Strategies to ‘Hydrophobize’ Systemic siRNA Vectors and Selectively Inhibit mTORC2 in Breast Tumors Through RNA Interference

By

Thomas Anthony Werfel

Dissertation
Submitted to the Faculty of the
Graduate School of Vanderbilt University
in partial fulfillment of the requirements
for the degree of

DOCTOR OF PHILOSOPHY
in
Biomedical Engineering
May, 2017
Nashville, Tennessee

Approved:

Craig L. Duvall, Ph.D.

Todd D. Giorgio, Ph.D.

John T. Wilson, Ph.D.

Rebecca S. Cook, Ph.D.

Dana M. Brantley-Sieders, Ph.D.

Justin M. Balko, Pharm.D., Ph.D.

This work is dedicated to my mother, Karen Werfel, a brave survivor of breast cancer.

ACKNOWLEDGEMENTS

I must begin by thanking my advisor, Dr. Craig Duvall, who has laid the foundation for the work I am able to do and whose guidance is constantly elevating this work. Dr. Duvall never lets his students settle and is always driving us toward the attainment of higher goals. This attribute is noticeably present throughout his publication record. I must thank all the amazing members of Dr. Duvall's Advanced Therapeutics Laboratory at Vanderbilt University for their support and comradery. Particularly, I thank Drs. Hongmei Li, Chris Nelson, Dana Brantley-Sieders, and Rebecca Cook. Dr. Li, as she was the first to train me as a scientist and whose mentorship initiated my interest in research. Dr. Nelson, as his work and ideas serve as the basis for the optimization of siRNA delivery materials presented here. Drs. Brantley-Sieders and Cook, as their ideas motivated pursuing a selective mTORC2-targeting therapeutic. I would also like to thank the remaining direct contributors to the work presented herein: Martina Miteva, Taylor Kavanaugh, Kellye Kirkbride, Meredith Jackson, Shan Wang, Meghan Morrison Joly, Donna Hicks, Violeta Sanchez, Linus Lee, Somtochukwu Dimobi, Samantha Sarett, Corban Swain, Kameron Kilchrist, Brian Evans, Irene Chandra, Madison Hattaway, Rebecca Cook, Todd Giorgio, and Craig Duvall. Thank you to Rene Colehour and Sarah Satterwhite who first introduced me to the great family here at Vanderbilt and who continue to stay in touch. Thank you to Dan Balikov for many meals and coffees and the conversations which accompanied and helped to strengthen us through graduate school. Thank you to Ashton Werfel, my wife and the love of my life, for her continued support and constant grace as I pursue a career in science.

I am grateful to the Vanderbilt Institute for Nanoscale Science and Engineering (VINSE) for access to DLS and TEM (NSF EPS 1004083) for polyplex characterization. I am grateful to the

Vanderbilt Translational Pathology Shared Resource (TPSR) for tissue sectioning and staining and blood chemistry analysis. I am grateful to Vanderbilt Breast Specialized Program of Research Excellence (S.P.O.R.E.) program for support of resources for immunohistochemistry. I am grateful to the Vanderbilt Digital Histology Shared Resource (DHSR) for access to a slide scanner and assistance with histology quantification. This work was supported by the Vanderbilt School of Engineering, the NIH through the following grants: NIH R21EB012750, NIH R01 EB019409, NIH P30 CA068485, and NCI R01 CA148934, the DOD through the CDMRP OR130302 grant, and the NSF through the NSF CAREER BMAT 1349604 grant and the following NSF GRFP fellowships: 1445197, 1445197, and 0909667.

TABLE OF CONTENTS

LIST OF TABLES

LIST OF FIGURES

LIST OF EQUATIONS

CHAPTER I

INTRODUCTION TO POLYMERIC NANOPARTICLES FOR GENE DELIVERY

Text for Chapter I taken from:

TA Werfel, CL Duvall. Polymer Nanoparticles for Gene Delivery. *Polymers and Nanomaterials for Gene Therapy*. Woodhead Publishing: Edited by Ravin Narain. 2016, 7, 147-188.

Background

Gene therapies have emerged as a part of the revolution in cell and molecular biology over the second half of the 20th century. While viral gene therapies represent the gold standard in terms of efficiency, therapeutic use of viruses remains shadowed by concerns with safety. Due to the tremendous opportunity for gene therapies to impact medicine, there is great motivation to work toward safer and targeted viral vectors and to also carry out parallel efforts toward engineering more efficient nonviral systems that can achieve safe, efficacious gene therapy in humans. This chapter will focus on the primary barriers that have limited clinical translation of nonviral gene therapies and outline recent advances in polymeric nanoparticles that have the potential to overcome these challenges. Many of the recent breakthroughs in nonviral gene therapy are a result of advances in materials science, chemistry, and engineering that have enabled the synthesis/fabrication of more homogeneous materials with an array of well-defined and tunable functionalities, in addition to the evolution of technologies for more rigorous characterization of chemical composition and biological interactions of nanomaterials. Taken together, rapid advances in materials synthesis and characterization, combined with tremendous progress in our ability to manipulate the genome and molecular-level and nanoscale phenomena, are predicted to yield

clinically-relevant breakthroughs in nonviral gene therapies that provide new and improved treatments for some of our most challenging diseases. This chapter provides and overview of advances in the design and testing of polymeric nanoparticles that continue to motivate our quest for clinical translation of nonviral gene therapies for both gene expression and silencing.

Nucleic acid-based drugs are sought for the replacement of missing, mutated, or deficient genes and for the suppression of gene expression by RNA interference (RNAi). Common classes of nucleic acid-based drugs include plasmid DNA (pDNA), messenger RNA (mRNA), short interfering RNA (siRNA), short hairpin RNA (shRNA), microRNA (miRNA), miRNA inhibitors, peptide nucleic acids (PNA), RNA-based adjuvants, and clustered regularly interspaced short palindromic repeats/Cas (CRISPR/Cas) gene editing systems. This chapter will focus on the more heavily investigated delivery strategies for siRNA and pDNAs, but note that strategies are similar for other nucleic acid-based drug classes reviewed elsewhere[1-4]. miRNA, miRNA inhibitor, RNA-adjuvant and PNA delivery strategies typically coincide with siRNA delivery, while mRNA (although trafficking to the nucleus is not needed), shRNA and CRISPR/Cas systems typically coincide with pDNA. Gene replacement/addition is the more mature field but comes with the extra challenges associated with delivering pDNA into the nucleus and the limitation that plasmids often do not stably integrate and thus do not have high potential for curing chronic genetic diseases. By contrast, RNAi by siRNA only requires delivery into the cytosol where the RNA-induced silencing complex (RISC) machinery is located. The activated RISC complex contains the antisense siRNA strand and mediates the recognition and subsequent enzymatic degradation of complementary mRNA. Both approaches require some common and disparate delivery considerations based on the desired intracellular pharmacokinetics. For instance, both require accumulation at the tissue compartment of interest and must cross the outer cell membrane. However, RNAi by siRNA will

only require a carrier with endosomal escape mechanisms while gene augmentation/replacement achieved through delivery of pDNA requires intracellular trafficking into the nucleus.

In general, three major delivery barriers are considered when developing polymeric nanoparticles for gene therapy: 1) preferential biodistribution to the site of action, 2) cellular internalization by the targeted cell type, and 3) trafficking to and unpackaging within the intracellular compartment where the nucleic acid cargo will be active (**Figure 1.1**). Viruses have evolved mechanisms to efficiently overcome these barriers and are the inspiration for the design of biomimetic polymer nanoparticles. Continued breakthroughs in the elucidation of the mechanisms of action of viruses, combined with rapid advances in synthetic fabrication and characterization of virus-mimetic polymeric nanoparticles, suggests that more safe and effective nonviral gene therapies will continue to emerge.

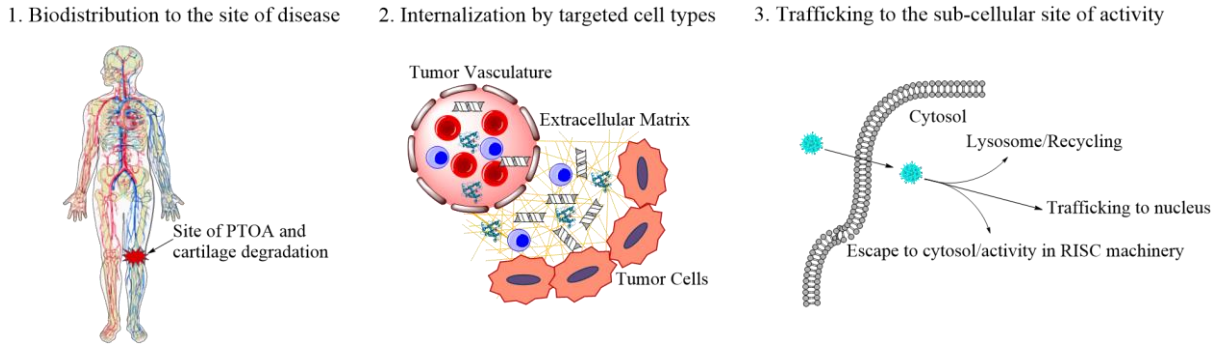

Figure 1.1) Schematic of the three major systemic and intracellular barriers to delivery of gene therapies. 1. The drug should be able to accumulate at the site of pathology, whether passively or by active targeting. 2. The drug should escape the circulation, navigate the ECM, and be internalized by the targeted cell types. 3. The drug should be trafficked to and released within the sub-cellular compartment where it is active.

Five classes of polymer nanoparticles are reviewed herein with the goal of highlighting techniques for synthesis and characterization and the gene therapy applications for each. The

classes of materials to be discussed are: micelles/polyplexes, cross-linked micelles, polymersomes, and microgels/nanogels.

Micelles

"Block copolymers with amphiphilic character, having a large solubility difference between hydrophilic and hydrophobic segments, are known to assemble in an aqueous milieu into polymeric micelles with a mesoscopic size range."[5] -Kazunori Kataoka et al. 2001

Micelles are self-assembling amphiphilic block copolymers with a core-shell (hydrophilic-hydrophobic) architecture. They are typically assembled in aqueous solutions by methods such as dialysis, pH adjustment, and dropwise addition of concentrated organic solutions. The formation of core-shell architecture is driven by entropic processes, resulting in segregation of a hydrophobic core from solution by a hydrophilic outer corona. This is an attractive architecture for drug delivery applications because it is possible to load hydrophobic small molecule therapeutics into the hydrophobic micelle core. The hydrophilic outer shell is often composed of PEG and serves as an aide for increased blood circulation and reduced cytotoxicity. In many gene therapy applications, the outer corona or the core are endowed with cationic functionalities that enable the electrostatic packaging of nucleic acids. Pre-assembled micelles with a cationic corona can be used to load nucleic acids, forming "micelleplexes". In other approaches, a diblock polymer with one core-forming, cationic block and one neutral hydrophilic block (typically PEG) is assembled into PEGylated polyplexes, also known as polyion complex (PIC) micelles, upon mixing with anionic nucleic acid cargo. In this chapter, we will utilize the "micelle" as an umbrella term to describe both of these sub-classes of delivery systems. Physicochemical attributes such as size, shape,

chemical composition, and charge are all important factors when considering the design of micelles as therapeutic carriers because they have a profound impact on their effectiveness in overcoming *in vivo* delivery barriers. This section reviews researched approaches for modulating the physicochemical properties of micellar gene therapies to approach the delivery efficiency of viral gene vectors.

The earliest approaches to using micelles as non-viral gene vectors employed cationic, amine-rich polymers such as poly(ethyleneimine) (PEI), poly(2-(dimethylamino)ethyl methacrylate) (PDMAEMA), and poly(L-lysine) (PLys). The amines of this class of cationic polymers are used for three purposes: 1) condensation/nuclease protection of negatively charged nucleic acids, 2) enhanced cellular uptake, and 3) endosomolytic escape. The positively charged amines form electrostatic interactions with and very efficiently condense nucleic acids. They also drive cellular uptake through mechanisms that are not yet fully elucidated, but are likely mediated through anionic, heparin sulfate proteoglycans present on cell surfaces.[6] After internalization, polymers with secondary and tertiary amines with pKa values at or just below pH 7 drive endosomolytic escape through the proton-sponge effect.[7,8]

Polyplexes formed of solely of cationic homopolymers have shown promise as *in vitro* tranfection agents but have many translational issues.[9] Their cationic character causes cytotoxicity and limits their utility for systemic delivery. The cationic surface charge causes aggregation with serum proteins and red blood cells, generally thought to be the reason for their eventual disproportionate accumulation in the capillary beds of the lungs, liver, and spleen and rapid clearance by the reticuloendothelial system (RES). In extreme cases, this can lead to rapid blockage of pulmonary capillaries and acute mortality in animal models. Therefore, cationic polymers are typically synthesized as diblock copolymers with hydrophilic polymers such as PEG and used to

form PIC micelles.[5] Kataoka's group pioneered the development of these micelles and their application as gene vectors. They used PEG-PLys as a diblock copolymer to condense DNAs and form PIC micelles that utilize PEGylation to shield their cationic character. This approach has served as the basis for numerous subsequent designs that utilize polyion complex formation to produce stable, nucleic acid-loaded micelles.

Other "micelleplex" approaches have leveraged diblock copolymers that pre-assemble into stable micelles in the absence of polyanionic nucleic acids. These stable micelles incorporate a cationic outer shell that can be utilized to condense nucleic acids into their corona. Stayton et al. developed a diblock polymer capable of forming stable micelles in the absence of any nucleic acids and condensing siRNA onto their surfaces, while the micelle core provided active endosome disruption behavior.[10] These micelles consist of a 100% PDMAEMA block and a random terpolymer block of 50% butyl methacrylate (BMA), 25% DMAEMA, and 25% propylacrylic acid (PAA). When a concentrated stock of the polymer in ethanol is added dropwise into excess PBS, micellar nanoparticles (~50 nm diameter) form with a PDMAEMA shell and p(DMAEMA-co-BMA-co-PAA) core. The hydrophobic BMA and electrostatic stabilization between DMAEMA and PAA provide core stability at physiological pH. The highly cationic PDMAEMA block provides stable siRNA loading into the outer micelle shell. The core stabilization is disrupted at pH values representative of the endolysosomal pathway (~5-6) due to concurrent protonation of the secondary amines of DMAEMA and carboxylic acid of PAA, leading to net cationic charge and electrostatic repulsion/destabilization of the core. The exposed p(DMAEMA-co-BMA-co-PAA) core-forming block exhibits pH-dependent lipid bilayer membrane disruptive activity, driving endosomolysis and escape of siRNA into the cytosol (**Figure 1.2a, b**).

While they are very effective for *in vitro* delivery and potentially for topical/local delivery *in vivo*, these micelleplexes possess highly cationic surface charge, resulting in similar limitations as the cationic homopolymers described above with regard to systemic delivery applications *in vivo*. To overcome this shortcoming, Stayton et al. have extended the use of the endosomolytic p(DMAEMA-co-BMA-co-PAA) micelle core-forming composition by combining it with a charge neutral corona containing sites for siRNA conjugation (rather than electrostatic loading).[11] The corona of these charge neutral polymeric micelles consists of neutral, hydrophilic poly[N-(2-hydroxypropyl)methacrylamide-co-N-(2-(pyridine-2-yldisulfanyl)ethyl)methacrylamide)] (p[HPMA-co-PDSMA]). This block promotes aqueous stability and provides pyridyl disulfide functionalities amenable to conjugation of thiol-functionalized siRNA. This approach shows mRNA knockdown and excellent biocompatibility and represents a potential alternative approach to PEGylation of cationic micelles, although the efficiency of siRNA conjugation is still much lower than electrostatic condensation.

Approaches that promote micelle surface charge neutrality, such as PEGylation, covalent siRNA loading as described above, and others also have limitations. By shielding of the cationic surface charge, the mechanism for cellular uptake of the micelles is also significantly neutralized. Attempts at modulating the effects of PEGylation are currently under investigation. Groups are elucidating what effect different lengths and densities of PEG on surfaces of micelles have on uptake and *in vivo* pharmacokinetics.[12] Two promising approaches for overcoming reductions in bioactivity due to PEGylation are: 1) the addition of targeting moieties on micelle surfaces that engage actively-internalized cell surface receptors (rather than depending on nonspecific electrostatic interactions with the cell surface for uptake) and 2) reversible PEGylation.

Micelle surface functionalization with targeting moieties can be beneficial for both PEGylated and non-PEGylated micelles. Stayton et al. employed this approach to their cationic micelles by conjugating folate for cancer cell targeting.[13] They were able to exhibit folate receptor specific interaction of the folate conjugated micelles as well as *in vitro* gene knockdown, though this system is not optimized for intravenous delivery due to high residual surface charge. More commonly, targeting moieties are added to the surface of PEGylated micelles. Kataoka et al. attached targeting molecules to their PEGylated PIC micelles for various applications.[14] They attached lactose for targeting the ASGP receptor of HepG2 cells, showing a significant increase in cellular transfection efficiency compared with micelles lacking lactose.[15] They also employed the cyclic RGD (Arg-Gly-Asp) peptide as a means to target $\alpha_v\beta_3$ integrin receptors. This integrin is expressed on many cell types that play an important role in angiogenesis, and is a potentially useful means to target anti-angiogenic tumor therapies. Hydrophobic stabilization of the core in PIC micelles has also been employed in order to achieve better pharmacokinetics *in vivo*.[16] By balancing cationic DMAEMA with hydrophobic BMA within the core of PEG-b-P(DMAEMA-co-BMA) PIC micelles, significantly higher endosomal escape and luciferase protein level knockdown was achieved *in vitro*. Further, knockdown of the model gene PPIB was achieved *in vivo* without any active targeting moiety.

Similar targeting approaches have been taken for more traditional (Non-PIC) micelles as well. For example, Xiong et al. recently coined a "virus-mimetic" targeted micelle for siRNA delivery.[17] They targeted PEG-poly(ε-capralactone) (PEG-PCL) micelles by decorating the PEG shell with a combination of RGD targeting peptide and transactivator of transcription (TAT)-derived cell-penetrating peptide. They observed an increase in cellular uptake for micelles with the targeting moieties, seeing the largest increase for the combined targeting with RGD and TAT

peptides. Increased cellular uptake also led to increased levels of P-glycoprotein (P-gp) knockdown at the mRNA and protein levels, re-sensitizing the cancer cells to doxorubicin treatment. A follow up study was conducted where doxorubicin (Dox) was co-delivered with siRNA within the RGD- and TAT-targeted PEG-PCL micelles.[18] The co-delivery technique improved the efficacy of Dox in multi-drug resistant (MDR) MDA-MB-435 tumor cells overexpressing P-gp. Cell viability *in vitro* was reduced 2-3-fold by co-delivery of MDR-1 siRNA and Dox in RGD/TAT targeted micelles verses untargeted micelles or targeted micelles with scrambled siRNA. Like most studies in this area to date, these are preliminary results and require more investigation in preclinical animal trials. These results do, however, provide proof of concept and promise of future success of this targeting approach for increased therapeutic efficacy *in vivo*.

The second approach that has recently evolved as a means for overcoming reduced activity due to micelle PEGylation is to use reversible / sheddable conjugation chemistry for micelle PEG attachment. By this approach, micelles will contain a cellular transfection moiety, most commonly cationic charge, which is shielded by PEG. PEG shields the micelles from uptake until it is removed within the pathological environment of interest. Giorgio et al. pioneered a form of enzyme activation of quantum dot nanoparticles (QD-NPs) coined as "proximity-activated" targeting.[19] With this approach, QD-NPs are only activated in proximity of the pathological environment where matrix-metalloproteinase (MMP) enzymes are expressed in higher concentrations than in circulation and normal tissue environments. A modification of this approach has been applied for reversible PEGylation of micelles for siRNA delivery.[20] In this approach, pDMAEMA-b-p(DMAEMA-co-BMA-co-PAA) cationic micelles were PEGylated through PEG attachment to the micelle surface using an MMP-7 cleavable peptide. PEGylation shields the cationic pDMAEMA shell utilized for siRNA loading, providing stealth in circulation. This PEG

shielding of the cationic layer is reversed in pathological environments of high MMP-7 expression (e.g., aggressive metastatic tumors), exposing cationic character of the micelles and driving cellular uptake. The surface charge of responsive micelles was increased 2.5-3-fold after exposure to MMP-7, indicating the potential of this design to shed PEGylation in pathological microenvironments (**Figure 1.2c**). In the preliminary studies, MMP-7 responsive micelles showed significant increases in knockdown of the model enzyme luciferase in R221A-Luc mammary tumor cells following MMP-7 activation.

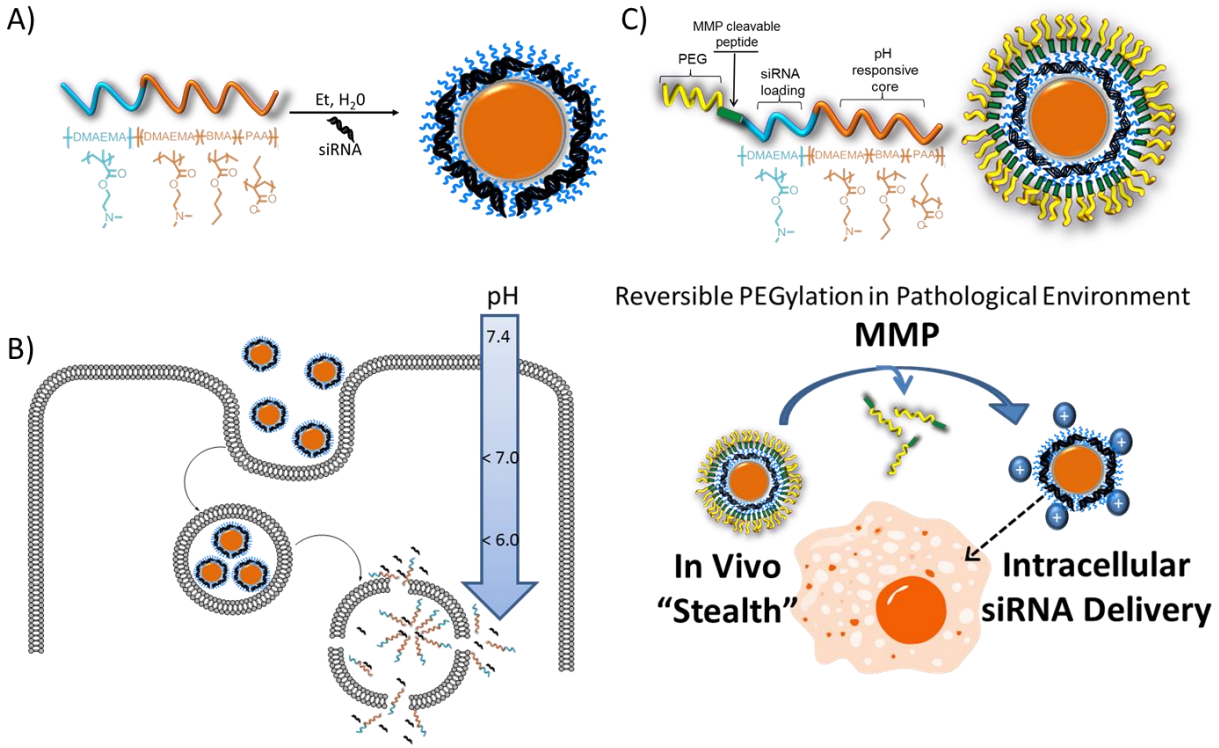

Figure 1.2) Endosomolytic Micelles for siRNA packaging and delivery.[20,21] (A) siRNA loading and micellization in aqueous solution. (B) Cellular internalization of the cationic nanocarriers and pH-responsive endolysosomal escape of siRNA. (C) PEGylation of the cationic nanocarriers for *in vivo* stealth and MMP-triggered, reversible PEGylation for preferential siRNA delivery into pathological sites.

The use of biodegradable micelles is a separate approach that has been explored, predominantly as a means to lower toxicity profiles of micelles. Poly(beta-amino esters) (PBAEs) are a particularly promising class of cationic, biodegradable micelles showing better transfection

efficiency *in vitro* than Lipofectamine 2000 (LF2K).[22,23] Langer and Green et al. developed a high-throughput system for synthesizing and screening combinatorial libraries of PBAEs to discover polymers that provide high cell transfection efficiency with low toxicity profiles.[24] Initially, they identified an ideal PBAE polymer candidate through high-throughput screening. A library of end group functionalities was then screened to identify which would give the greatest increase in transfection efficiency while maintaining cytocompatibility. It was found that PBAEs with primary alkyl di-amines were more effective than PBAEs with di-amine PEG spacers. Most importantly, they reported transfection efficiencies comparable to adenoviruses and orders of magnitude above PBAEs without end-group functionalities. Further studies of similar systems [i.e. poly(amine-co-esters)] have shown a continuum of success for cationic, biodegradable systems in pre-clinical studies and suggest that these classes of non-viral gene delivery systems are moving closer to replicating virus-like efficiency and becoming a clinical reality.[25]

To this point, most of the micellar systems discussed were of fully synthetic origin. Many micellar delivery systems employ amino acid-based monomers as well. The PEG-P(Lys) derived PIC micelles discussed earlier were one of the first delivery systems to employ "natural" monomers. Other micelles have been developed since using natural source monomers such as histidine, chitosan, β-cyclodextrins, and glycoamidoamines that show promise as non-viral gene vectors.

Poly(histidine) [P(His)] has a secondary amine containing imidazole group with its pKa around 6.0, appropriate for the proton sponge effect in late endosomes where the pH is shifted to below 6.0. P(His) is typically combined with P(Lys) in either a grafted or highly branched copolymer. The primary amines of lysine are fully protonated at physiological pH and serve to efficiently condense nucleic acids. The lower pKa secondary amines of P(His) provide an

endosomal escape mechanism by the proton sponge effect.[26] However, it was shown that the addition of endosomal disruption agent, chloroquine, significantly improved the transfection efficiency of these micelles, indicating that they are still prone to entrapment in the endolysosomal pathway.[27] Other approaches to hybrid micelles using P(His) have also been investigated such as a promising chitosan-P(His) hybrid, where the histidine residues are incorporated into a chitosan backbone in order to enhance endosomal escape and transfection efficiency.[28]

Chitosan, a polysaccharide composed of N-acetyl glucosamine units bonded via β(1→4) glycosidic bonds, has been extensively investigated as a saccharide polymer-based delivery vector. Chitosan is a 'green' approach because it is a biodegradable, renewable resource derived from chitin. Howard et al. conducted a series of successful experiments in which they delivered siRNA to knockdown enhanced green fluorescence protein (eGFP). They achieved high levels of eGFP knockdown in H1299 human lung carcinoma cells and murine peritoneal macrophages (77.9% and 89.3%, respectively).[29] In their *in vivo* studies, the siRNA loaded chitosan micelles achieved 37% and 43% reduction in eGFP in bronchiolar epithelial cells in transgenic eGFP mice after nasal administration as compared to mismatched and untreated controls, respectively. Although promising results have been reported, chitosan micelles are limited by poor solubility in physiological buffers and poor escape from the endolysosomal pathway. Therefore, several variants such as chitosan-PEI hybrids and the chitosan-P(His) hybrid mentioned above have been developed in an attempt to increase solubility and endosomal escape.[30]

Reineke and Davis have published a wealth of data on natural source-based micelles, reporting some of the most convincing results that non-viral gene vectors could have profound clinical impacts. The Reineke lab developed a class of glycopolycations, the poly(glicoamidoamines) (PGAAs).[31] Initially, a library of PGAAs was made through condensation

reactions of carbohydrates with oligoamine co-monomers. PGAAs were varied based on parameters such as carbohydrate size, hydroxyl number and stereochemistry, amine number, and presence of heterocyclic groups. The library was screened for gene delivery and optimized formulations were identified that facilitate efficient DNA packaging and intracellular delivery. The Reineke group also investigated the effectiveness of trehalose-based "click" polymers and are optimizing aqueous RAFT synthesized formulations for *in vivo* performance.[32,33] Through these studies, they have found formulations of diblock glycopolymers that effectively condense pDNA and siRNA while promoting stability under physiological salt and serum conditions. Moreover, the diblock glycopolymer formulations were made even more stable in physiological conditions when surface functionalized with poly(trehalose) as an alternative to PEGylation.[34] The poly(trehalose) functionalized diblock glycopolymer micelles showed rapid internalization into glioblastoma cells and tunable rates of siRNA delivery.

The Davis Lab has pioneered the use of β-cyclodextrin (β-CD) based polymers for non-viral gene delivery. Cationic β-cyclodextrin-based polymers (βCDPs) were synthesized by the condensation of diamino-cyclodextrin monomers with diimidate co-monomers and were capable of forming polyplexes with nucleic acids.[35] βCDPs are unique in that their large, interior cavities are capable of forming inclusion complexes with hydrophobic moieties which can then be functionalized with PEG or targeting ligands.[36,37] The Davis lab was the first to translate a targeted βCDP-based micelle into the clinic for RNA interference (RNAi) human trials. They reported on the first targeted delivery of siRNA in humans using a βCDP, PEGylated for increased circulation and targeted by way of a human transferrin (Tf) targeting ligand.[38] The success of this approach was realized just a year later when the Davis Lab reported the first evidence of RNAi in humans using targeted polymeric NPs.[39] In the study, a reduction of the targeted mRNA and the protein

level expression was observed as compared to "pre-dosing tissue." The presence of predicted mRNA cleavage fragments further demonstrated the siRNA-mediated degradation of mRNA leading to RNAi. This initial report is a profound accomplishment, verifying the potential of siRNA and other forms of RNAi (discovered in 1998, won Nobel Prize in Physiology and Medicine in 2006[40]) as potent and specific therapeutics which could transform the treatment of a variety of hard to drug pathologies in the future.

Cross-Linked Micelles

"Supramolecular self-assembly techniques have provided a versatile means by which to selectively assemble polymer molecules into well-defined three dimensional core–shell nanostructures. The covalent stabilization and tailoring of these dynamic nanostructures can be achieved using a range of chemistries within the assembly to afford robust functional nanoparticles."[41] –Karen Wooley et al. 2006

Micelles, as described above, are supramolecular self-assemblies of amphiphilic di-block copolymers. Their self-assembly is driven by the hydrophobic effect – an entropic phenomenon where water molecules move from their ordered architecture along the polymer (water "cage") and into solution. Self-assembled micelles can suffer from lack of stability in biologic environments. Often, micellar systems are susceptible to dynamic changes such as temperature, salinity, and concentration. Cross-linking has been employed as a strategy to overcome micelle instability by introducing covalent linkages between polymer chains that make up the micelles. Cross-linking can be used to offer greater stability to micelles by reinforcing the weaker intermolecular forces which drive micelle self-assembly.[41]

Two major categories of cross-linking are employed for the stabilization of micelles. Core cross-linking is the process by which cross-linkable groups are introduced onto the hydrophobic segment of the di-block copolymer of the micelle. The cross-linking reaction is performed after micellization, resulting in a core cross-linked micelle with increased stability over its micellar precursor. Alternatively, cross-linkable groups can be incorporated onto the hydrophilic portion of the polymer that forms the micelle shell. In this case, the cross-linking reactions can be similarly performed post-assembly, but the result is a shell cross-linked micelle. Both strategies have been investigated for increasing micellar stability and used for a variety of applications (therapeutics, molecular imaging agents, nano/micro-electronics, etc,).[41] Moreover, each strategy comes with its advantages and limitations. The choice of core versus shell crosslinking strategies is often based on the eventual application. However, shell cross-linked micelles are considered by many to have greater potential as delivery agents than their core cross-linked counterparts due to their higher core mobility, increased diversity of core composition, and improved encapsulation efficiency by the membrane-like, cross-linked shell layer.

Several chemistries have been employed for micelle core and shell cross-linking. Core cross-linking is commonly achieved by the copolymerization of monomers containing cross-linkable groups during the polymerization of the hydrophobic polymer block. The introduction of cross-linking reagents or external stimuli (such as photo/UV-irradiation) can be used to drive the cross-linking reactions within the core following polymer synthesis and micelle self-assembly. Recently, induction of core cross-linking by external cues such as pH and temperature have been investigated as alternative strategies.[42,43] Radical polymerization techniques were first reported for the cross-linking of the shell of micelles and condensation reactions were reported soon after.[44,45] However, the most common shell cross-linking technique is achieved by introducing cross-linking

reagents (**Figure 1.3**). A diamine reagent can cross-link carboxylic acid groups of the polymer backbone in the presence of a carbodiimide activator in aqueous solution. Alkylation is an alternative cross-linking strategy for cross-linking shells comprised of hydrophilic monomers, such as *N*,*N*-dimethylaminoethyl methacrylate, that do not contain carboxylic acid functionalities.[46]

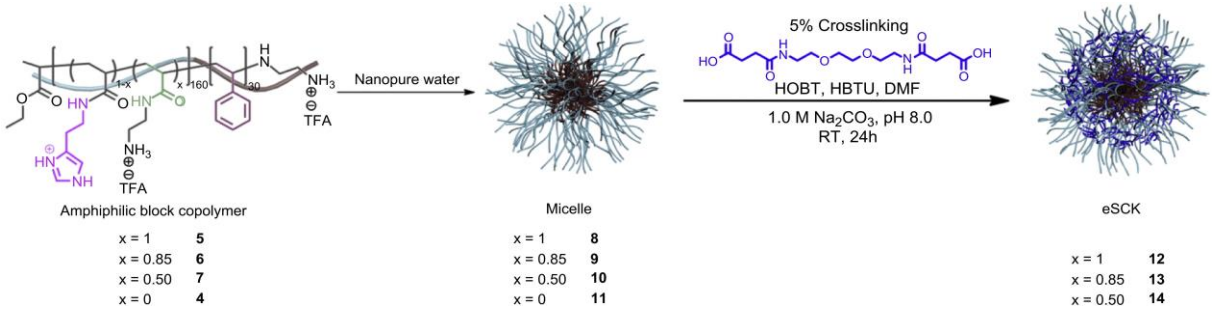

Figure 1.3) Schematic of polymerization and cross-linking of shell cross-linked micelles. *Adapted with permission from reference [44]. Copyright 2012, Elsevier.*

Selectively achieving intramicellar and not intermicellar coupling is a critical criterion for producing consistent batches of cross-linked micelles. Intramicellar couplings lead to the desired shell or core cross-linked micelles while intermicellar couplings lead to the formation of large, covalently bound aggregates. Two major approaches are taken to overcome this potential limitation. By one approach, cross-linking is simply done at extremely dilute concentrations. The extreme dilution greatly reduces the probability of intermicellar cross-linking in solution and typically leads to consistent intramicellar cross-linking. Translation to an industrial scale is a limitation of this approach, and therefore, cross-linking of ABC copolymers has been introduced as an alternative. AB copolymers consist of a hydrophobic-hydrophilic di-block architecture. ABC copolymers consist of an additional intermediate “B” segment of polymer which contains the

cross-linking moieties (**Figure 1.4**). For example, Armes et al. developed an ABC copolymer consisting of a poly(propylene oxide) (PPO) core, poly(2-(dimethylamino)ethyl methacrylate) (DMAEMA) intermediate layer, and methoxy capped poly(oligo(ethylene glycol) methacrylate) (OEGMA) shell.[47] The DMAEMA intermediate layer residues were cross-linked using the bifunctional quaternizing agent, 1,2-bis(2-iodoethoxy)ethane (BIEE). The introduction of this intermediate layer for coupling allows for cross-linking at higher concentrations, and offers a more desirable approach for promoting intramicellar cross-linking over intermicellar.

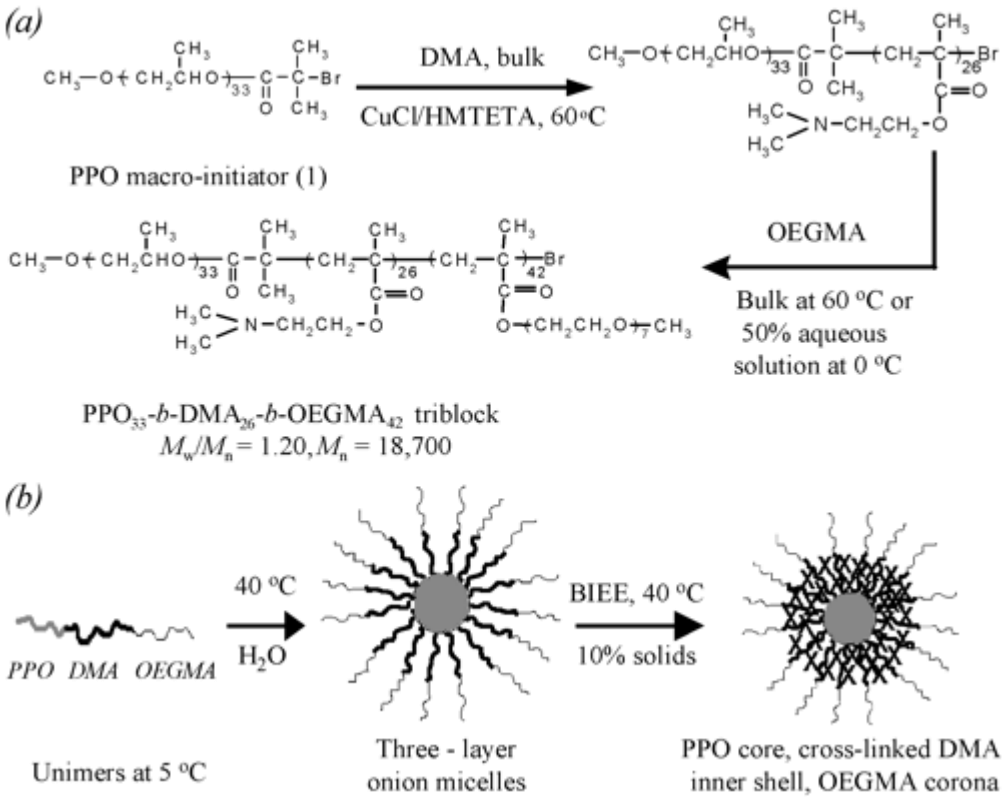

Figure 1.4) Schematic of Intra-micellar cross-linking by ABC tri-block copolymers. *Adapted with permission from reference [45]. Copyright 2001, American Chemical Society.*

Although the two approaches described above have been used for developing cross-linked micelles with good functionality, more effective cross-linking strategies are still sought after. The traditional cross-linking reactions are inherently inefficient and hard to quantify. Orthogonal cross-linking chemistries have been more recently investigated as a more efficient alternative. Namely,

'click' chemistry has been an increasingly popular approach. One of the most used 'click' chemistries employs the copper(I)-catalyzed Huisgen 1,3-dipolar cycloaddition reaction between alkynes and azides. The reaction is highly efficient, selective, and results in good compatibility and orthogonality with a variety of biological molecules. Hawker et al. demonstrated the potential for this approach by incorporating click-reactive functional groups in either the core or shell of micelles in aqueous solution.[48] Using azide/alkyne click-functionalized fluorescent dyes, they showed the selective reactivity of these groups to complementary azide/alkyne groups within their micelle architectures. Further work has followed up on this initial report, verifying 'click' chemistry as a powerful cross-linking approach and investigating its utility for the surface-functionalization of micelles.[49,50] Reversible or environmentally-responsive cross-linking, such as Katoaka's disulfide cross-linked PIC micelles[51], is also a more recent evolution and has been developed to ensure that micelles can unpackage their cargo (*i.e.*, so that micelle overstabilization doesn't hinder drug release/bioactivity).

Wooley et al. pioneered synthesis of shell cross-linked micelles for packaging nucleic acids.[52] McCormick and Armes et al. investigated another shell cross-linked system which they described as for the release of "bioactive agents".[42] Their design incorporated a reversible cross-linking moiety into the B-block of their ABC triblock copolymer to achieve controlled release. The thermoresponsive and reducible nature of these SCL micelles made the drug release profile responsive to changes in environmental conditions. Other groups focused on further optimizing shell cross-linked micelle chemistry for more efficient encapsulation and improved biocompatibility for gene delivery. Stenzel et al. thoroughly investigated cationic polymers made by RAFT polymerization for their application as shell cross-linked micelles for gene delivery.[53] They showed that shell cross-linked micelles were more biocompatible than their cationic non-

cross-linked micelle counterparts and that cross-linked micelles retained desirable levels of transfection. Wooley's group published a set of articles also demonstrating the effective transfection of mammalian cells by shell cross-linked micelles.[54,55] Their initial study highlighted a shell cross-linked micelle composed of poly(acrylamidoethyl amine)-*b*-polystyrene (PAEA-*b*-PS). They demonstrated the ability to condense oligonucleotides and pDNA and to effectively transfect mammalian HeLa cells, indicating that a 6:1 N/P ratio provided the highest transfection efficiency. The follow-up study optimized transfection efficiency and cytotoxicity by investigating various relative quantities of primary versus tertiary amines and exploring a range of N/P ratios used for nucleic acid condensation. They showed that cationic shell cross-linked nanoparticles (cSCKs) with 25% primary amines and 75% tertiary amines (cSCK-pa_{25}-ta_{75}) transfected pDNA into HeLa cells best at a 20:1 N/P ratio. Alternatively, cSCK-pa_{50}-ta_{50} micelles at a 10:1 N/P ratio were best for transfecting oligodeoxynucleotides (ODNs). Importantly, they also demonstrated that the incorporation of tertiary amines into the shell of micelles was an effective strategy for maintaining transfection efficiency while reducing cytotoxicity.

Building upon these initial proof of concept and optimization studies, other groups have recently further investigated the effectiveness of both shell and core cross-linked micelles as gene delivery vectors. Kataoka's group employed their environmentally-responsive, disulfide core cross-linked micelles to this end.[56] The PIC micelles were formed from iminothiolane-modified PEG-*b*-PLL (PEG-*b*-(PLL-IM)). This polymer efficiently condensed siRNA and formed a cross-linked core through linkages between iminothiolane groups. They showed that reductive conditions (such as those within the cytosol) destabilize the core of these micelles and lead to increased gene silencing compared to a non-reducible analog. Finally, they also demonstrated that

tuning of the ratio of PEG-b-(PLL-IM) to siRNA was imperative for achieving gene silencing activity.

Wooley et al. have recently investigated additional shell-cross linked micellar designs for siRNA and peptide nucleic acid (PNA) delivery. Interestingly, their first report in this vein was on the packaging and efficient delivery of PNAs.[57] PNAs are a synthetic hybrid molecules comprising a polypeptide backbone but with nitrogenous base R-groups which enables Watson-Crick base pairing with nucleic acids. PNAs are a promising class of therapeutics because they are not susceptible to degradation by nucleases that are classically linked to the *in vivo* degradation of gene therapies. Yet PNAs still suffer from short circulation half-lives, low transfection efficiency, and a lack of endolysosomal escape mechanisms. Therefore, the Wooley group investigated the packaging of PNAs into their previously developed cSCKs. They took two approaches to packaging PNAs: 1) electrostatic complexation of PNA-ODN hybrid, and 2) bioreducible, covalent disulfide linkage. They showed that both versions of the cSCKs were as effective at transfection as LF2K and had higher cell viabilities. They also showed that cSCKs were more effective than previously developed Arg-mediated methods of PNA delivery. This attributed to cSCK facilitation of PNA endosomal escape, while PNAs alone suffered from entrapment within endosomes. Next, the Wooley Lab investigated the cSCKs for their ability to enhance the delivery of siRNA.[58] In particular, they studied the effect of altering the cSCKs buffering capacity on siRNA binding, transfection, endosomal escape, and cytotoxicity. The buffering capacity of cSCKs was tuned by altering the amount of histamine verse primary amines in the shell cross-linking region. The addition of histamine was shown to reduce the siRNA encapsulation efficiency as well as cellular binding. However, cytotoxicity was significantly reduced, and the increased buffering capacity led to an increase in transfection efficiency.

Theranostic nanomaterials represent another recent development for shell cross-linked micelles capable of both delivery and diagnostic sensing. The Wooley Lab has recently developed a hierarchically assembled theranostic material from the cSCK platform described above.[59] The material is capable of delivering siRNA as a therapeutic and can be radiolabeled for potential diagnostic applications. The hierarchical assembly is initiated by preparing anionic, shell cross-linked nanorods of the amphiphilic block copolymer poly(acrylic acid)-*b*-poly(*p*-hydroxystyrene) (PAA-*b*-P*p*HS) in nanopure water. Cationic shell cross-linked nanoparticles are then added to coat the nanorod surfaces. These theranostic, hierarchically assembled nanostructures were demonstrated to condense siRNA, transfect several cell lines *in vitro*, and have sufficient radiolabeling yield. The nanostructures condensed siRNA at lower N/P ratios and achieved higher intracellular delivery of Cy3-labeled siRNA compared to LF2K or cSCKs alone. The hierarchically assembled theranostic nanostructures also showed had higher radiolabeling efficiency compared to cSCKs, suggesting their potential for use with PET imaging. A follow up study by the Wooley group incorporated paclitaxel, a hydrophobic anticancer drug, into the nanostructures and also introduced a targeting ligand onto the surface of cSCKs.[60] Multifunctional approaches such as the hierarchically assembled theranostic nanostructures may expect to be met with significant regulatory barriers for clinical use yet represent key advances in basic science that are adding to our understanding of how nanomaterials interact with biological systems.

Polymersomes

"Polymersomes are polymer-based vesicular shells that form upon hydration of amphiphilic block copolymers."[61] -Dennis Discher et al. 2009

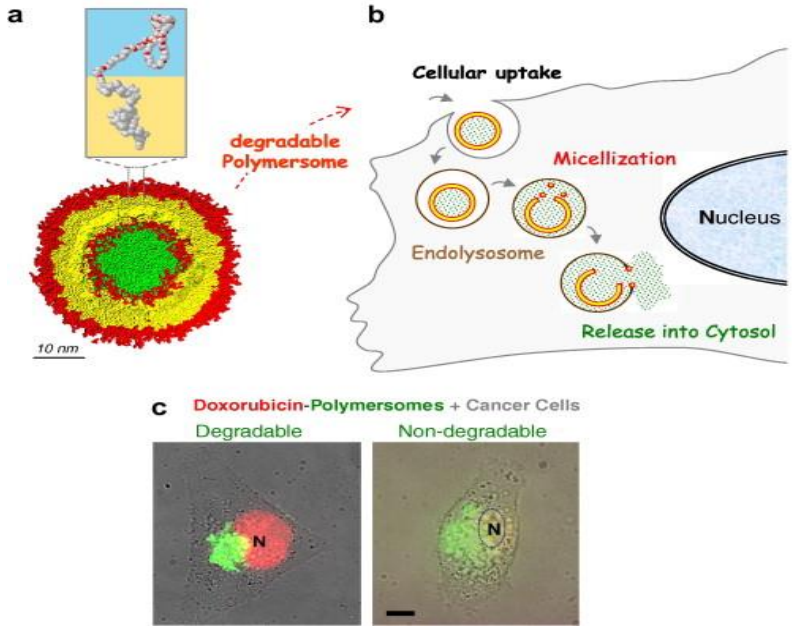

Figure 1.5) Polymersomes. (A) Polymersome assembly and structure in aqueous milieu. (B) Cellular uptake and endolysosomal escape. (C) Fluorescent microscopy imaging of doxorubicin delivery from polymersomes. *Adapted with permission from reference [58]. Copyright 2009, Elsevier.*

Discher et al. developed a novel class of polymeric nanoparticles at the turn of the 21st century termed "polymersomes". This term was derived from being a polymer-based "liposome" because they adopt a vesicular structure similar to previously-described liposomes but were composed of amphiphilic di-block copolymers rather than lipids (**Figure 1.5**).[62] Polymersomes create unique capabilities relative to micellar structures, which are typically utilized to load hydrophobic drugs into their core, because they can encapsulate a wide variety of therapeutics, including entrapment of larger, water soluble biologics such as nucleic acids and proteins, within the aqueous interior. Like other polymer-based nanoparticles, one can also incorporate additional polymer functionality (i.e. responsiveness to environmental stimuli) to improve delivery. For example, recent developments on controlled disassembly, degradation, targeting, and endolysosomal escape have further increased the potential of polymersomes as nanocarriers for therapeutics. These developments are discussed herein with a focus on applications in gene therapy.

Polymersomes have a large range of tunable properties based on the polymer molecular weight (MW), composition, and chemistry, a key advantage relative to classical liposomes. Using a reletively inert, synthetic di-block copolymer, poly(ethelyne glycol)-polybutadiene (PEG-PBD), the effect of the molecular packing factor (a measure of the ratio of hydrophobic to hydrophilic sections of an amphiphilic copolymer) on morphology of copolymer aggregates has been elucidated. By changing the length of the hydrophilic block, the resulting aggregates could be tuned to form either spherical micelles, worm-like micelles, or polymersomes.[63] For hydrophobic:hydrophilic ratios that form polymersomes, the vesicle interior diameter correlates with the total MW of the block copolymer.[64] Further, it is only for lower MW copolymers that the polymer bilayer exhibits mid-planes of low density ("methyl troughs") reminiscent of lipid bilayers. Higher MW copolymers form a single thick shell of homogeneous density.[65,66] Membrane fluidity generally decreases with increasing MW, most drastically once an entanglement threshold is crossed. Polymersomes have generally been described as having mechanical properties somewhere between lipid vesicles (optimized for fluidity) and viral capsids (evolved to possess robustness and stability).[61]

Polymersome activity *in vivo* is largely dependent upon the ability to tune the material chemistry to create ideal pharmacokinetic properties. The earliest polymersomes were formed from inert polymers, such as PEG-PBD and poly(ethylene gycol)-polyethyleneethylene (PEG-PEE). These polymersomes exhibit long circulation half-lives, being 100% PEGylated to provide serum stability. However, the need for controlled release to enable effective *in vivo* bioactivity has motivated the recent development of biodegradable and environmentally- and stimuli-responsive polymersome chemistries. The bioactivity of therapeutics delivered through nanocarriers are dependent upon the ability of the carrier to overcome physiological barriers such as rapid clearance

through the reticuloendothelial system (RES), transfection across the plasma membrane, escape from endolysosomes, and appropriate intracellular trafficking. Groups have, accordingly, focused on mechanisms to overcome these barriers and increase the efficiency of polymersomes. External cues such as temperature and UV light, as well as internal cues such as pH and redox changes have been investigated.[67]

Temperature and ultraviolet (UV)-light exposure are popular examples of using externally applied cues to stimulate endolysosomal escape and release of therapeutics from polymersomes. Kros et al. and Jiang et al. have explored two different UV-sensitive polymersomes. Kros et al. investigated a system based on the polymer PEG-poly(methylphenylsilane).[68] This polymersome is capable of encapsulating hydrophilic drugs, and the Si-Si bond is cleaved upon exposure to UV-light, shifting polarity of the hydrophobic core and triggering disassembly of and cargo release form the polymersomes. Jiang et al. investigated a system based on the polymer PEG-(Malachite Green-CN) (PEG-MG-CN).[69] A similar mechanism of core disruption is employed by PEG-MG-CN where UV-light induces the loss of cyanide anions from MG and the resultant PEG-MG disassembles and releases its hydrophilic cargo. UV exposure presents many challenges *in vivo* and is therefore more likely to be used for *in vitro* or *ex vivo* applications. As an alternative, temperature responsive motifs have been investigated which could be of more utility *in vivo*. The polymer, poly(N-isopropylacrilamide) (PNIPAm), is a prototypical lower critical solution temperature (LCST) polymer that has been pursued for thermally responsive polymersomes.[70,71] PNIPAm solubility is temperature-dependent ($T > 32^oC$ – hydrophobic; $T < 32^oC$ – hydrophilic). As an example, the di-block polymer PEG-PNIPAm is amphiphilic at temperatures above 32^oC and can self-assemble into polymersomes when the appropriate relative block lengths of PEG and PNIPAm are used. As the temperature drops below 32^oC, amphiphilicity is lost and the

polymersomes disassemble, providing a controlled release mechanism for the encapsulated drugs (such as doxorubicin). As is to be expected, it is necessary to use these carriers in combination with some form of hypothermic therapy to stimulate the temperature-dependent response, which is below normal physiologic temperature (37°C).[71]

Leveraging endogenous, physiologic cues for polymersome disassembly are desirable, relative to externally actuated systems, because they are not as limited by accessibility for applications deeper within the body. For example, changes in pH and redox conditions have been investigated as ways to internally trigger the release of therapeutics within the desired cellular microenvironment. Polymersomes experience a change in pH during endocytosis, from extracellular pH of 7.4 to ~5.0 in late endolysosomes. Triggered release can be achieved with polymer chemistries which are sensitive to this change in pH. Two primary approaches have been taken to develop polymersomes that respond to pH change: 1) leveraging changes in rate of polyester hydrolysis with decreasing pH [72,73] and 2) incorporation of acidic/basic monomers whose protonation state effects polymer water solubility.[74] The first approach is less desirable as degrading polymersomes already nonspecifically release therapeutics prior to the decrease in pH (lower pH only accelerates the process). Alternatively, designs based on a shift in polymer hydrophobicity in response to pH changes typically more stably encapsulate therapeutics, and more switchlike release behavior. Poly(2-vinylpyridine)-PEG (P2VP-PEG)[74] and poly(2-(methacryloyloxy)ethyl phosphorylcholine)-*b*-poly(2-(diisopropylamino(ethyl methacrylate) (PMPC-*b*-PDPA)[75] are two examples of diblock polymers that have been utilized to fabricate pH responsive polymersomes that release their cargo within the pH of the endolysosomal pathway. Redox conditions within the endolysosomal pathway can also be leveraged for controlled release. Hubbell et al. developed reduction[76] and oxidation[77,78] responsive polymersomes. They developed

a triblock amphiphile composed of PEG-poly(propylene-sulfide)-PEG that self assembles into polymersomes. Upon exposure to reactive-oxygen species (ROS) such as hydrogen peroxide (H_2O_2), PPS (initially hydrophobic) is oxidized to more polar poly(sulfoxides) and poly(sulfones), triggering polymersome disruption. To employ a reduction-responsive mechanism, they incorporated a disulfide linkage into the di-block version of the previous polymer (PEG-SS-PPS). The disulfide bond is broken in reducing environments such as by high concentrations of intracellular glutathione[79], driving polymersome disassembly and release of therapeutics.

Over the last ten years, polymersome design principles have begun to be applied for development of carriers that overcome nonviral gene therapy barriers such as low transfection efficiency, rapid degradation, transient expression, and off-target toxicity. Korobko et al. were one of the first to apply polymersomes to effectively deliver genes *in vitro*.[80,81] They used a cationic and amphiphilic diblock copolymer poly-(butadiene-*b*-*N*-methyl-4-vinyl pyridinium) (PBD-P4VPQI) to encapsulate DNA in the vesicle lumen as well as being electrostatically condensed with the cationic P4VPQI. The DNA was efficiently encapsulated and controlled release was achieved by osmotic pressure (proton sponge-like effect driven by cationic P4VPQI monomer) triggered disruption of the polymersomes. They further showed that the polymersomes could encapsulate pDNA, thus overcoming a shortfall of many previous polymersome designs that could only encapsulate very small genetic materials. Though promising, downfall significant limitation of this design was that the overly cationic character of the polymersomes drives non-specific uptake and cytotoxicity, making this design less applicable for *in vivo* use. Brown et al. developed seminal poly(amino acid) [poly(AA)] based polymersomes. Their design utilizes amphiphilic triblock copolymers of methoxy-(PEG), palmitic acid, and either poly-L-lysine (PLL) or poly-L-orthinine (PO).[82] These triblocks self-assemble into polymersomes. Importantly, the cationic

charge of this system can be tuned by the ratio of polymer to DNA (polymer:DNA). Effective *in vivo* delivery to the lungs and liver were shown when the charge was tuned to be overall slightly anionic, but significant cytotoxicity was seen *in vitro* at very low concentrations.[83] Thus, more biocompatible designs have been a focus for continued polymersome development.

PEG-polylactic acid (PEG-PLA or 'OLA') polymersomes were a promising initial design for balancing cellular transfection efficiency and cytotoxicity, which are often competing considerations.[84] The PEGylated surface increases blood circulation half-life, decreases cytotoxicity, and doesn't affect nucleic acid encapsulation. The OLA polymersomes (OLA-Psomes) were effectively applied to deliver siRNA *in vitro* at comparable levels to the commercial transfection reagent Lipofectamine 2000 (LF2K). The OLA-Psomes + siRNA and LF2K + siRNA showed about a 33% knockdown effect while free siRNA showed no knockdown. The OLA-Psomes are promising for further development because their PEGylated surfaces make them more translatable *in vivo* relative to highly cation lipoplexes formed with LF2K and similar reagents.

More recently, several designs have been investigated with the goal of increasing circulation half-lives and balancing the efficiency of therapeutic delivery and off-target cytotoxicity. Like all classes of nanoparticles, PEGylation is heavily investigated for increasing the circulation half-lives of polymersomes. It is generally understood that PEGylation of nanoparticles decreases their interaction with plasma proteins in circulation and decreases the immune response to the carrier. In order to address the problem of inefficient and non-specific delivery, groups have also begun employing active targeting mechanisms. Development of multifunctional polymersomes with long circulation time and efficient uptake through active targeting may enable discover of gene therapies that approach the efficiency of viral vectors.

Several approaches to targeting have been investigated and are still in development. Initially, conventional receptor ligands and antibodies have been sought for active targeting.[85] Nonspecific cell penetrating peptides (CPPs) such as the HIV-derived Tat peptide (TATp) have also been utilized for increasing cell uptake. As an example, Christian et al. conjugated TATp to PEG-PBD polymersomes to target dendritic cells [86] Antibodies have the potential to be utilized as a more specific targeting mechanism. Lecommandoux et al. recently functionalized magnetic polymersomes with an antibody (trastuzumab) in order to target and image overexpressing HER-2 cells in a metastatic breast cancer model.[87] Biotin and polyguanacyclic acid have also been used to achieve active targeting with polymersomes.[88,89] All of these mechanisms have been shown to be effective *in vitro*, but none have yet been well characterized *in vivo*. It will be crucial to see the translation from *in vitro* studies to preclinical *in vivo* studies and to observe how well these modified polymersomes perform *in vivo* relative to other classes of carriers.

Other targeting peptides have also been explored by Kokkoli et al. for polymersome-based gene therapies. Initially, they pursued a PEG-poly(γ-methyl-ε-caprolactone) (PEG-PMCL) polymersome containing a vinyl sulfone electrophile in the corona.[90] The electrophile reacted preferentially with thiol-containing peptides for active targeting. They also utilized a bio-orthogonal "click" chemistry approach to attachment of targeting peptides.[91] In this case, polymersomes were modified with a fibronectin mimetic peptide (PR_b) to target to areas of higher $\alpha_5\beta_1$ integrin (various cancer cells). The polymersomes were found to significantly outperform non-targeted analogs in terms of cytotoxicity and delivery efficiency. Recently, this group showed enhanced delivery of siRNA to highly expressing $\alpha_5\beta_1$ integrin breast cancer cells using PR_b targeting.[92] In this study, PEG-PBD polymersomes surface-functionalized with PR_b by click chemistry were used to encapsulate and deliver siRNA. Down-regulation of Orai3

(calcium channel protein) was shown to reduce breast cancer cell viability in previous studies and was therefore chosen as a target for siRNA knockdown in this study. The PR_b functionalized polymersomes knocked down Orai3 significantly better than unfunctionalized polymersomes in T47D breast cancer cells in vitro. Although commercial transfection agents had higher levels of knockdown, the polymersomes represent a more translatable system with regardsto potential *in vivo* biocompatibility. This, and other, studies serve as a promising proof of concept for application of polymersomes for targeted gene delivery, motivating continued preclinical development of this approach.

Microgels/Nanogels

"Hydrophilic polymers are the center of research emphasis in nanotechnology because of their perceived "intelligence". They can be used as thin films, scaffolds, or nanoparticles in a wide range of biomedical and biological applications."[93] –Langer et al. 2006

Over the last few decades, advances in materials engineering have enabled synthesis of defined networks of hydrophilic polymers with finely controlled physicochemical and mechanical properties. These networks of hydrophilic polymers can be physically or chemically cross-linked to yield "hydrogels". Hydrogels have a high affinity for water because of their hydrophilic nature, and their cross-linked architecture results in swelling. Hydrogel chemistry can be utilized for loading and controlled release of biologics such as proteins, nucleic acids, and cells. Defined functionalities can also be engineered into hydrogels to control host cell infiltration into and response to hydrogels following implantation *in vivo.* Their high water content and similarity in

structure to native extracellular matrices makes hydrogels especially useful for tissue engineering, but they are currently under investigation for a broad variety of biomedical applications including drug delivery, biosensing, microarrays, and diagnostic imaging.[93]

Hydrogels are conventionally synthesized at the macro/tissue scale, but new methods are amenable to creating hydrogels of varied size and shape for specialized applications such as gene therapy (**Figure 1.6**). Three of the most important parameters for characterizing hydrogel bulk structure are the swollen state polymer volume fraction, molecular weight of polymers between cross-links, and the mesh size (consult this recent review for mathematical models of these parameters[93]). While bulk hydrogels are often utilized as tissue engineering implants, microgels and nanogels offer flexibility that is often harnessed for drug delivery applications. Microgels are typically in the hundreds of nanometers to micrometer scale. Preparation into thin films is the most common approach for their application in drug delivery.[94] Recent advances in fabrication techniques have also allowed the production of nanogels, nano-sized networks of cross-linked hydrophilic polymers. Nanogels are created using specialized fabrication approaches and are typically administered similarly to the other categories of nanoparticles discussed in this chapter.

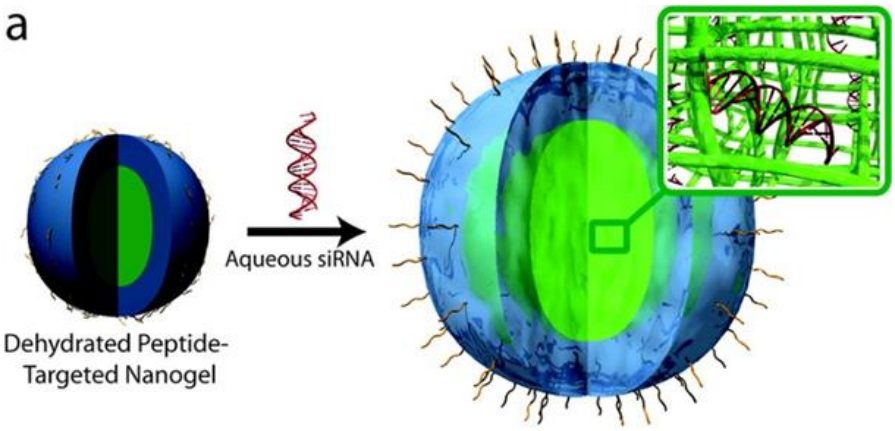

Figure 1.6) Peptide-targeted Nanogels. Schematic of the swelling and encapsulation of siRNA in aqueous milieu. *Adapted with permission from reference [91]. Copyright 2011, American Chemical Society.*

Like other classes of gene therapy nanoparticles, hydrogels can be derived from natural and synthetic sources. Neutral synthetic polymers commonly utilized to generate hydrogels are PEG, poly(hydroxyethyl methacrylate) (PHEMA), and poly(vinyl alcohol) (PVA), with PEG being the most heavily investigated. Multi-arm PEG precursors with various reactive end chemistries are commercially available that can used to form cross-linked hydrogel networks that are resistant to protein adsorption and do not generate significant cytotoxicity or excessive immune response.[95] A strength of basic PEG hydrogels is that they block protein or cell adhesion and are largely nondegradable. Thus, PEG provides a "blank slate", enabling engineering of the hydrogels to possess carefully tuned properties such as degradation and cell adhesion. PEG hydrogel crosslinking is achieved using end functional groups such as silane, acrylate, thiols, and groups that participate in ionic and hydrogen bonding. Often, peptides are engineered into hydrogels, both to provide degradation mechanisms (e.g. MMP dependent) that mimic native ECM and to provide sites for cell adhesion (e.g. RGD peptide).[96-98] Like PEG, PHEMA is extremely stable in water and has robust mechanical properties. PHEMA is especially well-known for its application in contact lenses, but it is also an attractive material for drug delivery.[99] A variety of modifications have been employed to enhance the properties of PHEMA hydrogels (e.g., copolymerization with other monomers has been utilized to tune degradability, swelling, and mechanical properties). PVA hydrogels are generated by repeated freeze-thaw cycles or through covalent cross-linking. Physical cross-linking is also possible with PVA and is of particular utility in drug delivery as it is more amenable to achieving biodegradability.[100,101]

Biological hydrogels formed from naturally-derived polymers or biohybrids of both natural and synthetic materials are also a topic of heavy investigation. Commonly used natural polymers include collagen, hyaluronic acid (HA), fibrin, alginate, agarose, dextran, and chitosan.[102] These

natural polymers are derived from mammalian extracellular matrix (collagen), tissues (HA), or from marine algae sources (alginate and agarose), and they are advantageous for their low levels of cytotoxicity. Collagen provides an especially conducive cell-material interface because it is a natural matrix for cellular growth and inherently possesses a multitude of cell-signaling domains that is difficult to replicate using synthetic methods. However natural polymers like collagen also suffer from poor mechanical properties, and cross-linking strategies are commonly employed to improve its mechanical strength.[103] Alginate and chitosan are linear polysaccharides that can be cross-linked to form hydrogels. Alginate generates gels upon the formation of ionic bridges in the presence of divalent cations. It degrades slowly over time, and the mechanical integrity of the alginate hydrogels is concurrently lost. Natural polymers typically possess inherent degradation mechanisms, which is advantageous for most *in vivo* applications. For example, collagen is naturally degraded by collagenases and HA is degraded by cells through the release of enzymes like hyaluronidase.[93]

Biohybrid hydrogel systems attempt to synergize the advantages of synthetic and biologic materials by combining them into a single platform that enable one to retain synthetic control while also integrating biologic signals that enhance biocompatibility and overall performance. A common approach is the addition of degradable or biologically active peptides into the matrix of synthetic hydrogels.[104,105] Another approach is the addition of enzymes or genetically-engineered proteins into the mesh space of hydrogels.[106,107] Both approaches are used to enhance cell-adhesion and invasion into the interior of the gels as well as to provide the possibility for cell-mediated degradation. Growth factors can also be included in hydrogels by covalent attachments and regulate cellular function and migration within the gels.[108,109] Biologics such as peptides, chitosan, alginate, agarose, and dextran can also be copolymerized with synthetic monomers.[110-112]

Polypeptide approaches such as the elastin-like class of polypeptides are particularly popular and can be designed and synthesized using genetic engineering protocols.[113] Expense and synthetic complexity are potential limitations for polypeptide-based technologies, but recent advances are making their production more scalable and cost efficient.[114]

Microgels

Microscopic scale hydrogels, or microgels, are useful for applications in drug delivery and the controlled release of bioactive therapeutics. Mucoadhesive microgels for oral and non-oral drug delivery to areas such as the nasal and pulmonary cavities are under particularly heavy investigation.[115,116] Hydrophilic microgels composed of mucoadhesive polymers (e.g. hydroxypropylcellulose, chitosan, carbopol, carboxymethylcellulose, hyaluronic acid, polyacrylic acid) naturally adhere to mucus layers, a property which makes them a natural fit for these applications.[115] Recent research has also explored functionalizing the surface of microgels with anionic or thiolated moieties, or both. These targeting moieties could allow for better interpenetration into and adhesion within mucus layers.[117,118] These mucoadhesive microgels can be used to encapsulate a variety of therapeutics and serve as a drug depot for the sustained release of therapeutics. A few particularly exciting formulations have been developed for oral delivery of therapeutics.[119] For example, an oral polymer microgel drug delivery system was optimized with varying amounts of poly(acrylic acid) (PAA) and Pluronic®.[120] Nine Pluronic® copolymers were grafted to PAA with a range of molecular weights and varying poly(propylene oxide) (PPO) and PEG content, with or without cross-linking. The longest Pluronic® polymers with grafted PAA attachments resulted in the microgels with the strongest mucoadhesive properties. Another mucoadhesive microgel system incorporated cysteine-modified PAA polymers.[121] The thiol

moieties of cysteine were shown to form disulfide bonds and intermolecular cross-links with mucus material and increase the mucoadhesive properties 14-fold over unmodified microgels. Microgels show promise for mucoadhesive applications, and these recent studies suggest that microgels will make an impact on oral and pulmonary drug delivery.

The Lyon group has innovated functional microgel-based drug delivery systems. They initially published on the synthesis and characterization of environmentally responsive core-shell morphology microgels.[122] They tested two compositions: 1) PNIPAm-co-acrylic acid (AAc) core/PNIPAm shell and 2) PNIPAm core/PNIPAm-co-AAc shell. It was found that the location (core verses shell) of PNIPAm and AAc have an effect on the temperature (PNIPAm) and pH (AAc) dependent swelling. Importantly, it was found that there were only small differences in the effect on pH between the two core-shell particles, indicating that the spatial organization of temperature responsive PNIPAm dominates the behavior in this system. They also reported an application of PNIPAm-co-AAc microgels in which they loaded microgel thin films with Dox and thermally regulated its loading and release.[123] In this study, they used a spin coating, layer-by-layer (scLBL) approach to prepare thin films of anionic PNIPAm-co-AAc alternating with layers of cationic poly(allylamine hydrochloride) (PAH). They showed that doxorubicin could be loaded into 10, 20, and 30 layer thick microgel films and that release kinetics of doxorubicin from the films could be controlled using temperature. They were further able to tune the swelling kinetics of core-shell microgels by the incorporation of the hydrophobic monomer butyl methacrylate (BMA) into the shell.[124] This showed the ability to control the kinetics of microgel de-swelling simply by modifying the periphery of particles. Alternatively, the incorporation of hydrophilic PEG moieties into PNIPAm core-shell microgels was studied with the goal of reducing protein absorption into the gels.[125] Their results confirmed that protein absorption was reduced by the

incorporation of PEG chains, especially when PEG was located within the microgel shell. They further showed that once PNIPAm undergoes its phase transition from hydrophobic to hydrophilic, PEG grafts can interpenetrate or flip with the PNIPAm layer. They also showed early evidence for the ability to target microgel therapies using folate-conjugated PNIPAm microgels.[126] In sum, their studies on an array of PNIPAm-based, thermo-responsive microgels have provided the field with significant mechanistic insights into the synthesis, characterization, and functionality of microgel drug delivery platforms.

Peppas and Elbert have also deeply influenced the development of microgels as drug delivery systems. Peppas laid much of the groundwork for how we understand swelling and drug release from hydrogel networks.[127-129] More recently, his group has investigated the incorporation of biological molecules such as insulin into microgels/microparticles.[130] They have showed highly efficient encapsulation of insulin within poly(methacrylic acid-*g*-ethylene glycol) [P(MAA-*g*-EG)] microgels with preferential release in neutral/basic media over acidic media, with the goal of protecting insulin during passage through acidic environments within the body (i.e. stomach). They tested the encapsulation of other hydrophilic model drugs, namely theophylline, vancomycin, and fluorescently labeled dextrans. Insulin showed the highest loading efficiency into their P(MAA-g-EG) formulation. One could envision this technology as an oral carrier for insulin and also imagine the possibility of tailoring this formulation to increase encapsulation of other therapeutics for oral delivery. Elbert's group has developed many PEG-based materials for the coating of biomedical materials. In work with Hubbell, he developed approaches for coating biomaterials for increasing biocompatibility by reducing the absorption of serum proteins and cell adhesion.[131-135] Elbert's group more recently pioneered a microgel-based system aimed at reducing late-term thrombosis on drug-eluting stents.[136] In this approach, glass or poly(ethylene terephthalate) substrates were

dip-coated with PEG-octavinylsulfone(OVA)-BSA microgel conjugates. The difference in nucleophilicity of thiols verse primary amines was used to avoid macrogelation and then induce rapid covalent attachment of microgels to the glass surface under diluted conditions. The PEG-OVA-BSA coated surfaces reduced protein absorption. Cellular adhesion and migration were inhibited by the microgel formulation and promoted by a control, fibrinogen-capped coating. The authors proposed that this microgel-based coating could serve as a useful surface modification for blood-contacting devices through resistance of protein and cell adhesion.

Only very recently have microgels been developed with the capability of encapsulating gene therapies and nucleic acid based therapeutics. Moreover, the delivery of nucleic acids from hydrogels is strongly biased to nanogel formulations over microgels. To our knowledge, two approaches have been taken in delivering nucleic acids from microgels: direct incorporation and incorporation of nucleic acid containing nanoparticles into microgels.

De Smedt et al. introduced a microgel system by which they could induce the time-controlled release of siRNA.[137] They started by testing two microgel preparation techniques. They found that it was ideal to load siRNA into neutral dextran microgels prior to cross-linking and gel formation, while the copolymerization of cationic DMAEMA monomers allowed for post-gelation siRNA loading. Time-controlled siRNA release was achieved from the microgels by varying the density of cross-linking incorporated during gelation. Microgels with higher orders of cross-linking led to much slower release profiles. The authors argue that this is particularly desirable for siRNA delivery because of the transient nature of its activity. Therefore, the functional impact of gene knockdown should be increased if siRNA delivery can be sustained over time periods that span its transient activity profile. The authors also allude to the major setback of attempting siRNA delivery from a microgel platform; many microgels are too large for cellular internalization. To

address this shortcoming, they filtered out larger microgels to obtain a mean population size between 2 and 3 μm before applying them as cell treatments. Queiroz et al. co-loaded a similar system with pDNA against a gene for p53 and the anti-cancer drug Doxorubicin.[138] They showed effective encapsulation of both and observed modest sustained release for up to 5 days. They propose application of this delivery system for local chemotherapy/gene delivery approaches where the therapeutics would diffuse from the microgels and into the local tumor microenvironment.

The second microgel-based gene therapy approach has involved loading of nucleic acid loaded-nanoparticles into the microgels. This stategy has been attempted recently by both Peppas and Roy. The Peppas group loaded cationic nanoparticles into anionic poly(methacrylic acid-*co*-*N*-vinylpyrrolidone) (P(MAA-co-NVP)) microgels and performed chemical characterization of the system.[139] They demonstrated that swelling of the system was dependent upon both pH and the cross-linking density of the microgels. Although they used a protein and small molecule as models for loading and release studies, one could easily envision using the cationic nanoparticles to condense siRNA and incorporating siRNA loaded cationic nanoparticles into anionic microgels. Roy et al. developed a similar but more functional system for pulmonary delivery of biologic drugs.[140] Their system incorporates an enzymatically degraded peptide sequence into the backbone of the microgel as a cross-linker. After cross-linking, the microgel is also loaded with either nanoparticles, biologic drugs, or biologic drugs within nanoparticles. The "nano-inside-micro" formulation exhibited desirable properties for pulmonary delivery: it was mucoadhesive, enzymatically degraded, protected from clearance by alveolar macrophages, and induced better penetration into/through pulmonary mucus membrane verses a microgel alone. The authors argue that the formulation can be versatile and tailored to the delivery of DNA, siRNA, and proteins.

Moreover, they argue that the system is able to encapsulate biologic-loaded nanoparticles in the range of 20-200 nm. The "nano-inside-micro" approach is certainly a step towards overcoming the physical size limitation of delivering nucleic acids from a microgel platform. It should be noted that similar systems have also been developed as scaffolds and also porous silicon microparticles, where drug-loaded nanoparticles are incorporated into polymer or other "bulk" scaffolds for applications in controlled/sustained release and tissue engineering.[141-147]

Nanogels

Nanogels have been significantly more developed for gene therapies relative to their microscale counterparts. Size is the major distinction between the two classes of hydrogels and is the motivating factor for choosing nanogels as gene delivery vectors over microgels. Nanogels, or hydrogel nanoparticles, are typically in a similar size range to the other classes of nanoparticles discussed up to this point (20 – 200 nm). Systemic delivery by intravenous injection of therapeutics into the blood circulation is the preferable gene delivery strategy for many potential applications (e.g., dispersed cancers). Therefore, the size range of nanogels is preferable over the size of microgels for most gene delivery applications as microgels risk getting lodged within and blocking the capillaries of the systemic circulation. Moreover, the polydispersity of microgel samples is typically larger than that of nanogels. The ability to better control the polydispersity in nanogels is highly desirable, ensuring more consistency and reduced toxicity of treatments *in vivo*.

While microgels are typically polymerized by emulsion or precipitation polymerizations (although controlled polymerizations are becoming more popular), nanogels are typically prepared by controlled polymerizations and cross-linking reactions.[148] The controlled polymerization techniques such as RAFT, ATRP, and ROMP are needed to achieve better control over size

distribution in nanogels. This, in turn, leads to the production of consistent gene vectors that can encapsulate nucleic acids efficiently and provide some tuning of their release kinetics based on swelling, biodegradability, diffusion, or environmental responsiveness.

Vinogradov et al. initially reported nanogel formulations for delivering oligodeoxynucleotides (ODNs).[148-151] Their formulation consisted of a cross-linkable copolymer of PEG-*b*-PEI prepared via an emulsification/solvent evaporation technique. Gel permeation chromatography (GPC) was used to fractionate the resulting nanogels and separate the smallest size range for use in the studies (~120 nm). The ODN-loaded nanogels were condensed to a smaller size (~80 nm) and had a decreased zeta potential. These nanogels facilitated better accumulation of ODNs in multidrug resistant (MDR) carcinoma cells compared to ODNs free in solution. Moreover, ODNs encapsulated in the nanogels demonstrated increased inhibition of P-glycoprotein efflux pumps in MDR cell lines when compared with free ODNs. This approach was adapted for a follow up study aimed at delivering ODNs to the brain. The previously reported nanogel delivery system was tested for its ability to transport across the blood-brain barrier (BBB) using polarized monolayers of bovine brain microvessel endothelial cells as an *in vitro* model. They demonstrated that nanogel-ODN formulations facilitated increased transport across the BBB and that surface modification of the nanogels with transferrin and insulin further increased the transport efficiency. The accumulation of ODN in the brain was increased 15-fold one hour after intravenous injections and decreased 2-fold in the liver and spleen. Delivery of nucleoside analog 5'triphosphates was also attempted in the same nanogel system. 5-fluoroadenosine arabinoside (FATP) was electrostatically complexed into the nanogels and delivered *in vitro*. The nanogels protected 90% of encapsulated FATP from nuclease degradation and folate-targeted nanogels resulted in a 10-fold increase in transfection of human breast carcinoma MCF-7 cells.

Several other research groups have followed up Vinogradov's initial findings and have effectively developed nanogel formulations for siRNA and pDNA delivery. One of these applications utilized co-delivery of pH-responsive nanogels with PIC micelles loaded with pDNA.[152] Co-delivery of the nanogels and PIC micelles led to increased transfection efficiency compared to delivery by PIC micelles alone, suggesting the importance of the pH-responsive nanogels in this strategy. With this approach, it was assumed that the pH-responsive nanogels are co-localized with PIC micelles within endolysosomal vesicles and that the nanogels introduce the proton sponge buffering capacity needed to promote PIC micelle endolysosomal escape and trafficking to the nucleus.

The most common nanogel gene therapy strategy has been synthesis of surface PEGylated nanogel carriers with cross-linked, cationic cores amenable to nucleic acid loading. For example, nanogels consisting of a cross-linked PDEAMA core and PEGylated surface were investigated for their ability to deliver siRNA and compared with delivery from a PEG-*b*-PDEAMA PIC micelle analog.[153] The nanogel/siRNA complexes showed enhanced salt and serum stability compared with their PIC micelle analogs. Importantly, the nanogel/siRNA complexes greatly enhanced gene silencing over the PIC micelles and demonstrated a more pronounced tendency for endosomal escape as observed by confocal microscopy. This system was further studied with the addition of quaternary ammonium groups for enhanced siRNA binding and nanogel stability, and the effect of tertiary verse quaternary amine groups in the core was analyzed.[154] The introduction of quaternary ammonium groups was shown to improve siRNA binding at lower N/P ratios as well as increase nanogel stability against polyanion displacement reagents. However, the zeta-potential of these nanogels was over +20 mV, potentially limiting the use of this strategy *in vivo*, especially for intravenous delivery applications. Interestingly, it was found that quaternization increased

uptake of nanogel/siRNA complexes but showed no effect on the uptake of the unloaded nanogels. The buffering capacity of the nanogels was reduced with increasing quaternization, and it was concluded that the ratio of quaternary ammonium groups to tertiary amine groups should be optimized in this kind of system since they have competing effects on cellular uptake and proton sponge-based endosomal escape. Another effective nanogel gene delivery system was made by conjugating branched PEI onto preformed gelatin nanoparticles.[155] The nanogels showed less toxicity than PEI alone and significantly higher gene silencing than LF2K *in vitro*. The nanogels also effectively escaped the endolysosomal pathway, and increasing the N/P ratio from 10 to 30 in the formulation doubled the intracellular uptake. Again, the zeta-potential of these nanogels, up to +40 mV, causes concerns for *in vivo* delivery applications. In sum, these initial preclinical studies on nanogel/nucleic acid formulations show great promise but need further development to become translatable into *in vivo* models and the clinic.

A series of nanogels has also been synthesized from natural polymeric sources. The gelatin-PEI hybrid system described above represents one example. Hyaluronic acid (HA) nanogels were also synthesized in the size range of 200 to 500 nm and used to encapsulate siRNA by an inverse water-in-oil emulsion.[156] The siRNA was physically entrapped within the nanogels after cross-linking by this method. The HA/siRNA complexes effectively targeted HA receptor positive cells (HCT-116 cells). The nanogels showed selective uptake by HCT-116 cells via receptor mediated endocytosis, but addition of glutathione was necessary to reduce the nanogel cross-links and induce siRNA release. De Smedt et al. also investigated a nanogel analog to their previously described dextran-based microgels.[157] Dextran-based nanogels with [2-(methacryloyloxy)-ethyl]trimethylammonium chloride (TMAEMA) and 2-aminoethyl methacrylate (AEMA) cationic cross-linkers were used to electrostatically condense siRNA. The nanogels were then co-delivered

alongside amphiphilic photosensitizers (photochemical internalization (PCI)) in order to destabilize endosomal vesicles and prolong the effects of gene silencing. The De Smedt group followed up this study by investigating a PEGylated model of the dextran-nanogel, concluding that the non-PEGylated system was effective *in vitro* but would be too cationic for effective *in vivo* delivery.[158] The PEGylation technique was used, as has been discussed with many carriers, to improve circulation and minimize aggregation with serum proteins after intravenous injections. Multiple methods of PEGylation were tested, with the authors concluding that covalent attachment of PEG to the nanogels was the most effective fabrication technique. Importantly, PEGylated nanogels were also internalized by the cell types used in this study, and gene silencing was achieved. Therefore, the modification of cationic dextran nanogels with PEG was an effective method for increasing the translatability of the system without removing its functionality. Biodegradable, carbohydrate-based nanogels are another promising platform from natural sources. The chemistry of a carbohydrate-based nanogel system was recently optimized and tested for its efficacy for pDNA delivery to hepatocytes *in vitro*.[159,160] An optimized design was ultimately identified with transfection efficiency comparable to branched PEI model systems, and the addition of small amounts PEI into the carbohydrate-based nanogels further increased delivery of pDNA to hepatocytes. The biodegradability of this system was an advantage to many other nanogels and was shown to promote controlled release of pDNA.

Multi-functional nanogels designed to overcome multiple *in vivo* delivery barriers have shown particular promise during preclinical investigations. Lyon's peptide-functionalized nanogels serve as a good example.[161] They developed PNIPAm-based core/shell nanogels made through seeded precipitation polymerization. The nanogels were then surface-functionalized with a peptide for targeting the EphA2 receptor of ovarian carcinoma cell types. The nanogels protected

siRNA and achieved targeted gene knockdown of the EGF receptor. A chemosensitization analysis was conducted in a follow up study by co-delivering docetaxel with the siRNA-loaded, targeted nanogels.[162] EphA2 positive Hey cells showed decreased EGFR levels and cell viability after co-delivery of the nanogels with docetaxel while EphA2 negative SK-OV-3 cells were not chemosensitized by the nanogels. This study suggests that targeted co-delivery of siRNA is a promising strategy for increasing the efficacy of established chemotherapies. DeSimone et al. developed a multifunctional, reductively-responsive nanogel for siRNA delivery (**Figure 1.7**).[163]

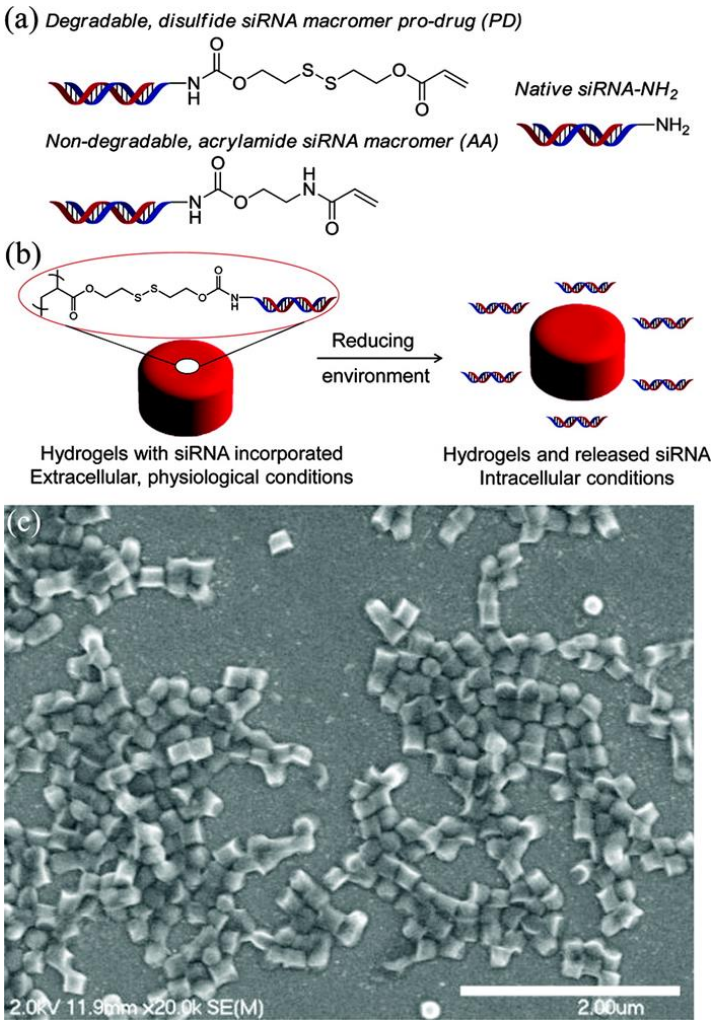

Figure 1.7) Reductively-responsive Nanogels for siRNA delivery. (A) siRNA macromer pro-drugs used for nanogel synthesis. (B) Schematic of the hydrogels and their response to reducing environments. (C) SEM of the reductively-responsive nanogel architecture. *Adapted with permission from reference [161]. Copyright 2012, American Chemical Society.*

Initially, siRNA was incorporated into the nanogels by electrostatic condensation, but siRNA loading and function was increased by polymerizing a siRNA prodrug with reducible, disulfide linkages directly into the PEGylated nanogels. The nanogels released the siRNA cargo under reducing conditions (indicative of the cytosol) while remaining stable in other physiological

environments. Moreover, the amine content of the nanogels was optimized in order to achieve gene silencing while maintaining cytocompatibility.

Roy et al. directly investigated the function of nanogel shape on cellular internalization.[164] Based on the knowledge that nanorods are internalized at a higher rate than spherical nanoparticles, Roy's group extended this field by then comparing the internalization of nanorods versus nanodiscs. They found that mammalian epithelial and immune cells preferentially internalize nanodiscs over nanorods. They also showed that larger sized nanorods and nanodiscs were internalized more than smaller sized rods and discs, although the opposite has been seen with nanospheres. They concluded that nanoparticle internalization should be thought of as a manifestation of the following shape- and size-dependent parameters: particle surface-to-cell membrane contact area, strain energy for membrane deformation, and local particle concentration at the cell membrane. These results suggest the need for more optimal carriers that leverage all, or as many as possible, of the above functionalities in concert.

Outlook

Two to three decades of research into gene therapy has revealed both the great potential and technical challenges of implementing successful therapies. Initial successes such as the first clinical trial for viral-based gene therapy against adenosine deaminase severe combined immunodeficiency (ADA-SCID) affirm the great clinical potential of gene therapies and motivate further investigation.[165-167] However, several studies in gene therapy have been halted, and the clinical trials have been canceled due to safety concerns and lack of efficacy.[168-170] These setbacks provide motivation for continued development of new, multifunctional nanocarriers that meet both safety and efficacy thresholds. Advances in our ability to synthesize nanocarriers using 21st century

rational design principles are affording rapid advances towards this goal. For example, liposomal formulations of DNA vaccines have shown increased uptake of pDNA by cells and increased immunogenicity of the vaccines in clinical trials.[171,172] Over half of the clinical trials for RNA interference by siRNA currently employ formulations of liposomes or polymeric conjugates (**Table 1.1**).[173] We refer readers to the recent review on worldwide clinical trials up to year 2012 for more detailed information on over 1800 gene therapy clinical trials that have been attempted to date.[174]

The recent advances in polymeric nanoparticles have begun yielding multi-functional, virus-mimetic vectors that offer increasingly effective spatiotemporal control over biodistribution, controlled release, and intracellular delivery *in vivo*. Current formulations require tuning to achieve application-dependent optimization. For example, formulations for systemic delivery (i.e. intravenous injection) should maximize circulation time and accumulation at the site of interest while minimizing opsonization by the RES and off-target or nonspecific cellular uptake. By contrast, local delivery formulations should aim for rapid cell recognition and uptake while minimizing diffusion from the site of interest. In all cases, strategies for increasing the therapeutic index of the genetic agents are crucial for developing more efficacious systems with fewer side effects.

It is important to note that rapid progress in the understanding of both cellular and molecular biology has led to the ability to create rationally designed delivery vehicles based on the new knowledge of the cellular and molecular environments. It is expected that this progress will only grow in scope and continue to accelerate discovery by enabling more effective design of gene vectors. For example, nanoparticle diffusion through tissue and cellular internalization is still

Drug	Target	Delivery system	Disease	Phase	Status	Company	ClinicalTrials.gov identifier
DPC, dynamic polyconjugate; LNP, lipid nanoparticle; NP, nanoparticle; shRNA, short hairpin RNA.							
ALN–VSP02	KSP and VEGF	LNP	Solid tumours	I	Completed	Alnylam Pharmaceuticals	NCT01158079
siRNA–EphA2–DOPC	EphA2	LNP	Advanced cancers	I	Recruiting	MD Anderson Cancer Center	NCT01591356
Atu027	PKN3	LNP	Solid tumours	I	Completed	Silence Therapeutics	NCT00938574
TKM–080301	PLK1	LNP	Cancer	I	Recruiting	Tekmira Pharmaceutical	NCT01262235
TKM–100201	VP24, VP35, Zaire Ebola L-polymerase	LNP	Ebola-virus infection	I	Recruiting	Tekmira Pharmaceutical	NCT01518881
ALN–RSV01	RSV nucleocapsid	Naked siRNA	Respiratory syncytial virus infections	II	Completed	Alnylam Pharmaceuticals	NCT00658086
PRO-040201	ApoB	LNP	Hypercholesterolaemia	I	Terminated	Tekmira Pharmaceutical	NCT00927459
ALN–PCS02	PCSK9	LNP	Hypercholesterolaemia	I	Completed	Alnylam Pharmaceuticals	NCT01437059
ALN–TTR02	TTR	LNP	Transthyretin-mediated amyloidosis	II	Recruiting	Alnylam Pharmaceuticals	NCT01617967
CALAA-01	RRM2	Cyclodextrin NP	Solid tumours	I	Active	Calando Pharmaceuticals	NCT00689065
TD101	K6a (N171K mutation)	Naked siRNA	Pachyonychia congenita	I	Completed	Pachyonychia Congenita Project	NCT00716014

AGN211745	VEGFR1	Naked siRNA	Age-related macular degeneration, choroidal neovascularization	II	Terminated	Allergan	NCT00395057
QPI-1007	CASP2	Naked siRNA	Optic atrophy, non-arteritic anterior ischaemic optic neuropathy	I	Completed	Quark Pharmaceuticals	NCT01064505
I5NP	p53	Naked siRNA	Kidney injury, acute renal failure	I	Completed	Quark Pharmaceuticals	NCT00554359
			Delayed graft function, complications of kidney transplant	I, II	Recruiting	Quark Pharmaceuticals	NCT00802347
PF-655 (PF-04523655)	RTP801 (Proprietary target)	Naked siRNA	Choroidal neovascularization, diabetic retinopathy, diabetic macular oedema	II	Active	Quark Pharmaceuticals	NCT01445899
siG12D LODER	KRAS	LODER polymer	Pancreatic cancer	II	Recruiting	Silenseed	NCT01676259
Bevasiranib	VEGF	Naked siRNA	Diabetic macular oedema, macular degeneration	II	Completed	Opko Health	NCT00306904
SYL1001	TRPV1	Naked siRNA	Ocular pain, dry-eye syndrome	I, II	Recruiting	Sylentis	NCT01776658
SYL040012	ADRB2	Naked siRNA	Ocular hypertension, open-angle glaucoma	II	Recruiting	Sylentis	NCT01739244
CEQ508	CTNNB1	*Escherichia coli*-carrying shRNA	Familial adenomatous polyposis	I, II	Recruiting	Marina Biotech	Unknown

RXi-109	CTGF	Self-delivering RNAi compound	Cicatrix scar prevention	I	Recruiting	RXi Pharmaceuticals	NCT01780077
ALN–TTRsc	TTR	siRNA–GalNAc conjugate	Transthyretin-mediated amyloidosis	I	Recruiting	Alnylam Pharmaceuticals	NCT01814839
ARC-520	Conserved regions of HBV	DPC	HBV	I	Recruiting	Arrowhead Research	NCT01872065

Table 1.1) RNAi-based drugs in clinical trials. *Adapted with permission from reference [173]. Copyright 2013, Nature.*

poorly understood. Elucidation of the mechanisms involved in cellular internalization and endosomal escape of nanoparticles is also critical. It is not fully understood how particle size, sterics, targeting, cargo chemistry, and shape influence internalization and subsequent intracellular trafficking, nor which properties are most important. Moreover, it is not yet understood which properties are most important for different cell and tissue types. Better elucidation of these structure-function properties will provide engineers with the ability to design more rational systems with universally better characteristics as well as application-specific advantages. The recent advances in top-down synthesis approaches suggest that we will ultimately be able to manipulate understood pathways in order to influence uptake in only desired cell types through specified internalization routes.

This chapter overviews a multitude of nanocarriers with significant promise for overcoming the delivery barriers that have crippled the advancement of gene therapies into the clinic. The benefits of nucleic acid protection, increased circulation, active and passive targeting, evasion of immune system, cellular internalization, and endolysosomal escape, all hallmarks of

virus functionality, have been demonstrated in preclinical models and are being realized in ongoing clinical trials. Further investigation is needed in order to fully understand the relative importance of each of these design considerations and to develop multi-functional nanocarriers that address these delivery concerns as comprehensively as possible. Through the advancement of nanoparticle fabrication techniques, further understanding of physiological mechanisms, and investigation of biomaterial-biological system interactions, methods of gene delivery will continue to advance toward safe and efficacious clinical gene therapies.

Clinical Significance

Breast cancer is the leading malignancy and second-deadliest form of cancer among western women. Approximately 20% of breast cancers overexpress human epithelial growth factor receptor 2 (HER2), which activates the phosphatidyl inositol-3-kinase (PI3K)/Akt/mammalian target of rapamycin (mTOR) signaling cascade and drives tumor cell growth, survival, metabolism, and motility[175]. Breast cancers with *HER2*-amplification are among the most aggressive, exhibiting marked increases in local and regional recurrence and metastases after breast-conserving surgery (BCS) or mastectomy[176,177]. Targeting HER2 therapeutically using Trastuzumab[178,179], Pertuzumab[180,181], and/or receptor tyrosine kinase (RTK) inhibitors (e.g., lapatinib[182-184], neratinib[185]) inhibits PI3K/Akt/mTOR signaling and decreases growth and survival of HER2-positive (HER2+) breast cancers. These treatment strategies have significantly improved clinical treatment options and improved outcomes for patients with HER2+ breast cancers. However, a significant portion of patients still relapse and die from their malignancy.

Both inherent and acquired resistance to HER2 inhibitors is common and typically associated with incomplete inhibition of PI3K and Akt activity[186]. RTK-addicted HER2+ BCs

respond well to HER2-targeted therapies where inhibition of the RTK leads to a down-regulation of PI3K/Akt/mTOR signaling[187]. Inherently resistant BCs are thought to feed their PI3K/Akt/mTOR addiction through alternative signaling aberrations such as *PIK3CA* mutations[188,189], loss of *PTEN*[188,190,191], and the *AKT1*-E17K mutation[192], which result in constitutive activation of the pathway independent of HER2. Acquired resistance mechanisms such as increased HER1[193] or HER3[194-196] expression, IGF-1R expression[197], and *MET* amplification[198], also lead to a resurgence in PI3K/Akt/mTOR signaling after treatment with trastuzumab or lapatinib. Thus, new treatment strategies which can more universally target PI3K/Akt/mTOR signaling and more potently inhibit Akt activity downstream of HER2 are desirable.

RNAi was initially observed by Mello and Fire et al. in 1998[40], and soon thereafter exogenously-delivered short double-stranded nucleic acid molecules were confirmed to be capable of potent and highly specific gene inhibition in mammalian cells[199,200]. Since its discovery, small interfering RNA (siRNA) has emerged as a powerful research tool and potentially transformative clinical therapeutic. Due to its mode of action at the mRNA level, siRNA is a promising class of therapeutics for inhibiting targets considered to be hard-to-drug by conventional pharmacological approaches, such as intracellular enzymes, transcription factors, and protein–protein interactions[201,202]. Currently, cellular and systemic delivery barriers limit the therapeutic applications of siRNA[203]. Naked siRNAs do not readily enter cells, have no inherent mechanism for endosome escape, and are rapidly cleared through filtration in the kidneys after systemic administration[173,204,205]. Thus, the use of siRNA as a safe and efficacious therapeutic is contingent upon its effective delivery to the desired tissue, cell type, and sub-cellular compartment of interest.

Packaging of siRNA by cationic lipids or polymers into electrostatically-driven formulations is one of the most investigated strategies for overcoming the challenges of siRNA delivery[173,206]. By this approach, siRNA is packaged into nanocarriers with a large excess of cationic charge which serves to drive cellular uptake through interaction with the anionic cellular membrane[207]. This approach has been particularly successful for hepatic siRNA targets as many of the formulations display preferential hepatic distribution, which is advantageous for the clinical development of RNAi drugs which target hepatocytes.

For delivery to non-hepatic targets, especially solid tumors, a broader set of pharmacokinetic and nanocarrier design parameters are important. Although the magnitude of the enhanced permeability and retention (EPR) effect in spontaneously-formed tumors in humans and large animals is known to be variable, it is accepted that for many tumor types, there is a significant correlation between nanocarrier tumor accumulation and blood circulation persistence (related to avoidance of clearance through organs such as liver and kidney)[208-211]. Likewise, it has been observed that the magnitude of passive tumor uptake of siRNA nanopolyplexes si-NPs is directly related to circulation time[212,213]. Commonly, lipoplex or polyplex nano-formulations designed for intravenous administration are PEGylated to impart colloidal stability and to reduce opsonization and clearance by the mononuclear phagocyte system (MPS)[214-217]. However, siRNA delivered by PEGylated polyplexes stabilized solely through electrostatic interactions with polyplex core-forming cationic polymers is susceptible to rapid clearance through the kidney due to polyplex disassembly triggered by the competing interactions between the cationic polymer and the polyanionic heparan sulfates of the glomerular basement membrane (GBM)[218,219]. As a result, electrostatically-stabilized or polyion complex nanoparticle formulations impart only minor differences in pharmacokinetics (i.e., blood persistence half-life) relative to free siRNA ($t_{1/2}$ siRNA

~1 – 2 min, $t_{1/2}$ siRNA nanoparticles ~3 – 5 min)[216,218,220-222]. Thus, a crux in the application of anti-tumor RNAi therapies is the ability to design delivery systems which increased circulation time, divert siRNA from clearance organs (liver, spleen, and kidneys), and increase distribution to tumors.

Innovation

The serine-threonine kinase, mTOR, exists in two structurally and functionally distinct complexes, mTORC1 and mTORC2. The mTORC1 complex requires co-factor Raptor for function and is activated downstream of PI3K/Akt, while mTORC2 requires the co-factor Rictor for function and directly phosphorylates Akt at S473[223,224]. The structurally distinct nature of the two complexes and their independent physiologic roles suggest that they could also serve non-overlapping roles in the pathophysiology of PI3K/Akt/mTOR signaling. Emerging pre-clinical evidence increasingly supports this concept. Analysis of breast cancer expression arrays from clinical samples curated by The Cancer Genome Atlas (TCGA) revealed an inverse correlation between *RICTOR* gene amplification and disease-free survival in patients with invasive breast cancer. Moreover, Immunohistochemistry (IHC) of clinical BC tissue microarrays showed Rictor levels were higher in invasive breast carcinomas compared to normal breast and ductal carcinoma *in situ* specimens[225]. The mTOR kinase inhibitors which block both mTORC1 and mTORC2 activity show increased efficacy over rapalogues which only inhibit mTORC1 activity[226]. A direct link between mTORC2 and PI3K-driven cancer progression have been made in prostate[227] and glioblastoma[228] models, and preliminary studies have shown that genetic mTORC2 inhibition reduced tumor cell motility and survival *in vitro* in breast cancer cell lines[229]. Importantly, genetic Rictor ablation has revealed that Rictor/mTORC2 (but not Raptor/mTORC1) is required during

postnatal/pubertal mammary gland development for ductal lengthening, secondary branching, mammary epithelial cell (MEC) motility and MEC survival, while Raptor/mTORC1 (but not mTORC2) is necessary for MEC proliferation[230]. Moreover, results from genetically engineered mouse models (Rictor ablation) of HER2+ breast cancer recently elucidated that Rictor/mTORC2 drives tumor cell survival through Akt activation *in vivo* and, loss of Rictor delayed HER2-driven tumor formation[225]. Although these studies all underscore the likely therapeutic benefit of mTORC2-specific inhibition, existing small molecules can only inhibit mTORC1 (e.g. rapalogues) or both mTORC1 and mTORC2 together (e.g. mTOR kinase inhibitors). No current therapeutic approach exists which can preferentially inhibit mTORC2.

Akt is a critical signaling effector of HER2 in HER2+ BCs, promoting cell survival and motility. Overexpression of *Akt1*, *Akt2*, or *Akt3* mRNA and protein occurs more frequently in HER2-enriched breast tumors as compared to Luminal A/B, Basal-like, or Claudin-low breast tumors in TCGA-curated datasets[225]. Moreover, abundant pre-clinical evidence suggests that full Akt inhibition is needed for a therapeutic response in HER2+ BCs and resistance to therapy is associated with resurgence in Akt activity[175,186].

Many studies have focused on the role of mTORC1 in HER2+ BCs, likely due to its position as a downstream effector of HER2/PI3K and the availability of mTORC1-specific inhibitors. However, mTOR kinase inhibitors which inhibit mTORC1 and mTORC2 have been more efficacious than mTORC1-specific inhibitors, suggesting mTORC2 may be independently important for tumor cell survival[226]. Interestingly, it is well-known that Akt signaling stimulates tumor cell survival[231,232], mTORC2 directly phosphorylates Akt at S473[233], recent studies showed that Rictor/mTORC2 genetic ablation increased cell death *in vivo*, and restoration of Akt was sufficient to fully rescue tumor cell survival after Rictor/mTORC2 ablation[225]. Since mTORC1 is

important for homeostasis of many physiologic processes such as macromolecule synthesis, growth, and metabolism, systemic toxicity is a potential concern for pan-mTOR inhibition. For example, the dual mTORC1/2 kinase inhibitor, AZD8055, induced transaminitis in human trials, indicating liver toxicity and immunosuppression[234,235]. It is possible that specific inhibition of mTORC2, while sparing other arms of the PI3K/mTOR pathway, can have a more direct effect on Akt activity and reduce systemic toxicity. Finally, it is well known that inhibition of mTORC1 releases its negative feedback on PI3K (through IRS-1) and potentially exacerbates aberrant PI3K/Akt signaling. Although it is currently unclear how much selective inhibition of mTORC2 will affect the expression of mTORC1, mTORC2-specific inhibition may reduce Akt reactivation associated with mTORC1-based negative regulation of PI3K.

RNAi using siRNA can potently and specifically inhibit many currently "undruggable" targets, potentially offering new treatment options for hard-to-drug diseases[202]. Unfortunately, clinical translation of RNAi therapies is hamstrung by the formidable physiologic barriers which prevent intracellular siRNA bioavailability in target cells of interest (e.g. tumor cells)[203]. Cellular barriers such as lipid membrane translocation (i.e. cell uptake and endosomal escape) and systemic barriers such as poor stability, intravenous pharmacokinetics, and tissue penetration, in addition to preferential hepatic biodistribution are all detrimental to siRNA bioactivity. Effective nanocarriers for RNAi in oncology will seek to overcome these collective barriers and increase siRNA bioavailability within tumor cells. To this end, a multiparametric *in vitro* screening approach will be conducted on a small library of nanocarriers to identify a lead formulation for *in vivo* studies. The strategy aims develop a lead candidate which is optimized to overcome both cell level (uptake and endosomolysis) and systemic (size, stability, circulation time, and tumor uptake) delivery barriers. To pass our screening conditions, a candidate formulation must have appropriate size (~

100 nm) and surface charge (~ 0 mV), low polysidpersity (< 0.3), stability in salt solutions, low toxicity, high cell uptake, endosomolytic potential, and potent *in vitro* target gene silencing. Importantly, we focus on increasing the physicochemical stability of polyplexes through the incorporation of hydrophobicity based on our previous observations that balanced cationic and hydrophobic polyplexes perform better both *in vitro* and *in vivo*[16]. Lead candidates will be administered *in vivo* to affirm the multiparametric screening approach and identify new formulations with improved pharmacokinetics, tumor biodistribution, and siRNA bioactivity.

Specific Aims

PI3K/Akt/mTOR signaling is dysregulated in over 60% of clinical breast cancers across all three major clinical subtypes driving tumor cell growth, survival, metabolism, and invasion[236,237]. The distal effector of this pathway, mTOR, is found within two functionally distinct complexes, mTORC1 and mTORC2[223,238,239]. Recent work has implicated a distinct physiologic role for mTORC2 in PI3K hyperactivated breast cancers[225], where it drives tumor survival and motility, but no current small molecules exist which can preferentially inhibit mTORC2 activity, while sparing mTORC1. Thus, the overall goal of this project is to develop an *in vivo*-ready RNA interference (RNAi) technology to hinder PI3K/Akt/mTOR pathway signaling through the specific inhibition of mTORC2. To this end, ternary siRNA nanopolyplexes (si-NPs) will be optimized through a combinatorial approach and used as an enabling technology for potent RNAi of mTORC2 signaling through target gene silencing of the mTORC2-specific co-factor Rictor.

Specific Aim 1. Hydrophobic stabilization of siRNA nanopolyplexes through a combinatorial approach: overcoming cell-level and systemic delivery barriers. Motivated by recent work that suggests balancing cationic and hydrophobic character of siRNA polyplexes is

crucial for *in vivo* stability and bioactivity, a small library of si-NPs which incorporate hydrophobic character into the ternary polyplex core, corona, or both will be generated. This library will be screened through a multiparametric approach to identify lead si-NPs which are optimized to overcome both cell-level (uptake and endosomal escape) and systemic (size, opsonization, stability) delivery barriers. Lead si-NP candidates will be benchmarked against our previous "gold-standard" PDB si-NPs[16] for *in vivo* biodistribution, pharmacokinetics, and pharmacodynamics. Ternary and PDB si-NPs will be compared for bioactivity against the model gene luciferase in orthotopic MDA-MB-231 (engineered to constitutively express luciferase) xenografts.

Specific Aim 2. Stabilization of siRNA nanopolyplexes by matching hydrophobic interactions of a lipid-modified siRNA and polymeric carrier: overcoming systemic delivery barriers. Formation of stable siRNA polyplexes which persist for long time periods in the circulation remains a significant challenge. Due to the balance of cationic and hydrophobic character within the core of PDB polymer-based polyplexes, we propose that hydrophobization of siRNA through lipid-modification will increase siRNA packaging into polyplexes, increase polyplex stability in the circulation, and improve delivery to solid breast tumors. We will modify siRNA with a simple palmitic-acid lipid moiety, and measure polyplex loading through gel retardation assays. Polyplex stability will be measured physicochemically by observing changes in polyplex size and morphology in response to increasing salt concentrations. Stability will further be assessed using a FRET readout to track siRNA packaging in response to challenge with heparin and serum. Lastly, we will measure the pharmacokinetics, biodistribution to tumor tissue, and *in vivo* intratumoral bioactivity (measured by gene silencing of the model gene luciferase) of polyplexes containing hydrophobized siRNA in mice harboring orthotopic MDA-MB-231 xenografts.

Specific Aim 3. Selective inhibition of mTORC2, without inhibiting mTORC1, through RNA interference in models of HER2-amplified breast cancer. New si-NPs optimized for systemic delivery will be used as an enabling technology to inhibit Rictor through RNAi in a panel of HER2+ breast cancers (MDA-MB-361, BT-474, SKBR3). Rictor RNAi will be validated at the gene and protein level through PCR and western blot analysis, respectively. Further, we will independently ablate Rictor (mTORC2) and Raptor (mTORC1) through sequence-specific RNAi, monitoring their effects on each other's expression as well as expression of downstream effectors, mTOR complex assembly, and cell killing. In vivo studies performed in MDA-MB-361 xenografts will elucidate the therapeutic effect of Rictor RNAi. Tumor growth will be quantified and post-mortem tissue analysis will focus on quantifying Rictor and P-Akt expression as well as cell death (TUNEL immunofluorescence (IF)). Lastly, Rictor RNAi will be used as an adjuvant to lapatinib treatment in MDA-MB-361 xenografts to test for synergistic efficacy.

CHAPTER II

HYDROPHOBIC STABILIZATION OF SIRNA NANOPOLYPLEXES THROUGH A COMBINATORIAL APPROACH: OVERCOMING CELL-LEVEL AND SYSTEMIC DELIVERY BARRIERS.

Text for Chapter II taken from:

TA Werfel, MA Jackson, TE Kavanaugh, KC Kirkbride, M Miteva, TD Giorgio, CL Duvall. Combinatorial Optimization of PEG Architecture and Hydrophobic Content Improves siRNA Polyplex Stability, Pharmacokinetics, and Potency In Vivo. *In Review*.

Abstract

A rationally-designed library of ternary siRNA polyplexes was developed and screened for gene silencing efficacy *in vitro* and *in vivo* with the goal of overcoming both cell-level and systemic delivery barriers. [2-(dimethylamino)ethyl methacrylate] (DMAEMA) was homopolymerized or colpolymerized (50 mol% each) with butyl methacrylate (BMA) from a reversible addition – fragmentation chain transfer (RAFT) chain transfer agent (CTA), with and without pre-conjugation to polyethylene glycol (PEG). Both single block polymers were tested as core-forming units, and both PEGylated, diblock polymers were screened as corona-forming units. Ternary siRNA polyplexes were assembled with varied amounts and ratios of core-forming polymers to PEGylated corona-forming polymers. The impact of polymer composition/ratio, hydrophobe (BMA) placement, and surface PEGylation density was correlated to important outcomes such as polyplex size, stability, pH-dependent membrane disruptive activity, biocompatibility, and gene silencing efficiency. The lead formulation, DB4-PDB12, was optimally PEGylated not only to ensure colloidal stability (no change in size by DLS between 0 and 24 hr)

and neutral surface charge (0.139 mV) but also to maintain higher cell uptake (>90% positive cells) than the most densely PEGylated particles. The DB4-PDB12 polyplexes also incorporated BMA in both the polyplex core- and corona-forming polymers, resulting in robust endosomolysis and *in vitro* siRNA silencing (~85% protein level knockdown) of the model gene luciferase across multiple cell types. Further, the DB4-PDB12 polyplexes exhibited greater stability, increased blood circulation time, reduced renal clearance, increased tumor biodistribution, and greater silencing of luciferase compared to our previously-optimized, binary parent formulation following intravenous (*i.v.*) delivery. This polyplex library approach enabled concomitant optimization of the composition and ratio of core- and corona-forming polymers (indirectly tuning PEGylation density) and identification of a ternary nanomedicine optimized to overcome important siRNA delivery barriers *in vitro* and *in vivo*.

Introduction

RNA interference (RNAi) was initially observed by Mello and Fire et al. almost twenty years ago[40], yet cellular and systemic delivery barriers have continued to limit the clinical application of siRNA.[203] Naked siRNAs do not readily enter cells, have no inherent mechanism for endosome escape, and are rapidly cleared through filtration in the kidneys after systemic administration.[204,205] Thus, the use of siRNA as a safe and efficacious therapeutic is contingent upon its effective delivery to the desired tissue, cell type, and sub-cellular compartment of interest. To date, a variety of methodologies have been developed to overcome the challenge of siRNA delivery, including covalent modifications[201,240], antibody-protamine fusion[241], liposomal encapsulation[242], and nanoparticle formulations of cationic lipids or polymers.[243-245]

Packaging of siRNA into cationic polymer- or lipid-based nanoparticles is one of the most investigated approaches.[173,206] By this approach, siRNA is packaged onto nanocarriers with an excess of cationic charge which serves to drive cellular uptake through interaction with the anionic cellular membrane.[207] Moreover, surface PEGylation has been widely employed as a strategy to neutralize siRNA nanocarriers to reduce opsonization and increase stealth from the mononuclear phagocyte system (MPS) following systemic administration.[214-216] However, polyplexes formulated from diblock polymers comprising PEG and a purely cationic polymer block suffer from a lack of stability *in vivo*.[245-248] This class of polyplexes, formed solely through electrostatic interactions, is disassembled at the glomerular basement membrane (GBM) and cleared primarily through the kidneys, resulting in modest increases of circulation time over naked siRNA.[218,219] In previous work, we endeavored to improve the performance of cationic polyplexes through incorporation of hydrophobicity into the core of the polyplex to create siRNA nanocarriers stabilized by a combination of both electrostatic and hydrophobic interactions.[16,249] This approach produced polyplexes with improved stability against destabilization by polyanions such as the herapan sulfates found in the GBM, longer *in vivo* circulation times, enhanced intracellular delivery of siRNA due to pH-dependent membrane disruptive function tuned to the endolysosomal environment, and improved *in vivo* bioactivity in the liver, kidneys, and spleen.

Efforts to develop effective siRNA transfection reagents through combinatorial approaches have yielded potent reagents that rival viral constructs. For example, the laboratories of Green, Langer, Anderson, *et al.* have developed large libraries of poly(β-amino esters) (PBAEs) and lipid or lipid-like chemistries through combinatorial methods with great success. Green *et al.* initially developed a library of cationic PBAEs in which the lead reagents were able to achieve pDNA transfection comparable to adenoviruses[24] and have more recently developed libraries which

yielded PBAE derivatives highly effective at delivering siRNA and pDNA to glioblastomas.[250,251] Anderson, Langer, and others have used combinatorial synthesis methods to develop large libraries of cationic lipid and lipid-like nanoparticles, reporting the most potent *in vivo* siRNA knockdown in multiple animal models to date.[243,252-255] Recently, Siegwart and coworkers utilized combinatorial synthesis to build new chemical classes of biodegradable dendrimer and polymer constructs that were incorporated as the cationic component of lipid nanoparticles.[256,257] This combinatorial approach allowed for the rapid screening and narrowing of a large chemical space which produced lead compounds highly effective for both siRNA and miRNA delivery *in vivo*.

Library-based screens, such as those highlighted above, used high throughput synthesis methods to screen different compositions of cationic lipids[243,253,254,258,259] or polymers[24,250,255-257,260-262]. This approach has proven powerful in elucidation of siRNA carrier structure-function relationships, especially for endpoints focused on *in vitro* activity and/or *in vivo* liver gene silencing. In these studies, the authors did not utilize a PEGylation component[24,250,260,261] or used a simple amphiphile (*i.e.*, (mPEG2000-carbamoyl)-1,2-di-O-tetradecyl-sn-glyceride (PEG-DMG) lipid) to sterically stabilize the surface of the resultant nanoparticles[243,253,254,256-259,262]. Here, we sought to create a library for simultaneous investigation of the composition (cationic versus balanced hydrophobic/cationic) and the relative quantity of both core- and (PEG-containing) corona-forming polyplex components. Moreover, we chose to focus our analysis on polyplex characteristics that are important for overcoming systemic barriers (stability for long circulation and reduced renal clearance) in addition to cell-level barriers (uptake/endosomal escape) that drive *in vitro* activity; the outcome that most previous screens have focused on. This multiparametric approach[253] expands upon our previous findings showing the importance of hydrophobe incorporation into the core of PEG-stabilized cationic polyplexes[16,249] and provides a systematic

study of structure-function relationships of this class of new class of ternary, PEGylated siRNA polyplexes.

In this study, poly(2-(dimethylamino)ethyl methacrylate) (pDMAEMA, D), poly[(2-(dimethylamino)ethyl methacrylate)-*co*-(butyl methacrylate)] (p(DMAEMA-*co*-BMA), DB), poly[(ethylene glycol)-*b*-(2-(dimethylamino)ethyl methacrylate)] (PEG-*b*-p(DMAEMA), PD), and poly[(ethylene glycol)-*b*-[(butyl methacrylate)-*co*-(2-(dimethylamino)ethyl methacrylate)]] (PEG-*b*-p(BMA-*co*-DMAEMA), PDB) were synthesized via RAFT polymerization (**Supplementary Figure B.1**). Ternary siRNA polyplexes (si-NPs) were formed at varying N^+:P^- ratios (ratio of polymer amines:nucleic acid phosphates) and varying ratios of the core- (D/DB) to corona-forming polymers (PD/PDB) for three classes of formulations: DB core/PD corona [DB-PD], DB core/PDB corona [DB-PDB], and D core/PDB corona [D-PDB] to produce a library of precisely defined polyplexes with a range of physicochemical properties (**Figure 2.1**). This strategy affords surface charge neutral, siRNA core-loaded si-NPs stabilized by electrostatic and hydrophobic interactions with the ability to rapidly tune the polyplex core-corona composition and degree of surface PEGylation. Through this combinatorial ternary si-NP approach, we were able to systematically study important polyplex characteristics such as surface PEGylation density, size, stability, endosomolysis, biocompatibility, cell uptake, and target gene silencing.

Materials and Methods

All chemicals were purchased from Sigma-Aldrich (St. Louis, MO, USA) unless otherwise specified. DMAEMA and BMA monomers were passed twice through a basic alumina gravity column prior to use in order to remove inhibitors. 2,2-Azobis(2-methylpropionitrile) (AIBN) was recrystallized twice from methanol. All cell culture reagents were purchased through Fischer

Scientific unless otherwise specified. Cell culture media and reagents, including Dulbecco's modified eagle medium (DMEM), fetal bovine serum (FBS), PBS (-/-), PBS (+/+), Pen/Strep, and gentamycin were purchased through Life Technologies (Grand Island, NY, USA). For DLS experiments, dsDNA was used as a model for siRNA. DLS measurements confirmed that si-NPs formed with dsDNA and siRNA are the same size (**Supplementary Figure B.1**). For all fluorescent measurements, fluorophore-labeled dsDNA was used a model of siRNA. A list of oligonucleotides is provided in the supplement (**Supplementary Table B.1**).

4-cyano-4-(ethylsulfanylthiocarbonyl)sulfanylpentanoic acid (ECT), the RAFT CTA, was synthesized according to a previously reported procedure[10]. The terminal carboxylic acid of ECT was then conjugated to PEG[16]. Briefly, methoxy-PEG (2 mmol, 10 g, Mn = 5000 Da), ECT (4 mmol, 1.045 g), and Dimethylaminopyridine (DMAP, 0.08 mmol, 10 mg) were dissolved in dry DCM (50 mL), and dicyclohexylcarbodiimide (DCC, 4 mmol, 0.82 g) was added while stirring. The reaction mixture was stirred for 48 h at room temperature (RT). Precipitated cyclohexyl urea was removed by filtration (0.2 μM pore size). The DCM layer was concentrated and precipitated into diethyl ether twice. The precipitated PEG-ECT was washed thrice with diethyl ether and dried under vacuum. ^{1}H NMR (400 MHz Sprectrometer, Bruker, $CDCl_3$) showed 94% ECT conjugation to PEG[16].

RAFT controlled polymerization was used to synthesize four polymers, either from ECT or the PEG-ECT macro-CTA. P(DMAEMA-*co*-BMA) (DB) and pDMAEMA (D) were synthesized from ECT (**Supplementary Figure B.1**). In both cases, the target degree of polymerization was 150, reaction volume was 3 mL (Dioxane), degassing was done for 30 min by nitrogen purge, and polymerizations proceeded at 70°C for 20 h using AIBN as an initiator at 5:1 (CTA:AIBN) molar ratio. Reactions were stopped by removing the flask from heat and opening

the reaction to air. The reaction mixtures were transferred to dialysis tubing and dialyzed one day against methanol and subsequently one day against diH_2O to remove unreacted monomers prior to lyophilization. PEG-*b*-pDMAEMA (PD) and PEG-*b*-p(BMA-*co*-DMAEMA) (PDB) were synthesized from the PEG-ECT macro-CTA (**Supplementary Figure B.1**). The target degrees of polymerization were both 150. Reaction volumes were 3 mL (Dioxane), and degassing was done for 30 min by nitrogen purge. The polymerizations proceeded at 70 °C for 24 h, and AIBN was used as an initiator at 5:1 (macro-CTA:AIBN) molar ratio. Reactions were stopped by removing the flask from heat and opening the reaction to air. The resulting diblock copolymers were precipitated in a cold solution of pentane:diethyl ether (90:10). The isolated polymers were dried, re-dissolved in ethanol, dialyzed one day against diH_2O and lyophilized to yield the final product.

Polymers were characterized for composition and molecular weight (Mn) by ^{1}H NMR (400 MHz Sprectrometer, Brüker) in either D_2O (D) or $CDCl_3$ (DB, PD, and PDB). Absolute molecular weight and polydispersity (PI) were further determined by gel permeation chromatography (GPC) using DMF + 0.1 M LiBr as the mobile phase with inline Agilent refractive index and Wyatt miniDAWN TREOS light scattering detectors. Serial dilutions (10 mg/ml – 0.25 mg/ml) in DMF were measured on a digital refractometer to determine dn/dc values which were used for calculating absolute molecular weight on GPC.

Three combinations of polymers were utilized for forming ternary si-NPs: DB-PD, DB-PDB, and D-PDB. All polymers were dissolved in pH 4.0 citric acid buffer (10 mM). The dsDNA was pre-condensed with the binary, core-forming polymer at each specified N^+:P^- ratio for 15 min at 0.5 mg/ml polymer concentration. Next, differing amounts of ternary, corona-forming polymer (3.33 mg/mL, 10 mM citric acid buffer at pH 4.0) were added in order to give the appropriate final N^+:P^- ratio, and these solutions were incubated at room temperature for an additional 30 min.

Polymer amounts needed to yield final N^+:P^- ratios were determined according to the following two equations for binary (1) and ternary (2) si-NPs:

(2.1) $$nmol\ Pol = \frac{(nmol\ NA)(bp\ NA)(2)(N{:}P)}{(RU\ DMAEMA)(0.5)}$$

(2.2) $$nmol\ Pol_2 = \frac{(nmol\ NA)(bp\ NA)(2)(N{:}P) - (nmol\ Pol_1)(RU\ DMAEMA_1)(0.5)}{(RU\ DMAEMA_2)(0.5)}$$

where nmol Pol is the nmol of binary core-forming polymer, nmol NA is the nmol of nucleic acid, N:P is the ratio of amines to phosphates, RU DMAEMA is the number of repeating units of DMAEMA within the polymer backbone, nmol Pol_2 is the nmol of ternary corona-forming polymer, nmol Pol_1 is the nmol of binary core-forming polymer, RU $DMAEMA_1$ is the number of repeating units of DMAEMA within the binary core-forming polymer backbone, and RU $DMAEMA_2$ is the number of repeating units of DMAEMA within the ternary corona-forming polymer.

After formulation of both the core- and corona-forming polymers with the siRNA at pH 4, a 5-fold excess of pH 8.0 phosphate buffer (10 mM) was added to the samples before filtering through 0.45 μm pore syringe filters. The hydrodynamic diameter (D_h) and zeta potential (ζ) of the resulting ternary si-NPs were then measured at 0 and 24 h using dynamic light scattering (DLS) (Malvern Zetasizer Nano ZS, Malvern, UK). The naming scheme used for ternary si-NP formulations is as follows: [Binary Polymer](Binary N^+:P^-)-[Ternary Polymer](Ternary N^+:P^-). For example, the lead ternary si-NP which contains a DB core formulated at 4:1 N^+:P^- and PDB corona formulated to a final N^+:P^- of 12:1 is referred to as DB4-PDB12.

The hemolysis assay was used to assess all ternary si-NP formulations for cytocompatibility and the potential to escape the endolysosomal pathway. Red blood cells (RBCs) were obtained from anonymous donors and isolated by a well-established protocol[263]. After isolation, RBCs were incubated with varying concentrations (5, 15, and 30 μg/mL total polymer concentration) of each ternary si-NP formulation at four pH's representative of extracellular and endolysosomal ranges (7.4, 6.8, 6.2, 5.6). After 1 h of incubation, intact RBCs and cellular debris were centrifuged out, and supernatants were removed. The supernatants were measured for absorbance at 451 nm (hemoglobin absorbance) and percent hemolysis was determined relative to 1% Triton-X100 detergent.

Human triple negative breast cancer cells (MDA-MB-231) were cultured in DMEM supplemented with 10% FBS and 50 μg/mL gentamicin. Mouse embryonic fibroblasts (NIH3T3), and mouse mesenchymal stem cells (MSCs) were cultured in DMEM supplemented with 10% FBS and 1% Pen/Strep. MDA-MB-231, NIH3T3, and MSC cells were transduced with lentivirus encoding firefly luciferase, Green Fluorescent Protein (GFP), and Blasticidin resistance, enabling the generation of stable luciferase expressing-MDA-MB-231 (L231), NIH3T3 (L3T3), and MSC (LMSC) cell lines.

Cytocompatability of all ternary si-NP formulations was evaluated by adding scrambled siRNA containing ternary si-NPs to L231 and L3T3 cells and measuring relative cell number based on cellular luminescence. L231 and L3T3 cells were seeded to 96-well black-walled plates at a density of 5,000 cells/well and allowed to adhere overnight. Ternary si-NP formulations were then added to each well in full serum media (DMEM, 10% FBS, 50 μg/mL gentamicin/1% Pen/Strep) at a final siRNA concentration of 100 nM and incubated for 24 h. After 24 h, media was replaced with luciferin containing media (150 μg/ml) and luminescence signal was collected on a Lumina

III IVIS system (Xenogen Corporation, Alameda, CA, USA). Cell viability was then calculated as the ratio of luminescence of siScrambled siRNA treated cells to non-treated cells.

Cell uptake was evaluated in both MDA-MB-231 and NIH3T3 cell types by flow cytometry. MDA-MB-231 and NIH3T3 cells were seeded into 24-well plates at a density of 30,000 cells/well and allowed to adhere overnight. Alexa488-labeled model siRNA was loaded into ternary si-NPs which were added to each well to give a final nucleic acid concentration of 100 nM. These treatments were incubated with cells in full serum media (DMEM, 10% FBS, 50 μg/mL gentamicin/1% Pen/Strep) for 24 h. After 24 h, media with treatments was removed, and cells were washed with PBS (-/-), trypsinized (0.25%), transferred to microcentrifuge tubes, and centrifuged at 420g for 7 min to yield a cell pellet. Pellets were re-suspended in 0.4 mL PBS(-/-) with 0.04% trypan blue to quench extracellular fluorescence, and intracellular si-NP delivery was measured by FACS (FACSCalibur, BD Biosciences, Franklin Lakes, NJ, USA) at excitation wavelength of 488 nm and emission wavelength of 519 nm.

The gene silencing profile of ternary si-NP formulations was screened within L3T3s, L231s, and LMSCs. Cells were initially seeded in black-walled, 96-well plates at a density of 2,000 cells/well and allowed to adhere overnight. Cells were then treated for 24 h in full-serum media (DMEM, 10% FBS, 50 μg/mL gentamicin/ 1% Pen/Strep) with all ternary si-NP formulations prepared as described above and containing an anti-luciferase or scrambled siRNA sequence (100 nM). After 24 h, treatment media was replaced by luciferin containing media (150 μg/ml), and cellular luminescence was measured using an IVIS Lumina III imaging system (Xenogen Corporation, Alameda, CA, USA). The cells were then incubated for an additional 24 h after luciferin containing media was replaced by low-serum media (DMEM, 1% FBS, 50 μg/mL gentamicin/1% Pen/Strep), which was used to minimize cellular overgrowth. Cellular

luminescence was re-measured at 48 h and normalized to treatment with analogous formulations containing a scrambled control siRNA sequence in all cases.

Cell uptake and endosomal escape of ternary si-NPs were imaged by confocal microscopy. MDA-MB-231 cells were seeded in 8-well chamber slides (Lab-Tek II Chambered Coverglass, Thermofisher) at a density of 20,000 cells/well and allowed to adhere overnight. Alexa488-labeled ternary si-NPs were added to each well to give a final nucleic acid concentration of 25 (LF2K) or 100 (PDB, DB4-PDB12) nM and incubated with cells in full serum media (DMEM, 10% FBS, 50 μg/mL gentamicin) for 24 h. After 24 h, treatment media was removed, cells were washed once with PBS (-/-) and imaged in PBS (-/-) containing DAPI nuclear stain. For visualizing endosomal escape after 2 h, cells were washed once with PBS (-/-) and incubated in PBS (-/-) containing DAPI nuclear stain and Lysotracker Red (75 nM) at 37 °C. Cells were imaged after 1 h incubation with Lysotracker Red. All images were processed using imageJ and colocalization was analyzed using Just Another Colocalization Plugin (JACoP) [264]. Using JACoP, Mander's overlap coefficients were calculated to represent the fraction of green signal (Alexa488-dsDNA) overlapping with red signal (LysoTracker Red) to quantify colocalization ($n \geq 4$ images).

PDB and DB4-PDB12 si-NPs were loaded with Förster Resonance Energy Transfer (FRET, using Alexa Fluor 488 and Alexa Fluor 546) pair-labeled dsDNAs. Fluorescence intensity was measured using a microplate reader (Tecan Infinite F500, Männedorf, Switzerland) with an excitation wavelength of 488 ± 5 nm. Alexa Fluor 488 emission was collected at 519 ± 5 nm, and Alexa Fluor 546 emission was obtained at 573 ± 5 nm. FRET was calculated as a ratio of the fluorescent intensity as follows:

(2.3) $$\text{FRET} = \frac{I_{573}}{I_{519}}$$

The stability of PDB and DB4-PDB12 si-NPs was measured in the presence of 2 to 100 U/mL of heparin sodium salt in DPBS [16]. The fluorescence emission at both wavelengths was measured over time following addition of heparin sodium salt. The EC_{50} of dissociation for PDB and DB4-PDB12 si-NPs was calculated according to the following equation:

(2.4)
$$y = \frac{-1}{1+\left(\frac{x}{K_d}\right)^b} + 1$$

Blood was collected retro-orbitally at 5 min and 10 min post-injection, not exceeding two collections per animal. After 20 min, animals were sacrificed, and blood was immediately collected via the renal vein. Blood samples were centrifuged at 2000 x g for 5 min, and 5 μL of plasma was taken from the supernatant and diluted into 95 μL PBS (-/-). Fluorescence was quantified on an IVIS Lumina III imaging system (Xenogen Corporation, Alameda, CA, USA) at excitation wavelength of 620 ± 5 nm and emission wavelength of 670 ± 5 nm. A standard curve was generated by measuring the fluorescence of the initial fluorescent si-NP solution in PBS (-/-) over the range of 200% - 1.5% of the injected dose. The standard curve was utilized in order to calculate the percent of injected dose in each blood sample, and the calculated values were used to determine nucleic acid concentration in the plasma at each time point as well as area under the curve (AUC) values.

Athymic nude female mice (4-6 weeks old, Jackson Laboratory, Bar Harbor, ME, USA) were injected in each mammary fat pad with 1 x 10^6 L231 cells in DMEM:Matrigel (50:50). After 17 days, tumor-bearing mice were injected via the tail vein with 1 mg/kg (Cy5-dsDNA dose) of fluorescent si-NPs. After 20 min, animals were sacrificed and the organs of interest (heart, lungs, liver, spleen, kidneys, and tumors) were excised. The organs were fluorescently imaged and quantified on an IVIS Lumina III imaging system (Xenogen Corporation, Alameda, CA, USA) at excitation wavelength of 620 ± 5 nm and emission wavelength of 670 ± 5 nm.

Athymic nude female mice (4-6 weeks old, Jackson Laboratory, Bar Harbor, ME, USA) were injected in each mammary fat pad with 1 x 10^6 L231 cells in DMEM:Matrigel (50:50). After 17 days, tumor-bearing mice were injected via the tail vein with 1 mg/kg (Cy5-dsDNA dose) of fluorescent si-NPs. After 180 min, animals were sacrificed and tumors were excised. Tumor tissue was immediately submerged in optimal cutting temperature (OCT) compound and snap frozen. Cryo-sections were then cut at 5 μm thickness by the Vanderbilt Translational Pathology Core and imaged in PBS containing DAPI on a C1si confocal microscope system (Nikon Instruments, Melville, NY, USA) equipped with differential interference contrast transmitted light detector.

Athymic nude female mice (4-6 weeks old, Jackson Laboratory, Bar Harbor, ME, USA) were injected in each mammary fat pad with 1 x 10^6 L231 cells in DMEM:Matrigel (50:50). After 17 days, tumor-bearing mice were injected i.p. with luciferin substrate (150 mg/kg) and imaged for bioluminescence on an IVIS Lumina III imaging system (Xenogen Corporation, Alameda, CA, USA) 20 minutes post-injection. Next, the mice were injected via the tail vein with 1 mg/kg (siRNA dose) si-NPs containing either anti-luciferase siRNA, a scrambled control siRNA, or saline. Mice were imaged and dosed at days 17 and 18 and also imaged on days 19 and 20. Relative luminescence was determined by measuring the raw luminescent intensity of each tumor on each day and comparing to the initial signal at day 17.

Treatment groups were compared using either two-tailed student's t-test or one-way ANOVA test coupled with Tukey means comparison test, where a p-value < 0.05 was deemed representative of a significant difference between treatment groups. No outliers were removed from data. For all data, the arithmetic mean and standard error are shown.

The animal studies were conducted with adherence to the guidelines for the care and use of laboratory animals of the National Institutes of Health (NIH). Mice were fed a standard chow

diet ad libitum and had free access to water. All protocols were approved by the Institutional Animal Care and Use Committee of Vanderbilt University and done in accordance with the National Institutes of Health Guide for the Care and Use of Laboratory Animals. Hemolysis assays were done on blood samples taken under a protocol approved by the Vanderbilt Institutional Review Board (IRB).

Results and Discussion

Two core-forming polymers, pDMAEMA (D; M_n = 21 kDa and PDI = 1.02) and p(DMAEMA-*co*-BMA) (DB; M_n = 18 kDa and PDI = 1.05), and two corona-forming diblock polymers, PEG-*b*-pDMAEMA (PD; M_n = 22 kDa and PDI = 1.16) and PEG-*b*-p(BMA-*co*-DMAEMA) (PDB; M_n = 23 kDa and PDI = 1.03), were synthesized using RAFT polymerization to achieve polymers with low polydispersity and controlled monomer composition and molecular weight (**Figure 2.1a, Table 2.1, and Supplementary Figures B.2 and B.3**). RAFT polymerization is advantageous for synthesizing biomacromolecules of complex architectures with precision and low polydispersity.[265,266] Moreover, the simple and single-step polymerizations used herein are scalable and yield polymers which can be rapidly purified.

Polymer	DP (NMR)	Composition (%BMA, NMR)	Mn (Da, NMR)	PI (GPC)
D	133	0	20,900	1.02
DB	117	49.6	17,500	1.05
PD	110	0	22,300	1.16
PDB	119	49.6	22,800	1.03

Table 2.1) Polymer degrees of polymerization (DP), composition (%BMA), number-average molecular weight (Mn), and polydispersity (PI) characterization.

The well-defined D, DB, PD, and PDB polymers served as the base units of thirty ternary si-NPs formed by varying polymer to siRNA charge ratios (N^+:P^-) and the ratio of core:corona polymers within each ternary si-NP class (DB-PD, DB-PDB, and D-PDB) (**Figure 2.1b-e**). The

D-PD combination[267] was not extensively pursued because of its lack of a hydrophobic component. Instead, we focused on "hydrophobized" ternary si-NPs which we hypothesized would outperform purely cationic ternary polyplexes based on our previous findings that balancing cationic and hydrophobic content of binary polyplexes increases stability, endosomolysis, and bioactivity.[16,249] The three sub-classes are characterized primarily by the placement of the hydrophobic BMA monomer into either the core- (DB-PD), corona- (D-PDB), or both core- and corona-forming polymers (DB-PDB, **Figure 2.1b**). Within each sub-class, the amount of non-PEGylated, core-

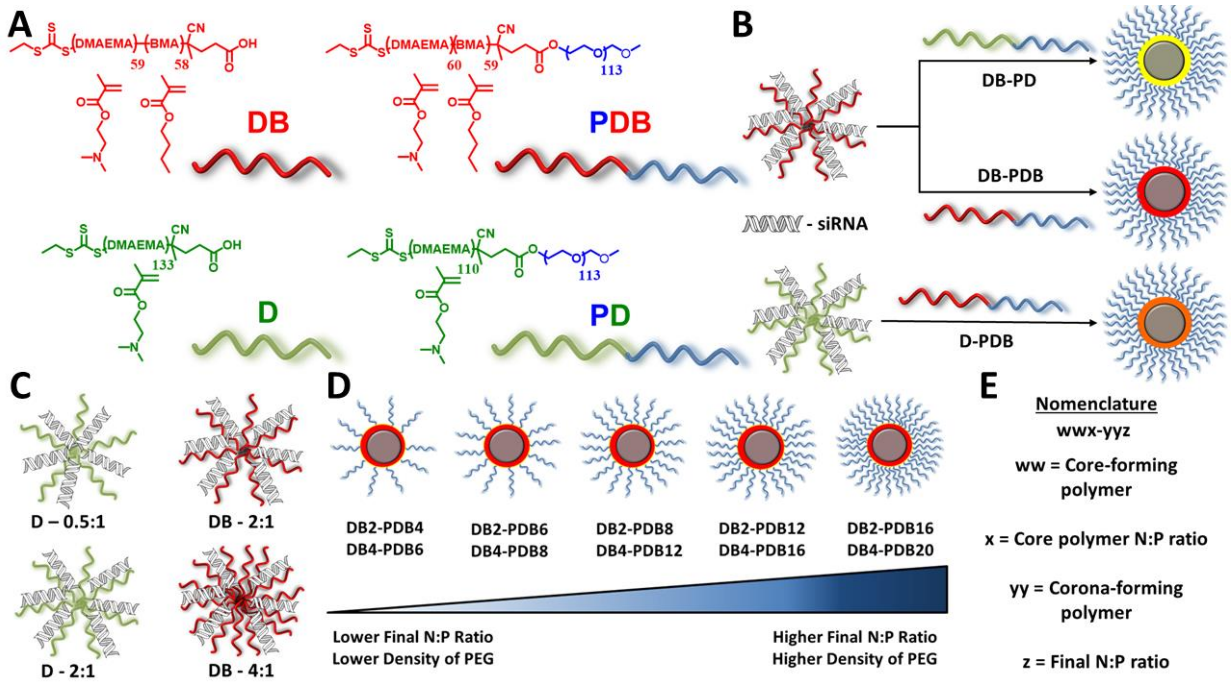

Figure 2.1) Ternary si-NP synthesis and structural characterization. (A) The four RAFT-synthesized polymers utilized for siRNA packaging and delivery. (B) Three sub-classes of ternary si-NPs were formed with a balance of hydrophobic BMA monomer copolymerized with cationic DMAEMA in either the core (DB-PD), corona (D-PDB), or both (DB-PDB). For formulation of ternary si-NPs, (C) core-forming, binary pre-NPs were made at varying N:P ratios (D: 0.5:1, 2:1; DB: 2:1, 4:1). (D) Ternary si-NPs were then formed by adding a PEGylated, corona-forming polymer to the binary complexes. The relative amount of the second polymer added dictates the degree of surface PEGylation. (E) Nomenclature used to identify ternary si-NPs.

forming polymer was varied (**Figure 2.1c**) to form si-NP precursors (pre-NPs, **Supplementary Figure B.4**). The amount of PEGylated, corona-forming polymer was also varied to generate different degrees of surface PEGylation and ratio of core:corona polymers within each sub-class (**Figure 2.1d**).

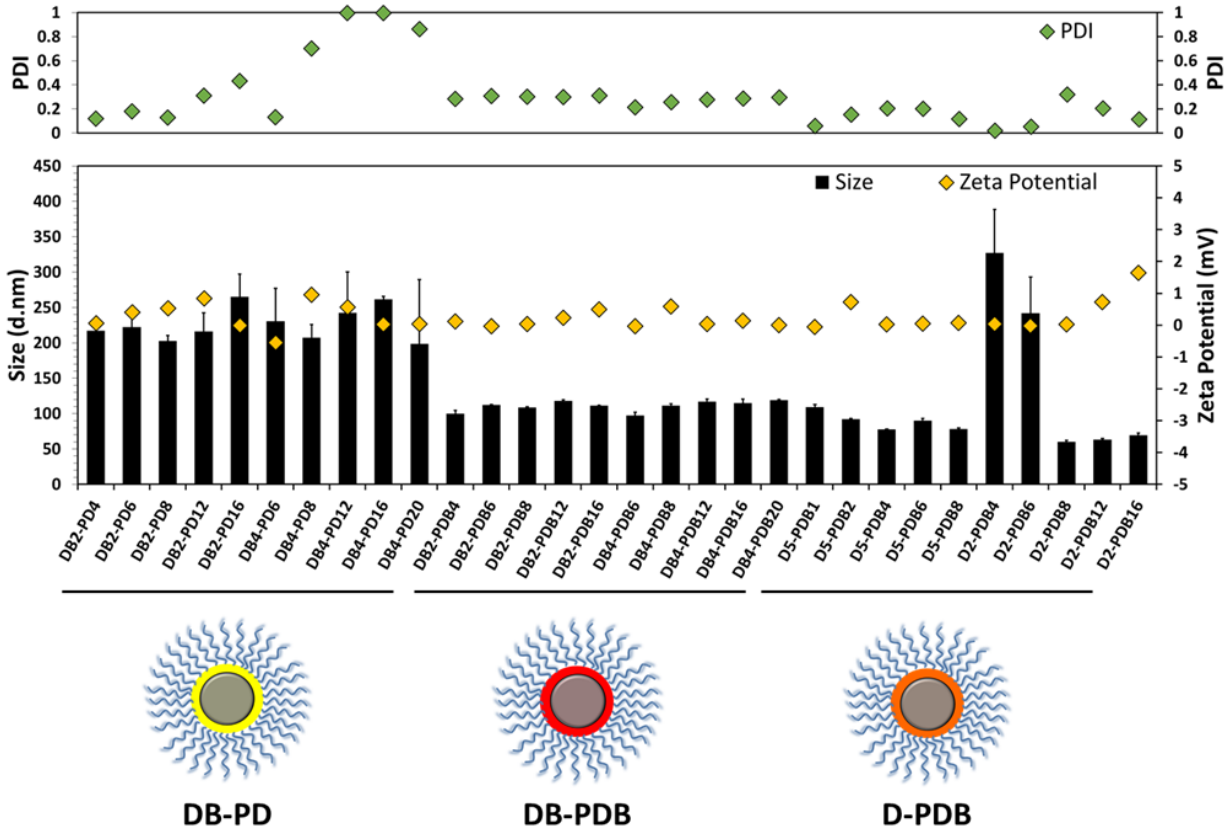

Figure 2.2) Physicochemical characterization of ternary si-NP library including si-NP size, surface charge (zeta potential), and polydispersity (PDI). (Yellow: DB-PD, Red: DB-PDB, Orange: D-PDB)

The physicochemical properties of si-NPs from each class were screened, including hydrodynamic diameter, polydispersity, and surface charge (zeta potential) at 0 h and 24 h post-fabrication. DB-PD, DB-PDB, and D-PDB ternary si-NPs each formed stable and compact si-NPs (~100–300 nm) (**Figure 2.2, Supplementary Table B.2**). While D2-PDB4 and D2-PDB6 si-NPs

significantly increased in size over 24 h, all other si-NPs retained their initial size. All si-NPs had approximately neutral surface charge which is ideal for systemic administration, with zeta potentials for each si-NP ranging from -1 to +2 mV. Ternary si-NPs utilizing the corona-forming polymer PDB (DB-PDB and D-PDB) displayed PDIs < 0.3, as compared to highly variable PDIs (0.1 – 1.0) seen in the PD-coated si-NPs (**Figure 2.2, Supplementary Table B.2**). In addition, the non-PEGylated, pre-NPs (DB4) rapidly aggregate, forming large and extremely polydisperse structures (**Supplementary Figure B.5**) at neutral pH (7.4). By contrast, PDB coating of DB4 to form ternary si-NPs gives nanoparticles in the same size range as the binary, parent PDB si-NPs (~120 nm; **Supplementary Figure B.5**). Moreover, PDB polymer not loaded with nucleic acid exists as very small micelles at pH 7.4 (**Supplementary Figure B.5**). In DLS spectra of DB4-PDB12 si-NPs, neither aggregates of the uncoated DB4 pre-NPs or small micelles of the empty PDB micelles appear, suggesting that PDB (when added to pre-NPs in a solution of pH 4) associates with the DB4 pre-NPs and successfully coats the pre-NPs, producing stabilized ternary nanoparticles. In sum, the initial physicochemical screening of this library of ternary si-NPs highlighted the promise of a subgroup of formulations (DB-PDB and D-PDB), which leveraged the PDB polymer as a corona-forming component. These two classes yielded stable si-NPs ~100 nm in diameter, with neutral surface charge and low polydispersity.

Entrapment in the endolysosomal pathway and subsequent degradation or trafficking out of the cell limit the effectiveness of many biologic drugs including siRNA.[268-270] Here, the pH-dependent hemolysis assay was used as a measure of active (non-proton sponge) endolysosomal escape capacity of the different ternary si-NP formulations[271]. The composition of the corona-forming polymer profoundly influenced si-NP hemolysis. PDB-containing si-NPs harbored "switch-like" endosomolytic behavior that is turned on at endosomal pH (6.8 and below) but not

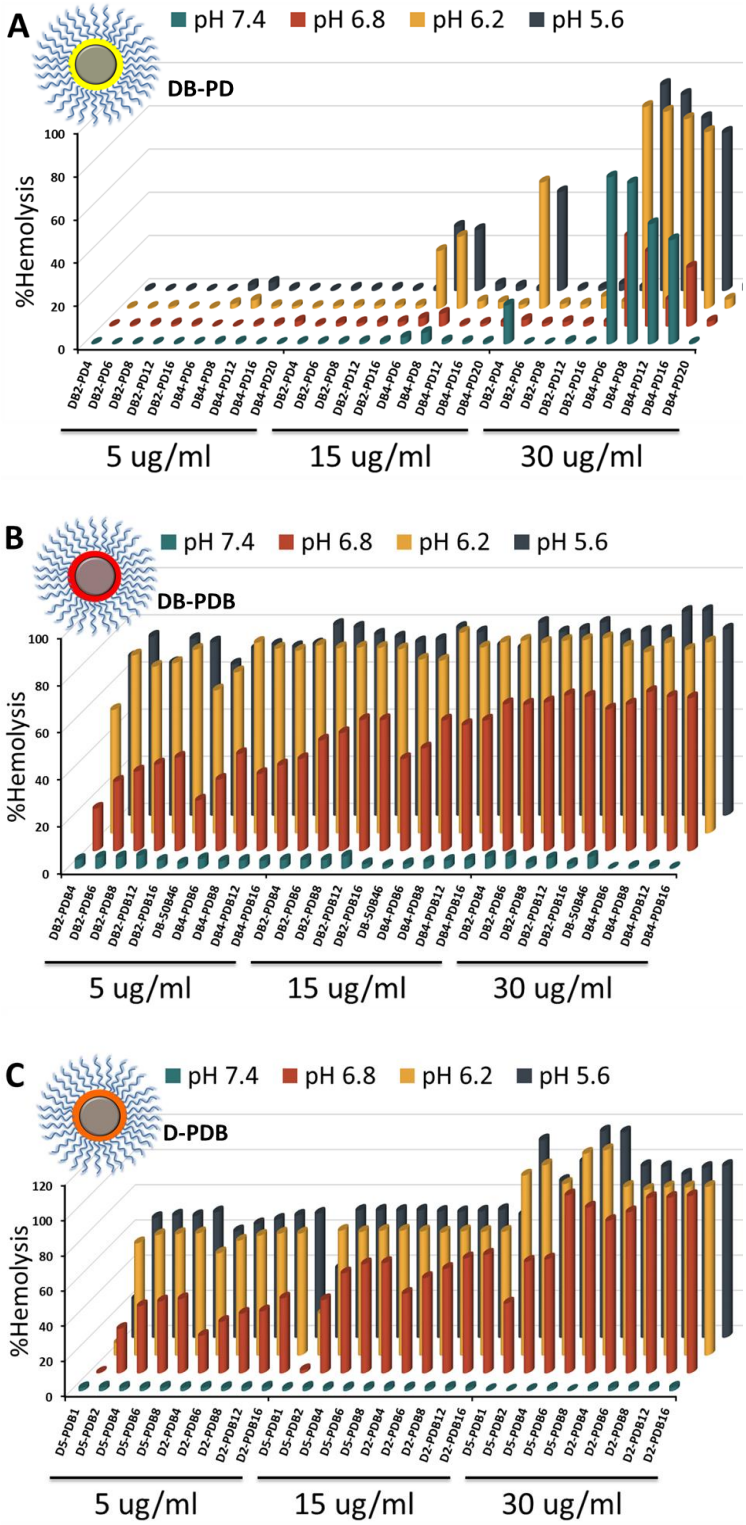

Figure 2.3) Hemolysis profiles of (A) DB-PD, (B) DB-PDB, and (C) D-PDB ternary si-NPs.

extracellular pH (7.4) (**Figure 2.3**). In contrast, PD-containing si-NPs showed weak hemolysis and were also hemolytic at pH 7.4, which is indicative of the potential for cytotoxicity (**Figure 2.3a**). For DB-PDB and D-PDB formulations, hemolysis increased proportionally with increasing amounts of the endosomolytic PDB, corona-forming polymer (**Figure 2.3b, c**). Therefore, ternary polyplexes which contained PDB as the corona-forming polymer exhibited optimal pH-dependent membrane disruptive behavior while PD-corona ternary polyplexes exhibited sporadic hemolysis and in some cases showed hemolysis at pH 7.4, which is generally correlated with cytotoxicity.

The relative cell uptake of all ternary si-NPs was initially

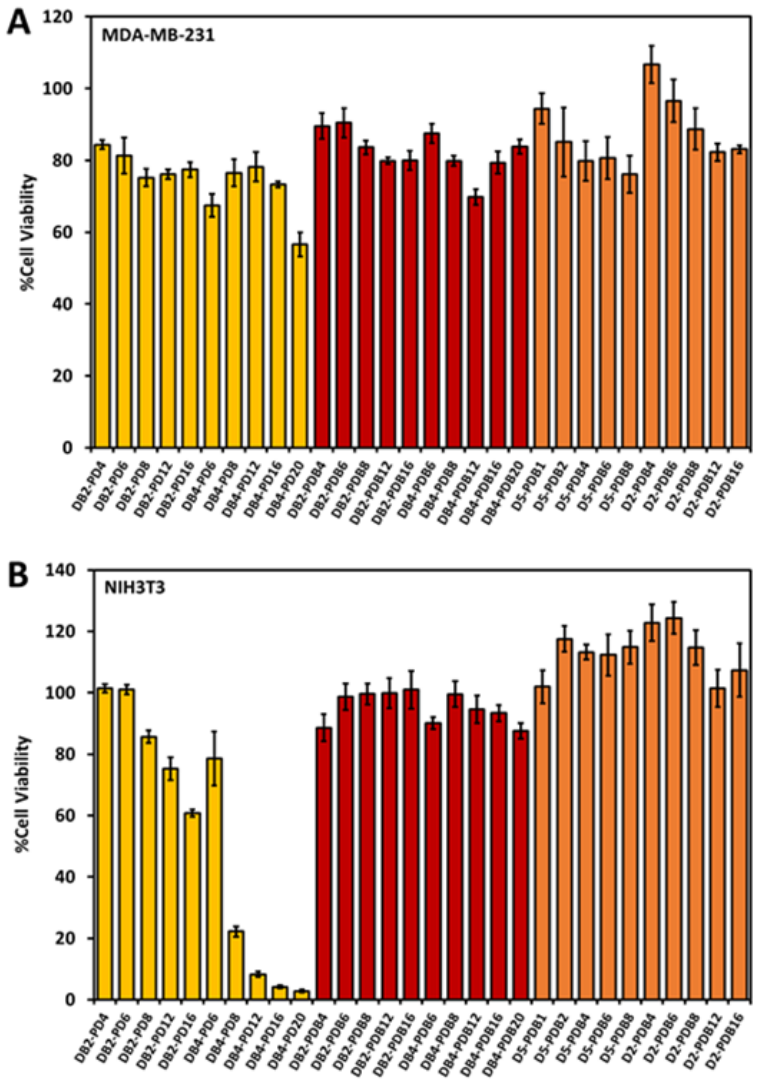

Figure 2.4) Cytocompatibility of DB-PD, DB-PDB, and D-PDB ternary si-NPs in (A) MDA-MB-231 and (B) NIH3T3 cells.

screened in MDA-MB-231 (human triple negative breast cancer) and NIH3T3 (murine embryonic fibroblasts) cells, and cytocompatibility was assessed in MDA-MB-231 and NIH3T3 cells lentivirally-transduced to constitutively express luciferase (L231 and L3T3, respectively). Treatment of L231s for 24 h with all ternary si-NP formulations was well tolerated, although DB-PD si-NPs trended toward increased cytotoxicity as amount of PD polymer was increased (**Figure 2.4a**). Incubation of L3T3s for 24 h with DB-PD si-NPs loaded with scrambled siRNA exhibited increasing cytotoxicity proportional to the amount of polymer (**Figure 2.4b**). This is consistent with the observed hemolytic membrane disruption at pH 7.4 for DB-PD polyplexes. DB-PDB or D-PDB si-NPs were not significantly toxic in L3T3s, consistent with observations that they did not cause membrane disruption at pH 7.4 in hemolysis assays (**Figure 2.4a, b**). Finally, DB2 and DB4 pre-NPs are toxic to the L3T3 cells (~40% and ~80% toxicity, respectively) until being coated by the PEGylated, corona-forming PDB polymer (**Supplementary**

Figure B.6). Upon coating, cytotoxicity of the DB pre-NPs is entirely mitigated, further suggesting their successful coating and surface presentation of the biocompatible PEG molecules (**Supplementary Figure B.6**). These results underscore the potential cytotoxicity of hemolytic materials which are not well-stabilized (such as DB-PD) and agree with previous reports of cell-type dependent cytotoxicity of nanomaterials[262,272,273].

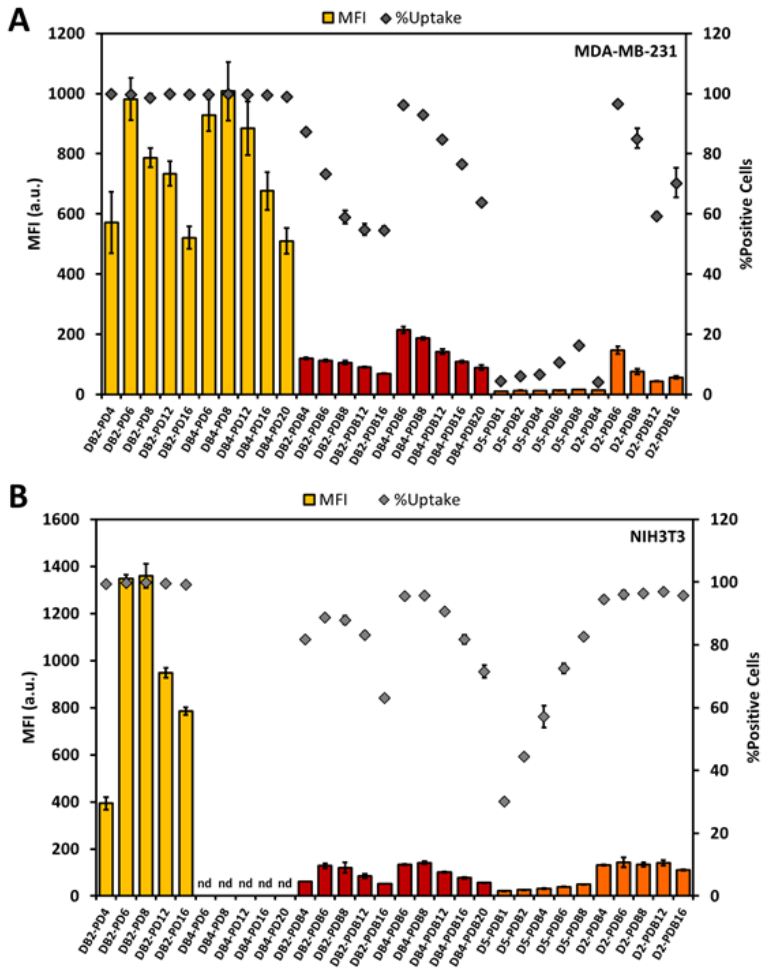

Figure 2.5) Cell uptake of DB-PD, DB-PDB, and D-PDB ternary si-NPs in (A) MDA-MB-231 and (B) NIH3T3 cells. (nd = no data)

Next, ternary Alexa488-labeled si-NPs were used to track cell uptake of si-NPs by MDA-MB-231 and NIH3T3 cells. Cellular uptake was dependent upon the chemistry of the cationic block of the corona-forming ternary polymer as well as the ratio of the PEGylated, ternary and the core-forming, binary cationic polymers. Although cells treated with DB-PD ternary si-NPs exhibited nearly 10-fold higher mean fluorescence intensity than DB-PDB and D-PDB si-NPs (**Figure 2.5**), the total fraction of the cellular population positive for uptake of fluorescent nucleic acid cargo approached 100% for all ternary si-NPs tested. Further, cells treated with the D-PDB and

DB-PDB ternary si-NP formulations displayed 5-fold higher mean fluorescence intensity than cells treated with the parental PDB binary si-NPs (**Supplementary Figure B.7**). Decreasing cellular si-NP uptake was observed with increasing degree of PEGylation in both cell types. After reaching an ~ 8:1 final N^+:P^- ratio, each subsequent addition of more corona-forming PEGylated polymer generally decreased cell uptake (**Figure 2.5**). Importantly, being able to control the amount of corona-forming polymer and thereby the density of PEGylation affords the ability to choose an optimal PEGylation state which provides colloidal stability and also a high level of cell uptake.

The panel of ternary si-NPs was initially evaluated for function based on *in vitro* target silencing of the model gene luciferase in L3T3 cells. After 24 h of treatment with ternary si-NPs loaded with anti-luciferase siRNA (siLuc), both DB-PD and DB-PDB classes of si-NPs significantly reduced protein-level expression of luciferase (**Supplementary Figures B.8 and B.9**). The DB-PDB group of ternary si-NPs (DB4-PDB6 – DB4-PDB20) achieved 65–85% reduction in luciferase activity at 48 h post-treatment (**Supplementary Figures B.8 and B.9**), which was greatest of all si-NP classes within our screen. Thus, despite their lower levels of cellular uptake, si-NPs from the DB-PDB are less toxic to cells at physiological pH, exhibit superior potential to escape endolysosomal compartments, and achieve more efficient target gene silencing in treated cells.

The panel of siRNA formulations was developed based on the idea that si-NPs that concomitantly overcome multiple siRNA delivery barriers will perform best in *in vivo* models of disease. By integrating data regarding size, zeta potential, cytotoxicity, uptake, pH-dependent hemolysis, and target gene silencing for each si-NP formulation in our library, we were able to generate a heatmap to visualize the performance of each si-NP across a number of assays simultaneously[253] (**Figure 2.6a**). Importantly, ternary si-NPs that perform well across multiple

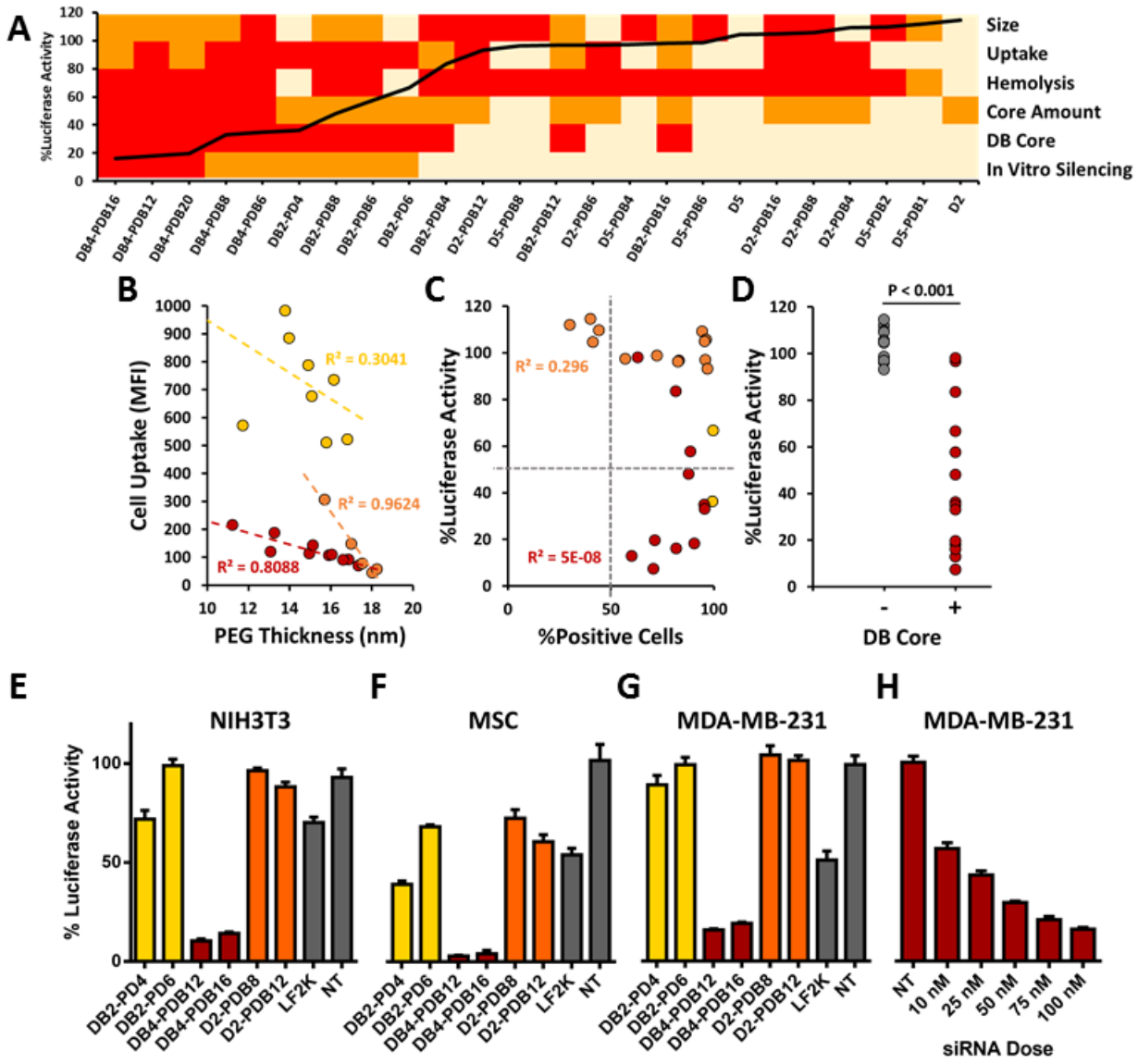

Figure 2.6) Multiparametric screen of ternary siRNA polyplexes reveals lead si-NP formulation DB4-PDB12. (A) si-NPs which are optimally tuned to overcome multiple siRNA delivery barriers such as size range, cell uptake, and endosomal escape achieve the highest target gene silencing *in vitro* (heat map parameters and thresholds are shown in Table S3; overlaid black line indicates level of residual luciferase activity for each si-NP formulation loaded with anti-luciferase siRNA). (B) Cell uptake trended inversely to si-NP surface PEG thickness (see PEG thickness calculations in Figure S8). (C) High cell uptake did not directly predict target gene silencing *in vitro*. (D) Incorporation of the hydrophobic and endosomolytic DB-core was the strongest predictor of gene silencing *in vitro* ($p < 0.001$). Lead si-NP formulations (DB4-PDB12 and DB4-PDB16; indicated in red) achieve > 80% gene silencing in (E) fibroblast (3T3s), (F) mesenchymal stem cells (MSCs), and (G) triple negative breast cancer (MDA-MB-231) cells. (H) The IC_{50} for DB4-PDB12 in MDA-MB-231 cells is 15.4 nM. (Yellow: DB-PD, Red: DB-PDB, Orange: D-PDB)

screening assays achieve the greatest level of gene silencing *in vitro* (**Figure 2.6a**). The ternary si-NP surface PEG density (calculated as described in **Supplementary Figure B.10**), cell uptake, and incorporation of the core-forming polymer DB were assessed more closely for correlation to knockdown activity. Within each class of ternary si-NPs, cell uptake was inversely proportional to the surface PEG density (**Figure 2.6b**). Although cell uptake was necessary for achieving knockdown, it was not sufficient, as many si-NPs with nearly 100% cellular uptake did not exhibit any knockdown (**Figure 2.6c**). Interestingly, the inclusion of the DB core was a key factor in achieving effective knockdown; nearly all DB-containing compounds produced target gene reduction, while all si-NPs without the DB core failed to knock down the target gene (**Figure 2.6d**).

The model gene silencing results were confirmed using murine fibroblast (NIH3T3), murine mesenchymal stem cell (MSC), and human breast cancer (MDA-MB-231) cell lines, each with stable luciferase expression. Two lead candidates from each ternary si-NP class were screened for target (luciferase) gene silencing, revealing that cells treated with the DB-PDB class si-NPs achieved greater gene silencing (>80% protein level knockdown) as compared to analogous si-NPs loaded with scrambled siRNA or other classes of siLuc si-NPs (**Figure 2.6e-g**). Dose response analysis for MDA-MB-231 cells revealed an IC_{50} silencing value of 15.4 nM for DB4-PDB12 ternary si-NPs (**Figure 2.6h**).

A crux in the development of translatable siRNA therapies is the design of delivery systems which are stable in circulation and divert siRNA from clearance organs (liver, spleen, and kidneys) in order to consequently improve distribution to pathological sites. Effective nanocarriers will overcome systemic pharmacokinetic barriers, in addition to classical subcellular endolysosomal pathway barriers, in order to increase siRNA bioavailability within target cells. Previous

combinatorial screens have yielded potent siRNA transfection reagents, but have focused primarily on *in vitro* and hepatic gene silencing[24,243,253,254,258,274]. Alternatively, we envisioned the design of a combinatorial library with parallel aims of increasing *in vitro* potency (dictated largely by intracellular barriers) and preserving physicochemical characteristics that reduce clearance by organs such as the kidneys, liver, and spleen for better *in vivo* delivery to alternate sites (*e.g.*, to tumors). With a set of comprehensive cell- and system-level barriers in mind, a multiparametric *in vitro* screening approach was conducted on this small library of rationally-designed nanocarriers. The initial physicochemical screening of this library of ternary si-NPs identified a subgroup (DB-PDB and D-PDB) of promising formulations for systemic administration, with appropriate size (~100 nm), zeta potential (~ 0 mV), and long-term colloidal stability in salts. Ternary si-NP cytotoxicity, cell uptake, and hemolysis assays subsequently revealed formulations (DB4-PDB6 – 20) which were ideally tuned for low toxicity and high potential to overcome siRNA delivery barriers. Importantly, these leading formulations achieved the highest gene silencing, and incorporation of the balanced cationic and hydrophobic DB core-component was identified as a crucial parameter for achieving potent RNAi *in vitro*.

The lead ternary si-NP, DB4-PDB12, was selected for further analysis *in vitro* and *in vivo*, benchmarking against the parental PDB binary si-NPs[16]. The DB4-PDB12 ternary si-NPs were 124.4 nm in diameter (**Figure 2.7a**) with approximately neutral surface charge (0.139 mV; **Supplementary Table B.2**), had nearly 4-fold higher cell uptake than the parental PDB binary si-NPs, and decreased colocalization of nucleic acid cargo with endolysosomes (labeled with LysoTracker Red) by 8.7- and 2.5-fold compared to Lipofectamine 2000 (LF2K) and PDB si-NPs, respectively (**Figure 2.7b-e and Supplementary Figures B.11 and B.12**). Increased cytosolic

delivery of nucleic acid cargo from DB4-PDB12 si-NPs through the endolysosomal pathway was also visualized by confocal microscopy of cells treated with fluorescently-tagged si-NPs and co-stained with Lysotracker Red (**Figure 2.7e and Supplementary Figure B.12**). Thus, the ternary analog, DB4-PDB12, maintained the important physicochemical characteristics of PDB for systemic administration (size and surface charge) while increasing lipid bilayer translocation (cell uptake and endosomal escape) of the siRNA delivery system.

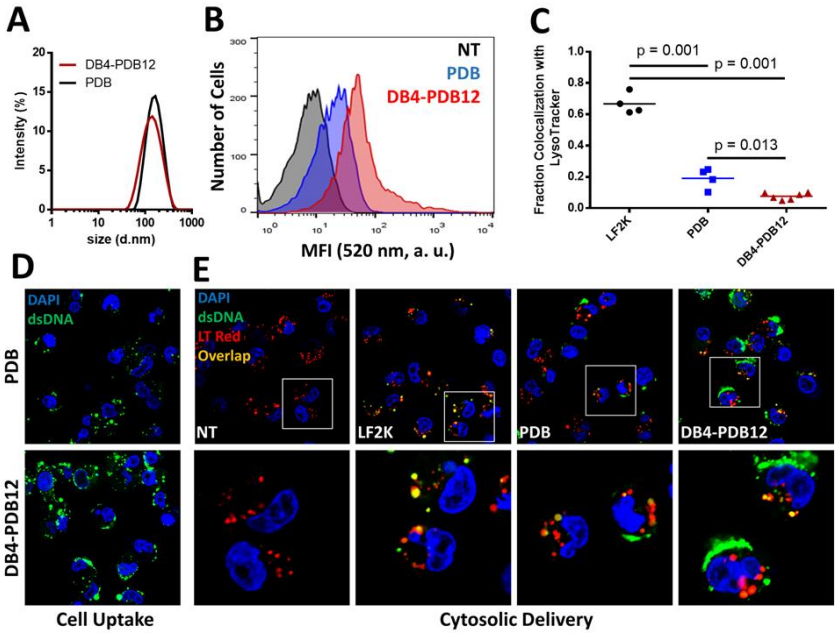

Figure 2.7) Leading DB4-PDB12 ternary si-NPs have higher cytosolic delivery than the parent binary si-NPs. (A) DB4-PDB12 si-NPs are similar size (DB4-PDB12: 124.4 vs PDB: 129.5 nm) as PDB si-NPs. (B) DB4-PDB12 have increased cell uptake over the PDB parent si-NPs (60x mag). (C) DB4-PDB12 si-NPs exhibit significantly lower endolysosomal colocalization than PDB or Lipofectamine 2000 (LF2K; administered at the maximum tolerated dose of 25 nM) si-NPs ($n \geq 4$ fields of view; 60x mag). (D) Increased DB4-PDB12 cell uptake visualized by confocal microscopy. (E) Increased cytosolic delivery of cargo by DB4-PDB12 si-NPs visualized by confocal microscopy.

To assess the stability of si-NPs in an assay that models the microenvironment of the kidney GBM, we measured binary PDB and ternary DB4-PDB12 si-NP stability in the presence of heparan sulfate. Using a FRET-based readout, DB4-PDB12 si-NPs were significantly more resistant to heparin-mediated disassembly over time when compared to PDB binary si-NPs (**Figure 2.8a and Supplementary Figures B.13 and B.14**). Consistent with these results, the fluorescently-labeled cargo of DB4-PDB12 ternary si-NPs exhibited lower concentration in the

kidneys of athymic female tumor-bearing mice relative to PDB binary si-NPs following *i.v.* injection (**Figure 2.8b and Supplementary Figure B.15**), suggesting that the ternary si-NPs have decreased susceptibility to GBM-triggered disassembly and renal clearance *in vivo*. In agreement with better stability within the circulation, DB4-PDB12 ternary si-NPs had a 1.6-fold greater area under the curve (AUC) value compared to PDB binary si-NPs (**Figure 2.8c**). Greater stability and bioavailability of DB4-PDB12 ternary si-NPs also correlated to a 2.6-fold increase in accumulation within orthotopic MDA-MB-231 breast tumor xenografts following *i.v.* injection relative to PDB binary si-NPs (**Figure 2.8d and Supplementary Figures B.15 and B.16**). The correlation between higher circulation time and greater tumor biodistribution is consistent with the principles of enhanced permeability and retention-(EPR-) based tumor accumulation[212,213]. In total, DB4-PDB12 si-NPs showed increased blood plasma AUC, reduced kidney accumulation, and increased tumor accumulation when compared to our previously optimized PDB binary si-NP composition[16], all advantageous characteristics for effective systemic delivery of siRNA to solid tumors.

The siRNA silencing efficacy of lead DB4-PDB12 ternary si-NPs was evaluated *in vivo* in orthotopic L231 (MDA-MB-231 triple negative breast cancer cells constitutively expressing luciferase) tumors. DB4-PDB12 ternary si-NPs or PDB binary si-NPs loaded with siLuc siRNAs were injected *i.v* in two doses, (days 17 and 18 after tumor inoculation), and tumor luciferase expression was assessed using intravital bioluminescence. As early as 24 h after treatment, luciferase was diminished by ~ 45% knockdown in tumors of mice treated with siLuc-loaded DB4-PDB12 si-NPs as compared to siScrambled control si-NPs ($p = 0.01$). Increased silencing by the DB4-PDB12 si-NPs was detected at 48 h and 72 h after treatment, with ~ 51% ($p < 0.01$) and ~ 59% ($p < 0.01$) luciferase attenuation, respectively (**Figure 2.8e**). Moreover, DB4-PDB12 ternary siLuc-NPs decreased luciferase signal significantly more than PDB binary siLuc-NPs at 24, 48,

and 72 h (45% vs. -23%, 51% vs. 20%, and 59% vs. 42% reduction, respectively; **Figure 2.8e**) when compared head-to-head.

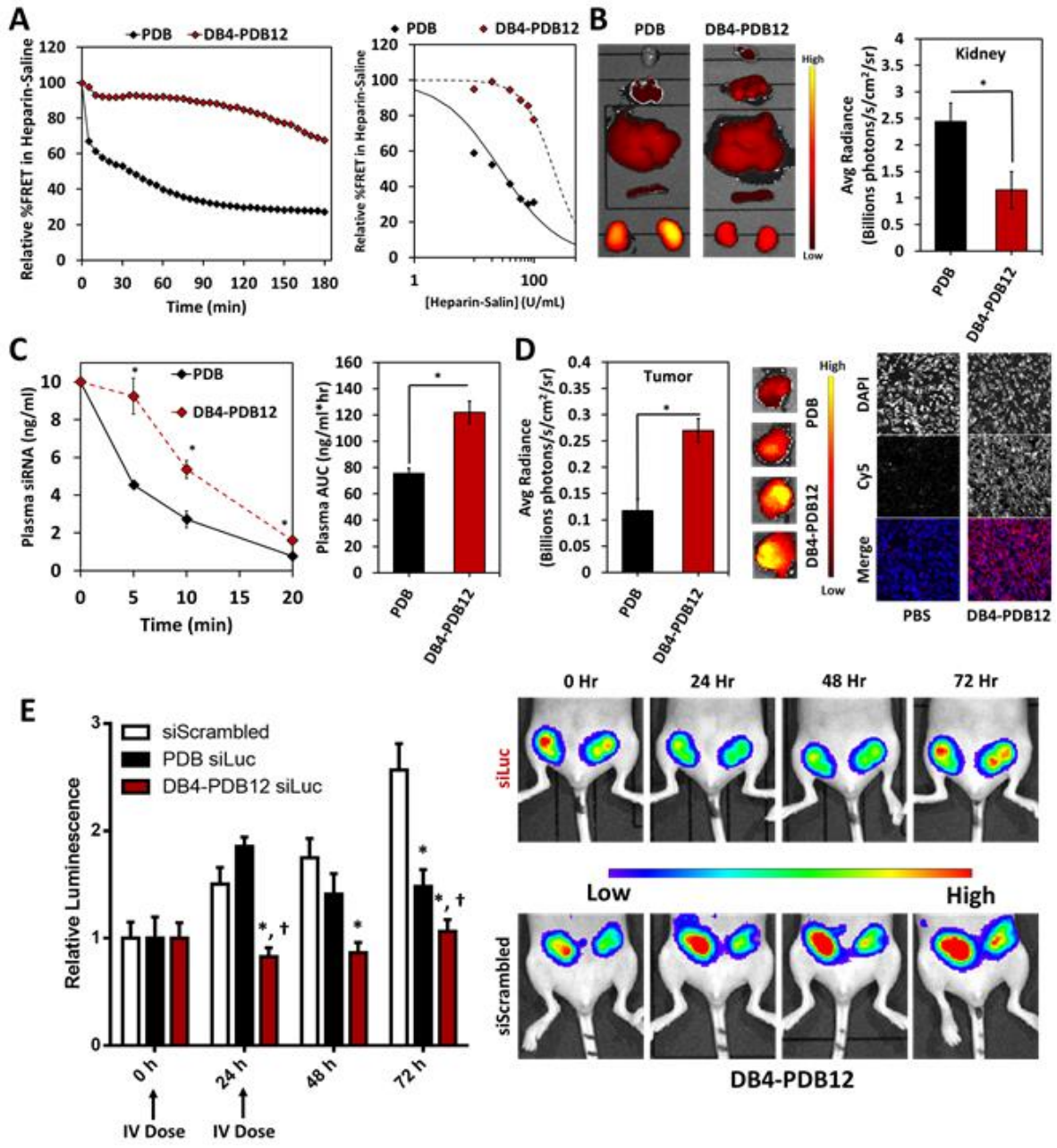

Figure 2.8) Ternary DB4-PDB12 si-NPs improve pharmacokinetics and bioactivity of siRNA relative to binary PDB si-NPs after *i.v.* administration. (A) Ternary si-NPs have increased resilience to disassembly by polyanionic heparin in saline solution. (B) Biodistribution of si-NPs after *i.v.* administration (1 mg/kg Cy5-labeled dsDNA). Ternary si-NPs have significantly reduced concentration in the kidneys compared to parent PDB si-NPs in male CD-1 mice ($n = 6$; $p < 0.001$). (C) Ternary si-NPs persist longer in blood ($n \geq 3$; $p = 0.008$) and (D) increase uptake into orthotopic breast tumors after *i.v.* administration relative

to PDB binary si-NPs (n = 6; p = 0.03). (E) Treatment with 2 doses (0 and 24 h) at 1 mg/kg siRNA silences the model gene luciferase in luciferase-expressing orthotopic MDA-MB-231 xenografts and arrests growth in luminescence signal. DB4-PDB12 si-NPs enhance siRNA bioactivity over parent PDB binary si-NPs ($n \geq 5$; $p = 0.05$).

Recent studies have identified the kidneys as the major route for *in vivo* clearance of *i.v.*-injected siRNA polyplexes assembled by electrostatic interactions[218,219]. In these studies, anionic proteoglycans such as heparan sulfates of the GBM were identified as culprits for polyplex disassembly and clearance through the kidneys/urine. Therefore, it is functionally significant that the DB4-PDB12 ternary si-NPs resist heparin-mediated disassembly, reduce clearance through the kidneys, and consequently achieve higher AUCs after *i.v.* administration when benchmarked against PDB binary si-NPs which previously were optimized to outperform PD (100% cationic) si-NPs[16]. Importantly, the optimized DB4-PDB12 formulation only accumulated ~50% within the kidneys (**Supplementary Figure B.15B)**, whereas siRNA polyplexes reported in the literature typically show > 75% renal accumulation[221,245,247,248,252,275-277], severely attenuating the amount of injected dose available for delivery to non-renal target organs. The increased AUC of DB4-PDB12 ternary si-NPs also correlated to higher siRNA delivery to orthotopic breast tumors in our studies. Although recent studies highlight the variability of the EPR effect[209,278], Clark et al. recently observed EPR-based tumor accumulation of CRLX101 in gastrointestinal adeno- or squamous cell carcinomas in human patients while the nanomedicine was absent in surrounding, non-neoplastic tissue[279]. Generally, it is accepted that EPR-based accumulation of nanoparticles within tumors occurs when particles fall within the appropriate size range and correlates with circulation AUC as observed within the current study[212,213]. In addition to passive targeting by the EPR effect, active targeting through receptor-ligand interactions (*e.g.*, transferrin, folic acid, RGD, HER2-ScFv) is a popular approach for increasing tumor retention after *i.v.* administration of si-NPs, but active targeting is inherently limited if the nanocarrier is rapidly cleared. For this reason, we focused on

initially improving the pharmacokinetics of our ternary si-NPs through modulation of the si-NP core chemistry, and it is anticipated that inclusion of active targeting will further improve our lead si-NPs in the future.

Conclusions

Many siRNA transfection reagents have been primarily optimized to achieve gene silencing *in vitro*, and therefore, utilize design principles (*e.g.*, extreme cationic charge for cell internalization[207]) which do not translate well to *in vivo* settings, especially for delivery to non-hepatic targets. Due to the shortcomings of strictly cationic polyplexes (such as colloidal instability and short persistence in circulation *in vivo*), we combinatorially incorporated hydrophobicity into the core, corona, and both core and corona of a rationally-designed library of 30 distinct ternary architecture si-NPs to stabilize them through both electrostatic and van der Waals forces. Within each class, the amount of core-forming polymer, corona-forming polymer, and the ratio of the two were varied in order to systematically study the effects of each component as well as investigate structure-function relationships. The full library was screened by a multiparametric strategy that facilitated identification of a lead candidate that is optimized to overcome both cell-level (*e.g.*, lipid bilayer translocation) and systemic (*e.g.*, stability in blood and rapid renal clearance) delivery barriers. Our lead candidate from this screen, DB4-PDB12, is small (~100 nm), stable in size, efficiently internalized by cells, potently endosomolytic, and effective at gene silencing *in vitro*. DB4-PDB12 si-NPs were benchmarked against our previous "gold-standard" PDB si-NPs[16] and exhibited superior cell internalization and cytosolic delivery of nucleic acid cargo, increased resilience to heparan sulfate-mediated disassembly, reduced renal clearance, increased blood circulation AUC, and improved target gene silencing within tumors after intravenous delivery.

These results confirmed that a multiparametric screening approach identified new lead formulations within the PEGylated polyplex class of siRNA carriers. New insights were also gleaned regarding the value of ternary over binary formulations, tuning of PEG density, and comprehensive incorporation of balanced cationic and hydrophobic content within both core- and corona-forming polyplex components.

CHAPTER III

STABILIZATION OF SIRNA NANOPOLYPLEXES BY MATCHING HYDROPHOBIC INTERACTIONS OF A LIPID-MODIFIED SIRNA AND POLYMERIC CARRIER: OVERCOMING SYSTEMIC DELIVERY BARRIERS.

Text for Chapter III taken from:

SM Sarett, TA Werfel, I Chandra, MA Jackson, TE Kavanaugh, ME Hattaway, TD Giorgio, CL Duvall. Hydrophobic Interactions between Polymeric Carrier and Palmitic Acid-Conjugated siRNA Improve PEGylated Polyplex Stability and Enhance In Vivo Pharmacokinetics and Tumor Gene Silencing. *Biomaterials.* 2016, 97, 122-132.

Abstract

Formation of stable, long-circulating siRNA polyplexes is a significant challenge in translation of intravenously-delivered, polymeric RNAi cancer therapies. Here, we report that siRNA hydrophobization through conjugation to palmitic acid (siPA) improves stability, *in vivo* pharmacokinetics, and tumor gene silencing of PEGylated nanopolyplexes (siPA-NPs) with balanced cationic and hydrophobic content in the core (relative to the analogous polyplexes formed with unmodified siRNA, si-NPs). Hydrophobized siPA loaded into the NPs at a lower charge ratio (N^+:P^-) relative to unmodified siRNA, and the siPA-NPs had superior resistance to siRNA cargo unpackaging in comparison to si-NPs upon exposure to the competing polyanion heparin and serum. *In vitro*, siPA-NPs increased uptake in MDA-MB-231 breast cancer cells (100% positive cells vs. 60% positive cells) but exhibited equivalent silencing of the model gene luciferase relative to si-NPs. *In vivo* in a murine model, the circulation half-life of intravenously-injected siPA-NPs was double that of si-NPs, resulting in a >2-fold increase in siRNA biodistribution to orthotopic

MDA-MB-231 mammary tumors. The increased circulation half-life of siPA-NPs was dependent upon the hydrophobic interactions of the siRNA and the NP core component and not just siRNA hydrophobization, as siPA did not contribute to improved circulation time relative to unmodified siRNA when delivered using polyplexes with a fully cationic core. Intravenous delivery of siPA-NPs also achieved significant silencing of the model gene luciferase *in vivo* (~40% at 24 hours after one treatment and ~60% at 48 hours after two treatments) in the murine MDA-MB-231 tumor model, while si-NPs only produced a significant silencing effect after two treatments. These data suggest that stabilization of PEGylated siRNA polyplexes through a combination of hydrophobic and electrostatic interactions between siRNA cargo and the polymeric carrier improves *in vivo* pharmacokinetics and tumor gene silencing relative to conventional formulations comprising only electrostatic interactions.

Introduction

Small interfering RNA (siRNA) has the potential to become a transformative class of therapeutics due to its ability to potently and specifically silence expression of genes, including targets considered to be "undruggable" by conventional small molecule inhibitors. However, clinical translation of siRNA therapies has been limited, primarily due to the formidable physiological barriers that must be overcome for siRNA to reach its intracellular site of action[280-282]. When delivered intravenously (e.g., for tumor therapy), siRNA molecules are rapidly cleared through the kidneys[218,220]. If siRNA reaches target cells, it lacks a mechanism to translocate bilayer membranes, limiting both cellular uptake and endosomal escape. To combat these myriad challenges, lipidic and polymeric carrier systems as well as a variety of siRNA conjugates have been developed that feature mechanisms to improve siRNA pharmacokinetics, stability, cellular

uptake, release, endosomal escape, and/or site-specific targeting[10,36,283-294]. However, clinical efficacy of these delivery systems remains limited, due in large part to a preferential distribution to and systemic clearance through the hepatic and renal systems. As evidenced by therapies currently in advanced clinical trials, the natural targeting of lipid-based nanoparticles to the liver can be leveraged to successfully modulate gene expression in hepatocytes, but delivery of siRNA to other target tissues remains a challenge[289,295-299]. It is thus of high significance to identify systemic siRNA delivery systems that accumulate at other target sites, such as tumors.

Although the magnitude of the enhanced permeability and retention (EPR) effect in spontaneously-formed tumors in humans and large animals is known to be variable, it is accepted that for many tumor types, there is a significant correlation between nanocarrier tumor accumulation and blood circulation persistence (related to avoidance of clearance through organs such as liver and kidney)[208-211]. Likewise, it has been observed that the magnitude of passive tumor uptake of nucleic acid-based nanopolyplexes is directly related to circulation time[212,213]. Commonly, lipoplex or polyplex nano-formulations designed for intravenous administration are PEGylated to impart colloidal stability and to reduce opsonization and clearance by the mononuclear phagocyte system (MPS)[214-217]. However, siRNA delivered by polyplexes that are stabilized solely through electrostatic interactions with polyplex core-forming cationic polymers is susceptible to rapid clearance through the kidney. This clearance is due to polyplex disassembly triggered by the competing interactions between the cationic polymer and the polyanionic heparan sulfates of the glomerular basement membrane (GBM). As a result, electrostatically-stabilized or polyion complex nanoparticle formulations impart only minor differences in pharmacokinetics (i.e., blood persistence half-life) relative to free siRNA ($t_{1/2}$ siRNA ~1 – 2 min, $t_{1/2}$ siRNA nanoparticles ~3 – 5 min)[216,218,220-222]. While siRNA-encapsulating nanoparticles fabricated

through water-oil-water (W/O/W) emulsion methods impart significant pharmacokinetic advantages[300], loading of highly anionic and hydrophilic siRNA into a hydrophobic core nanoparticle formulation is not very efficient, resulting in loss of expensive siRNA during fabrication, exposure of siRNA to potentially damaging organic solvents, and formation of nanoparticles with high weight ratios of carrier polymer(s) relative to siRNA cargo. The aim of the current report was to increase the stability of PEGylated siRNA polyplexes against polyanion-induced disassembly, limiting removal of intravenously-delivered polyplexes from the circulation while obviating complex and inefficient siRNA-loaded nanoparticle formulation processes.

Here, we sought to improve pharmacokinetics for tumor applications by developing a PEGylated nanopolyplex formulation that is core-stabilized by both electrostatic and hydrophobic interactions between the polymeric carrier and the siRNA cargo. We recently developed PEGylated, core-loaded siRNA nanopolyplexes (si-NPs) with a combination of both electrostatic and hydrophobic stabilization due to the optimized balance of cationic and hydrophobic content within the polymer block that forms the polyplex core[16]. These si-NP formulations comprised unmodified siRNA and the diblock polymer poly(ethylene glycol)-*b*-poly(dimethylaminoethyl methacrylate-*co*-butyl methacrylate) (PEG-*b*-p(DMAEMA-*co*-BMA)) with 50 mole percent of both cationic DMAEMA and hydrophobic BMA monomer in the core-forming block (polymer termed "50B"). Relative to the analogous PEG-*b*-p(DMAEMA) diblock polymer (termed "0B" and characterized by a fully cationic core), the 50B formulation exhibited improved resistance to disassembly by heparin sulfates, circulation time, and endosomal escape, as well as superior gene silencing bioactivity both *in vitro* and *in vivo*. Here, we utilized the 50B polymer for packaging and delivery of hydrophobized siRNA to evaluate the impact of providing both electrostatic and hydrophobic interactions between the polymeric carrier and the siRNA cargo.

To test the hypothesis that a combination of electrostatic and hydrophobic interactions between the 50B polymer and siRNA cargo increases formulation stability and performance, we compared pharmacokinetics and bioactivity of 50B-based nanopolyplexes loaded with unmodified siRNA to those loaded with siRNA conjugated to the hydrocarbon palmitic acid (PA). Conjugation of siRNA to lipid-like moieties (e.g. cholesterol, α-tocopherol, and palmitic acid) improves stability and enhances cellular uptake of siRNA by increasing the hydrophobicity of the siRNA molecule[290,301,302]. Furthermore, conjugation to hydrophobic molecules such as cholesterol or palmitic acid (PA) can make siRNA more effective when delivered via polymeric delivery carriers[283,287,302-304]. Similarly, incorporation of hydrophobic components into the polymer carrier has been proven to enhance polyplex stability and cellular uptake and transfection of unmodified nucleic acids[260,291,305-309]. The Kataoka group has specifically illustrated improvements in stability of a polyplex micelle delivery system via separate investigations into cholesterol modification of the siRNA molecule or micellar components. The approach in the current work is unique in that we investigate the interplay between hydrophobized siRNA and a partially hydrophobic polymer nanocarrier (50B), facilitating hydrophobic as well as electrostatic interactions between cargo and carrier. To isolate the pharmacokinetic significance of hydrophobic interactions between hydrophobized siRNA and the 50B polyplex core versus hydrophobization of each component individually, both the 0B (purely cationic) polymer and unmodified siRNA were used as controls for *in vivo* pharmacokinetics studies. This experimental design elucidates the functional benefit of dual hydrophobization for improving *in vivo* stability and target gene silencing in an orthotopic triple negative breast cancer (MDA-MB-231) model.

Materials and Methods

Amine-modified single-stranded DNA (modification at 5' end) or RNA (modification at 3' end) and complementary single-stranded Cy5-, Alexa Fluor 488- or Alexa Fluor 546-modified DNA or unmodified RNA were all obtained from Integrated DNA Technologies (Coralville, Iowa). The pGreenFire1-CMV plasmid was obtained from System Biosciences (Mountain View, CA), and packaging plasmids pMDLg/pRRE, pRSV-Rev, and pMD2.G were purchased from Addgene (Cambridge, MA). Lipofectamine 2000 and NucBlue Fixed Cell ReadyProbes were purchased from Life Technologies (Grand Island, NY). CytoTox-ONE Homogeneous Membrane Integrity Assay (a lactate dehydrogenase (LDH) assay) was purchased from Promega (Madison, WI). PD10 desalting columns were purchased from GE Healthcare (Waukesha, WI). Quant-iT RiboGreen RNA Assay Kit was purchased from ThermoFisher Scientific (Waltham, MA). All other reagents were purchased from Sigma-Aldrich (St. Louis, MO).

The RAFT chain transfer agent ECT was synthesized as previously described, and the R-group of the CTA was subsequently conjugated to PEG[10,265]. Briefly, dicyclohexylcarbodimide (4 mmol, 0.82 g) was added to the stirring solution of monomethoxy-poly(ethylene glycol) (Mn = 5000, 2 mmol, 10 g), ECT (4 mmol, 1.045 g), and DMAP (10 mg) in 50 mL of dichloromethane. The reaction mixture was stirred for 48 h. The precipitated cyclohexyl urea was removed by filtration, and the dichloromethanane layer was concentrated and precipitated into diethyl ether twice. The precipitated PEG-ECT was washed three times with diethyl ether and dried under vacuum (yield ~10g). ^{1}H-NMR (400 MHz $CdCl_3$) revealed 91% substitution of the PEG (data not shown)[16].

RAFT polymerization was used to synthesize a 50:50 [BMA]:[DMAEMA] copolymer using the PEG-ECT macro-CTA. The target degree of polymerization was 160, and the monomer

plus CTA was 40% weight per volume in dioxane. The polymerization reaction was carried out at 70^{o}C for 24 hours using AIBN as the initiator with a 5:1 [CTA]:[Initiator] molar ratio. A monomer feed ratio of 50:50 mol % or 0:100 mol % [BMA]:[DMAEMA] was used (to generate 50B and 0B respectively), and a double alumna column was utilized to remove inhibitors from DMAEMA and BMA monomers prior to polymerization. The reactions were stopped by removal from heat and exposure of the polymerization solution to air. The resulting polymers were precipitated into a co-solvent of 90% pentane and 10% diethyl ether. The isolated polymers were vacuum-dried, redissolved in water, further purified by dialysis for 24 hours, and lyophilized. Polymers were characterized for composition and molecular weight by ^{1}H-NMR spectroscopy (Bruker 400 MHz spectrometer equipped with a 9.4 T Oxford magnet). Absolute molecular weight and polydispersity of the polymers was determined using DMF mobile phase gel permeation chromatography (GPC, Agilent Technologies, Santa Clara, CA, USA) with inline Agilent refractive index and Wyatt miniDAWN TREOS light scattering detectors (Wyatt Technology Corp., Santa Barabara, CA, USA).

Single-stranded amine-modified oligo was reacted with 100-fold molar excess of PA *N*-hydroxysuccinimide ester pre-dissolved at 40 mM in *N*,*N*-dimethylformamide (DMF). The reaction was carried out for 18 hours at room temperature in 45% water, 45% isopropyl alcohol, and 10% DMF. The oligo-PA was purified by reversed-phase HPLC using a Clarity Oligo-RP column (Phenomenex, Torrence, CA) under a linear gradient from 95% water (50 mM triethylammonium acetate), 5% methanol to 100% methanol. The conjugate molecular weight was confirmed using MALDI-TOF mass spectrometry (Voyager-DE STR Workstation, Grand Island, NY) using 50 mg/mL 3-hydroxypicolinic acid in 50% water, 50% acetonitrile with 5 mg/mL ammonium citrate as a matrix. The yield of the oligo-PA was quantified based on absorbance at

260 nm. The purified oligo-PA was annealed to its complementary strand to generate Cy5-, Alexa Fluor 488- or Alexa Fluor 546-modified DNA-PA or siPA. Conjugation and annealing was also confirmed via agarose gel electrophoresis.

Polyplex NPs loaded with siRNA (si-NPs) or siPA (siPA-NPs) were made by mixing pH 4.0 stock solutions of 50B polymer (10 mM buffer, 3.33 mg/mL polymer) and siRNA (50 μM) at N:P ratios of 1, 2, 5, 7, 10, or 20. Control polyplexes comprising the 0B polymer (termed si-0B-NPs and siPA-0B-NPs) were made according to the same procedure. The final charge ratio was calculated as the molar ratio of cationic amines on the DMAEMA (50% are assumed to be protonated at physiologic pH) to the anionic phosphates on the siRNA/siPA. After mixing, these solutions were diluted 5-fold to 100 μL with pH 8.0 phosphate buffer (10 mM) to adjust the final pH to 7.4. After mixing, samples were incubated for 30 min, and 100 ng of siRNA/siPA for each sample was loaded onto a 2% agarose gel containing ethidium bromide to assess siRNA/siPA packaging efficiency. The gels were run at 100 V for 35 min and imaged with a UV transilluminator. Hydrodynamic diameter and zeta potential of the polyplex NPs at the N:P ratios described above were measured in triplicate using dynamic light scattering (DLS) (Malvern Zetasizer Nano ZS, Malvern, UK). DLS measures were used to evaluate salt stability of polyplex NPs; concentrated NaCl solution was added to si-NP or siPA-NP solutions in 10 mM phosphate buffer to yield final NaCl concentrations of 0, 0.1, 0.5, or 1 M where the final solution was 80% phosphate buffer by volume. For the cell uptake studies (where no functional effects were studied) DNA and DNA-PA was used as a model molecule for siRNA and siPA, respectively. Hereafter, NPs loaded with these molecules are referred to as si-NPs and siPA-NPs to avoid confusion.

Human epithelial breast cancer cells (MDA-MB-231) were cultured in Dulbecco's modified Eagle's medium (DMEM, Gibco Cell Culture, Carlsbad, CA) supplemented with 10% fetal bovine serum (FBS, Gibco) and 0.1% gentamicin (Gibco).

To produce lentivirus, the pGreenFire1-CMV plasmid and packaging plasmids pMDLg/pRRE, pRSV-Rev, and pMD2.G were transfected into HEK-293Ts using Lipofectamine 2000. Media was changed after 24 hours and supernatant containing lentivirus was collected at 48 and 72 hours. Viral supernatant was added directly to MDA-MB-231s with 6 μg/mL polybrene. Media was changed after 24 hours. Lentiviral transduction and was confirmed by GFP expression as analyzed by flow cytometry (BD LSR II Flow Cytometer, San Jose, CA). This was followed by selection with 8 μg/mL puromycin for two weeks to eliminate non-transduced cells.

MDA-MB-231s were seeded at 30,000 cells/well in 24-well plates and allowed to adhere overnight. After adhering, cells were treated with 100 nM Alexa Fluor 488-labeled si-NPs or siPA-NPs in 10% serum for 24 hours. Lipofectamine was used as a positive control (with treatment at 25 nM to minimize toxicity). After 24 h, media with treatments was removed, cells were washed with PBS (-/-), trypsinized (0.25%), transferred to microcentrifuge tubes, and centrifuged at 420xG for 7 min to pellet the cells. Pellets were re-suspended in 0.4 mL PBS(-/-) with 0.04% trypan blue to quench extracellular fluorescence and monitored by FACS (FACSCalibur, BD Biosciences, Franklin Lakes, NJ, USA) at excitation wavelength of 488 nm and emission wavelength of 519 nm to quantify intracellular delivery.

MDA-MB-231s were treated with si-NPs or siPA-NPs; the siRNA was either designed against the luciferase gene (luc siRNA) or was a scrambled sequence (scr siRNA). Cells were seeded at 2,000 cells/well in 96-well black-walled plates and allowed to adhere overnight. Cells were then treated in 10% serum for 24 hours at a dose of 100 nM siRNA. After 24 h, media was

replaced with luciferin-containing media (150 μg/mL) before imaging with an IVIS Lumina III imaging system (Caliper Life Sciences, Hopkinton, Massachusetts) every 24 hours for 10 days. Fresh low serum media (2% FBS) was replaced after each imaging session, and cells were passaged every 3 days. Growth in low serum was used to reduce the confounding influence of proliferation and allowed more direct investigation of gene silencing longevity. To evaluate treatment cytotoxicity, scr siRNA si-NP treatments were removed at 24 hours and cellular bioluminescence was quantified on a Lumina III IVIS (Caliper Life Sciences, Hopkinton, Massachusetts) and compared to no treatment as a measure of relative cell number.

NPs were loaded with Förster Resonance Energy Transfer (FRET, using Alexa Fluor 488 and Alexa Fluor 546) pair-labeled doubled-stranded 23mers (FRET-NPs). Fluorescent intensity was measured using a microplate reader (Tecan Infinite F500, Männedorf, Switzerland) with an excitation wavelength of 488 ± 5 nm. Alexa Fluor 488 emission was collected at 519 ± 5 nm, and Alexa Fluor 546 emission was obtained at 573 ± 5 nm. FRET was calculated as a ratio of the fluorescent intensity as follows:

(3.1) $$\text{FRET} = \frac{I_{573}}{I_{519}}$$

Because siRNA decomplexation by heparan sulfate-containing glomerular basement membrane in the kidney is a primary cause for rapid systemic clearance of polycation-siRNA nanoparticles, the stability of FRET-NPs was measured in the presence of 2 to 100 U/mL of heparin sodium salt in DPBS[218,220]. The fluorescence emission was measured over time following addition of heparin sodium salt. The heparin concentration at which the FRET signal was reduced 50% (EC50) for siRNA and siPA polyplexes was calculated as according to the following equation where y is the FRET ratio, x is the heparin concentration, and b is a fit parameter.

(3.2) $$y = \frac{-1}{1+\left(\frac{x}{EC50}\right)^{b}} + 1$$

The same assay was performed in the presence or absence of 10, 40, and 50% of FBS as well. In this study, si-NPs and siPA-NPs were prepared as described above and incubated with either FBS or an equal volume of PBS. FRET was calculated according to the equation above, and %FRET was calculated at each time point by dividing the FRET ratio of FBS-treated NPs by PBS-treated controls. The Quant-iT RiboGreen RNA Assay Kit was used to quantify the amount of unpackaged siRNA before and after addition of 100 U/mL heparin for si-NPs, siPA-NPs, si-0B-NPs, and siPA-0B-NPs.

Fluorescent (Cy-5-labeled) si-NPs and siPA-NPs were formed at an N:P ratio of 10:1 As a comparison, siRNA and siPA were loaded into 0B at a ratio of 10:1. NPs were injected into the tail vein of CD-1 mice (4-6 weeks old, Charles Rivers Laboratories, Wilmington, MA, USA) at 1 mg/kg. Blood was collected retro-orbitally at 5 min and 10 min post-injection, not exceeding two collections per animal. After 20 min, animals were sacrificed, and blood was immediately collected via cardiac puncture. Blood samples were centrifuged at 2000 G for 5 min and 5 μL of plasma was taken from the supernatant and diluted into 95 μL PBS (-/-). Fluorescence was measured and quantified on an IVIS Lumina III imaging system (Xenogen Corporation, Alameda, CA, USA) at excitation wavelength of 620 ± 5 nm and emission wavelength of 670 ± 5 nm (n = 6). A standard curve was generated by measuring the fluorescence of the initial fluorescent polyplex solution in PBS (-/-) over the range of 200% to 1.5% of the injected dose. The standard curve was utilized in order to calculate the percent of injected dose in each blood sample, and the calculated values were used to determine siRNA concentration in the plasma at each time point as well as area under the curve (AUC) values (see Table S1 for equations).

Athymic nude female mice (4-6 weeks old, Jackson Laboratory, Bar Harbor, ME, USA) were injected in each mammary fat pad with 1 x 10^6 MDA-MB-231 cells in DMEM:Matrigel

(50:50). After 17 days, tumor-bearing mice were injected via the tail vein with 1 mg/kg (nucleic acid dose) of fluorescent siNPs or siPA-NPs. After 20 minutes, animals were sacrificed and the organs of interest (heart, lungs, liver, spleen, kidneys, and tumors) were excised. The fluorescence intensity in the organs was quantified on an IVIS Lumina III imaging system (Xenogen Corporation, Alameda, CA, USA) at excitation wavelength of 620 ± 5 nm and emission wavelength of 670 ± 5 nm (n = 3 animals, n = 6 tumors).

Athymic nude female mice (4-6 weeks old, Jackson Laboratory, Bar Harbor, ME, USA) were injected in each mammary fat pad with 1 x 10^6 MDA-MB-231 cells in DMEM:Matrigel (50:50). After 17 days, tumor-bearing mice were injected i.p. with luciferin substrate (150 mg/kg) and imaged for bioluminescence on an IVIS Lumina III imaging system (Xenogen Corporation, Alameda, CA, USA) 20 minutes post-injection. Next, the mice were injected via the tail vein with 1 mg/kg (siRNA dose) NPs containing either luc siRNA / siPA, a scr siRNA / siPA, or saline. Mice were imaged and treated at days 17 and 18 following tumor cell inoculation and imaged on day 19. Relative luminescence was determined by measuring the raw luminescent intensity of each tumor on each day and comparing to the initial signal at day 17 (n =10 tumors per group).

Tumor-bearing mice used for *in vivo* luciferase silencing studies were sacrificed on day 20 following tumor cell inoculation (and following treatment with 1 mg/kg siRNA on days 17 and 18). Blood was collected by cardiac puncture and then centrifuged at 2000 G for 5 min. Then, plasma was harvested and tested by the Vanderbilt Translational Pathology Shared Resource (TPSR) for systemic levels of alanine aminotransferase (ALT), aspartate aminotransferase (AST), and blood urea nitrogen (BUN).

The treatment groups were statistically compared using a one-way ANOVA test coupled with a Tukey means comparison test; a p-value < 0.05 was deemed representative of a significant

difference between groups. For all data shown, the arithmetic mean and standard error are reported, and the sample size (n) is indicated.

The animal studies were conducted with adherence to the guidelines for the care and use of laboratory animals of the National Institutes of Health (NIH). All experiments with animals were approved by Vanderbilt University's Institutional Animal Care and Use Committee (IACUC).

Results and Discussion

A previously reported RAFT polymerization scheme was used to synthesize the 50B polymer from a 5 kDa PEG-ECT macro-CTA[16]. The scheme is desirable for its simplicity and scalability, and it consistently yields polymers at target molecular weight (MW) with low polydispersity index (PDI). The 50B polymer used here was synthesized from the macro-CTA with a final degree of polymerization (DP) of 152 (Target DP: 160) and PDI of 1.03 as determined by ^{1}H-NMR and GPC, respectively (**Figure 3.1**). The RAFT-polymerized block monomer composition and MW were quantified by ^{1}H-NMR using characteristic peaks from PEG (-O-C$\mathbf{H_2}$C$\mathbf{H_2}$-, δ 3.65s), BMA (-O-C$\mathbf{H_2}$CH$_2$-, δ 3.95s), and DMAEMA (-O-C$\mathbf{H_2}$CH$_2$-, δ 4.05s), showing 49:51 (BMA:DMAEMA) mol% ratio in the polyplex core-forming block and total MW of 27,800 Da (including 5kDa PEG; **Supplementary Figure C.1**). The control 0B polymer was synthesized by the same 5route and had a 110 DP, 1.16 PDI, 0:100 mol% ratio, an0 d 22,300 Da MW (data not shown).

Single-stranded DNA or RNA was successfully conjugated with PA in a one-step reaction and purified from the reactants via HPLC. Isolation of the desired products was confirmed by MALDI-TOF analysis (**Figure 3.1**) and also by shift upward of the free siPA band in comparison to the unmodified siRNA band in a gel retardation assay (**Figure 3.2**).

Unmodified siRNA completely loaded into the PEGylated nanopolyplexes at an N:P ratio of 20:1, while siPA was fully loaded at a ratio of 5:1, as characterized by gel retardation assays (**Figure 3.2a**). This result suggests that hydrophobization of the siRNA molecule enhances interactions with 50B and improves efficiency of loading into NPs. DLS measurements reveal that siPA-NPs are of equivalent size and exhibit enhanced stability to elevated salt concentration relative to si-NPs (**Figure 3.2b and Supplementary Figure C.2**). The zeta potential does not differ significantly between siPA-NPs and si-NPs, with each displaying a slight negative charge which is optimal for intravenous administration (data not shown).

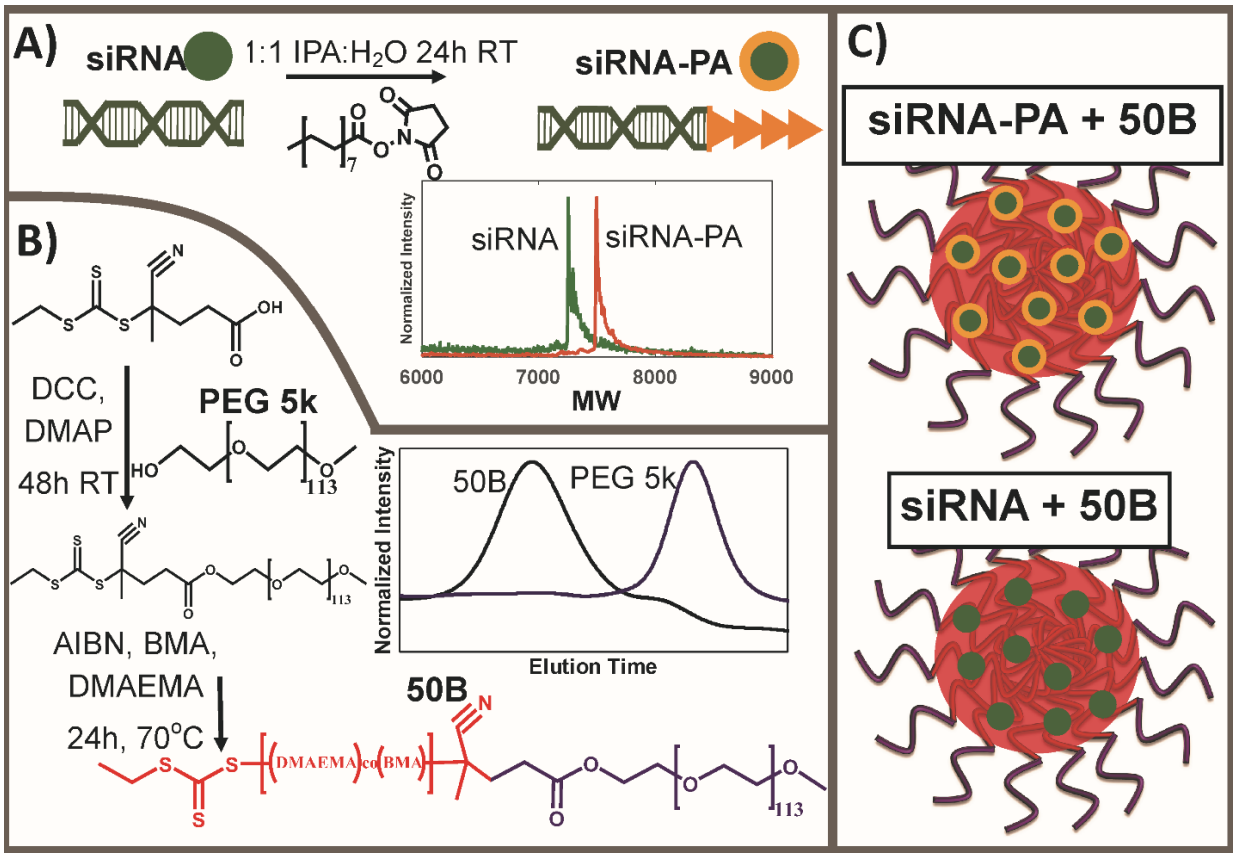

Figure 3.1) Generation of si-NPs and siPA-NPs. (A) Synthesis of siPA and product confirmation via MALDI-TOF. (B) Synthesis of 50B and GPC analysis. (C) Schematic of core-loaded siPA-NP and si-NP polyplexes.

This result is in agreement with previous reports from our group and others showing that lipid-modified siRNA loads more efficiently into nanocarrier systems with completely electrostatically-driven siRNA complexation mechanisms[283,304,310]. However, the siPA-NP system is unique in that it is the first to elucidate the importance of hydrophobic interactions between lipid-modified siRNA and hydrophobized cationic polymer components. We posit that the hydrophobization of the siRNA stabilizes the nanoparticles by introducing interaction between the lipophilic moieties on different siRNA molecules and, unique to the siPA-NPs, with the hydrophobic BMA monomer which is ~50 mol% of the core-forming block of the carrier polymer in the current system. This overall result indicates that a combination of electrostatic and hydrophobic interactions between siPA and 50B improved its

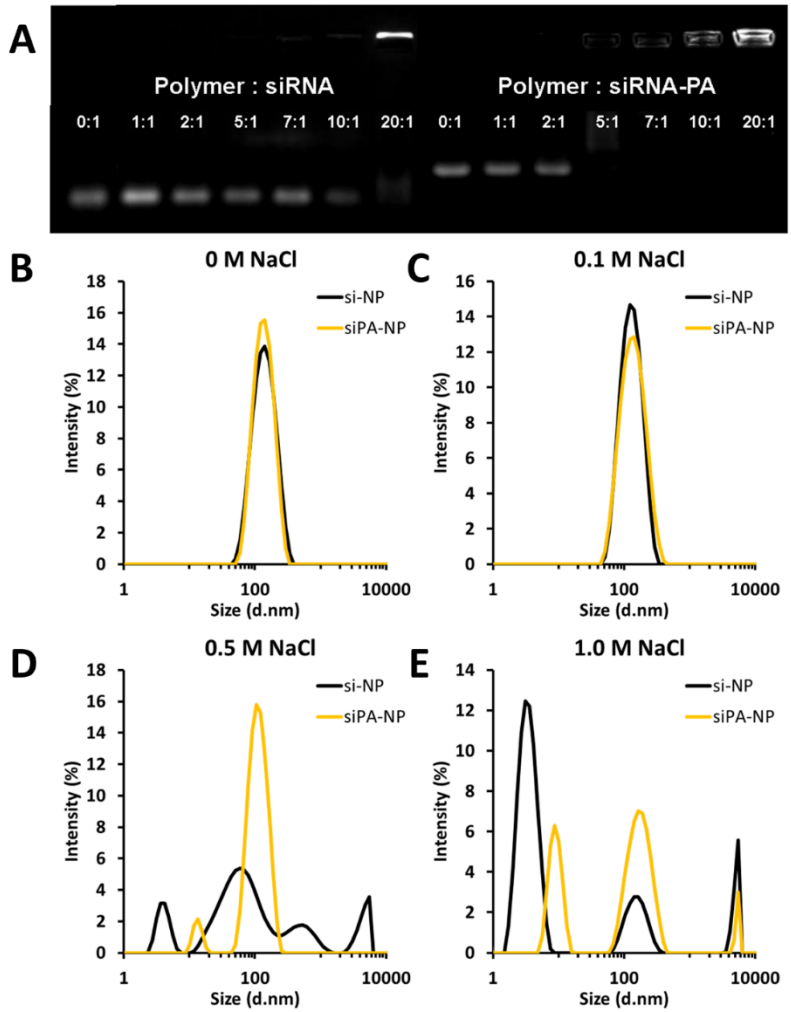

Figure 3.2) siPA is packaged more efficiently and stably with 50B polymer than unmodified siRNA. (A) As evaluated by gel retardation assay, siPA loads fully at a lower N:P ratio than unmodified siRNA; note that the upward shift of siPA compared to siRNA also confirms PA conjugation. (B-D) As evaluated by dynamic light scattering, siPA-NPs are more stable to elevated salt concentrations than si-NPs at N:P = 10:1.

loading efficiency and stability in the presence of competing polyelectrolytes (akin to those encountered in systemic administration), motivating further characterization of the stability and function of siPA-NPs in biological contexts.

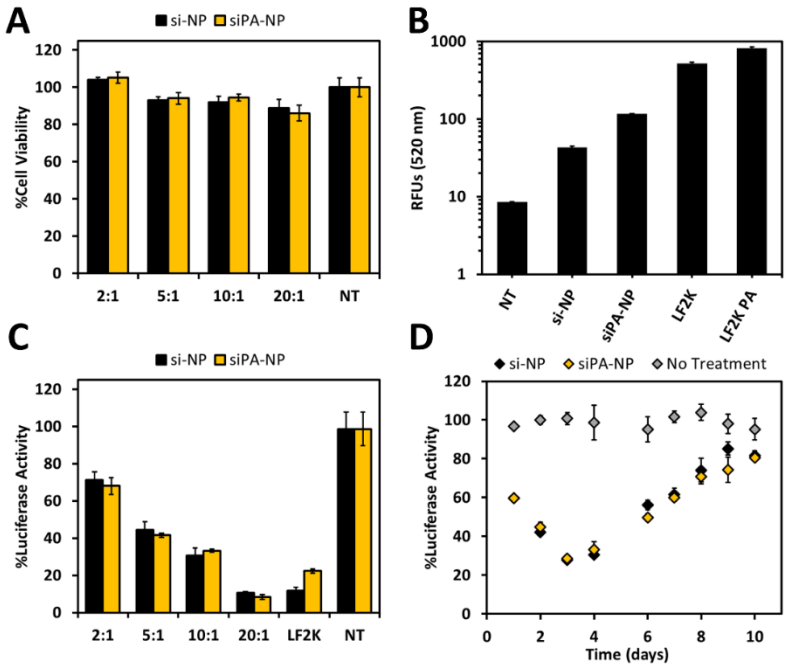

Figure 3.3) *In vitro* characterization of siPA-NPs vs. si-NPs. (A) Both formulations exhibit >80% cell viability at all N:P ratios investigated as evaluated by percent difference in luciferase signal from that of no treatment (n = 4). (B) siPA-NPs are internalized by cells ~2-fold more than si-NPs after 24 hours of treatment (N:P = 10:1, n = 3). (C) siPA-NPs and si-NPs exhibit increasing luciferase silencing at higher N:P ratios but are not significantly different from each other. (n = 4). (D) Both siPA-NPs and si-NPs show prolonged luciferase silencing (over 10 days) at an N:P ratio of 10:1 (n = 3). For (C) and (D), all treatment groups are normalized to analogous scrambled siRNA controls to account for treatment effect on cell viability; no treatment is averaged each day by measuring luminescent signal of untreated cells (n = 3).

After establishing the improved loading efficiency of siPA relative to unmodified siRNA, we characterized the performance of si-NPs and siPA-NPs *in vitro* (**Figure 3.3**). Evaluation of the cytotoxicity of each demonstrated greater than 80% cell viability at all N:P ratios examined after 24 h (**Figure 3.3a**), with a trend toward decreased cell number for higher N:P ratios. This result confirms that the nanopolyplex system is generally well-tolerated but also emphasizes the translational significance of reducing the amount of polymer necessary to achieve a therapeutic effect, for example through improved siRNA loading and delivery using a lower N:P ratio.

Next, the cellular uptake of siPA-NPs was compared to si-NPs. After treatment with siPA-NPs, nearly 100% of cells were positive for the fluorescently-tagged nucleic acid (**Supplementary Figure C.3**). This was equivalent to the percentage positive cells observed after treatment with Lipofectamine® 2000, a commercial transfection reagent. The corresponding treatment of si-NPs resulted in a cell population 60% positive (**Supplementary Figure C.3**), revealing that PA conjugation increased NP cellular internalization. This is corroborated by evaluation of the mean fluorescent intensity of treated cells, which was approximately 2-fold higher for siPA-NPs compared to si-NPs (**Figure 3.3b**). Many physicochemical and biological factors such as particle size[311,312], surface charge[311], shape[313], PEG density[314], particle elasticity[315], internalization and trafficking route[316,317], etc., can contribute to differences in particle uptake. In our studies, the most obvious difference between the si-NPs and siPA-NPs was enhanced stability of siPA-NPs in the presence of serum (**Supplementary Figure C.4**). Therefore, it is likely that increased siPA-NP stability in the presence of serum contributes to the observed improvement in uptake, although this result may be multifactorial.

In *in vitro* gene knockdown screens, the si-NPs and siPA-NPs both exhibited potent and sustained silencing in MDA-MB-231 breast cancer cells (**Figure 3.3c, d**). For each, a higher level of gene silencing was observed as the N:P ratio was increased. Silencing between si-NPs and siPA-NPs did not differ significantly across the N:P ratios screened, despite the small increase in cell uptake observed for siPA-NPs. This could be due to the enhanced stability of the siPA-NPs, which may impede siRNA unpackaging from nanopolyplexes upon cellular internalization[318]. Although increased polyplex stability may limit siRNA intracellular bioavailability *in vitro*, this potentially negative impact is expected to be outweighed by the benefit gained *in vivo* by increasing circulation half-life and cell uptake. Also of note is the prolonged silencing effect observed in this

nanoparticle system, using both unmodified siRNA and siPA (**Figure 3.3d**). A potential factor in this sustained effect *in vitro* is the inherent endosomolytic capability of the 50B polymer carrier; by avoiding endosomal degradation and/or trafficking from the cell, endosomolytic carriers have been shown to elicit desirable durability of therapeutic action[319]. The prolonged effect of si-NPs and siPA-NPs *in vitro*, with significant silencing out to 10 days post-treatment, suggests that this delivery system achieves a sustained effect that would minimize the need for repeat dosing.

Targeting siRNA nanoparticles to cancer targets such as solid tumors *in vivo* is contingent upon the ability to avoid rapid clearance by the liver (phagocytosis) and kidneys (polyanionic disassembly), which extends circulation time and consequently passive tumor uptake by the EPR effect. Disassembly in the kidney, leading to clearance through the urine, is especially detrimental to siRNA polyplex circulation time[218]. We showed previously that 50B-based si-NPs, which have balanced cationic and hydrophobic character in the polymeric block that forms the polyplex core, are more resilient to heparan sulfate disassembly and have longer circulation than strictly cationic analogues[16]. These si-NPs are used as a benchmark to compare siPA-NPs which incorporate hydrophobicity into both the polymer backbone and siRNA molecule.

The siPA-NPs have increased stability upon exposure to heparin compared to si-NPs as monitored by %FRET over time. Neither si-NPs nor siPA-NPs had reduced %FRET in the presence of 2 U/mL heparin, a dose which was previously used to completely disassemble strictly cationic polyplexes (**Supplementary Figure C.5**)[16]. At each dose increasing from 10 – 90 U/mL heparin, siPA-NPs retained higher %FRET compared to si-NPs throughout the entire time course (180 min) (**Figure 3.4a and Supplementary Figure C.5**). Only at the highest heparin dose (100 U/mL) did siPA-NPs and si-NPs have similar kinetics of reduction in %FRET over 180 min. An EC_{50} (indicative of the half maximal concentration of heparin necessary to dissociate polyplexes)

was calculated at multiple time points (30, 60, 90, 120, 150, and 180 min) in order to quantify the dose response of heparin-dependent disassembly observed over time. The EC_{50} of siPA-NPs was ~2-fold greater than that of si-NPs at each time point analyzed (**Supplementary Table C.2**), meaning that double the concentration of heparin was required to disassemble siPA-NPs and suggesting that added hydrophobicity of siPA conjugates within siPA-NPs provide increased stability upon exposure to polyanionic challenge such as by heparin sulfates found within the GBM.

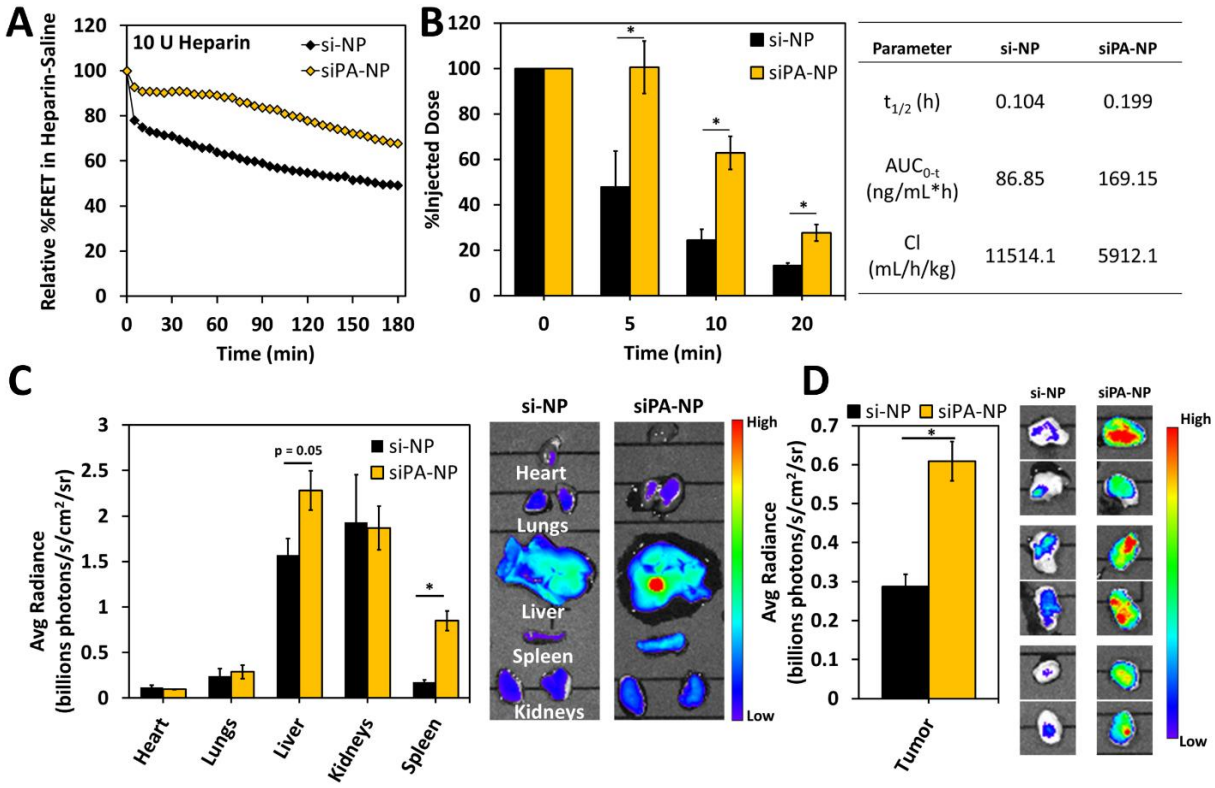

Figure 3.4) Higher stability of siPA-NPs relative to si-NPs corresponds to greater circulation time and increased accumulation in tumor tissue. (A) siPA-NPs are more stable than si-NPs in the presence of heparin, as evaluated by FRET measurements. (B) siPA-NPs injected intravenously in mice have a longer circulation half-life than si-NPs. (C, D) siPA-NPs accumulate more in tumor tissue and in the MPS organs (liver and spleen) than si-NPs in a mouse tumor model at 20 minutes following tail vein injection.

In blood pharmacokinetics experiments, increased fluorescence was detected within blood samples collected at each time point (5, 10, and 20 min) from siPA-NPs compared to si-NPs

(**Figure 3.4b**). The calculated circulation half-life of siPA-NPs (0.199 h) was ~2-fold greater than si-NPs (0.104 h), resulting in ~2-fold increase in area under the curve (AUC), and ~2 fold decrease in blood clearance (CL) (**Figure 3.4b**). The observation of increased circulation persistence is especially important due to its correlation with passive tumor accumulation, which was studied in athymic nude mice bearing orthotopic xenografts of MDA-MB-231 triple negative breast cancer cells in the mammary fat pad. Biodistribution in major organs of interest (heart, lungs, liver, kidneys, and spleen) after i.v. administration of 1 mg/kg nanoparticles (siRNA dose) was comparable between siPA-NPs and si-NPs (**Figure 3.4c**). As a result of decreased renal clearance and consequent increased exposure to other organs and tissues, the siPA-NPs exhibited higher levels of uptake within MPS organs (liver and spleen) than si-NPs. Importantly, a 2-fold increase in tumor uptake was observed by siPA-NPs (**Figure 3.4d**), confirming that increased circulation time of siPA-NPs translated to increased EPR-based passive tumor uptake. Commonly, active targeting ligands such as folic acid, hyaluronic acid, RGD peptide, or transferrin, are used as a strategy to increase tumor uptake and retention after i.v. administration[37,39,222,320-322]. Herein, tumor uptake was increased by tuning the core chemistry of polyplexes to increase polyplex stability and circulation time. Thus, it is expected that the addition of appropriate targeting ligands in the future will further increase tumor concentration due to improved tumor retention.

The in-depth studies above thoroughly compare the impact of PA-modified vs. unmodified siRNA with the hydrophobized 50B carrier. Conjugation of alkyl chains similar to PA has also been explored as a strategy to improve pharmacokinetics of therapeutics delivered carrier-free by leveraging lipid binding to serum proteins[323]. However, a comprehensive evaluation of lipid-modified siRNAs reveals that PA modification is insufficient to elicit serum protein binding and gene silencing[324]. Based on this prior work, we attributed the pharmacokinetic improvement of

siPA-NPs over si-NPs to their enhanced stability due to the impact of the hydrophobic interactions between the PA-modified siRNA and the hydrophobized 50B carrier. To confirm this, we ran a set of control experiments using the fully cationic polymeric carrier 0B. We investigated si-0B-NPs and siPA-0B-NPs in a subset of studies to rule out the possibility that our observations were driven solely by hydrophobization of the siRNA. The degree of siRNA unpackaging in the presence of heparin was evaluated for si-NPs, siPA-NPs, si-0B-NPs, siPA-0B-NPs. In accordance with previous reports si-NPs and siPA-NPs were more stable in response to heparin than si-0B-NPs and siPA-0B-NPs. siPA-NPs showed an additional enhancement in stability relative to si-NPs that was not observed in si-0B-NPs vs. siPA-0B-NPs (**Supplementary Figure C.6**). Significantly, 0B polyplexes loaded with siPA did not show any increase in blood circulation half-life relative to 0B polyplexes loaded with unmodified siRNA, while siPA increased circulation time approximately 2-fold relative to unmodified siRNA in 50B polyplexes (**Supplementary Figure C.7**). These data confirm that the hydrophobic interactions between siPA and the BMA of the 50B NP core are critical to the enhanced stability and circulation time observed for siPA-NPs.

To measure the impact of the improved pharmacokinetics of siPA-NPs on tumor bioactivity, the *in vivo* bioluminescence was tracked in mice bearing luciferase-expressing MDA-MB-231 orthotopic xenografts of the mammary fat pad after i.v. injection (1mg/kg siRNA dose) on days 17 and 18 after transplantation. The relative luminescence measured by intravital imaging increased steadily over 48 h (up to 2.5-fold) in mice administered saline, si-NP scrambled, and siPA-NP scrambled. Mice administered luciferase si-NPs did not show a treatment response after the first day, but they showed significant reduction in bioluminescence at 48 hours (after 2 consecutive treatments). The mice administered siPA-NPs showed a treatment response at both 24 h (after 1 treatment) and 48 h (after 2 consecutive treatments), with significant decreases in

bioluminescence compared to saline and scrambled controls (**Figure 3.5a**). Moreover, the bioluminescence of mice administered siPA-NPs did not significantly increase above the baseline measure at 0 h throughout the time course, indicating complete inhibition of luminescence associated with tumor growth over the 48 h treatment protocol. These data strongly support the effectiveness of siPA-NPs for tumor target gene silencing after i.v. administration and confirms the functional significance of the increased stability, circulation time, and tumor uptake of siPA-NPs. This increase in efficacy is expected to be impactful for knockdown of pathological genes, with these results suggesting that siPA-NPs would achieve a therapeutic response with a lower dose or fewer administrations relative to si-NPs.

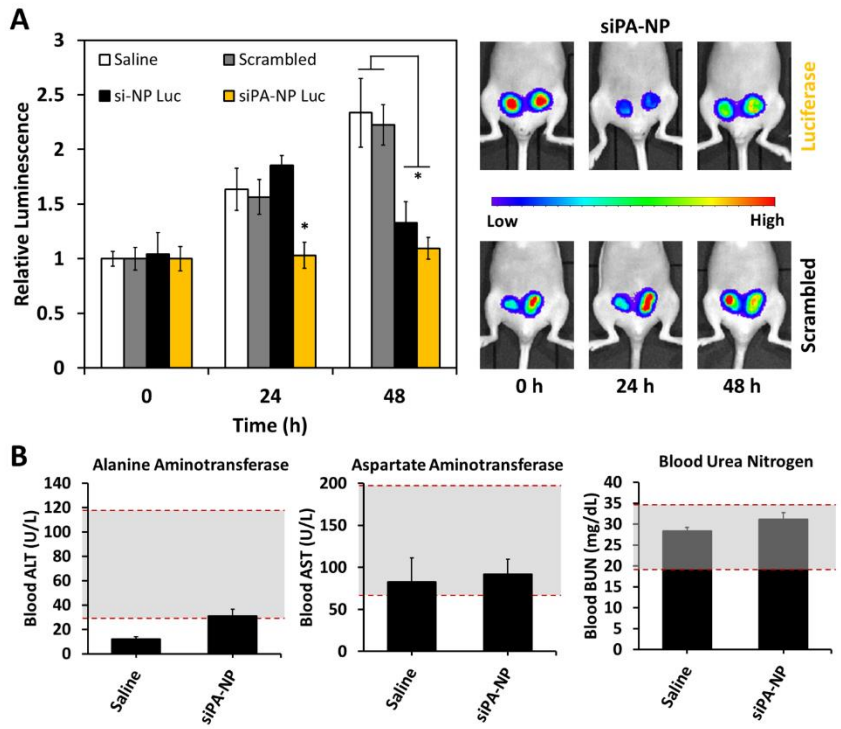

Figure 3.5) siPA-NPs delivered intravenously silence luciferase in an orthotopic MDA-MB-231 tumor model more effectively than si-NPs and cause no significant liver and kidney toxicity. (A) Luciferase silencing, compared to scrambled siRNA controls. (B) Measurements of liver (ALT and AST) and kidney (BUN) toxicity for si-NP and siPA-NPs 48 h after treatments.

Because there was significant accumulation of siPA-NPs in the liver and kidneys, ALT and AST (indicators of liver function / toxicity) and BUN (indicator of kidney function / toxicity) were assessed in the treated mice. Blood collected from mice at the time of euthanasia (48 h after the last treatment) showed that systemic levels of ALT,

AST, and BUN were not significantly elevated by the treatment protocol of si-NPs or siPA-NPs utilized. ALT and AST was increased in si-NPs above the mean levels of saline and siPA-NPs, but the increase was not statistically significant (**Figure 3.5b**).

Conclusions

The performance of PEG-*b*-p(DMAEMA-*co*-BMA) "50B", which forms siRNA-loaded NPs with balanced cationic and hydrophobic core content, can be improved through pairing with siPA hydrophobized siRNA. The hydrophobicity of both the polymer and siPA molecule was essential to improved polyplex stability, which can be attributed to increased van der Waals interactions between carrier and cargo. These interactions facilitated more efficient siPA loading into NPs and siPA-NP polyplexes were also more resilient to heparan sulfate-induced destabilization. Increased siPA-NP stability, when compared to our benchmark si-NPs, resulted in increased blood circulation time and EPR-driven passive uptake into orthotopic tumor xenografts after intravenous polyplex injections. The enhanced pharmacokinetics of siPA-NPs translated to increased bioactivity of siRNA, as assessed by target gene silencing of the model gene luciferase within orthotopic triple negative breast cancer (MDA-MB-231) tumors. Our results demonstrate that increasing the strength of associative forces, rather than solely utilizing electrostatic forces that are traditionally leveraged to drive polyplex assembly, can increase both polyplex stability and bioactivity *in vivo*. The data support continued efforts to stabilize siRNA NP systems to improve pharmacokinetics and pharmacodynamics of siRNA and increase clinical translatability for cancer applications.

CHAPTER IV

SELECTIVE INHIBITION OF MTORC2, WITHOUT INHIBITING MTORC1, THROUGH RNA INTERFERENCE IN MODELS OF HER2-AMPLIFIED BREAST CANCER.

Text for Chapter IV taken from:

TA Werfel, DM Brantley-Sieders, S Wang, MA Jackson, TE Kavanaugh, M Morrison Joly, DJ Hicks, VM Sanchez, L Lee, SC Dimobi, SM Sarett, RS Cook, CL Duvall. Selective mTORC2 Inhibition, without mTORC1 Inhibition, Using RNAi Nanomedicine In Vivo Provides Therapeutic Anti-Tumor Benefit.

Abstract

The PI3K/Akt/mTOR signaling cascade is dysregulated in over 60% of breast cancers across all three major clinical subtypes. There is mounting evidence that, within this pathway, mTORC2 plays a unique role in driving tumor cell survival, driving therapeutic resistance to cancer-targeted therapies through re-activation of Akt signaling. Importantly, mTOR-mediated therapeutic resistance was shown to be dependent upon mTORC2, but not mTORC1, in HER2-amplified breast cancers. Although mTORC1/2 dual kinase inhibitors exist, no current therapeutics selectively inhibit mTORC2 while sparing mTORC1. Here, specific mTORC2 therapy was enabled by genetic inhibition of the previously 'undruggable' molecule Rictor, which serves as an obligate and specific co-factor of the mTORC2 complex. Genetic Rictor inhibition was accomplished using ternary siRNA polyplexes (si-NPs), optimized to achieve potent endosomolysis, si-NP stability in plasma, persistence of the si-NP in circulation, and efficient siRNA delivery to solid breast tumors *in vivo*. Ternary si-NPs loaded with Rictor siRNA robustly

decreased Rictor protein expression, mTORC2 signaling, and tumor growth in HER2+ breast cancers through the induction of cell death. When combined with the HER2 tyrosine kinase inhibitor, lapatinib, Rictor-targeted si-NPs impaired Akt phosphorylation, tumor cell survival, and tumor growth to a greater extent that either agent used alone. These data demonstrate the previously elusive selective modulation of mTORC2 in a therapeutic setting, underscoring the potential utility of this approach for personalized molecular medicine, and highlighting the idea that selective mTORC2 targeting is both feasible and efficacious in HER2-amplified breast cancers.

Introduction

Breast cancer is the most prevalent malignancy and the second leading cause of cancer-related deaths among Western women. Approximately 20% of breast cancers overexpress human epithelial growth factor receptor 2 (HER2), which activates the phosphatidyl inositol-3-kinase (PI3K)/Akt/mechanistic target of rapamycin (mTOR) signaling cascade that drives tumor cell growth, survival, metabolism, and motility[325]. Targeting HER2 therapeutically using trastuzumab or tyrosine kinase inhibitors (TKIs; *e.g.*, lapatinib, neratinib) inhibits PI3K/Akt/mTOR signaling and decreases growth and survival of HER2-positive (HER2+) breast cancers. Anti-HER2 targeting has significantly improved clinical outcomes for patients with HER2+ breast cancers[175]. However, resurgent PI3K/Akt/mTOR signaling allows tumors to evade cell death in response to HER2 inhibition, is associated with tumor recurrence, and is a major cause of therapeutic resistance for anti-HER2 treatment strategies. Further, PI3K/Akt/mTOR signaling is aberrantly elevated in up to 60% of clinical breast cancers that are negative for *HER2* amplification, including estrogen receptor (ER)-positive breast cancers and triple negative breast cancers (TNBCs, those

that are negative for HER2, ER, and progesterone receptor), due to genetic alterations in *PIK3CA*, *AKT1-3*, *PTEN*, and increased expression or activity of growth factors and their receptors[232,237]. Given its prevalent activation in breast cancers, there is significant motivation to pursue new treatment strategies targeting the PI3K/Akt/mTOR signaling axis.

The serine-threonine kinase, mTOR, exists in two structurally and functionally distinct complexes, mTORC1 and mTORC2. The mTORC1 complex requires its co-factor Raptor for complex stability and substrate specificity, while mTORC2 depends on its co-factor Rictor. Interestingly, while mTORC2 directly phosphorylates Akt at S473 to drive Akt activation[223,224], mTORC1 does not phosphorylate or activate Akt. Rather, mTORC1 is activated by Akt. Further, mTORC1 is responsive to intracellular levels of oxygen, amino acids, and ATP, among others. Thus, mTOR complexes sit at a key juncture within the oncogenic PI3K/Akt/mTOR pathway, integrating signaling both upstream and downstream of Akt, as well as signals from key metabolic inputs.

mTORC1 and mTORC2 are structurally and functionally distinct, have unique roles in physiologic processes, and possess distinct oncogenic properties[230,233]. The impact of mTORC1 inhibition on tumor formation has been established by studies demonstrating decreased tumorigenesis in models treated with rapalogues, a family of inhibitors that primarily block mTORC1 activity[226]. Therapeutic efficacy of rapalogues as a single agent in breast cancers has not been demonstrated, although rapalogues used in combination with anti-estrogens provides an increased benefit to patients with ER+ breast cancers as compared to anti-estrogens alone[326,327]. Single agent use of mTOR kinase inhibitors (torkinibs), which block both mTORC1 and mTORC2 activity, show increased therapeutic efficacy over rapalogues[226], confirming that the mTOR complexes are not functionally redundant, and that tumors rely on mTORC2 for progression.

Indeed, direct links between mTORC2 and PI3K-driven tumor progression have been made in breast[225], prostate[227], pancreatic[328], lung[329], and glioblastoma[228] models. In the breast cancer setting, genetic mTORC2 deletion reduced tumor cell motility and survival *in vitro*[229], and decreased mammary ductal lengthening, secondary branching, mammary epithelial cell (MEC) motility and MEC survival *in vivo*[230]. Rictor ablation in spontaneous HER2+ murine mammary tumors impaired Akt phosphorylation at S473, signaling to Akt substrates, and cell survival, improving anti-tumor responses to lapatinib[225]. These studies support the idea that selective mTORC2 targeting may have therapeutic benefit, even without inhibition of mTORC1. Additionally, because mTORC1 inhibition relieves negative feedback on PI3K[330,331] and encourages cell growth in nutrient-deprived regions such as the tumor microenvironment[332], there is growing rationale for agents that specifically inhibit mTORC2, while sparing mTORC1. However, selective, therapeutic mTORC2 inhibition is not yet clinically available, as current drugs block mTORC1 (*e.g.*, rapalogues) only, or mTORC1/mTORC2 (*e.g.*, torkinibs) together.

Here, we engineered a Rictor-targeted siRNA nanomedicine and explored its therapeutic application because RNAi can be used to target 'undruggable' molecules, such as Rictor, at the mRNA level[202]. This new class of polyplexes incorporates a non-PEGylated core-forming component which forms binary "pre-NPs" with siRNA. The pre-NPs then serve as a scaffold for the addition of a corona-forming, PEGylated diblock copolymer (**Figure 4.1a**). Ternary siRNA polyplexes are confirmed to potently disrupt endosomes in living cells, achieve potent down-regulation of therapeutically-relevant siRNA targets, and deliver efficiently and homogenously to orthotopic breast tumors *in vivo*. These ternary siRNA polyplexes are used as an enabling technology to selectively silence Rictor *in vivo* for the first time. In addition, we monitor the

response of HER2+ breast cancers to Rictor monotherapy and combination therapy with lapatinib, an FDA-approved inhibitor of the receptor tyrosine kinase domain of HER2.

Materials and Methods

Overall survival of patients with Rictor and HER2 alterations >2 SD from mean of expression was analyzed within The Cancer Genome Atlas METABRIC data set. All 2509 samples from the METABRIC dataset were included and mutations, copy-number alterations, and mRNA expression >2 SD from the mean were included as alterations.

Human triple negative breast cancer cells (MDA-MB-231) and human HER2+ breast cancer cells (MDA-MB-361, BT474, and SKBR3) were cultured in DMEM supplemented with 10% FBS and 1% Anti-Anti reagent. A cohort of MDA-MB-231 cells were transduced with lentivirus encoding firefly luciferase, Green Fluorescent Protein (GFP), and Blasticidin resistance, enabling the generation of a luciferase expressing-MDA-MB-231 (L231) cell line[16]. Another cohort of MDA-MB-231 cells were transduced with VSV-G pseudotyped Moloney murine leukemia virus (MMLV) retroviral particles encoding yellow fluorescent protein-(YFP-)Galectin 8 and Blasticidin resistance, enabling the generation of a YFP-Galectin 8 expressing MDA-MB-231 (G8-231) cell line[333].

Human breast cancer cells were seeded (MDA-MB-231: 50,000 cells per well; MDA-MB-361, SKBR3, BT474: 250,000 cells per well) in 6-well plates and allowed to adhere overnight. Cells were treated with Lipofectamine 2000 (LF2K) carrying either Scrambled or Rictor siRNA (20 nM). After 24 h, treatments were replaced with full growth serum, and cells were allowed to grow 24 h more. RNA was isolated with an RNEasy Mini Kit (Qiagen) according to the

manufacturer's protocol at 48 h. The expression of Rictor and Raptor were evaluated by RT-qPCR by normalizing to the housekeeping gene GAPDH.

MDA-MB-361 (1e6 per dish) or MDA-MB-231 (0.5e6) cells were seeded in 10 cm dishes and allowed to adhere overnight. Cells were treated with LF2K carrying either Scrambled or Rictor siRNA (20 nM) for 24 h, and protein was harvested 48 h post-treatment. Western analyses using antibodies against Rictor (rabbit monoclonal, Sigma, 1:500), Raptor (rabbit monoclonal, Cell Signaling Technology, 1:1000), PSer473-Akt (rabbit monoclonal, Cell Signaling Technology, 1:1000), PThr389-S6K1 (rabbit monoclonal, Cell Signaling Technology, 1:1000), mTOR (rabbit monoclonal, Santa Cruz, 1:1000), and Tubulin (mouse monoclonal, Sigma, 1:1000) were performed on 20 micrograms cell lysate per lane resolved on 4-12% polyacrylamide gel (Novex) and transferred to nitrocellulose. Membranes were blocked in 3% gelatin in TBST (0.1% Tween-20) for 1 hour, incubated in primary antibody overnight at 4 degrees, washed 5 times for 5 minutes each in TBST, incubated in HRP-conjugated goat anti-rabbit secondary (Pierce) for 1 hour at room temperature, washed 5 times, and developed using Pico-ECL (Pierce).

MDA-MB-361, BT474, SKBR3, and MDA-MB-231 cells (5,000 cells per well) were seeded in black-walled 96-well plates and allowed to adhere overnight. After treatment, half of the media was removed (leaving 50 uL behind). To the remaining media and adherent cells, 50 uL of Caspase 3/7 Glo reagent (Promega) was added. After 1 h incubation on a shaker at RT, luminescence was measured on an IVIS Lumina III imaging system (Xenogen Corporation, Alameda, CA, USA).

G8-231 cells (5,000 cells per well) were seeded in 8-well chamber slides (Lab-Tek II Chambered Coverglass, Thermofisher) and allowed to adhere overnight. Ternary si-NPs were added to G8-231s at a final siRNA concentration of 100 nM and incubated for 7 and 16 hrs. After

incubation, media containing treatments were removed and replaced with PBS (-/-) containing DAPI nuclear stain. Images of cells were acquired using a Nikon C1si confocal microscope system (Nikon Instruments, Melville, NY, USA) equipped with differential interference contrast transmitted light detector. A two-step imaging mode was performed; in the first pass, a 405 laser was used to acquire channel 1 (DAPI); in the second pass, the 488 laser was used for excitation while channel 2 was used to acquire fluorescence at 520 nm (G8-GFP emission).

For biodistribution studies, athymic nude female mice (4-6 weeks old, Jackson Laboratory, Bar Harbor, ME, USA) were injected in each mammary fat pad with 1 x 10^6 L231 cells in DMEM:Matrigel (50:50). After tumors reached ~200 mm^3, tumor-bearing mice were injected via the tail vein with 1 mg/kg (Cy5-dsDNA dose) of fluorescent si-NPs. After 24 h, animals were sacrificed and the organs of interest (heart, lungs, liver, spleen, kidneys, and tumors) were excised. The organs were fluorescently imaged and quantified on an IVIS Lumina III imaging system (Xenogen Corporation, Alameda, CA, USA) at excitation wavelength of 620 ± 5 nm and emission wavelength of 670 ± 5 nm. After imaging, cells were immediately isolated from each tumor. Intracellular delivery of fluorescent si-NPs was evaluated by flow cytometry. Tumor cells were identified as the cell population expressing green fluorescent protein (GFP), while the GFP-negative cell population corresponded to native mouse cells.

MDA-MB-361 tumor cells (1 x 10^6) were suspended in 50% growth-factor reduced Matrigel/PBS and orthotopically transplanted in the mammary glands of 5 week old recipient athymic nude female mice (Jackson laboratories) as described previously[334]. Two contralateral tumors were injected into each mouse. Treatment was initiated two weeks post-transplantation [when tumors reached a volume of approximately 100 mm^3; tumor dimensions measured using a digital caliper and volume calculated as follows: volume = length x $width^2$ x 0.52)[335]. Briefly, si-

NPs loaded with 1 mg/kg scrambled or Rictor siRNA were injected *i.t.* every other day for 5 days, with tumor volume measured on treatment days. siRictor-NPs were injected into one tumor and siScr-NPs into the contralateral tumor. Tumors were harvested 24 hours following the final siRNA treatment (day 6) and processed for western blot and histologic analyses.

MDA-MB-361 cells (5,000 cells per well) were seeded in 6-well plates on day 0. Cells were treated with DB4-PDB12 si-NPs carrying either Scrambled or Rictor siRNA (100 nM each) on day 1. Cells were fed with fresh media containing 0.25 μM lapatinib in DMSO, or with an equal volume of DMSO (0.2 microliters). Cells were fed with fresh media containing DMSO or lapatinib every 3 days through day 10. Cells were stained with crystal violet on day 10, and scanned on a flatbed scanner.

MDA-MB-361 tumor cells (1×10^6) were suspended in 50% growth-factor reduced Matrigel/PBS and orthotopically transplanted in the mammary glands of 5 week old recipient athymic nude female mice (Jackson laboratories). Treatment was initiated two-four weeks post-transplantation [when tumors reached a volume of approximately 50 mm^3; tumor dimensions measured using a digital caliper and volume calculated as follows: volume = length x $width^2$ x 0.52). Animals were injected *i.t.* (on days 1, 3, and 5 after treatment initiation) or *i.v.* (on days 1, 3, 6, and 8 after treatment initiation) with DB4-PDB12 si-NPs containing either scrambled or Rictor siRNA. Animals were injected *i.p.* or by oral gavage (*o.g.*) daily with 100 mg/kg lapatinib or equal volume of vehicle control (16.7% DMSO, 0.1% Tween-80, 0.5% methyl cellulose). Tumor volume was measured every other day throughout the 21 and 28 day trials.

Treatment groups were compared using either two-tailed student's t-test or one-way ANOVA test coupled with Tukey means comparison test, where a p-value < 0.05 was deemed representative of a significant difference between treatment groups. Linear regression was used to

calculate R^2-values. For tumor growth kinetics, linear regression of the growth curves was performed, and a significant difference is indicated where the 95% confidence intervals of curves do not overlap. Outliers were removed from data using the Grubb's method with $\alpha = 0.05$ for a single outlier or ROUT method with a 1% Q-value for multiple outliers. For all data, the arithmetic mean and standard error are shown.

The animal studies were conducted with adherence to the guidelines for the care and use of laboratory animals of the National Institutes of Health (NIH). All experiments with animals were approved by Vanderbilt University's Institutional Animal Care and Use Committee (IACUC).

Results and Discussion

To assess the clinical relevance of inhibiting Rictor as a therapeutic target, The Cancer Genome Atlas (TCGA) data was used to generate Kaplan-Meyer survival curves for patients with and without Rictor alterations (*e.g.*, mutation, amplification, and/or mRNA overexpression). TCGA-curated data revealed that within a large cohort of breast cancer patients (n=2509) Rictor alterations correlated with decreased overall survival (OS) (**Figure 4.1a**, $p = 0.0294$). Patients with alterations in both Rictor and HER2 had a highly significant decrease in OS (**Figure 4.1b**, $p = 0.000375$), consistent with the prominent position of Rictor/mTORC2 within the oncogenic PI3K/Akt/mTOR signaling axis (**Figure 4.1c**), and with previous observations that genetic mTORC2 targeting[225], or pharmacological mTORC1/mTORC2 targeting[226], decreases tumor cell survival in cell culture-based models of HER2-amplified breast cancer. Together, these findings support the notion that selective mTORC2 blockade is an attractive therapeutic strategy warranting further exploration in HER2-amplified breast cancers.

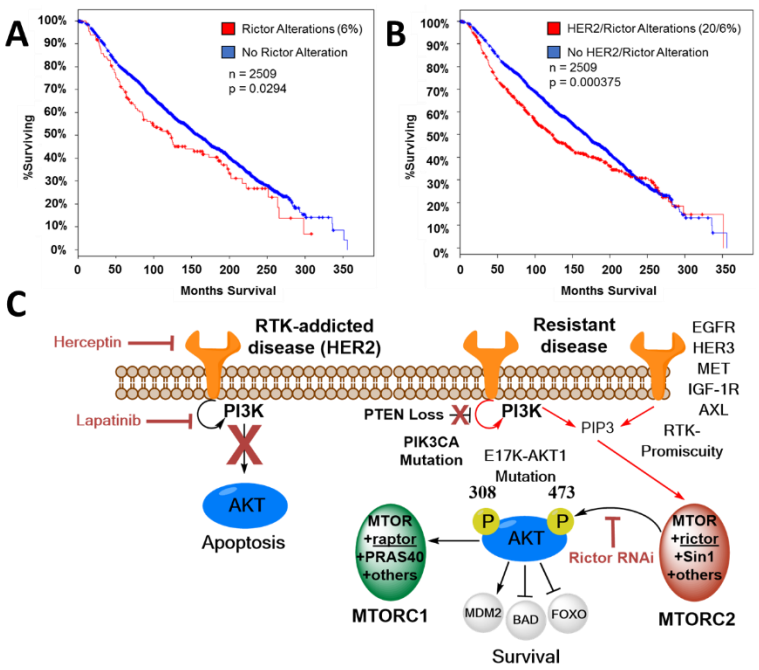

Figure 4.1) Breast cancer patients with Rictor alterations have decreased overall survival. TGCA-curated data (from the METABRIC cohort) indicates a statistically significant decrease in survival for patients that have genetic alterations in (A) Rictor and (B) Rictor as well as HER2. (C) The PI3K/Akt/mTOR signaling axis is a prominent resistance mechanism to HER2-targeted therapies. HER2-targeted therapies (*e.g.*, Herceptin, lapatinib) cause cell death through the inhibition of PI3K/Akt/mTOR signaling downstream of the HER2 receptor tyrosine kinase (left). Resistance to these therapies is often associated with PI3K/Akt/mTOR signaling independent of HER2 such as through mutations in PI3K, PTEN loss, or stimulation by other receptor tyrosine kinases. Inhibiting Rictor downstream of these mutations provides a direct modulator of Akt and in combination with HER2-targeted therapies allows inhibition of multiple converging survival pathways.

Although current agents exist for selective mTORC1 inhibition (rapalogues), or mTORC1/mTORC2 co-inhibition (torkinibs), therapeutic options for selectively inhibiting mTORC2 are unavailable. The central technological goal of this work was to selectively inhibit mTORC2 in a therapeutic setting, *in vivo*, for the first time. To achieve this goal, we used *RICTOR* siRNA in a panel of three HER2-amplified human breast cancer cell lines (MDA-MB-361, BT474, and SKBR3), as well as the TNBC cell line MDA-MB-231. In these cell lines, *RICTOR* siRNA knocked down *RICTOR* mRNA levels by 60 – 80%, but had no impact on *RPTOR* mRNA (**Figure 4.2a**). Supportive of the notion that mTORC2-blockade is an effective cell killing strategy, caspase activity was increased by *RICTOR* siRNA in the entire panel of breast cancer cells tested (**Figure 4.2b**). The downstream activity of mTORC1 was measured by the phosphorylation of its substrate S6 Kinase 1 (S6K1),

while mTORC2 activity was examined by the phosphorylation of its substrate Akt at the Ser473 motif (**Figure 4.2c**). *RICTOR* siRNA reduced *RICTOR* protein expression and inhibited the phosphorylation of Akt, indicating abrogated mTORC2 activity (**Figure 4.2d**). In contrast, *RICTOR* siRNA treatment had no effect on *RPTOR* protein expression and did not reduce the

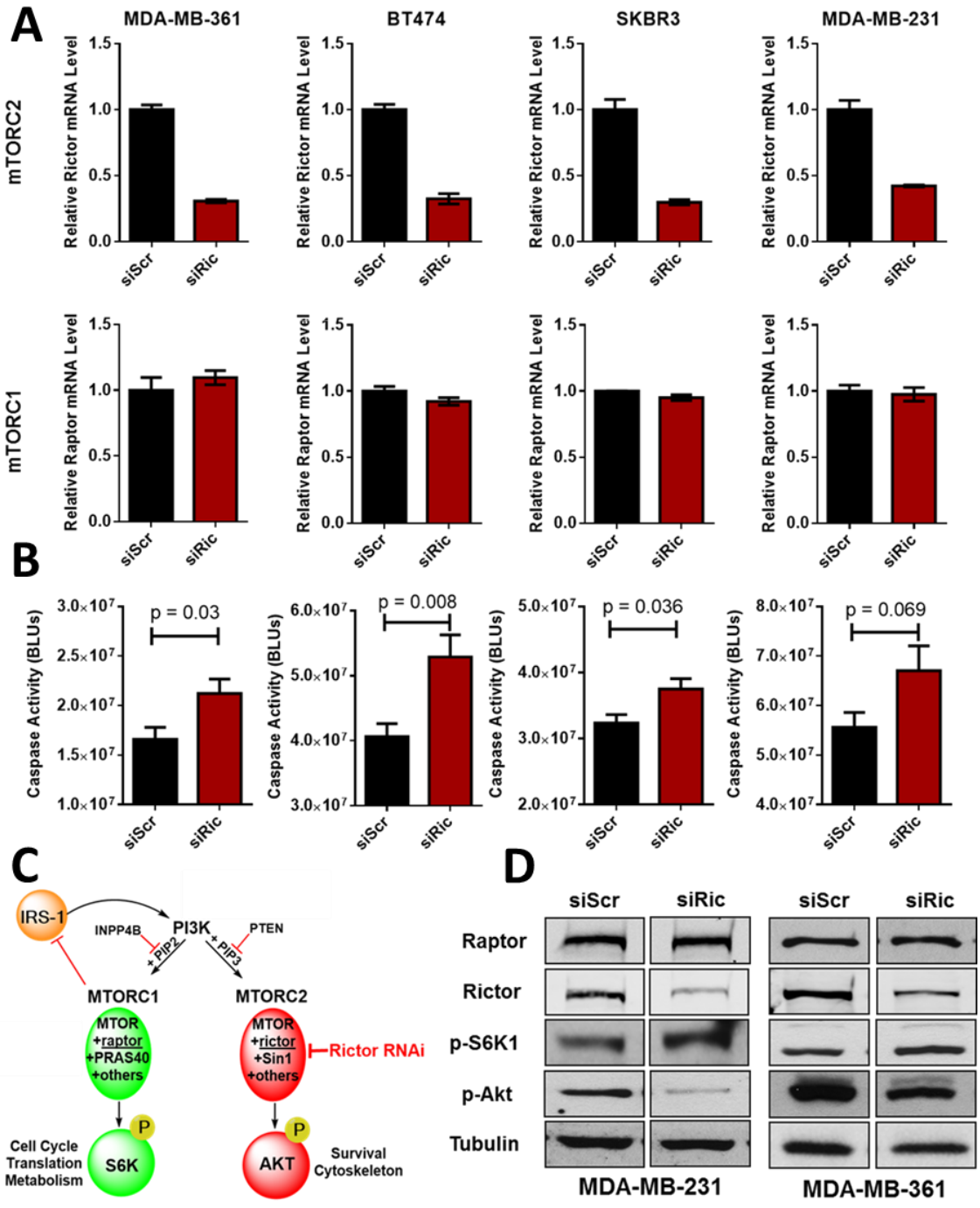

Figure 4.2) Rictor/mTORC2 is selectively silenced in a panel of human breast cancer cells. (A) Rictor RNAi silences *RICTOR* mRNA expression (~80%), while having no effect on *RPTOR* mRNA levels 48 h post-treatment with 20 nM Scrambled or Rictor siRNA. (B) Rictor RNAi induces apoptosis, measured by caspase 3/7 activity, in human breast cancer cells after 24 h siRNA treatment. (C) Signaling information for mTORC1 and mTORC2 complexes. (D) Rictor siRNA reduces protein expression of Rictor and phosphorylation of mTORC2 substrate Akt at Ser473, but does not reduce Raptor protein levels or the phosphorylation of mTORC1 substrate P-S6K1. Protein level expression was evaluated 48 h after start of siRNA treatment.

phosphorylation of mTORC1's substrate, S6K1. These results reveal the feasibility of selectively interrogating mTORC1 and mTORC2 using RNAi and confirm that mTORC2-specific inhibition kills HER2-amplified cells and can be achieved without concomitantly inhibiting mTORC1.

Ternary si-NPs leveraged as an *in vivo*-ready RNAi nanomedicine were formed using successive mixing of three components: siRNA, non-PEGylated, core-forming polymer (DB), and PEGylated, corona-forming polymer (PDB) (**Figure 4.3a**). Although binary "pre-NPs" of siRNA mixed with DB (4:1 N:P ratio) formed large and unstable structures at physiological pH, and the siRNA-free PDB micelles were small (~20 nm diameter) at physiological pH, the combination of binary pre-NPs with PDB at pH 4.0, followed by pH adjustment to 7.4, produced a stable ternary si-NP structure ~150-200 nm diameter (**Figure 4.3b, c**), lacking any evidence of binary pre-NPs aggregates or free PDB, and confirming formation of ternary si-NPs.

We and others have previously shown that siRNA polyplexes (si-NPs) with optimal PEG surface density and hydrophobic character outperform analogous systems *in vivo*[16,214,216,217,249,336], with greater *in vivo* stability, circulation time, and endosomal escape of the siRNA cargo, which allows delivery of siRNA to the cytosol. We confirmed that the ternary si-NPs, which incorporated the endosomolytic DB core and PDB corona, displayed potent and controlled pH-dependent membrane disruption at pH 6.8 and below, acidic pH values that mimic the endolysosomal interior (**Figure 4.3d**). Using yellow fluorescent protein (YFP)-tagged galectin 8 (YFP-G8) as a molecular marker to assess endosomal disruption in MDA-MB-231 cells (G8-231s)[333,337], we found that an

8 h treatment of G8-231 cells with ternary si-NPs induced YFP-G8 puncta accumulation at disrupted endosomes, while control cells displayed diffuse cytoplasmic YFP-G8 staining (**Figure 4.3e**), confirming potent endosomal disruption in ternary si-NP treated cells. Consistent with efficient cytosolic delivery of siRNA cargo, si-NPs loaded with Rictor siRNA sequences (siRictor-

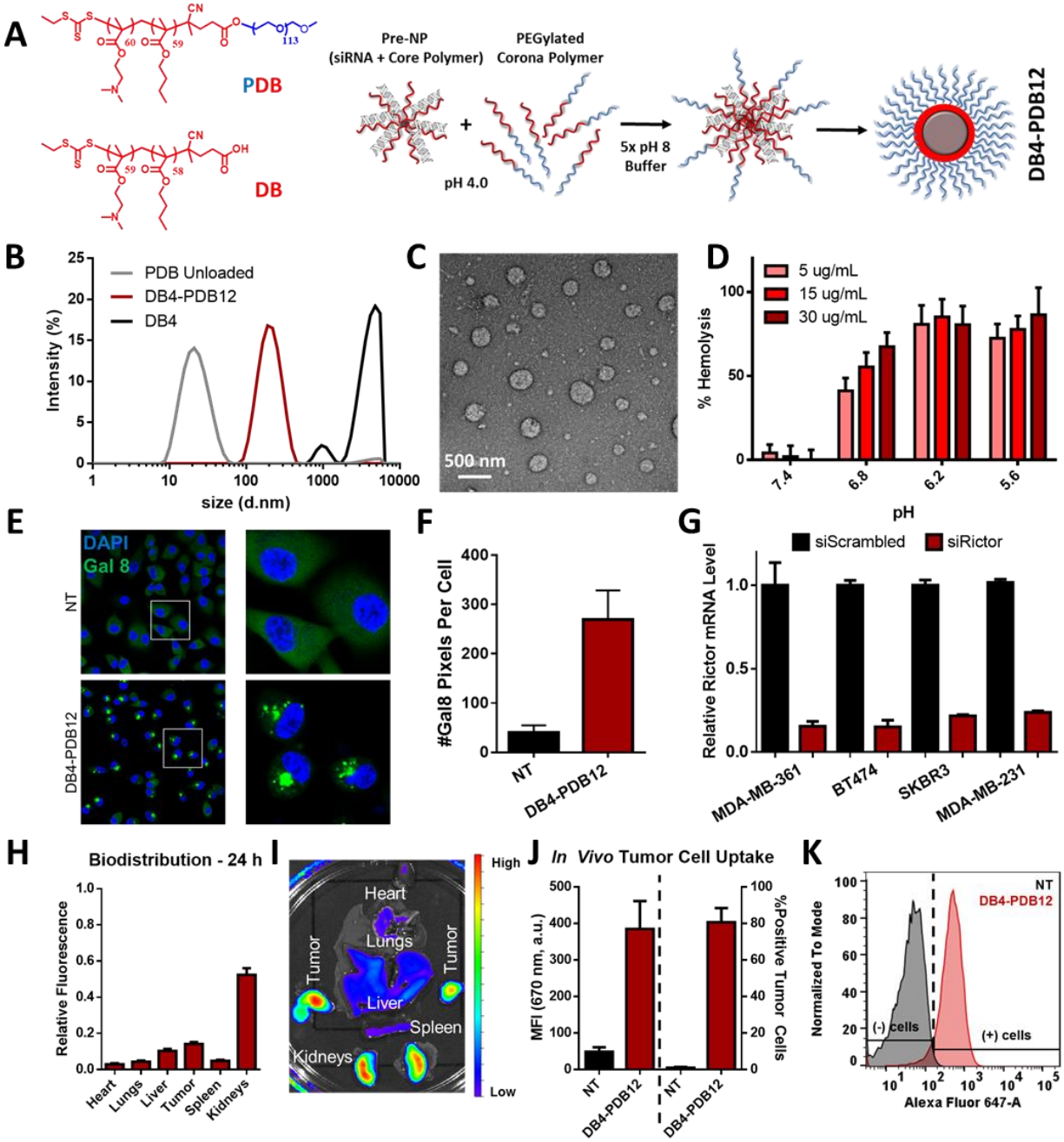

Figure 4.3) Physicochemical and biological characterization of DB4-PDB12 ternary si-NPs that enabled mTORC2 specific therapy *in vivo*. (A) Polymer chemistry and schematic of ternary si-

NP formation. (B) DLS size distribution of PDB polymer (w/o siRNA), DB4 pre-NPs at pH 7.4 with no PDB coating, and DB4-PDB12 si-NPs. (C) TEM images of DB4-PDB12 ternary si-NPs confirm expected size and morphology of nanoparticles. (D) %Hemolysis after incubation of human red blood cells with DB4-PDB12 si-NPs. (E) Confocal imaging of YFP-galectin 8 construct (20x mag). The shift of the autophagosomal marker galectin 8 from diffuse cytosolic to punctate staining indicates recruitment of galectin 8 to disrupted endosomes. (F) DB4-PDB12 si-NPs increase punctate YFG-Gal-8 puncta 6.7-fold over non-treated cells. (G) DB4-PDB12 si-NPs potently and specifically silence rictor in a panel of human breast cancer cell lines (HER2+: MDA-MB-361, BT474, SKBR3; TNBC: MDA-MB-231). (H) Biodistribution of DB4-PDB12 si-NPs 24 h after tail vein injection of 1 mg/kg siRNA in nude mice harboring orthotopic MDA-MB-231 xenografts. (I) Representative image of organ fluorescence (organs were excised 24 h after tail vein injection of 1 mg/kg siRNA). (J) DB4-PDB12 si-NPs deliver Cy5-labeled dsDNA intracellularly to MDA-MB-231 tumor cells *in vivo*. (K) Representative histogram of Cy5 fluorescence in isolated GFP+ MDA-MB-231 cells (NT vs. DB4-PDB12 treated).

NPs) produced 80%-90% Rictor knockdown as compared to si-NPs loaded with a scrambled siRNA sequence (siScr-NPs) in a panel of three HER2-amplified and one TNBC human breast cancer cell lines (**Figure 4.3g**).

We assessed intravenous (*i.v.*) delivery of ternary si-NPs to tumors grown in the mouse mammary fatpad, revealing substantial fluorescent signal within tumor tissue at 24 h post-injection (**Figure 4.3h, i**). Moreover, ternary si-NPs exhibited 1.4-fold more signal within tumors as compared to the liver (**Figure 4.3h, i**). The enhanced permeability and retention (EPR) effect was assessed in our model[278,279,338,339]. Although often overestimated, EPR is an informative measurement in mammary tumor models, and revealed here that a significant portion of the injected si-NP dose accumulated within tumor tissue as opposed heart, lungs, and spleen. Importantly, single cell suspensions of MDA-MB-231 tumors assessed by flow cytometry for uptake of fluorescently labelled si-NPs revealed that nearly 80% of cells assessed harbored fluorescent signal at 24 h after treatment with si-NPs, indicating a successful distribution of si-NP uptake throughout the tumor (**Figure 4.3j, k**). Although continued efforts will be required to achieve a more complete tumor distribution, these results are a substantial advancement over current siRNA delivery platforms using traditional binary formulations, and support the continued

investigation of this ternary siRNA polyplex within the context of Rictor/mTORC2 therapeutic targeting.

To test the therapeutic efficacy of acute inhibition of mTORC2 by Rictor RNAi therapeutically in a model of HER2+ breast cancer, we treated MDA-MB-361 tumors grown in athymic mice with siRictor-NPs or siScr-NPs using intratumoral (*i.t.*) delivery on treatment days 1, 3, and 5. Tumors harvested on day 6 were assessed by immunohistochemistry (IHC) revealing potent knockdown of Rictor in tumors treated with siRictor-NPs as compared to those treated with siScr-NPs (**Figure 4.4a, b**). Further, siRictor-NPs blocked intratumoral mTORC2 signaling, as demonstrated by impaired Akt phosphorylation at the mTORC2 motif, Ser473 (**Figure 4.4a, c**). Importantly, MDA-MB-361 tumors treated with siRictor-NPs were substantially smaller at treatment days 3 and 5, as compared to those treated

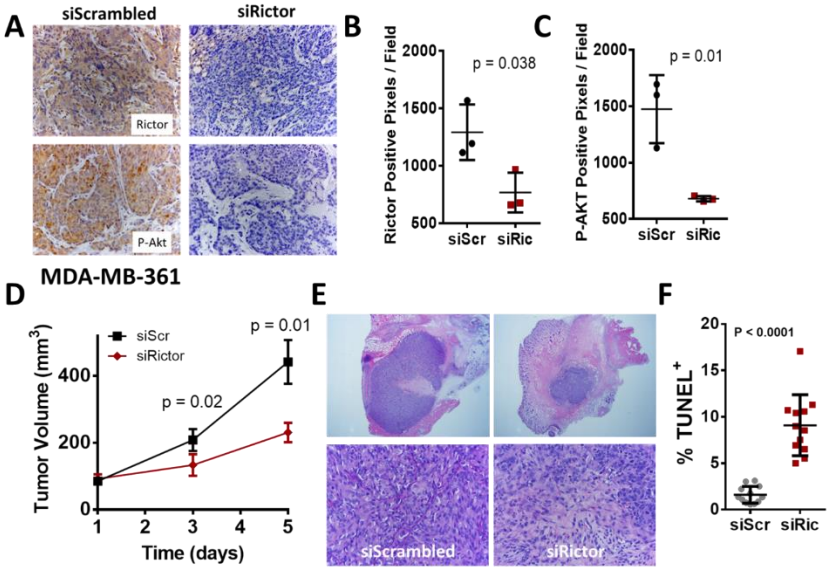

Figure 4.4) Rictor RNAi-mediated inhibition of mTORC2 signaling slows MDA-MB-361 HER2+ breast cancer growth primarily through cell death. (A) Rictor-directed RNAi prevents mTORC2 phosphorylation of Akt at Ser-473 and decreases cell survival. (B-C) IHC staining confirms protein level knockdown of Rictor and reduction in the Ser-473 phosphorylated form of the mTORC2 effector P-Akt in MDA-MB-361 xenografts (20x mag, 4 images per tumor, n = 3 different tumors, p = 0.038 and 0.01). (D) Tumor growth of MDA-MB-361 xenografts is significantly arrested at days 3 and 5 post-treatment with 1 mg/kg Rictor siRNA at days 1, 3, and 5 post-treatment initiation ($n \geq 4$). (E) H&E staining demonstrates that MDA-MB-361 xenografts treated with 1 mg/kg Rictor siRNA have reduced tumor size and cellular density (Top: 2x mag, Bottom: 40x mag). (F) Quantification of TUNEL+ confirms increased cell death in MDA-MB-361 xenografts treated with 1 mg/kg Rictor siRNA (4 images per tumor, n = 3 different tumors, $p < 0.0001$).

with siScr-NPs (**Figure 4.4d, e**). Tumor cell killing was increased nearly 10-fold in response to Rictor knockdown by ternary si-NPs, as indicated by TUNEL staining of DNA fragmentation in apoptotic cells (**Figure 4.4f**).

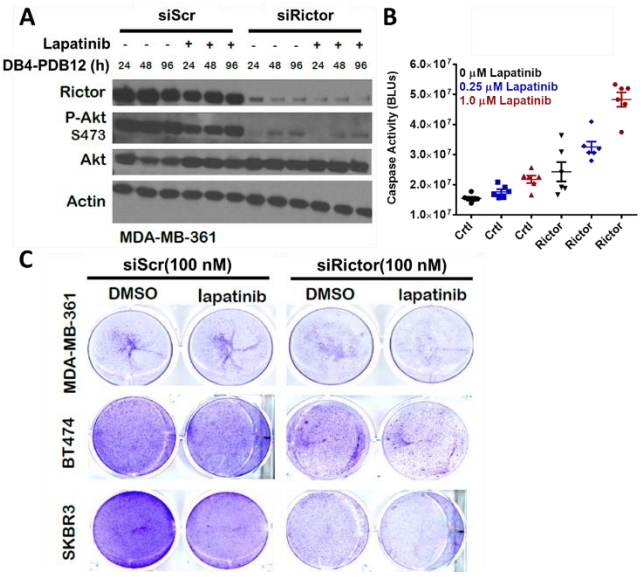

Figure 4.5) *In vitro* mTORC2 inhibition cooperates with lapatinib to kill MDA-MB-361 cells. (A) Relative protein levels of Rictor, P-Akt at Ser-473, total Akt, and Actin after 24 h treatment with siScr-NPs or siRictor-NPs followed by 24 h treatment with 0.25 μM lapatinib. (B) Caspase activity (indicating cellular apoptosis) measured after 24 h treatment with si-NPs followed by 24 h treatment with 0.25 or 1.0 μM lapatinib. (C) Representative images from cell growth assays at day 14 where MDA-MB-361, BT474, and SKBR3 cells were treated with siScr-NPs or siRictor-NPs on day 1 and fed 0.25 μM lapatinib-containing media every 3 days.

The therapeutic combination of Rictor RNAi with the FDA approved HER2 (and EGFR) TKI lapatinib was next investigated in culture. Rictor knockdown was confirmed in MDA-MB-361 cells by western analysis (**Figure 4.5a**). Lapatinib treatment at 0.25 μM in the presence of siScr-NPs modestly decreased P-Ser473 Akt, consistent with the role of HER2 as an activator of the PI3K/Akt/mTOR pathway. However, siRictor-NPs reduced P-Ser473 Akt to an even greater extent, while the combination of lapatinib and siRictor-NPs caused the greatest reduction in P-S473 Akt phosphorylation, particularly at extended time points of treatment, up to 96 hours. As expected, HER2 inhibition using lapatinib for 48 h increased caspase 3/7 activity (**Figure 4.5b**), suggesting induction of apoptosis. However, greater levels of caspase 3/7 activity were seen 48 h after treatment with siRictor-NPs, and the combination of siRictor-NPs with lapatinib produced the greatest level of caspase 3/7 activity, consistent with previous studies using stable shRNA-mediated Rictor knockdown in combination with

lapatinib[225]. A panel of HER2-amplified cells seeded at low density and cultured with lapatinib in the presence of siScr-NPs for 2 weeks produced colonies at a reduced level as compared to cells treated with siScr-NPs alone (**Figure 4.5c**). Similarly, acute Rictor knockdown using siRictor-NPs at treatment day 1, reduced colony growth over two weeks. However, the combination of lapatinib and siRictor si-NPs inhibited HER2-amplified breast cancer colony formation to a greater extent than either agent alone.

The therapeutic potential of the combination of lapatinib and siRictor si-NPs was assessed *in vivo* using MDA-MB-361 orthotopic xenografts. As a preliminary study to assess the combinatorial effect of siRictor-NPs with lapatinib, we used intratumoral injection of siRictor (Ric) and siScr-NPs (Crtl; 1 mg/kg siRNA) on treatment days 1, 3, and 5, in combination with daily lapatinib (Lap; 100 mg/kg, *i.p.*) on days 1-28. [Note that these experiments were followed with intravenous delivery of siRictor-NPs, described below.] Consistent with *in vitro* growth assays, lapatinib alone reduced tumor growth, as did intratumoral siRictor-NPs, while their combination decreased tumor growth to the greatest extent (**Supplementary Figure D.4a, b**). Intratumoral cell density confirmed reduced tumor cellularity in samples treated with siRictor-NPs plus lapatinib as compared to other treatment groups (**Supplementary Figure D.4c, d**). Interestingly, no difference in cell proliferation was observed between any of the treatment groups (**Supplementary Figure D.5**), consistent with previous observations that mTORC2 inhibition using stable Rictor ablation did not affect cell proliferation in HER2-amplified tumor models[225].

Next, tumor-bearing mice were administered siRictor-NPs (Ric) or siScr-NPs (Crtl) via intravenous delivery on treatment days 1, 3, 5, 8 and with lapatinib (Lap; 100 mg/kg) or vehicle (Veh) administration on treatment days 1-21 (**Figure 4.6a**). Tumors were assessed on treatment day 6 for *RICTOR* mRNA, revealing *RICTOR* knockdown in samples treated with siRictor-NPs

alone (~70% knockdown) or in combination with lapatinib (~60% knockdown) (**Figure 4.6b**). Rictor knockdown was confirmed further using IHC (**Figure 4.6c**). Importantly, IHC staining of

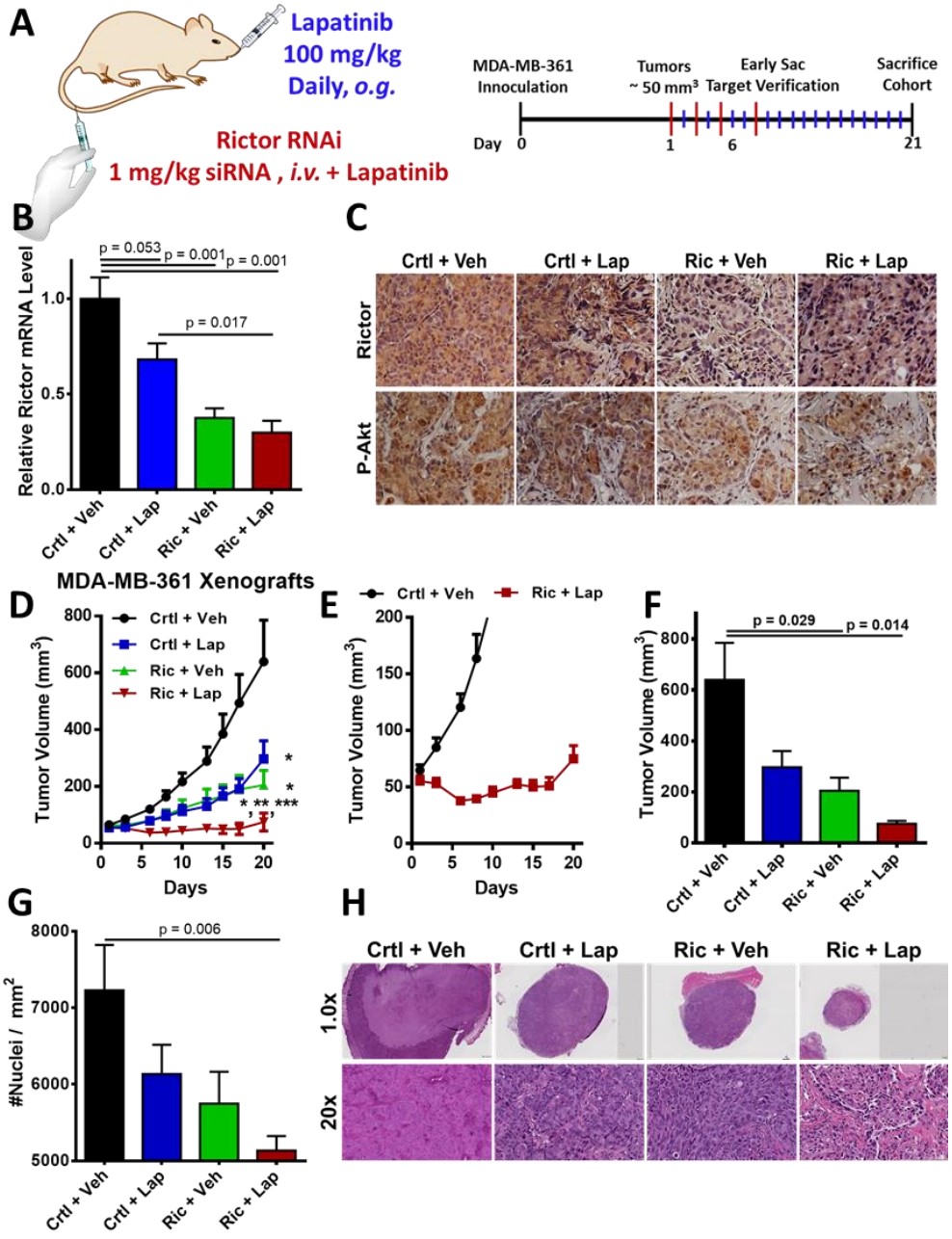

Figure 4.6) Intravenous anti-mTORC2 and oral lapatinib therapy inhibits HER2+ breast tumor growth *in vivo*. (A) Treatment protocol for Rictor RNAi and lapatinib combination therapy. (B) Rictor mRNA levels ($n \geq 4$) at treatment day 6 (1 mg/kg *i.v.* Rictor/Scrambled siRNA on days 1, 3, 6 and 8; 100 mg/kg *o.g.* lapatinib/vehicle daily on days 1-21). (C) IHC staining of Rictor protein expression and phosphorylation of Ser473-Akt at treatment day 6. Tumor growth curves for (D) all groups ($n \geq 7$) and (E) the comparison of siScr-NPs and vehicle (Crtl + Veh) vs.

siRictor-NPs and lapatinib (Ric + Lap). (F) Tumor volume at treatment day 21 ($n \geq 7$). (G) Quantification of tumor cell density ($n \geq 5$) and (H) representative H&E images show that dual therapy caused the largest reduction in tumor size and cellularity at treatment day 21 (Top: 1x mag, Bottom: 20x mag).

P-Ser473 Akt was reduced at treatment day 6 in samples treated with siRictor-NPs as compared to those treated with siScr-NPs, regardless of the lapatinib treatment status (**Figure 4.6c**). Although intravenous delivery of siRictor-NPs occurred only on treatment days 1, 3, 6, and 8, after which siRictor-NP treatment was halted, this treatment regimen produced a 3-fold reduction in tumor volume through treatment day 21 as compared to tumors treated with siScr-NPs (**Figure 4.6d**). This growth inhibition was better, albeit modestly, to daily treatment with lapatinib. However, the combination of intravenous siRictor-NPs and lapatinib (Ric + Lap) produced an initial tumor regression, followed by sustained arrest of tumor growth (**Figure 4.6d-f**). At day 21 of treatment, tumors treated with the combination of siRictor-NPs and lapatinib were 8.5-fold smaller than those treated with siScr-NPs and vehicle (**Figure 4.6f**). Histological examination revealed tumor cell death (**Supplementary Figure D.6**), decreased tumor cell density with increased histological debris, matrix deposition, and serous fluid accumulation in tumors treated with the combination of siRictor-NPs and lapatinib (**Figure 4.6g, h**). The *i.v.* delivery of ternary si-NPs for Rictor therapy was also well-tolerated by the mice, with no toxicity to liver and kidneys detected based on serum markers (**Supplementary Figure D.7**), and no change in animal body mass (**Supplementary Figure D.8**). These results highlight the therapeutic potential of this combination in HER2-amplified breast cancers, and the ability to increase specificity of target inhibition using next generation RNAi technologies.

Although phase 1 trials were completed for melanoma therapy using the PEGylated cationic siRNA polyplex, CALAA-01[39,340], no anti-tumor RNAi therapies have succeeded in late stage trials to date. One of the limitations of siRNA nanomedicines based on purely cationic

polymers such as the cationic cyclodextrin-based polymer utilized in formulation of CALAA-01 is lack of stability *in vivo*. These particles are rapidly disassembled at the glomerular basement membrane (GBM) and cleared through the kidneys, limiting circulation time, bioavailability, and tumor accumulation following *i.v.* administration[218,219]. Recent advancements have improved the cationic polyplex-mediated delivery of siRNA to solid tumors through the incorporation of hydrophobicity into the core of the polyplex and to the siRNA itself[16,249], providing resistance to heparan sulfate-mediated destabilization in the GBM and improved *in vivo* bioactivity. Moreover, the ternary siRNA polyplexes utilized within this study have been optimized to further increase particle stability, circulation persistence, and thus delivery to tumors through the combinatorial optimization of PEG architecture and hydrophobic content within the polyplexes. Importantly, we found that ternary polyplexes with optimally tuned PEG density and a hydrophobic and endosomolytic component within both the core- and corona-forming polymer unit achieved the highest delivery to tumors and intratumoral bioactivity. Here, these ternary si-NPs biodistributed efficiently and homogeneously to tumor cells, escaped the endolysosomal compartment of tumor cells, and enabled potent genetic silencing of Rictor to deactivate the mTORC2 complex.

The PI3K/Akt/mTOR axis is often activated downstream of receptor tyrosine kinases (RTKs) such as HER2, supporting the notion that alteration in both HER2 and Rictor would drive oncogenic signaling leading to growth and metastasis, and decreasing overall patient survival. Indeed, it is common for HER2+ breast cancers to develop resistance to HER2-targeted therapies, whereby they support PI3K-to-Akt signaling through alternative mechanisms such as PIK3CA hotspot mutation[188,189], PTEN loss[188,190,191], or activation by other receptor tyrosine kinases[194,195,197,198]. Akt/mTOR is a critical downstream signaling node downstream of receptor tyrosine kinases, PI3K, and PTEN, and abundant pre-clinical evidence suggests that Akt/mTOR

inhibition is necessary for a full therapeutic response of HER2+ breast cancers. Most studies have focused on inhibition of mTORC1, likely due to its position as a downstream effector of HER2/PI3K/Akt and the availability of mTORC1-specific inhibitors. Unfortunately, inhibition of mTORC1 relieves negative feedback loops of PI3K (through insulin receptor substrate 1 (IRS-1)), exacerbating PI3K-to-Akt signaling and attenuating the therapeutic efficacy of mTORC1-specific rapalogues[331,341]. Recent work has even proposed that inhibition of mTORC1 can be detrimental in certain contexts, increasing tumor cell metabolism and tumor growth in nutrient-deprived and hypovascular tumor microenvironments[332].

Considerably less is understood about the role of mTORC2 in breast cancer, but mTOR kinase inhibitors which inhibit mTORC1 and mTORC2 have been more efficacious than mTORC1-specific inhibitors, suggesting mTORC2 is important for tumor cell survival[226]. It is well known that Akt signaling stimulates tumor cell survival[231,232], and mTORC2 directly phosphorylates Akt at S473[233]. Further, restoration of Akt signaling was sufficient to overcome HER2+ breast cancer cell death induced by Rictor/mTORC2 genetic ablation, further highlighting the key role played by mTORC2 in tumor cell survival[225]. Our collective results provide seminal confirmation that these observations hold true within the therapeutic context as well. Specifically, we found that it is possible to independently silence each mTOR complex, targeting mTORC2 was an efficient cell killing strategy, RNAi-mediated inhibition of mTORC2 diminished the phosphorylation of Akt at Ser-473 both *in vitro* and *in vivo*, and therapeutically inhibiting mTORC2 triggered cell death in HER2+ breast tumors and delayed tumor growth similar to previous reports in genetically engineered mouse models[225].

The most effective breast cancer therapies to date have been combination therapies, *e.g.*, a recent clinical trial highlighted the exciting potential of combining dual HER2 inhibitors and

docetaxel to treat metastatic HER2+ breast cancers[342]. The combination of Rictor RNAi and lapatinib is a logical choice in HER2+ breast cancer because mTORC2 can activate Akt independent of HER2 and generate resistance to HER2-targeted agents such as lapatinib[225]. In combination, Rictor RNAi and lapatinib cooperated to abolish the phosphorylation of Akt, improve cell killing above either monotherapy, and completely halt tumor growth. The combination of Rictor RNAi and other HER2-targeted agents (*e.g.*, trastuzumab, pertuzumab, neratinib) should be similarly effective as it is widely acknowledged that full attenuation of PI3K-to-Akt signaling downstream of HER2 is necessary to achieve a therapeutic effect. In addition, we anticipate that Rictor RNAi will combine powerfully with neoadjuvant chemotherapy (NAC) since one of the most common pathway alterations identified in patients resistant to NAC is the PI3K/Akt/mTOR pathway[343].

Conclusions

In summary, this work introduces and validates a new therapeutic target for RNAi, Rictor/mTORC2, in PI3K/Akt/mTOR-dependent breast cancers. Effective RNAi of Rictor/mTORC2 *in vivo* was enabled by ternary siRNA polyplexes which safely and efficiently deliver siRNA to solid breast tumors. Efficacy studies confirmed the therapeutic value of selective mTORC2 inhibition in HER2+ breast cancers both alone and in combination with a FDA-approved agent, lapatinib. Our results confirm that mTORC2 is a viable therapeutic target in HER2+ breast cancers and provide mechanistic insight into response of HER2+ breast cancers to TKIs in combination with mTORC2-specific inhibition. Our collective results illustrate broad potential for identifying powerful new breast cancer therapies through RNAi and motivate our ongoing studies to catalog breast cancer subtypes sensitive to Rictor/mTORC2 RNAi, further elucidate relative

importance of mTORC2 versus mTORC1 signaling, compare relevant on- and off-target toxicities of mTORC2 versus dual mTORC1/2 inhibition, and identify drug combinations with the greatest clinical potential.

CHAPTER V

SUMMARY AND OUTLOOK

Small interfering RNA (siRNA) has emerged as a powerful research tool and potentially transformative clinical therapeutic[344]. RNA interference (RNAi) was intitially observed by Mello and Fire in 1998[40], and soon after siRNAs were confirmed to be capable of potent and highly specific inhibition by RNAi[345,346]. Due to their mode of action at the mRNA level, they are a promising approach to inhibiting targets that are the hardest to drug by conventional pharmacology (*i.e.*, intracellular enzymes, transcription factors, and protein-protein interactions)[201,202]. Moreover, siRNAs can be rapidly designed *in silico* through computational approaches and used to modulate theoretically every existing drug target in the genome. However, almost twenty years after Mello and Fire's initial discovery, systemic and cellular delivery barriers continue to limit the application of siRNAs as therapeutics[203]. After systemic administration, siRNAs are rapidly cleared through filtration in the kidneys and readily degraded by nucleases[204,205]. At the cellular level, siRNAs are unable to traverse the plasma membrane due to their size and negative charge and lack an inherent mechanism for endosomal escape[173,205]. Thus, their effective clinical use is contingent upon the ability to safely and effectively achieve delivery to the target tissue, cell type, and intracellular compartment of action. To date, a variety of methodologies have been developed to address the challenge of siRNA delivery, including covalent modifications[201,240], antibody-protamine fusion[241], liposomal encapsulation[242], and nanoparticle formulations of cationic lipids or polymers[243-245].

Chapter Summaries

Chapter 1 serves as a review of polymeric materials that have been investigated for improving siRNA delivery, as well as other genetic cargos such as pDNA, AON, miRNA, PNA, mRNA, and components of the CRISPR/Cas9 gene editing system. We discuss the rapid advances in polymer chemistry and materials science that have made it possible to rationally design non-viral nucleic acid vectors which can overcome delivery barriers and increase the efficacy and specificity of gene expression, editing, or inhibition. Specifically, we review five distinct classes of polymeric materials which have been heavily investigated for delivering genetic cargo: micelles/polyplexes, cross-linked micelles, polymersomes, microgels, and nanogels. These different classes of polymer delivery systems provide virus mimetic functionalities such as nucleic acid protection, increased blood circulation time, active and passive targeting, evasion of immune system, cellular internalization, and endolysosomal escape to varying extents. Recent studies are reviewed in order to showcase the potential for success within each class, and current ongoing clinical trials for RNAi are discussed to highlight the translatability of optimized nanoparticle designs.

The remainder of the work is focused on tailoring micelles/polyplexes to deliver siRNA to solid tumor tissues more efficiently upon systemic administration. Many siRNA transfection reagents have been primarily optimized to achieve gene silencing *in vitro*, and therefore, utilize design principles (*e.g.*, extreme cationic charge for cell internalization[207]) which do not translate well to *in vivo* settings, especially for delivery to non-hepatic targets. Strictly cationic polyplexes, PEGylated for colloidal stability, can be administered systemically[214,216], but are unstable in the presence of serum and competing polyanions such as heparan sulfates of the GBM[16,218,219]. Consequently, this class of electrostatically-stabilized polyplexes are still rapidly cleared through

the liver and kidneys and show only modest pharmacokinetic improvements over naked siRNA. Targeting siRNA nanoparticles to cancer targets such as solid tumors *in vivo* is contingent upon the ability to avoid rapid clearance by the liver (phagocytosis) and kidneys (polyanionic disassembly), which extends circulation time and consequently passive tumor uptake by the EPR effect. Disassembly in the kidney, leading to clearance through the urine, is especially detrimental to siRNA polyplex circulation time[218]. We showed previously that siRNA polyplexes which have balanced cationic and hydrophobic character in the polymeric block that forms the polyplex core, are more resilient to heparan sulfate disassembly and have longer circulation than strictly cationic analogues[16]. Due to the shortcomings of strictly cationic polyplexes and based on the revelation that hydrophobicity can be used as an alternative stabilizing force, we developed two independent but complimentary hypotheses: 1) Combinatorial incorporation of hydrophobicity into the core, corona, and both core and corona of polyplexes of ternary architecture will stabilize them through both electrostatic and van der Waals forces. 2) Hydrophobization of siRNA cargo through lipid-modification will improve association with balanced cationic and hydrophobic polyplexes, increasing stability through both electrostatic and van der Waals forces.

Our first hypothesis is presented in Chapter 2, where we develop a combinatorial library of ternary siRNA polyplexes which incorporate hydrophobic moieties within either the core-, corona-, or both core- and corona-forming polyplex components. A multiparametric screen established the impact of polyplex composition and hydrophobe placement on important performance outcomes such as polyplex size, stability, endosomolysis, biocompatibility, and RNAi efficacy. This screen revealed the importance of incorporating hydrophobicity within both the core- and corona-forming polyplex components, where increased stability and endosomolysis greatly improved gene silencing potency. Indeed, no ternary formulations that lacked the

incorporation of hydrophobicity in both the core- and corona-forming unit achieved appreciable gene silencing. The increased stability of our lead formulation, DB4-PDB12, had profound effects on its *in vivo* performance as well. When injected directly into the circulation (i.v.), this formulation exhibited increased blood circulation time, reduced renal clearance, increased tumor biodistribution, and greater silencing of the model gene luciferase compared to our previously-optimized, binary parent formulation (PDB). Thus, we found that a combinatorial optimization of the hydrophobic forces on the polymer component of ternary siRNA polyplexes improved performance *in vitro* and *in vivo* by refining polyplex design parameters that concomitantly address cell-level and systemic physiological delivery barriers.

The second hypothesis is presented in Chapter 3, where we modified siRNA with palmitic acid to add hydrophobic character to the molecule and increase its interaction with the balanced cationic and hydrophobic polymer PDB (referred to as 50B in chapter 3). Less than half the amount of polymer was required to fully bind/complex palmitic acid-modified siRNA, indicating increased affinity of the polymer and siRNA-lipid conjugate. Comparing to PDB complexed with unmodified siRNA, the stability of PDB complexed to palmitic acid-modified siRNA was comprehensively improved. Polyplexes made from complexing PDB and palmitic acid-modified siRNA resisted decomplexation at high concentrations of salt, serum, and heparan sulfate, three notorious mediators of polyplex decomplexation in the systemic circulation. Functionally, the increased stability of these polyplexes was realized by their increased circulation time and universally improved delivery to solid breast tumors after systemic administration (i.v.). Sustained gene silencing was observed within tumors of mice treated by PDB polyplexes containing palmitic acid-modified siRNA, while no signs of toxicity (e.g. ALT, AST, and BUN chemistry levels) were observed in the animals. Thus, we found through our work in chapters 2 and 3 that diverse

improvements to the hydrophobic content of siRNA polyplexes are simple yet effective methods to increase polyplex stability, in turn increasing the systemic circulation time and passive accumulation of siRNA polyplexes within tumor tissue by the EPR effect.

In chapter 4, we explored the use of our improved RNAi technology to modulate a previously 'undruggable' target in HER2+ breast cancer. PI3K/Akt/mTOR signaling is dysregulated in over 60% of clinical breast cancers across all three major clinical subtypes driving tumor cell growth, survival, metabolism, and invasion. The distal effector of this pathway, mTOR, is found within two functionally distinct complexes, mTORC1 and mTORC2. Recent work has implicated a unique physiologic role for mTORC2 in HER2+ breast cancers, where it drives tumor survival and therapeutic resistance[225], but no current small molecules exist which can preferentially inhibit mTORC2 activity. Additionally, the most effective breast cancer therapies have been drug combinations, e.g. a recent clinical trial highlighted the exciting potential of combining dual HER2 inhibitors and docetaxel to treat metastatic HER2+ breast cancers[342]. Thus, we were motivated to test the effect of combining mTORC2 inhibition through RNAi with a current standard of care to improve treatment of HER2+ breast cancers. We chose lapatinib because it is currently used to treat late-stage and metastatic HER2+ breast cancers, recent studies uncovered a role for mTORC2 in mediating cell survival in lapatinib-resistant HER2+ breast cancer cell lines, and lapatinib inhibits a separate signaling axis (HER2 / PI3K) than mTORC2 (directly acts on Akt). In our study, it was found that RNAi of Rictor, an obligate and specific co-factor of the mTORC2 complex, inhibited mTORC2 activity while sparing mTORC1 activity, becoming the first drug of its kind to do so. Specific inhibition of mTORC2 mediated cell killing of HER2+ breast cancer cell lines in culture and orthotopic xenografts *in vivo*. The combination of mTORC2 inhibition and lapatinib abolished Akt signaling and reduced cell growth in culture. Finally, this combination prevented

the growth of orthotopic HER2+ breast cancer xenografts *in vivo*. While monotherapy of mTORC2 inhibition and lapatinib both reduced tumor growth compared to controls, the combination therapy significantly reduced growth compared to either monotherapy and completely halted the growth of tumors over the course of our study. Our results highlight the vast potential for discovering newly druggable targets using RNAi and specifically illustrate the anti-tumor benefits of combining mTORC2-specific inhibition with the FDA-approved agent lapatinib to treat patients with HER2+ breast cancer.

Shortcomings

Though this work has highlighted our achievements producing improved nanomedicine-based delivery of siRNA to solid breast tumors, we have also discovered a number of potential shortcomings of the approach which warrant discussion. Potential shortcomings of our synthetic preparation, physicochemical characterization, biological performance, and experimental approach are briefly discussed below.

There are aspects of the synthetic preparation of ternary siRNA polyplexes that remain to be optimized. The preparation of our ternary siRNA polyplexes necessitates dilute solutions to prevent aggregation and precipitation of the polymer-nucleic acid complexes. This is no problem at all for studies in cell culture, but it becomes a technical challenge to make solutions of polyplexes which are concentrated enough to administer high doses to animals. Thus, we must perform a relatively harsh spin concentration step which has potential to alter the dose and physicochemical characteristics of the polyplexes before administration. Improved designs of the future will endeavor to remove this concentration step for *in vivo* studies. There also exists an inherent variability between batches in these synthetic materials. Although rigorous

characterization of our materials is performed, some materials which are identical from a characterization perspective do not always perform equivalently *in vivo*. It would be very valuable to discover new characterization methods that more accurately predict *in vivo* performance based on the chemical characteristics of a material. Moreover, although structure-activity relationships (SARs) which directly predict *in vitro* performance of polyplexes based on polymer chemistry have been discovered[309], more predictive SARs for *in vivo* settings have remained elusive and are extremely desirable. Finally, long-term storage of our polyplexes remains a concern. We prepare fresh batches of polyplexes each day we have an experiment requiring animal injections. This is arduous and not feasible from a clinical perspective. It would be desirable to produce polyplexes which could be either stored in their administration medium long-term or lyophilized to a dry powder and reconstituted just before injection. Our group has yet to extensively investigate the lyophilization of the polyplexes used in these studies, but a variety of excipients exist that stabilize the size and morphology of polyplexes through the lyophilization process[347]. It is likely that a systematic study of existing excipients would reveal an optimal formulation that could be lyophilized and maintain its physicochemical and biological properties, alleviating the need to make different batches of polyplexes for each experiment/clinical administration.

A primary goal of nanomedicine in oncology is to use phenomenon such as the EPR effect and active receptor-ligand targeting to preferentially deliver pharmaceutical agents (*i.e.*, drugs) to cancerous tissue while avoiding delivery to healthy tissue. In other words, our goal is to maximize the percent of the injected dose (%ID) at the tumor site and minimize %ID at all other sites. Unfortunately, a recent analysis of the literature across all qualifying nanomedicine studies in oncology revealed that only 0.7% ID is typically delivered to tumor tissue, and that value has not significantly improved over the last 20-30 years of research[348]. In our studies, there was an

improved average of 2.5-5% ID delivered to tumors depending on the quantification method used. However, this means that 95-97.5% ID is still accumulating in non-targeted, healthy tissues where the drug is likely to cause undesirable toxicities. Therapeutic indices (or therapeutic windows), which indicate the range of doses within which efficacy is achieved without toxicity, remain characteristically narrow for nanomedicines in oncology as a functional consequence. An analysis of biodistribution of our polyplexes to other major organs after i.v. administration revealed that ~20% ID and ~50% ID accumulate within the liver and kidneys, respectively. Although a literature survey shows that this is a significant improvement over currently existing polyplex technologies, there remains a critical need to reduce accumulation in these tissues further.

Other delivery limitations may occur directly at the tumor site. Two influential studies served to establish the optimal size of nanomedicines for leveraging the EPR effect. Both studies suggest that to achieve an optimal balance of vascular permeability, tissue penetration, and impermeability to lymphatic drainage, nanoparticles of size ~30-50 nm diameter are preferred[349,350]. Therefore, the size of our nanomedicine (~100-150 nm diameter) can still be further optimized through methods such as micro-mixing and nanoprecipitation to increase permeability to tumor tissue. Additionally, the EPR effect has generated intense scrutiny within the last two to three years. It appears that: 1. EPR is highly variable across cancer types, animal models, and patient populations. 2. Animal models often do not accurately predict the magnitude of EPR in the clinical setting. 3. Patients should be chosen on a case-by-case basis when evidence of EPR is present[339,351,352]. Based on these revelations, two recent studies offer a new way to approach the EPR effect[278,338]. In these studies, “companion” nanoparticles are administered alongside the nanomedicine and used as contrast agents for imaging. Thus, noninvasive imaging can predict whether a patient is likely to respond to the nanomedicine based on accumulation of

the companion nanoparticle. In this paradigm, patients predicted to benefit from nanomedicine will receive it and all other patients will be given the clinical standard of care. The EPR was readily apparent within our studies, conducted in cell line-based breast cancer xenografts, but it is unlikely that all patients in the clinic will exhibit EPR to the extent observed in these studies. A strategy such as EPR prediction with companion nanoparticles could thus be a powerful addition to our current approach when considering clinical translation in the future.

In our studies, all tracking of biodistribution and pharmacokinetic information was done by measuring fluorescent signal of nucleic acid cargos that were labeled with Cyanine5 fluorophore (ex.: 650 nm, em.: 670 nm). This technique provides meaningful comparisons within experiments and between very carefully controlled experiments, but absolute quantification is a challenge and experiments are inherently low-throughput, requiring the sacrifice of many animals to generate statistically powerful data. Moreover, measurement of pharmacodynamics in our studies required many additional animals (because of terminal analyses), arduous experiments, and remained semi-quantitative in many instances.

Future Work

Ongoing work will seek to improve delivery to tumors and overcome a number of the shortcomings above by: 1) further optimizing designs of the material delivery system, 2) seeking techniques to that alter animal physiology to improve tumor delivery, 3) pursuing alternative technologies which do not rely on the EPR effect, and 4) adopting techniques which more thoroughly quantify siRNA biodistribution, pharmacokinetics, and pharmacodynamics.

Materials chemistry approaches can be used to further improve the stability, endosomolysis, biocompatibility, pharmacokinetics, and potency of our current siRNA polyplex

design. We have found that the stability and endosomolysis of our polyplexes are largely dictated by the core polymer block (DB). Therefore, a systematic study of the effect of core block size on stability, endosomolysis, and potency is warranted. The core block can be tuned easily and very precisely through stoichiometric variation of the RAFT polymerization conditions. A library of core block-varied polymers could be used to elucidate important structure-activity relationships that are related to core block size. Crosslinking is a common strategy to increase micelle/polyplex stability against competing polyanions and serum upon dilution. Crosslinking can be synthetically incorporated into the current design through the incorporation of a sulfur containing monomer into the core or corona of polyplexes (to introduce disulfide crosslinks) or simply through the crosslinking of DMAEMA moieties that currently exist in the core of the polyplexes. To date, our work has focused on optimizing the core stability of our class of siRNA polyplexes but all the designs contain the same 5 kDa PEG corona-forming polymer block. Future work should aim to optimize the corona chemistry as well as the core block chemistry since PEG coronas (especially low molecular weights such as 5 kDa) do not completely resist protein adsorption and immune recognition[353]. Other recent articles have highlighted the enhanced pharmacokinetic profiles of emulsion nanoparticle-based siRNA delivery systems. These systems force the siRNA into a hydrophobic, polymer core through water-oil-water emulsions and show potential pharmacokinetic advantages over mix-and-go polyplex systems such as those used in our studies[300,354]. Lastly, although the focus of this work has been on nanomedicine-based siRNA delivery systems (most common siRNA delivery strategy), other delivery strategies such as siRNA conjugates are alternatives to nanomedicine which have high translatability due to their relative simplicity and broad therapeutic indices[355,356].

Many promising approaches to increase tumor delivery efficiency are extra-material, or they are techniques that do not directly change the materials chemistry but instead augment performance *in vivo*. As has been discussed, a major limitation of nanomedicines (for tumor delivery) is rapid accumulation within the liver. Although we have focused solely on materials design considerations to reduce liver accumulation, extra-material approaches also exist and may be used in concert with materials design to further decrease liver accumulation. Two examples are the saturation of phagocytic Kupffer cells of the liver by some inert substance other than the delivery material or transient depletion of the Kupffer cells prior to nanomedicine injection[357]. Both approaches have shown pre-clinical success, but they are an extreme manipulation of otherwise healthy and necessary aspects of the liver and immune system. Thus, the tolerability of these approaches in clinical settings is uncertain, warranting continued efforts to develop other extra-materials approaches with the same goal of reducing nanomedicine clearance by the liver. Another crucial goal in cancer nanomedicine is to increase tumor penetration and homogeneity of tumor delivery. Focused ultrasound has emerged as a technique to transiently disrupt the blood-brain barrier and increase delivery of small molecule drugs and nanomedicines to pathologies within the brain[358]. Since it has become clear that lack of vascular permeability in more advanced cancer models and patients dampen nanomedicine efficacy, it is likely that focused ultrasound can be implemented to increase permeability of tumors similar to opening the blood-brain barrier. One thing is clear, delivery of nanomedicines to tumors is not a magic bullet and off-target accumulation of delivery materials in the liver, kidneys, and spleen appears unavoidable. Thus, extra-materials approaches that "tune" the physiological environment to reduce off-target accumulation, improve tumor penetration and retention, or both should be pursued and implemented alongside new material designs.

In addition to next-generation designs, new experimental techniques have recently been developed that may be considered as alternative approaches to the techniques used within these studies. Intravital microscopy, whereby pharmacokinetic data is generated within a single animal over time is one powerful step forward[359]. This technique continues to rely on fluorescent measurements, but gives highly quantitative data and typically reduces the number of animals needed to produce statistical power. Moving beyond fluorescent measurements, which vary based on tissue absorbance and rely on the modification of the molecule of interest with an exogenous fluorescent moiety, stem loop PCR is a powerful technique borrowed from the miRNA field that should allow absolute quantification of siRNAs in blood and tissues of interest without any fluorescent moiety. In this modified version of RT-PCR, PCR reaction conditions are optimized for the amplification of the siRNA of interest[360]. The experimental workflow would follow: 1. Injection of natural, unmodified siRNA molecule (with/without delivery system), 2. Purification of siRNA from blood/tissues of interest, 3. Generation of standard curve of siRNA within stem loop PCR protocol, 4. Quantification of siRNA extracted from blood and tissues via comparison to standard curve after RT-PCR. Moreover, it is possible to immunoprecipitate the Argonaute 2 protein, which facilitates siRNA binding with the RISC complex, and subsequently perform stem loop PCR to quantify the amount of active, RISC-loaded siRNA that was delivered. DNA barcodes have recently been introduced as another non-fluorescent method for tracking biodistribution and pharmacokinetics[361]. By this technique, particles are loaded with distinct sequences of DNA which can then be extracted from tissue, sequenced using next-generation sequencing techniques, and quantified as an absolute number of DNA molecules detected. Stem loop PCR and DNA barcodes can both theoretically be used to screen many particles at once (provided they all contain unique sequences), introducing an exciting opportunity to perform high throughput analysis of

nanoparticle pharmacokinetics and biodistribution. Lastly, new techniques that allow non-invasive, non-terminal, and single-cell level monitoring of pharmacodynamics would revolutionize the design of pre-clinical anti-tumor efficacy studies.

Potential Applications

It is appropriate to conclude where we began, by highlighting the enormous impact that RNA interference and other gene therapies can have on human health. The ability to safely and efficiently deliver siRNA and other nucleic acid drugs to malignant tumors will transform the clinical treatment of cancers. siRNA can be rapidly designed by computer algorithms and modulate theoretically all drug targets, making it an ideal drug for the post-genomic world where tumors are known to harbor many mutations and have notoriously high genetic plasticity. In this work, we showed as a proof-of-concept that a previously 'undruggable' target, mTORC2, that breast cancer cells use to grow and resist therapy could be specifically inhibited through efficient siRNA delivery into tumors. Future work should develop a library of siRNA targets in breast cancer. There are many well-documented pathways that control cell growth (PI3K/mTOR/Akt, RAS/MAPK, Wnt, Myc), cell cycle (cyclins), and cell death (apoptosis pathways) in breast cancer cells. A myriad of new drug targets could be developed within these pathways using siRNA, and the ability to deliver multiple siRNAs could enable powerful new drug combinations. Moreover, siRNAs could be designed against specific oncogenic mutants that drive progression of cancers but are absent from other healthy tissues, generating unprecedented target specificity.

In addition to siRNA, the delivery strategies discussed herein can be employed with other similarly sized genetic cargo such as locked nucleic acids (LNAs), miRNAs, and immunomodulatory nucleic acids. miRNAs function as endogenous negative regulators of gene

expression and, in many cases, are powerful drug targets since single miRNAs can control the expression of whole gene networks (hundreds of genes). If the miRNA of interest is under-expressed, replacement of the miRNA can be achieved by delivering exogenous miRNA or miRNA mimetics. On the other hand, when the miRNA of interest is over-expressed, antisense oligonucleotides such as LNA can be designed to inhibit the miRNA and reduce its function. Recent studies have shown that aberrant miRNA expression (specifically, miR-125b, miR-145, miR-21, and miR-155) is common in breast cancers, and modulation of these miRNAs represents a promising new therapeutic strategy[362]. Immunomodulatory nucleic acids such as stimulator of interferon genes (STING) agonists and 5' triphosphate RNAs that induce RIG-I are also likely to require delivery vehicles for therapeutic relevancy. Simple adjustments of current vehicles such as those discussed in this work are an obvious starting place and have already shown efficacy in pre-clinical work[363]. Importantly, specific delivery to tumors for immunomodulation can often be achieved by direct injection or delivery to tumors is not necessary to achieve immunity, relaxing many systemic delivery constraints that exist for purely pharmaceutical modulation within tumors.

Conclusion

We sit at the precipice of a revolution in genetic therapy due to rapid advances in our understanding of genetic processes and the ability to engineer "smart" materials that therapeutically modulate these processes. While delivery of genetic cargo such as siRNA is reaching the efficiency necessary to achieve therapeutic efficacy, potential design and experimental improvements that can further enhance delivery are reviewed. Therapies that modulate underlying genetic drivers of breast cancer represent a paradigm shift from classic

pharmacology, and successes will transform the clinical treatment of breast and many other cancers.

APPENDIX A

HYDROLYTIC CHARGE-REVERSAL OF PEGYLATED POLYPLEXES ENHANCES INTRACELLULAR UN-PACKAGING AND ACTIVITY OF SIRNA.

Text for Appendix A taken from:

TA Werfel, C Swain, CE Nelson, KV Kilchrist, BC Evans, M Miteva, CL Duvall. Hydrolytic Charge-reversal of PEGylated Polyplexes Enhances Intracellular Un-packaging and Activity of siRNA. *Journal of Biomedical Materials Research: Part A.* 2016, 104, 917-927.

Abstract

Hydrolytically degrading nano-polyplexes (HDG-NPs) that reverse charge through conversion of tertiary amines to carboxylic acids were investigated to improve intracellular un-packaging of siRNA and target gene silencing compared to a non-degradable analog (non-HDG-NPs). Both NP types comprised reversible addition-fragmentation chain-transfer (RAFT) synthesized diblock copolymers of a poly(ethylene glycol) (PEG) corona-forming block and a cationic block for nucleic acid packaging that incorporated butyl methacrylate (BMA) and either dimethylaminoethyl methacrylate (DMAEMA, non-HDG-NPs) or dimethylaminoethyl acrylate (DMAEA, HDG-NPs). HDG-NPs decreased significantly in size and released significantly more siRNA (~40%) than non-HDG-NPs after 24 hours in aqueous solution. While both HDG-NPs and non-HDG-NPs had comparable uptake and cytotoxicity up to 150 nM siRNA doses, HDG-NPs achieved significantly higher target gene silencing of the model gene luciferase in vitro. High resolution FRET confocal microscopy was used to monitor the intracellular un-packaging of siRNA. Non-HDG-NPs had significantly higher FRET efficiency than HDG-NPs, indicating that

siRNA delivered from HDG-NPs was more fully un-packaged and therefore had improved intracellular bioavailability.

Introduction

Small interfering RNA (siRNA) has emerged as a powerful research tool and potentially transformative clinical therapeutic.[344] Due to its mode of action at the mRNA level, siRNA is a promising class of therapeutics for inhibiting targets considered to be hard-to-drug by conventional pharmacological approaches, such as intracellular enzymes, transcription factors, and protein-protein interactions.[201,202] However, systemic and cellular delivery barriers currently limit the application of siRNAs as therapeutics.[203] After systemic administration, siRNA molecules are rapidly cleared through filtration in the kidneys and do not have inherent properties that disposes them to distribute to tumors or other potential target sites.[204,205] At the cellular level, siRNAs are unable to traverse the cellular membrane due to their size and negative charge and lack an inherent mechanism for endosomal escape.[173,205] Thus, effective clinical use of siRNA is contingent upon the ability to safely and effectively deliver these molecules to the target tissue, cell type, and intracellular compartment of action.

The conventional approach for delivering siRNA is packaging with cationic polymers or lipids into nanosized polyplexes.[206] The nanocarriers are typically formulated with a large excess of cationic charge which enhances siRNA cellular uptake through interaction with the anionic cellular membrane.[207] Strictly cationic lipoplexes and polyplexes can be effective in vitro transfection reagents, but their highly positive zeta-potential and lack of stability make systemic administration a challenge.[364,365] Therefore, surface PEGylation has been widely employed as a strategy to neutralize these carriers for reduced opsonization and increased stealth from the

mononuclear phagocyte system (MPS) in vivo.[214-216] For example, first-in-man class clinical trials have tested a cationic, PEGylated siRNA delivery vehicle for systemic administration.[38,39,366]

The current work builds upon our previous report by introducing a hydrolytic charge-reversing mechanism for increased un-packaging and bioavailability of siRNA within the cytosol (**Figure A.1**). Introducing a mechanism to increase intracellular un-packaging of siRNA from polyplexes designed for in vivo applications is an important design consideration due to the desire to balance in vivo stability in circulation and intracellular interaction of siRNA with the RNA induced silencing complex (RISC) machinery. Ideally, in vivo-ready polyplexes will possess characteristics which increase blood circulation time and stability (PEGylation and hydrophobicity). However, these characteristics can decrease gene silencing potency; PEGylation reduces cell uptake and core stabilization potentially hinders intracellular siRNA bioavailability. We have previously shown that reversible PEGylation promotes siRNA uptake and activity.[20,367] To better understand the barrier of intracellular release for PEGylated polyplexes with balanced core hydrophobicity, the current project tested the impact of incorporating a hydrolytically degradable, charge-reversing cationic monomer and comparing the bioactivity and intracellular siRNA release relative to an analogous system made with a stable cationic monomer. Stimuli-

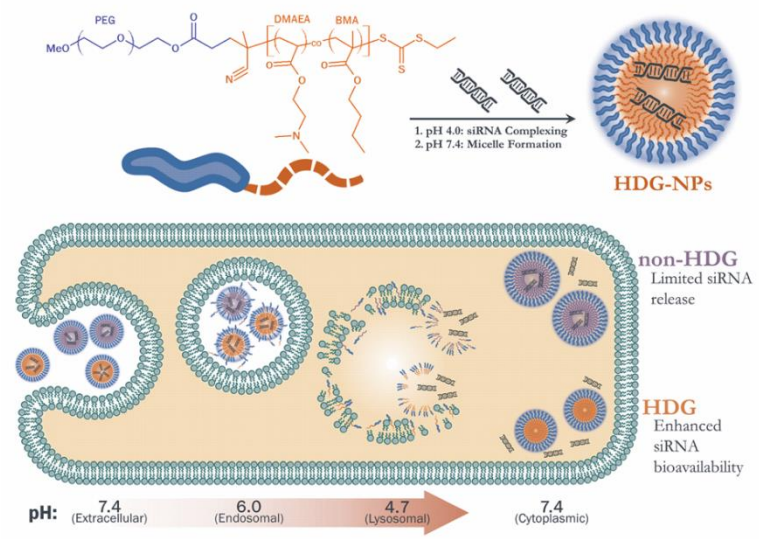

Figure A.1) Top: Polymer Chemistry and siRNA Loading Protocol. Bottom: Hypothesis for Enhanced Intracellular Release and Activity of siRNA Delivered by HDG-NPs.

responsive cues such as pH and ROS have been investigated for enhancing gene and drug delivery potency.[368-371] Specifically, charge-reversal has been investigated as a means to increase pDNA transfection[372] and siRNA potency from polyplexes.[373, 294] Moreover, dimethylaminoethyl acrylate (DMAEA) has been utilized by Monteiro et al. for the timed release of siRNA from micelleplexes.[373,374] However, our report represents the first use of hydrolytic charge-reversal in PEGylated polyplexes which have been optimized for systemic delivery in vivo, and the system reported effectively couples both endosomal escape and intracellular release mechanisms. Importantly, increased siRNA release from a charge-reversing carrier is measured in living cells for the first time using high resolution Förster Resonance Energy Transfer (FRET) confocal microscopy.

The hydrolytically-degrading nano-polyplexes (HDG-NPs) were developed by replacing DMAEMA as the cationic monomer of non-hydrolytically degrading nano-polyplexes (non-HDG-NPs) with DMAEA. Like DMAEMA, DMAEA contains a tertiary amine that enables siRNA complexing and pH-dependent membrane disruption. However, the lack of a pendant methyl group in the polymer backbone of DMAEA-containing polymers increases the rate of hydrolysis of the ester group, leaving behind a residual negatively-charged acrylic acid. Therefore, we hypothesized that incorporation of DMAEA would enable a polymer charge-reversal-based siRNA release mechanism that would increase cytosolic availability and therefore, activity of siRNA delivered by PEGylated polyplexes with core hydrophobicity. To test this hypothesis, we herein have compared the new HDG-NPs to the benchmark non-HDG-NPs for siRNA release kinetics in solution, cell uptake and viability, and target gene silencing. Finally, FRET confocal microscopy techniques were used to monitor the intracellular trafficking of siRNA delivered from both NPs.

Materials and Methods

All chemicals were obtained from Sigma-Aldrich and used as received unless otherwise noted. DMAEMA, DMAEA, and BMA monomers were passed twice through an alumina column to remove inhibitors prior to polymerization. 2,2-Azobis(2-methylprpionitrile) (AIBN) was recrystallized twice from methanol prior to use. Dioxane was distilled under vacuum prior to use. Luciferase and scrambled siRNA sequences were designed and purchased through IDT. Fluorophore labeled dsDNAs were purchased through IDT and Sigma. Lipofectamine 2000 was obtained through Invitrogen. 21-mer dsDNA was used in DLS and fluorescent studies as a model of siRNA.

ECT was synthesized according to previous protocols described by Convertine et al. and Moad et al.[375,376] Briefly, ethanethiol (4.72 g, 76 mmol) was reacted with carbon disulfide (6.00 g, 79 mmol) in the presence of sodium hydride (3.15 g, 79 mmol) in diethyl ether for 1 h. The resulting sodium S-ethyl trithiocarbonate was further reacted with iodine (6.3 g, 25 mmol) to obtain bis(ethylsulfanythiocarbonyl) disulfide, which was then refluxed with 4,4-azobis(4-cyanopentanoic acid) in ethyl acetate for 18 h to yield ECT. The crude ECT was purified by column chromatography using silica gel as the stationary phase and ethyl acetate:hexane (50:50) as the mobile phase. ^{1}H-NMR (400 MHz, CDCl3): 3.35 (q, 2H, S-CH_2-CH_3), 2.69 (t, 2H, -CH_2-CH_2-COOH), 2.36-2.58 (m, 2H, -CH_2-CH_2-CH_3), 1.88 (s, 3H, CH_3-C-CN), 1.36 (t, 3H, S-CH_2-CH_3)

ECT was conjugated to hydroxyl-functional PEG by a carbodiimide coupling strategy.[377] Briefly, dicyclohexylcarbodimide (4 mmol, 0.82 g) was added to the stirring solution of methoxy-poly(ethylene glycol)-hydroxyl (Mn = 5000, 2 mmol, 10 g), ECT (4 mmol, 1.045 g), and DMAP (10 mg) in 50 mL of dichloromethane. The reaction mixture was stirred for 48 h. The precipitated cyclohexyl urea was removed by filtration, and the dichloromethanane layer was concentrated and

precipitated into diethyl ether twice. The precipitated PEG-ECT was washed three times with diethyl ether and dried under vacuum (yield ~10g). RAFT polymerization was then used to synthesize diblock copolymers from the PEG-ECT macroCTA. Either DMAEMA (0.236 g, 1.5 mmol) or DMAEA (0.415 g, 2.9 mmol) and BMA (0.213 g, 1.5 mmol or 0.333 g, 2.34 mmol) were added to separate solutions of PEG-ECT (100 mg, 0.02 mmol) in 3 mL dioxane. The solutions were purged with N_2 for 30 min and then reacted at 70 °C for 24 h using AIBN as an initiator at a 10:1 [CTA]:[Initiator] molar ratio. The reactions were quenched by exposure to air, and the resulting polymers were precipitated thrice into a mixture of pentane:diethyl ether (90:10) and vacuum dried. The reactivity ratios for the BMA and DMAEA monomers were determined using the Fineman-Ross method after polymerization under the conditions described above at three molar feed ratios [DMAEA:BMA]: [40:60], [50:50], and [60:40].

Polymers were characterized for composition and molecular weight by ^{1}H-NMR (NMR, Bruker 400 MHz spectrometer equipped with a 9.4T Oxford Magnet). Polydispersity Index (PDI) of the polymers was determined using gel permeation chromatography (GPC) on a system running DMF + 0.1 M LiBr as the mobile phase (Agilent Technologies, Santa Clara, CA, USA) with inline Agilent refractive index and Wyatt miniDAWN TREOS light scattering detectors (Wyatt Technology Corp., Santa Barbara, CA, USA).

Both non-HDG and HDG micelles were initially dissolved in 100% ethanol (10 mg/mL), then diluted 10X with pH 7.4 PBS to give 1 mg/mL solutions of micelles. These solutions were frozen and lyophilized either immediately or after 24 and 48 hours of incubation in PBS at 37 °C. The lyophilized powder was then re-dissolved in $CDCl_3$ at 10 mg/mL and analyzed by ^{1}H-NMR (NMR, Bruker 400 MHz spectrometer equipped with a 9.4T Oxford Magnet). The percent

hydrolysis of each polymer was calculated by comparing the ratios of DMAEA/DMAEMA (-O-CH_2CH_2-, δ 4.05s) to PEG (-OCH_2CH_2-, δ 3.65s) and normalizing to t = 0 h.

To make empty micelles, the non-HDG and HDG polymers were initially dissolved in 100% ethanol (10 mg/ml), then diluted 10X with pH 7.4 PBS to yield 1 mg/ml solutions. For siRNA-loaded polyplexes, the non-HDG and HDG polymers were initially dissolved in 100% ethanol (33.3 mg/ml), then diluted 10x with pH 4.0 citrate buffer (10 mM). Next, dsDNA (50 μM, H_2O) was added to the polymers at pH 4.0 at an N:P ratio of 5:1. After 30 min, 5x pH 8.0 phosphate buffer (10 mM) was used to raise the pH to ~7.4. The size of both loaded polyplexes and empty micelles was monitored by DLS (Malvern Zetasizer Nano ZS, Malvern, UK) at 0 h and 24 h of incubation in aqueous solution.

The hydrolytically-dependent release of siRNA from NPs in aqueous solution was also monitored by FRET-based measurements. FRET can be used to measure siRNA loading and release of FRET-labeled siRNAs, where a reduction in FRET efficiency over time is indicative of siRNA release.[16,378] Polyplexes were loaded as described above with 50:50 mix of FRET-paired Alexa488- and Cy5-labeled dsDNAs. Fluorescence intensity was measured at each time point using a plate reader (Tecan) at an excitation wavelength of 488 ± 5 nm. Alexa488 (donor) emission was collected at 520 ± 5 nm, and Cy5 (acceptor) emission was collected at 670 ± 5 nm. The release of siRNA was quantified as loss of %FRET signal which was calculated as follows:

(A.1) $$\%FRET = \left(\frac{I_{670}}{I_{520} + I_{670}}\right) * 100$$

Whole blood was extracted from anonymous, consenting human donors, and red blood cells (RBCs) were isolated according to well-established protocols.[263] RBCs were then incubated with the HDG- and non-HDG-NPs (concentration of 5 μg/mL) in buffers of pH 7.4, 6.8, and 6.2, which model the environments in the extracellular space and in the more acidic vesicles of the

endolysosomal pathway. After 1 h of incubation, the RBCs were centrifuged and the supernatant was spectrophotometrically analyzed at 451 nm (Tecan Plate Reader) in order to determine percent hemolysis relative to 1% Triton X-100 detergent.

Human epithelial breast cancer cells (MDA-MB-231) were cultured in Dulbecco's Modified Eagle's Medium (DMEM, Gibco Cell Culture, Carlsbad, CA, USA) with 10% fetal bovine serum (FBS, Gibco) and 50 μg/mL gentamicin (Gibco). Some of the MDA-MB-231s used were lentivirally transduced to constitutively express firefly luciferase and green fluorescent protein (GFP). Luciferase-expressing MDA-MB-231s (L231) were used to assess cell viability and for screening efficiency of carrier delivery of luciferase siRNA.

MDA-MB-231 breast cancer cells were seeded in 24-well plates at 30,000 cells/well and allowed to adhere overnight. The cells were treated with polyplexes loaded with Alexa-488-labeled dsDNA at a final concentration of 100, 200, and 300 nM in DMEM supplemented with 10% FBS and 50 μg/mL gentamicin. After 24 h, cells were washed with PBS and trypsinized. Trypsin was inactivated by adding serum containing media, and cells were centrifuged and resuspended in PBS containing 0.04% Trypan Blue to quench extracellular fluorescence. Relative cell fluorescence was quantified via flow cytometry to measure intracellular delivery of siRNA (FACS Calibur, BD Biosciences, Franklin Lakes, NJ, USA).

Viability of cells treated with polyplexes was assessed by measuring relative cell number based on luciferase activity. Luciferase-expressing MDA-MB-231 (L231) breast cancer cells were seeded at 2,000 cells/well in black, clear bottom 96-well plates and allowed to adhere overnight. Polyplexes containing a scrambled siRNA sequence were added to cells at 2:1, 5:1, 10:1, and 20:1 N:P ratios and final concentrations of 50, 100, 150, and 200 nM in DMEM supplemented with 10% FBS and 50 μg/mL gentamicin. After 24 h incubation, cells were washed, and the media was

replaced with luciferin-containing DMEM (150 μg/mL). Bioluminescence was quantified using a Xenogen Lumina III series IVIS (Caliper Sciences) to determine relative cell number compared to no treatment.

Luciferase-expressing L231 cells were seeded in black, clear bottom 96-well plates at 2,000 cells/well and allowed to adhere overnight. Cells were treated with polyplexes containing either anti-luciferase siRNA (100 and 150 nM) or a scrambled sequence (100 and 150 nM) as a control in DMEM supplemented with 10% FBS and 50 μg/mL gentamicin. After 24 h, media was replaced with luciferin-containing DMEM (150 μg/mL), and bioluminescence was quantified using a Xenogen Lumina III series IVIS (Caliper Sciences). In all cases, bioluminescent signal of treatment samples was normalized to the corresponding scrambled control in order to determine percent luciferase activity (n = 5).

Intracellular un-packaging of siRNA was monitored in live cells by FRET microscopy methods recently established.[379] Briefly, MDA-MB-231 breast cancer cells were seeded in fibronectin-coated (50 μg/ml) 8-well chamber slides (Nunc, Thermo Fisher Scientific Inc., Waltham, MA, USA) at a density of 10,000 cells/well. The cells were treated with polyplexes containing a 50:50 mix of Alexa-488- and Alexa-546-labeled dsDNA as a FRET pair at a total concentration of 100 nM in DMEM supplemented with 10% FBS and 50 μg/mL gentamicin. After 24 h, cells were washed with PBS, and media was replaced with phenol red-free DMEM (10% FBS, 50 μg/mL gentamicin) containing DAPI nuclear stain. After 1 h incubation, cells were imaged using a Nikon C1si confocal microscope system (Nikon Instruments, Melville, NY, USA) equipped with differential interference contrast transmitted light detector. A two-step imaging mode was performed; in the first pass, a 405 laser was used to acquire channel 1 (DAPI); in the second pass, the 488 laser was used for excitation while channels 2 and 3 were simultaneously

acquired (Alexa 488 / Alexa 546). The optical system was equipped with the 405/488/543 dichroic mirror, the 450/35 filter cube in the first position (Ch1), and the 515/30, 605/75 filter cube in the second position (Ch2/Ch3). Sensitized emission in the red channel (i.e., the increased fluorescence in the acceptor fluorophore due to FRET) was analyzed in a blinded, high throughput, whole-image analysis using MATLAB (MathWorks, Natick, MA, USA) code that calculated the average per cell sensitized emission fluorescence intensity by summing Ch3 and normalizing to cell number (algorithmically counted using DAPI staining). These data representing >9,000 cells are presented in Figure A.5b.

All measurements are presented as mean ± standard error of the mean. One Way ANOVA coupled with post-hoc Tukey means comparison test was used to determine statistical significance, and $p < 0.05$ was considered significant.

Results and Discussion

A previously reported RAFT synthesis scheme was used to synthesize two diblock copolymers (**Supplementary Figure SA.1**).[16] In both cases, a carbodiimide coupling strategy using DCC and DMAP allowed the attachment of ECT to monohydroxyl-functional 5 kDa PEG and generation of a PEG-ECT RAFT macroCTA. ^{1}H-NMR (400 MHz $CDCL_3$) revealed 91% substitution of the hydroxyl-PEG to PEG-ECT (data not shown).[16] The second polymer block was then synthesized from the macroCTA and resulted in approximately equimolar (50:50) amounts of either DMAEMA and BMA (non-HDG) or DMAEA and BMA (HDG). ^{1}H-NMR (400 MHz $CDCL_3$) analysis of the products showed similar core compositions (non-HDG: 48.3% BMA, HDG: 55.9% BMA), overall degree of polymerizations (non-HDG: 120, HDG: 115), and

Polymer	DP[a]	%BMA[a]	%DMAEMA/ DMAEA[a]	Mn[a] (Da)	PDI[b]
non-HDG	120	48.3	51.7	22994	1.04
HDG	115	55.9	44.1	21404	1.35

[a]Determined by ^{1}H-NMR. [b]Determined by GPC.

Table A.1) Summary of the NMR and GPC Polymer Characterization of PEG-*b*-p(DMAEMA-*co*-BMA) [non-HDG] and PEG-*b*-p(DMAEA-*co*-BMA) [HDG] diblock copolymers.

molecular weights (non-HDG: 23 kDa, HDG: 21 kDa) (**Table A.1 and Supplementary Figure SA.2a**). Both polymers were relatively monodispersed (non-HDG: 1.04, HDG: 1.35) as determined by GPC (**Table A.1 and Supplementary Figure SA.2b**). The Fineman-Ross method was used to determine values of r_{BMA} and $r_{DMAEA,}$ which were close to 1, suggesting formation of a random copolymer. The reactivity ratios for the DMAEA/BMA system were r_{BMA}=1.21 and r_{DMAEA}=0.81, respectively. This result indicates the potential for compositional shifting, resulting in slightly longer segments of BMA. However, since the reactivity ratios are relatively close to 1 and the composition of the polymer was only ~6% off from the feed ratio, the copolymer can still be considered a random distribution of DMAEA and BMA (**Supplementary Figure SA.3**). The synthesis route employed is desirable for its simplicity and precision when compared to the complex schemes often employed for producing polymers with higher-order architecture to achieve particle stability, siRNA packaging, and endosomolytic functionality.

HDG-NPs were designed to self-hydrolyze in aqueous solutions by the incorporation of an unprotected ester bond adjacent to the polymer backbone. In contrast, the non-HDG polymer contains a pendant methyl group off the backbone which protects the ester from hydrolysis. ^{1}H-NMR analysis confirmed HDG polymer hydrolysis upon incubation in PBS at 37 °C. The decrease in signal from protons directly adjacent to the PDMAEA ester (δ 4.05s) and increase in signal from dimethylamino ethanol (DMAE) peaks (δ 3.3s and 3.7s) indicated significant polymer hydrolysis occurred over 24 - 48 h (**Figure A.2a**). The extent of hydrolysis was quantified for both non-HDG

and HDG polymers, and the HDG polymer showed ~25 % and 45 % hydrolysis at 24 and 48 h, respectively (**Figure A.2b**). In contrast, the non-HDG polymer showed ~3 % and 5 % hydrolysis

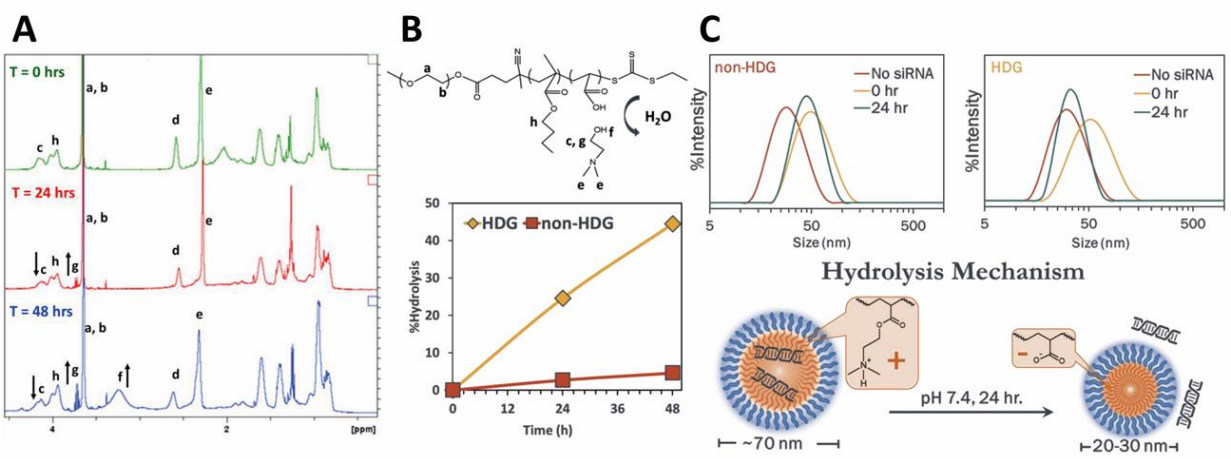

Figure A.2) Hydrolysis of siRNA-loaded polyplexes in aqueous solution. (A) ^{1}H-NMR analysis reveals HDG polymer hydrolysis at 24 and 48 h (arrows indicate either the appearance or disappearance of peaks over time due to hydrolysis). (B) Structure of hydrolyzed HDG polymer (top) and quantification of polymer hydrolysis at 24 and 48 h (bottom). (C) HDG-NPs (right) reduced in size after 24 h, indicating hydrolytically-dependent NP siRNA release.

at 24 and 48 h. DLS measurement of NP size was used as an additional indicator of this hydrolysis in aqueous solutions (**Figure A.2c**). Solutions of the non-HDG and HDG polymers assembled directly into micelles in PBS at pH 7.4 served as an empty micelle standard. Both empty micelles were ~25 nm. For both polymers, the freshly-made siRNA-loaded formulations were 60-70 nm. After 24 h of incubation in aqueous solution, the HDG-NPs were reduced to the size of empty micelles (~25 nm) while non-HDG-NPs retained their initial size. These data are an initial indication of siRNA release from HDG-NPs over time after exposure to aqueous environments.

Increased release of siRNA from HDG-NPs during incubation in aqueous solution was validated using a FRET-based readout (**Figure A.3**). The effect of hydrolysis of the HDG-NPs was apparent at extended time points based on the disappearance of FRET signal, indicating increased siRNA release relative to the non-HDG-NPs. At 24 hr, HDG-NPs released ~40% more siRNA than non-HDG-NPs at a 5:1 N:P ratio (which was therefore used in functional in vitro

studies). Increasing the N:P ratio partially mitigated the difference in siRNA release, likely due to the excess of cationic charge present in higher N:P ratio formulations. The rate of hydrolysis observed herein are comparable to previously reported homopolymers of DMAEA.[380]

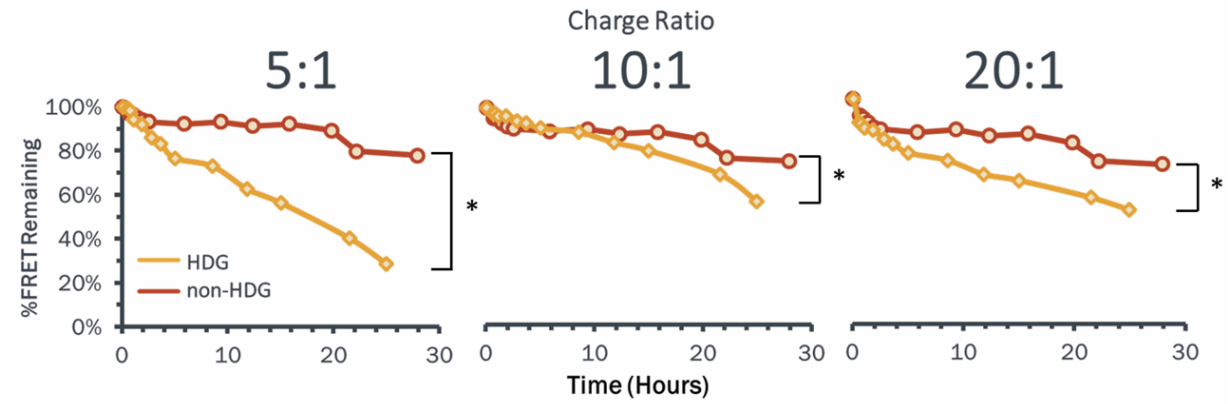

Figure A.3) HDG-NPs release siRNA cargo more efficiently than non-HDG-NPs. FRET signal is used to track siRNA release kinetics where loss of FRET is indicative of siRNA release. At 5:1 N:P ratio, HDG-NPs released ~40% more siRNA at 24 hr than non-HDG-NPs. Increasing the N:P ratio reduced the impact of the HDG chemistry, likely due to the presence of excess cationic charge.

In order to compare the non-HDG- and HDG-NPs directly for target gene silencing and intracellular un-packaging, we first endeavored to confirm that both formulations had comparable hemolysis, cell uptake, and effect on cell viability. The hemolysis assay allows for the quantitative measure of pH-dependent membrane disruption and indicates the ability of the NPs to achieve endosomal escape.[263] HDG- and non-HDG-NPs both exhibited switch-like, pH-dependent membrane disruption between pH 7.4 and 6.8 (**Supplementary Figure SA.4**). No significant difference in the hemolysis profiles of HDG- and non-HDG-NPs was observed, indicating that endosomal escape would not be a contributing factor to differences in silencing efficiency observed. Cell uptake was assessed in MDA-MB-231 breast cancer cells using flow cytometry to quantify the intracellular delivery of Alexa-488-labeled dsDNA from both non-HDG- and HDG-NPs. Both NPs exhibited intracellular delivery of the siRNA cargo, with intracellular fluorescence significantly above no treatment (**Figure A.4a, b**). The non-HDP-NPs exhibited higher cell uptake

over HDG-NPs at each siRNA dose tested (100, 200, and 300 nM), but uptake in both groups were significantly lower than Lipofectamine 2000 uptake. There was a small dose-dependent increase in cell uptake within each group, but this effect was modest due to the inherently low uptake of this class of PEGylated, surface-shielded polyplexes that have ζ-potential of approximately 0 mV.

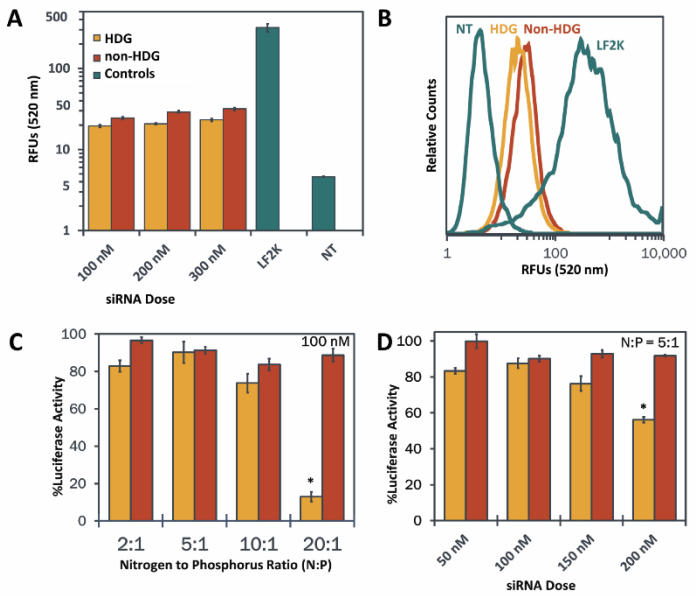

Figure A.4) Assessment of non-HDG- and HDG-NP cell uptake and cytocompatibility. (A) Intracellular delivery of siRNA by polyplexes as quantified by flow cytometry (n = 3). (B) Flow cytometry histogram of cell uptake at 100 nM siRNA dose. (C) Cell viability assessed at varying N:P ratios at 100 nM siRNA concentration (n = 4). (D) Cell viability assessed at varying siRNA concentrations at N:P ratio of 5:1 (n = 4). LF2K = Lipofectamine 2000.

The effect of both polyplexes on cell viability was assessed in luciferase-expressing MDA-MB-231 breast cancer cells across a range of siRNA concentrations as well as N:P ratios. First, siRNA concentration was kept constant at 100 nM and the N:P ratio was varied between 2:1 and 20:1 (**Figure A.4c**). Cell viability was not significantly different between either group up to 10:1 N:P ratios. At N:P ratio of 20:1, HDG-NPs were significantly more toxic to the cells than non-HDG-NPs. Next, the N:P ratio was held constant at 5:1 (where both polyplexes were most cytocompatible at 100 nM siRNA dose) and the siRNA concentration was varied between 50 and 200 nM (**Figure A.4d**). There was decreased cytocompatibility of HDG-NPs at 200 nM, but there was no significant difference between non-HDG- and HDG-NPs up to 150 nM siRNA dose. Cytotoxicity of large polymers (>5600 Da) containing the DMAEA monomer has been reported in the literature.[381] Our observations confirm that cytotoxicity is of concern with the DMAEA-

based polymers but suggest that toxicity can be mitigated for DMAEA copolymerized with BMA when complexed with oligonucleotides under conditions where a minimum effective dose is used and there is not a significant excess of polymer used in formulation.

Potential efficacy of HDG-NPs for target gene silencing was assessed in vitro in MDA-MB-231 cells constitutively-expressing luciferase (L231s) as a model gene. Both non-HDG- and HDG-NPs, as well as the commercial transfection agent Lipofectamine 2000 (LF2K), were used to deliver anti-luciferase siRNA through incubation with L231s for 24 h, and gene silencing was determined by quantifying cellular bioluminescence. At each dose investigated, the HDG-NPs achieved significantly greater protein level knockdown of luciferase relative to non-HDG-NPs (**Figure A.5**). Moreover, the knockdown of luciferase was dose-dependent for both non-HDG- and HDG-NPs with up to ~40% knockdown observed by HDG-NPs at a 150 nM siRNA dose.

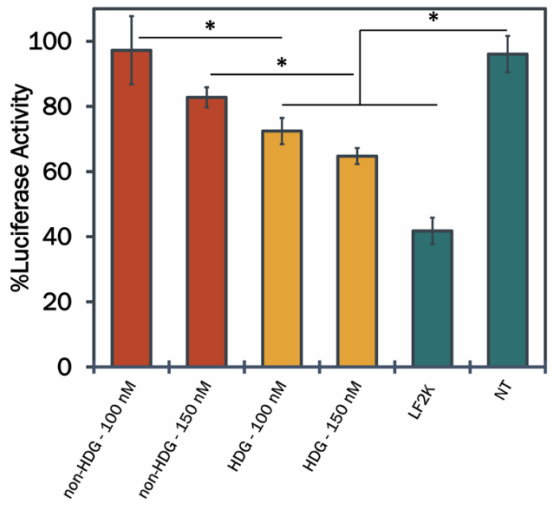

Figure A.5) Target gene silencing of the model gene luciferase by non-HDG- and HDG-NPs at N:P ratio of 5:1 (n = 5). HDG-NPs exhibited enhanced siRNA potency at both 100 and 150 nM doses. All gene silencing data are normalized to an analogous scrambled siRNA control with the same carrier (HDG-NP and non-HDG-NP) and at each dose (100 and 150 nM). LF2K = Lipofectamine 2000.

The level of knockdown from HDG-NPs did not match that of LF2K in vitro. This is not surprising, as LF2K has a very high zeta potential that drives cell interactions and internalization in vitro. However, non-PEGylated, cationic transfection agents such as LF2K are not suitable for systemic delivery in vivo, whereas the HDG-NPs are more amenable to in vivo intravenous siRNA delivery. The level of knockdown achieved in vitro does not reach that of some of the most

optimized transfection reagents, but the performance is comparable to other PEGylated or decationized delivery systems.[248,382] Overall, these data suggest that incorporation of mechanisms for un-packaging is a feasible route to improving the bioactivity of PEGylated polyplex delivery systems.

The observed increase in gene silencing by the HDG-NPs, despite having similar hemolysis, cell uptake, and viability as non-HDG-NPs under the conditions tested, suggests that the addition of a hydrolytic, charge-reversal-based siRNA release mechanism improved carrier release and intracellular bioavailability of the siRNA. To test this in vitro, we monitored the FRET efficiency of paired siRNAs co-loaded into both particle types to investigate whether charge reversal led to an increase in intracellular un-packaging of siRNA (**Figure A.6 and Supplementary Figure SA.5**). Non-HDG-NPs exhibited punctate regions of strong FRET efficiency within cells, suggesting that part of the siRNA delivered into the cells remained packaged tightly within the NPs (**Figure A.6a**). Quantification across all images acquired showed that non-HDG-NPs consistently retained significantly higher intracellular FRET signal than HDG-NPs (**Figure A.6b**). The HDG-NP and non-HDG-NP treatments administered to these cells were confirmed to have the same level of FRET efficiency at t = 0 h (**Figure A.6c**). Moreover, the increased loss of HDG-NP FRET was confirmed in solution at 24 h by re-measuring the same treatment aliquots after incubation in PBS (**Figure A.6c**). Presumably, the siRNA still packaged within non-HDG-NPs would not be bioavailable for assembly into the RISC complex because of steric and electrostatic hindrance of the associated polymer. On the other hand, HDG-NP-treated cells had negligible FRET signal. Our collective data indicate that the hydrolysis of the cationic siRNA-condensing moiety, and subsequent charge-reversal, of the HDG-NPs provided an

effective mechanism for enhanced siRNA intracellular un-packaging and improved gene silencing bioactivity.

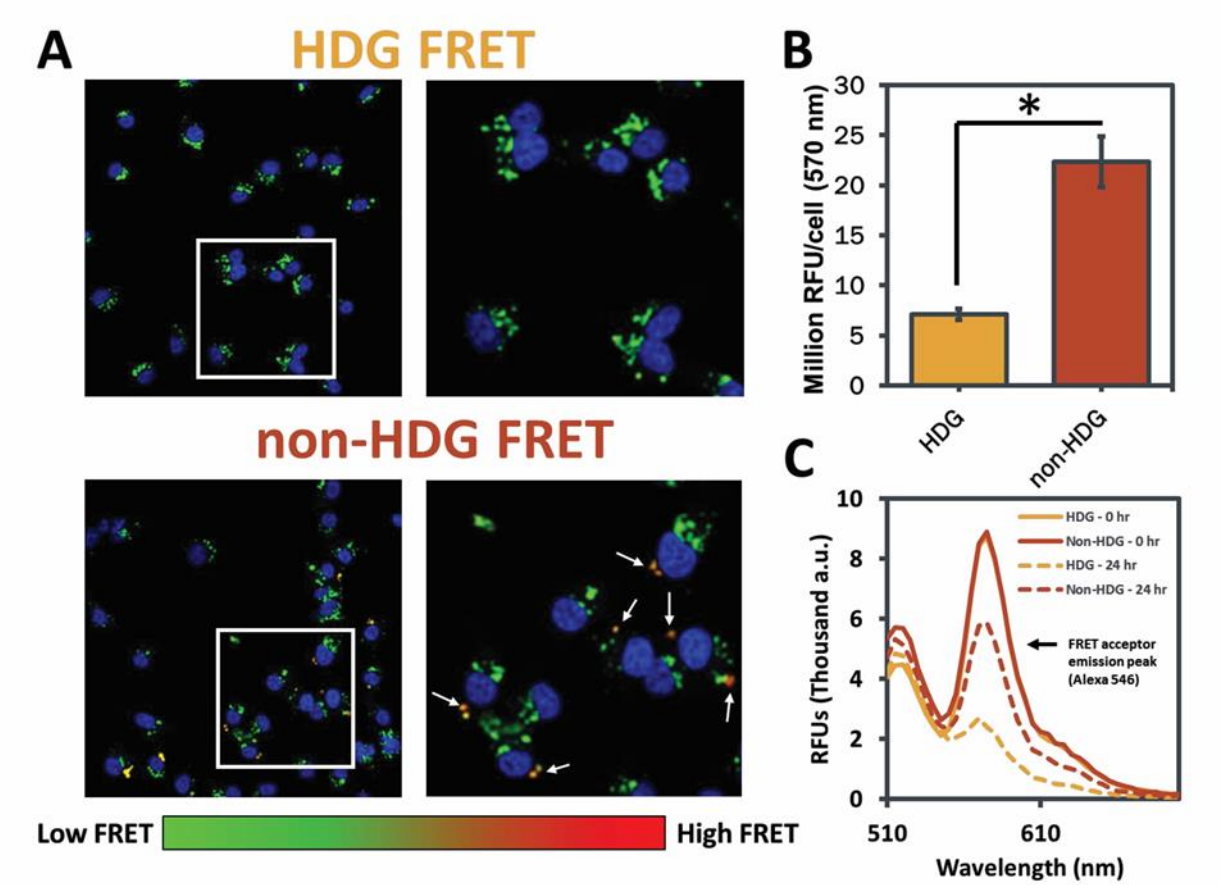

Figure A.6) Analysis of intracellular un-packaging of siRNA delivered from non-HDG- and HDG-NPs by FRET microscopy. (A) Representative microscopy images of MDA-MB-231s after delivery of FRET-labeled siRNA from non-HDG- and HDG-NPs. FRET signal is detected consistently within cells treated with non-HDG-NPs, whereas minimal FRET is detected within HDG-NP-treated cells. All images are presented at the same intensity scale. (B) Microscopy image quantification of emission intensity at 570 nm (FRET acceptor emission; n = 4, 9 images/n, > 9,000 cells total) (C) Fluorescence spectra of FRET-labeled NPs at 0 and 24 h incubation in PBS.

Conclusions

Cytosolic release of siRNA is often overlooked within non-viral gene delivery vector development. Here, a comparative study of HDG-NPs and non-HDG-NPs confirms that incorporation of a cytosolic release mechanism using the hydrolytically-degradable, charge-

reversing cationic monomer DMAEA improves intracellular release and bioactivity of endosomolytic, surface charge-neutral, PEGylated siRNA polyplexes. The HDG-NPs are stabilized upon initial formulation but have accelerated release of siRNA cargo in aqueous solutions relative to non-HDG-NPs; importantly, increased cargo release of the HDG-NPs was also confirmed intracellularly by FRET microscopy. Increased un-packaging of siRNA delivered by HDG-NPs correlated with significantly higher target gene silencing of the model gene luciferase in vitro compared to non-HDG-NPs, despite minimal differences in hemolysis, cell uptake, and viability under the test conditions. Overall, these results suggest that activity of endosomolytic, charge-neutral, PEGylated siRNA polyplexes can be increased by improving cytosolic release. This work motivates further exploration into charge-reversing systems, including carriers that respond to specific cues such as pH, oxidation / reduction, enzymatic cleavage, light activation, etc. to leverage “smarter” intracellular un-packaging triggers.

Supplementary material for Appendix A

Oligonucleotide	Sequence (5' -> 3')	Source
Alexa488-Sense	GTCAGAAATAGAAACTGGTCATC	IDT
Alexa488-Antisense	[Alexa488]GATGACCAGTTTCTATTTCTGAC	IDT
Alexa546-Sense	GTCAGAAATAGAAACTGGTCATC	IDT
Alexa546-Antisense	[Alexa546]GATGACCAGTTTCTATTTCTGAC	IDT
Cy5-Sense	GTCAGAAATAGAAACTGGTCATC	Sigma
Cy5-Antisense	[Cyanine5]GATGACCAGTTTCTATTTCTGAC	Sigma
Luc-Sense	CAAUUGCACUGAUAAUGAACUCC[dT][dC]	Sigma
Luc-Antisense	GAGGAGUUCAUUAUCAGUGCAAUUGUU	Sigma
Scr-Sense	CGUUAAUCGCGUAUAAUACGCGU[dA][dT]	Sigma
Scr-Antisense	AUACGCGUAU[mU]A[mU]ACGCGAU[mU]A[mA]C[mG][mA][mC]	Sigma

*Nomenclature: [d] = chiral DNA base, [m] = backbone 2'O-methyl modification

Supplementary Table SA.1) List of oligonucleotide sequences.

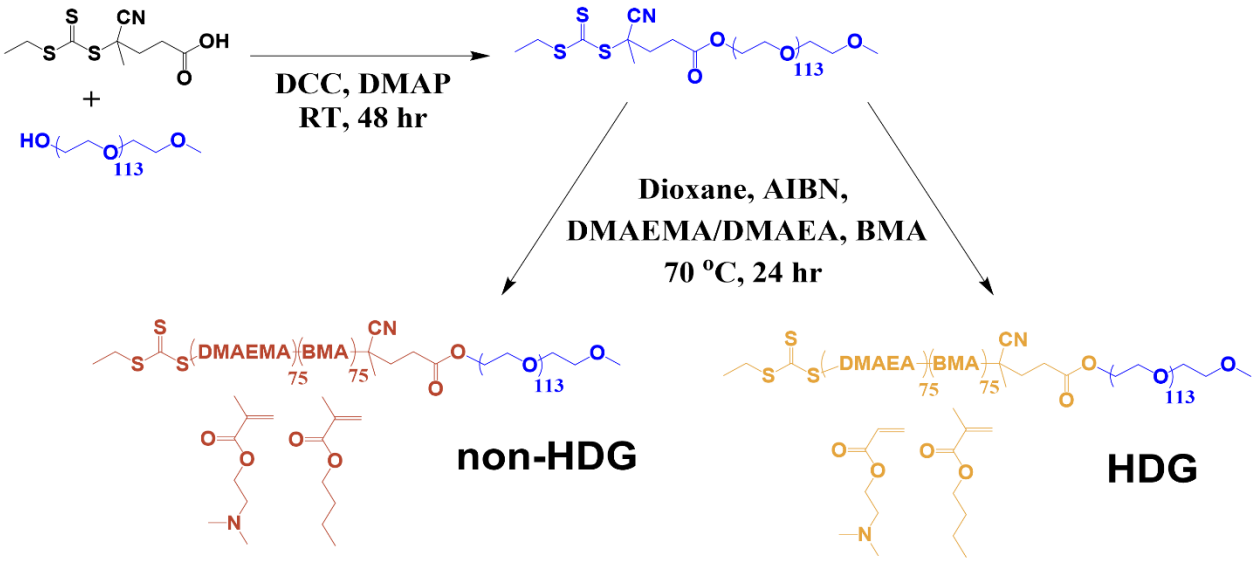

Supplementary Figure SA.1) Synthesis scheme for PEG-*b*-p(DMAEMA-*co*-BMA) (non-HDG) and PEG-*b*-p(DMAEA-*co*-BMA) (HDG). Non-HDG and HDG polymers were synthesized from a 5 kDa PEG reversible addition-fragmentation chain-transfer (RAFT) macro-Chain Transfer Agent (macro-CTA).

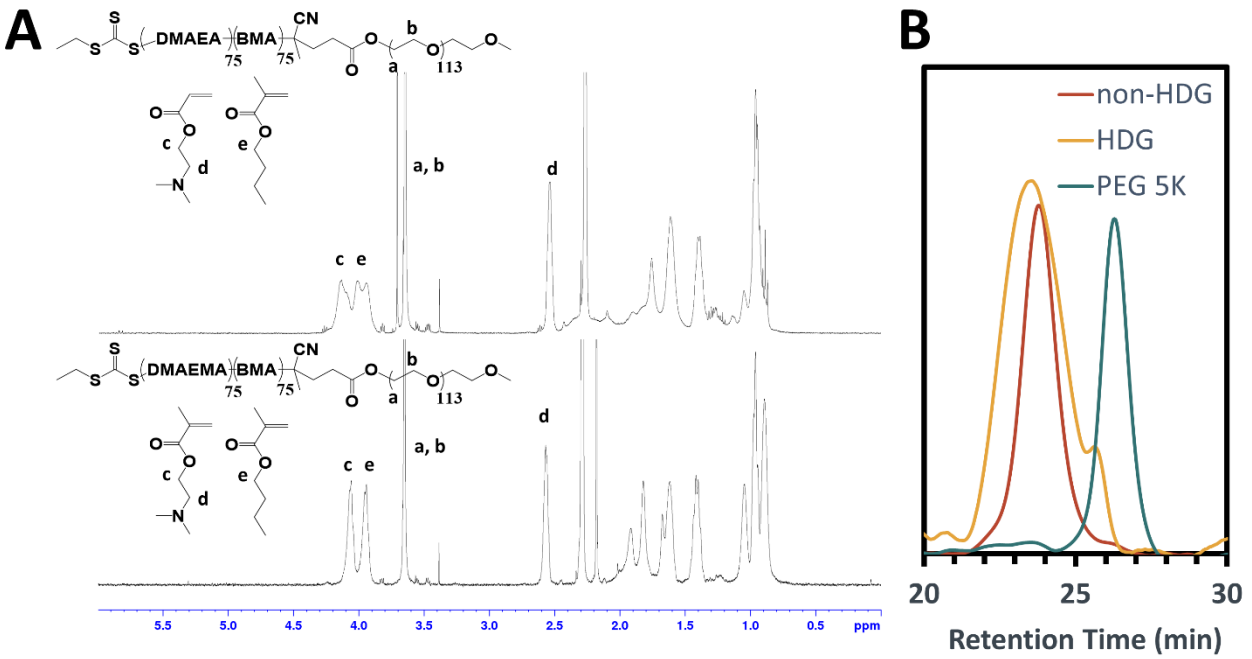

Supplementary Figure SA.2) Polymer characterization. (A) ^{1}H-NMR spectrums of HDG (top) and non-HDG (bottom) polymers. The molecular weight was quantified by integrating the PEG peak (d, -OC**H**$_2$C**H**$_2$-, δ 3.65s) and comparing to DMAEA/DMAEMA (a, -O-C**H**$_2$CH$_2$-, δ 4.05s) and BMA (c, -O-C**H**$_2$CH$_2$-, δ 3.95s). The %composition was quantified by integrating (a) and (c) together and then subtracting the amine peak of DMAEA/DMAEMA (b, -CH$_2$N**H**$_2$, δ 2.60s). (B) Gel permeation chromatography (GPC) elugrams for 5 kDa PEG macro-CTA, HDG, and non-HDG polymers.

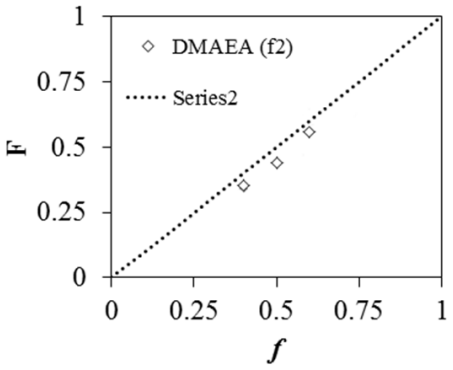

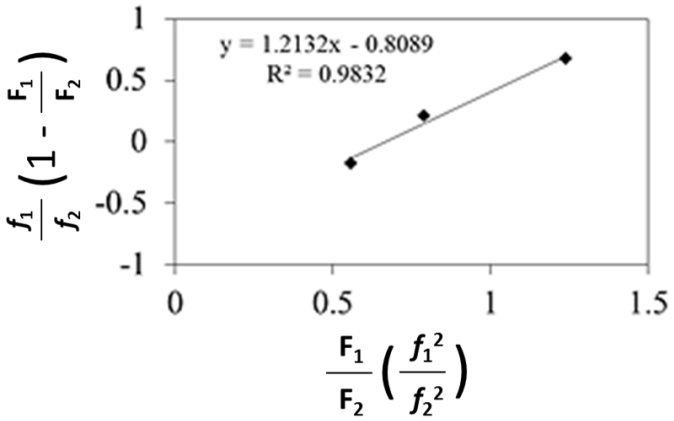

Ross Fineman Equation

$$M - \left(\frac{M}{P}\right) = - r_2 + r_1\left(\frac{M^2}{P}\right)$$

$$M = \frac{f_1}{f_2}$$

$$P = \frac{F_1}{F_2}$$

r_1 = Reactivity ratio of BMA

r_2 = Reactivity ratio of DMAEA

f_1 = Molar concentration of BMA in the monomer feed

f_2 = Molar concentration of DMAEA in the monomer feed

F_1 = Molar concentration of BMA in the polymer

F_2 = Molar concentration of DMAEA in the polymer

Supplementary Figure SA.3) Reactivity ratios of DMAEA and BMA determined by the Fineman-Ross method. HDG and non-HDG polymers were synthesized at the following three molar feed ratios [DMAEA:BMA] to determine polymerization kinetics: [40:60], [50:50], and [60:40]. Reactivity of DMAEA and BMA are close to 1, indicating a random copolymerization from the 5 kDa PEG macro-CTA.

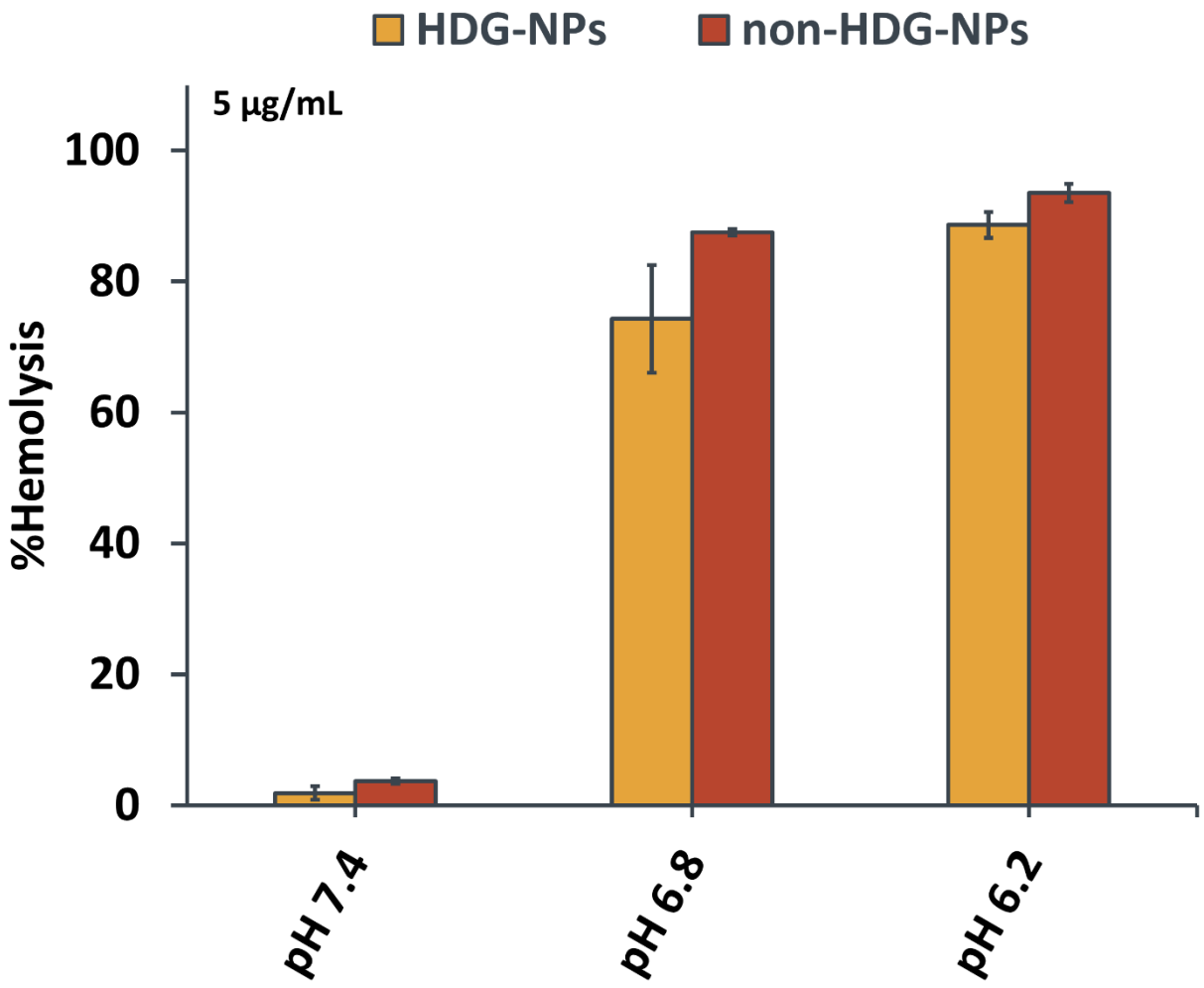

Supplementary Figure SA.4) Comparative hemolysis of HDG- and non-HDG-NPs. Both HDG- and non-HDG-NPs exhibit switch-like, pH-dependent membrane disruption starting at early endosomal pH (6.8) as indicated by the increase in hemolysis from ~0% at pH 7.4 to ~80% at pH 6.8.

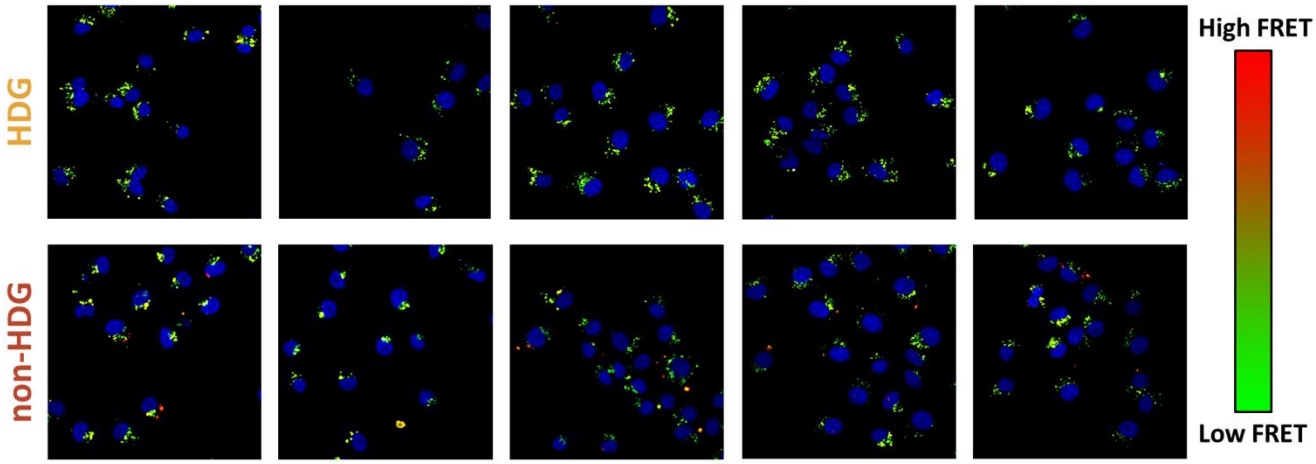

Supplementary Figure SA.5) Panel of representative FRET microscopy images. Strong punctate FRET signal is detected consistently across images of non-HDG-NP-treated cells while FRET signal is not apparent in HDG-NP-treated cells.

APPENDIX B

SUPPLEMENTARY MATERIAL FOR CHAPTER II

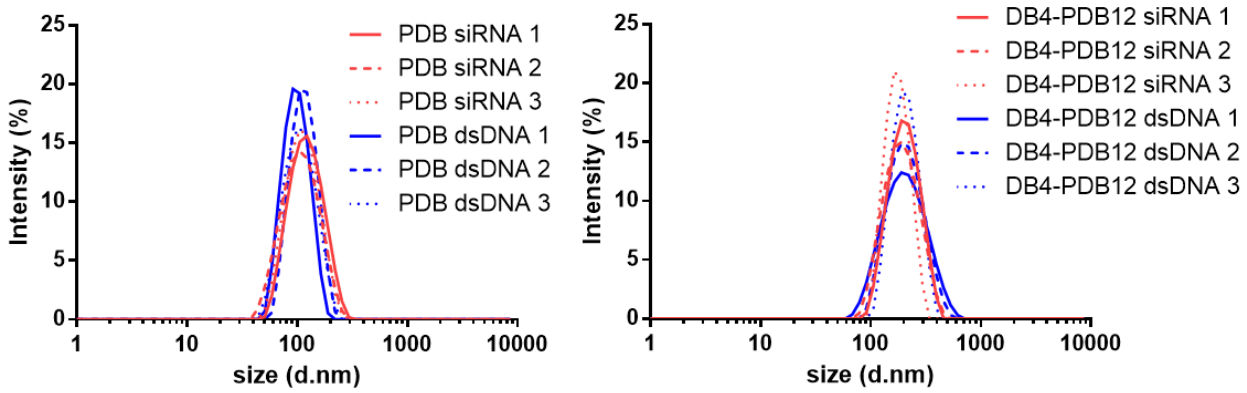

Figure B.1) PDB and DB4-PDB12 si-NPs form reproducibly and there is no appreciable size difference between si-NPs formed using siRNA or dsDNA.

Oligonucleotide	Sequence (5' -> 3')	Source
Alexa488-Sense	dGdTdCdAdGdAdAdAdTdAdGdAdAdAdCdTdGdGdTdCdAdTdC	IDT
Alexa488-Antisense	[Alexa488]dGdAdTdGdAdCdCdAdGdTdTdTdCdTdAdTdTdTdCdTdGdAdC	IDT
Cy5-Sense	dGdTdCdAdGdAdAdAdTdAdGdAdAdAdCdTdGdGdTdCdAdTdC	IDT
Cy5-Antisense	[Cyanine5]dGdAdTdGdAdCdCdAdGdTdTdTdCdTdAdTdTdTdCdTdGdAdC	IDT
Luc-Sense	rCrArArUrUrGrCrArCrUrGrArUrArArUrGrArArCrUrCrCdTdC	Sigma
Luc-Antisense	rGrArGrGrArGrUrUrCrAmUrUmArUrCrArGrUrGrCmArAmUrUmGmUmU	Sigma
Scr-Sense	rCrGrUrUrArArUrCrGrCrGrUrArUrArArUrArCrGrCrGrUdAdT	Sigma
Scr-Antisense	rArUrArCrGrCrGrUrArUmUrAmUrArCrGrCrGrArUmUrAmArCmGmAmC	Sigma

***Nomenclature: d = DNA base, r = RNA base, m = backbone 2'O-methyl modification**

Table B.1) Oligonucleotide sequences used in studies.

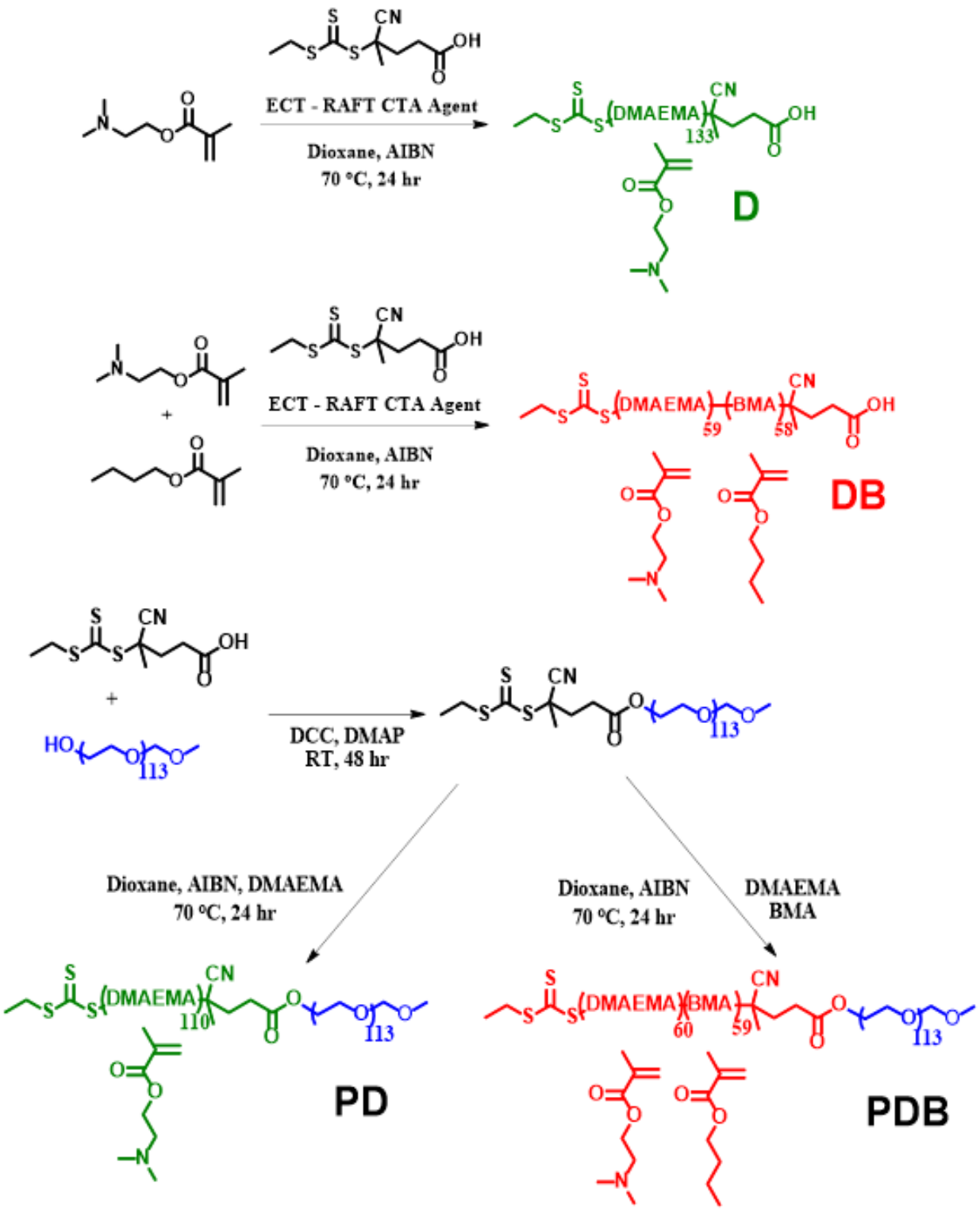

Figure B.2) Polymer synthesis schemes. Four single-pot reactions yield the D, DB, PD, and PDB polymer units for forming unique classes of ternary siRNA polyplexes (si-NPs).

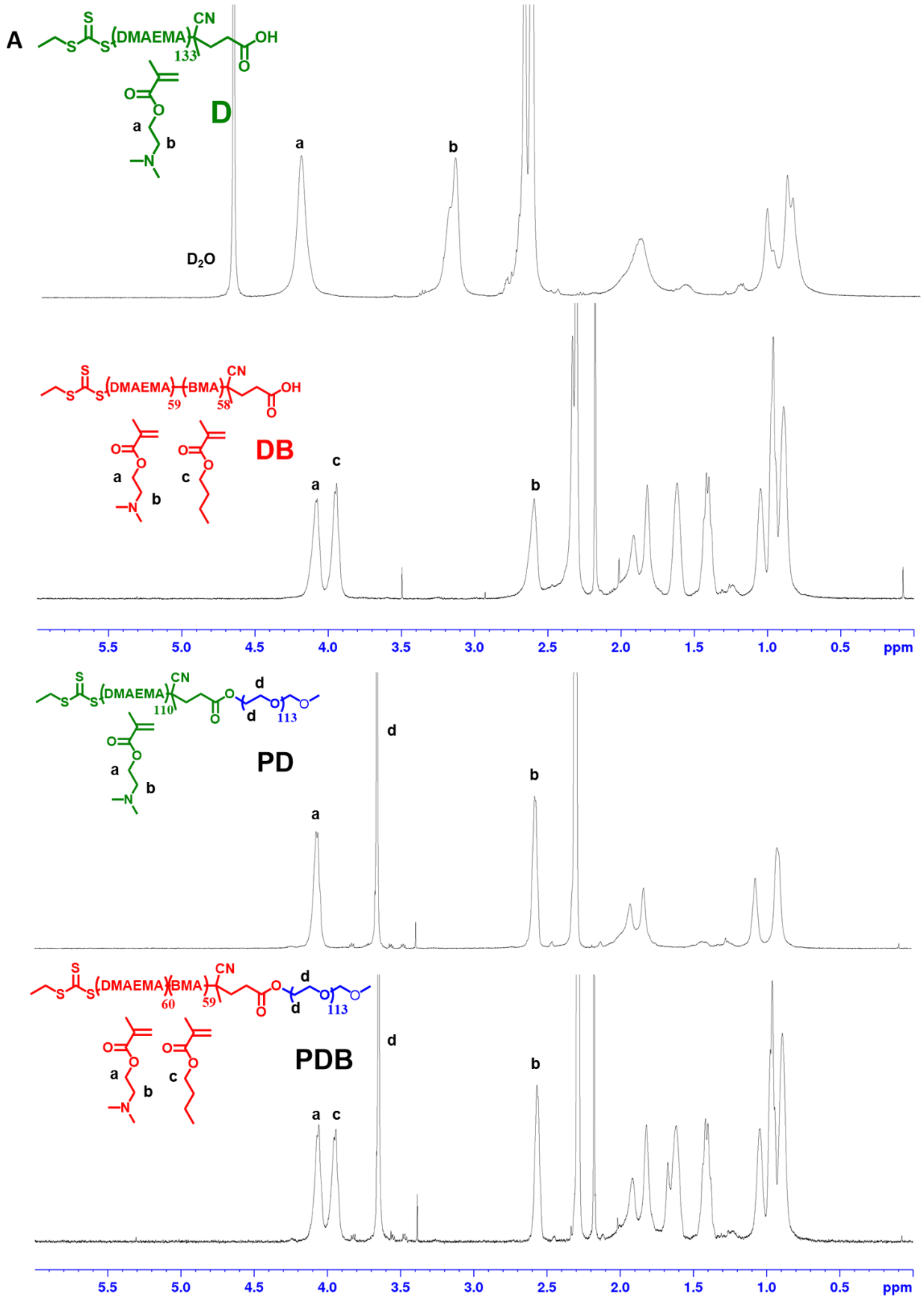
A
D
DB
PD
PDB
D2O
a
b
c
d
5.5
5.0
4.5
4.0
3.5
3.0
2.5
2.0
1.5
1.0
0.5
ppm

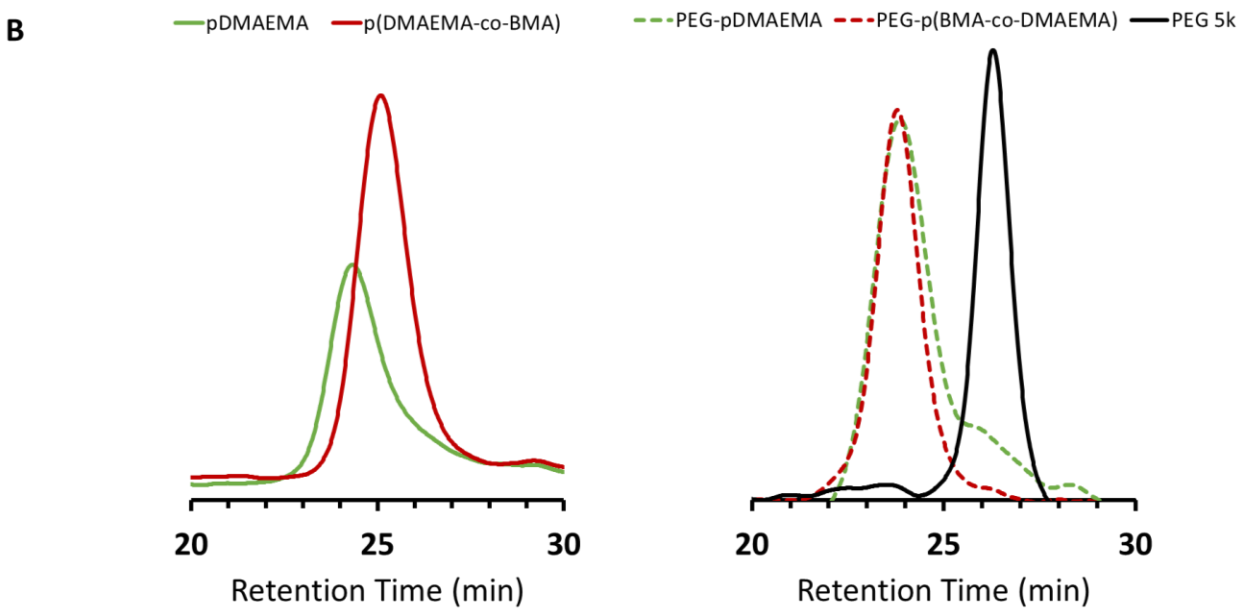

Figure B.3) Polymer characterization. (A) ^{1}H-NMR characterization of D (in D_2O) and DB, PD, and PDB (in $CDCl_3$) polymers used as base units of ternary polyplexes. (B) Gel Permeation Chromatography (GPC) elugrams of D, DB, PD, and PDB polymers used as the base units of ternary polyplexes.

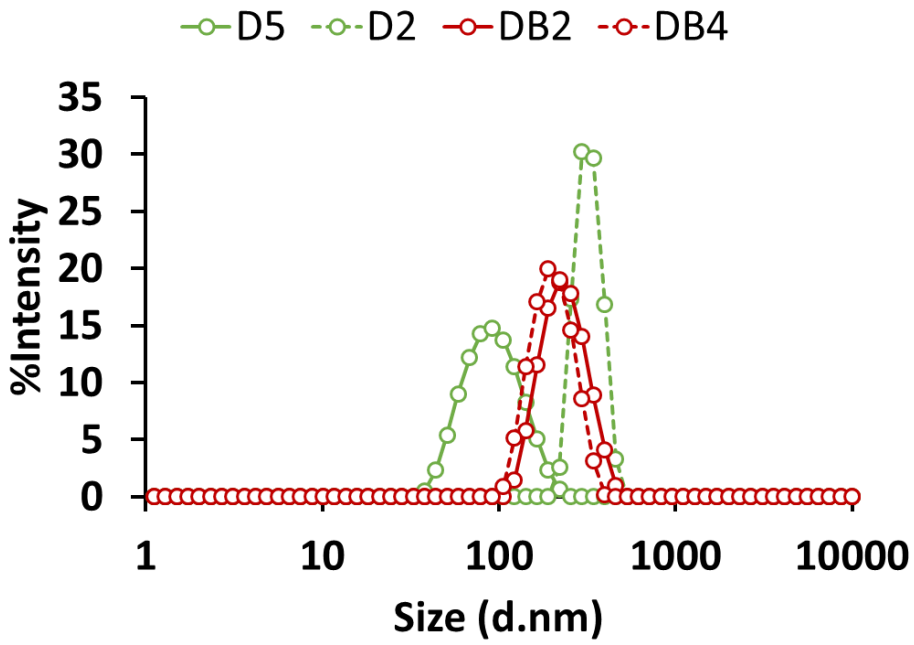

Figure B.4) DLS size characterization of binary polyplex precursors (pre-NPs) at pH 4.0.

	DB2-PD4	DB2-PD6	DB2-PD8	DB2-PD12	DB2-PD16
Size - 0 Hour (nm)	191.5	190.4	179.2	162.9	173.2
Size - 24 Hour (nm)	189.1	199.1	213.6	52.99	222.1
Polydispersity Index (PDI)	0.119	0.184	0.128	0.312	0.436
Zeta Potential (mV)	-0.139	0.486	0.479	0.45	0.0192
	DB4-PD6	DB4-PD8	DB4-PD12	DB4-PD16	DB4-PD20
Size - 0 Hour (nm)	201.4	119.3	38.23	52.78	26.48
Size - 24 Hour (nm)	361.3	371.9	350.1	292.8	18.59
Polydispersity Index (PDI)	0.134	0.705	1.0	1.0	0.866
Zeta Potential (mV)	-0.0833	1.25	0.729	1.1	-0.0389
	DB2-PDB4	DB2-PDB6	DB2-PDB8	DB2-PDB12	DB2-PDB16
Size - 0 Hour (nm)	99.85	111.4	108.6	118.2	111.2
Size - 24 Hour (nm)	109.4	113	110.8	116	110.4
Polydispersity Index (PDI)	0.247	0.249	0.269	0.279	0.254
Zeta Potential (mV)	0.476	0.00486	-0.0466	0.842	1.08
	DB4-PDB6	DB4-PDB8	DB4-PDB12	DB4-PDB16	DB4-PDB20
Size - 0 Hour (nm)	97.52	111.4	113.3	114.7	118.8
Size - 24 Hour (nm)	106.0	116.0	124.4	126.3	120.9
Polydispersity Index (PDI)	0.196	0.222	0.219	0.246	0.243
Zeta Potential (mV)	0.541	0.144	0.139	0.167	0.0878
	D5-PDB1	D5-PDB2	D5-PDB4	D5-PDB6	D5-PDB8
Size - 0 Hour (nm)	109.2	91.99	77.47	90.25	78.08
Size - 24 Hour (nm)	102.4	94.52	78.53	96.33	74.84
Polydispersity Index (PDI)	0.148	0.173	0.173	0.210	0.197
Zeta Potential (mV)	-0.315	0.566	0.00494	-0.504	0.0301
	D2-PDB4	D2-PDB6	D2-PDB8	D2-PDB12	D2-PDB16
Size - 0 Hour (nm)	327.1	242.1	61.64	63.3	69.37
Size - 24 Hour (nm)	450.3	344.4	55.9	60.03	76.16
Polydispersity Index (PDI)	0.023	0.186	0.237	0.255	0.34
Zeta Potential (mV)	0.0399	-0.0708	-0.052	0.98	1.21

Table B.2) Dynamic light scattering (DLS) values for polyplex size and zeta potential (surface charge).

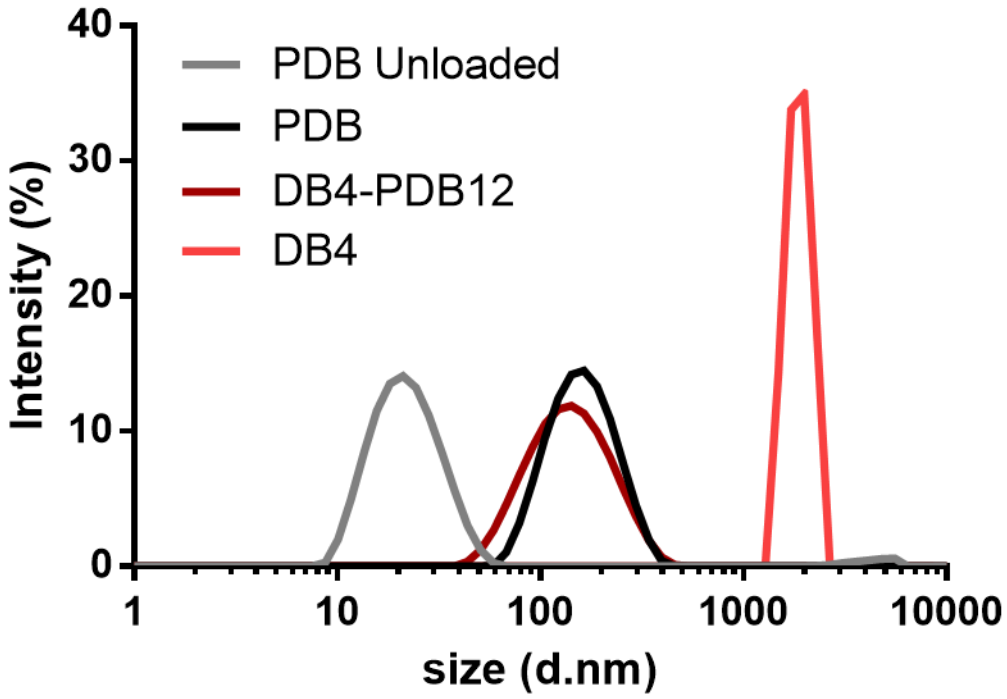

Figure B.5) DLS spectra showing unloaded PDB polymer and dsDNA-loaded PDB, DB4-PDB12, and DB4 si-NPs at pH 7.4. Key observations are that the PDB polymers form small micelles (~20 nm) in solution when not loaded with nucleic acid cargo and that the DB4 pre-NPs aggregate into large (>1 um) and polydisperse (0.5 – 1.0 PDI) structures at pH 7.4; neither of these structures are apparent in the DB4-PDB12 formulation.

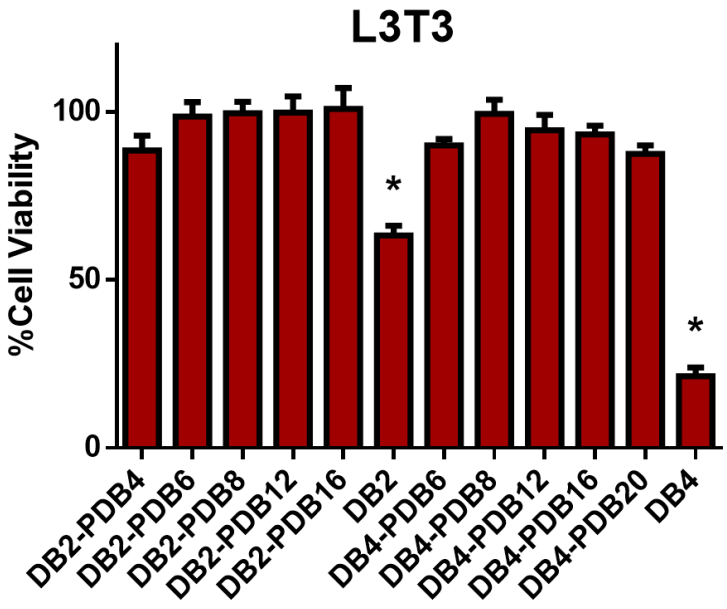

Figure B.6) Cytocompatibility of DB-PDB class of ternary si-NPs compared to the DB2 and DB4 pre-NPs. The coating of pre-NPs with the PEGylated, PDB polymer significantly increases si-NP biocompatibility.

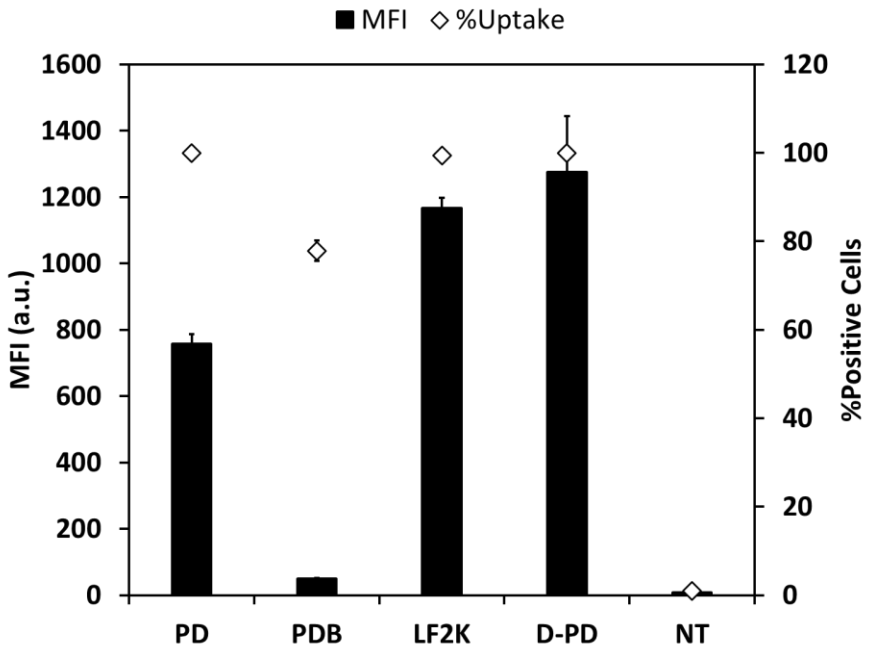

Figure B.7) Mean fluorescence intensity and percent positive cells indicating intracellular delivery of siRNA by PD, PDB, D-PD, LF2K, and NT. PD and PDB represent the binary si-NP formulation of the two corona-forming diblock polymers. D-PD represents ternary si-NPs formed with purely cationic components [pDMAEMA (D) and PEG-*b*-pDMAEMA (PD)]. (LF2K = Lipofectamine 2000, NT = No Treatment)

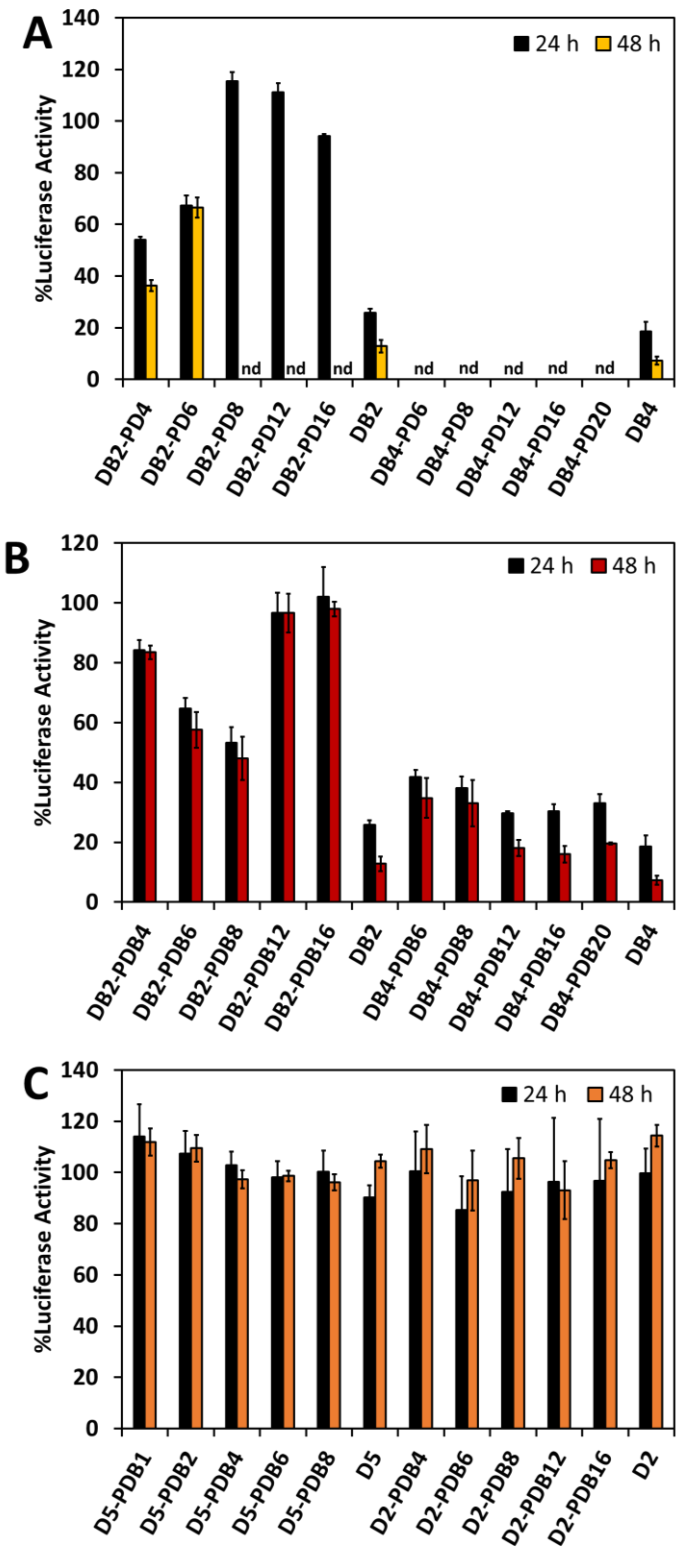

Figure B.8) *In vitro* target gene silencing of the model gene luciferase in luciferase-expressing mouse embryonic fibroblasts (L3T3s) by (A) DB-PD, (B) DB-PDB, and (C) D-PDB.

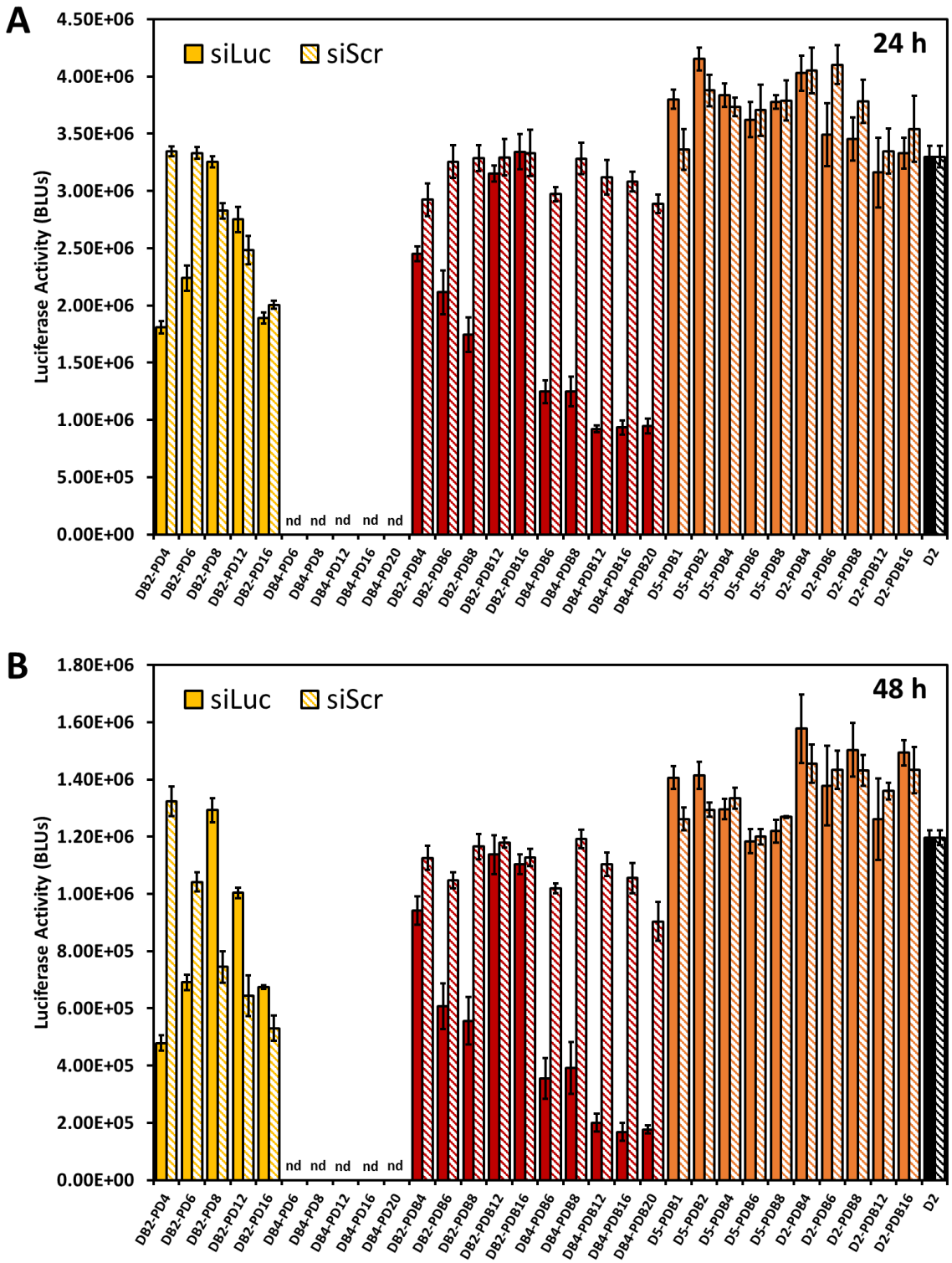

Figure B.9) Raw bioluminescence values of L3T3 cells after treatment with ternary si-NPs containing either luciferase (siLuc) or scrambled (siScr) siRNA sequences at (A) 24 and (B) 48 h post-treatment. (NT = no treatment)

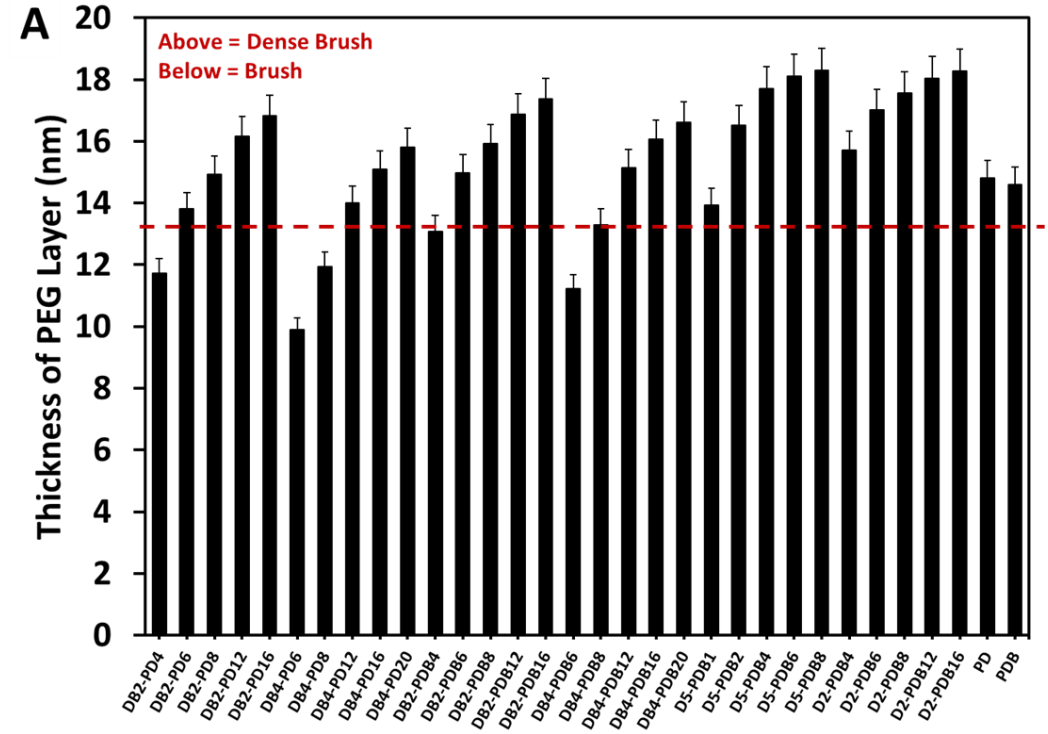

B

$$A = \frac{6M_{PEG}}{dN_A f \rho} \quad (1)$$

$$D = 2\sqrt{\frac{A}{\pi}} \quad (2)$$

$$L = \frac{Na^{5/3}}{D^{2/3}} \quad (3)$$

Definitions

A ≡ Area one PEG chain occupies
M_{PEG} ≡ PEG molecular weight
d ≡ nanoparticle diameter
N_A ≡ Avogadro's Number
f ≡ PEG mass fraction
ρ ≡ nanoparticle density
D ≡ distance between PEG chains
N ≡ number of monomers per PEG chain
a ≡ length of one PEG monomer
L ≡ Thickness of PEG layer

Constants

M_{PEG} = 5000 Da
N_A = 6.02e23
ρ = 1.1 – 1.3 g/mL
N = 113
a = 0.35 nm

Figure B.10) Calculated PEG density on surface of ternary polyplexes. (A) PEG thickness. (B) Series of equations used to calculate PEG density. Nanoparticle density was estimated based upon literature values (ρ_{min} = 1.1 g/mL and ρ_{max} = 1.3 g/mL). Standard deviation was calculated based on PEG thickness calculations for minimum and maximum particle densities.

Threshold	Red	Orange	Eggshell	Units
Size	< 100	100 < x < 200	> 200	nm
Uptake	> 100	50 < x < 100	< 50	MFI
Hemolysis (pH 6.8)	> 60	20 < x < 60	< 20	%
Core Composition	4.0	2.0	0.5	N:P Ratio
DB Core	+		-	N/A
In vitro Gene Silencing	< 20	20 < x < 70	> 70	%

Table B.3) Heat map (Figure 2.6a) parameters and thresholds.

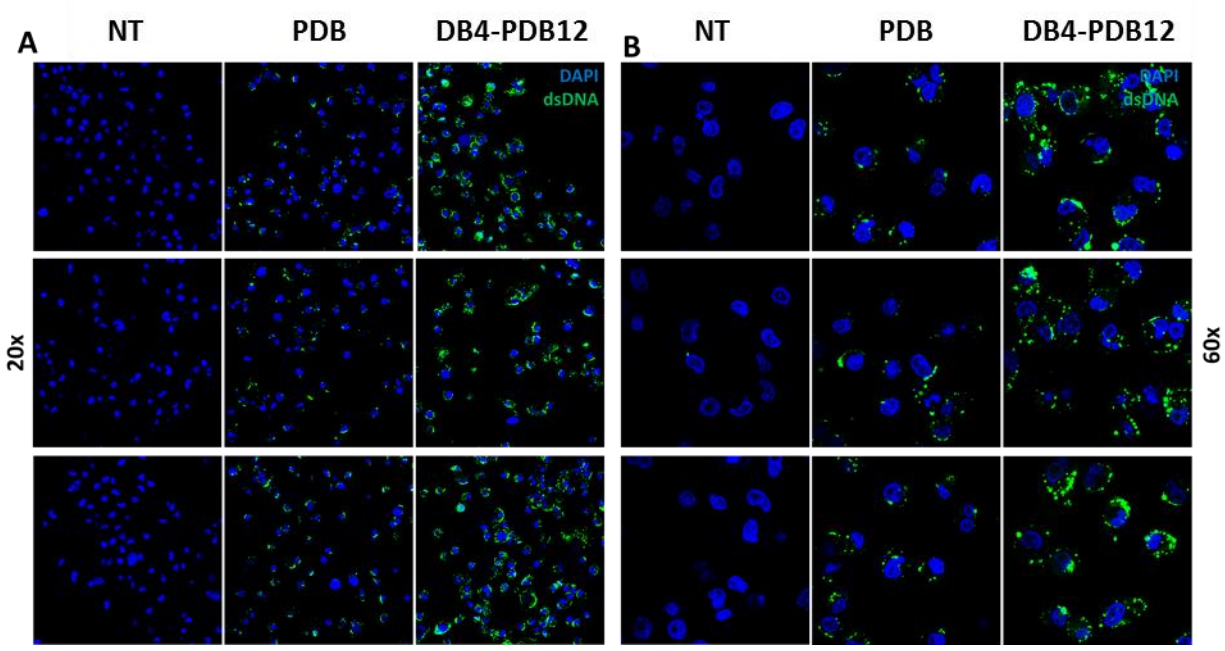

Figure B.11) Panel of confocal microscopy images at (A) 20x and (B) 60x magnification after 24 h treatment with PBS, PDB, or DB4-PDB12.

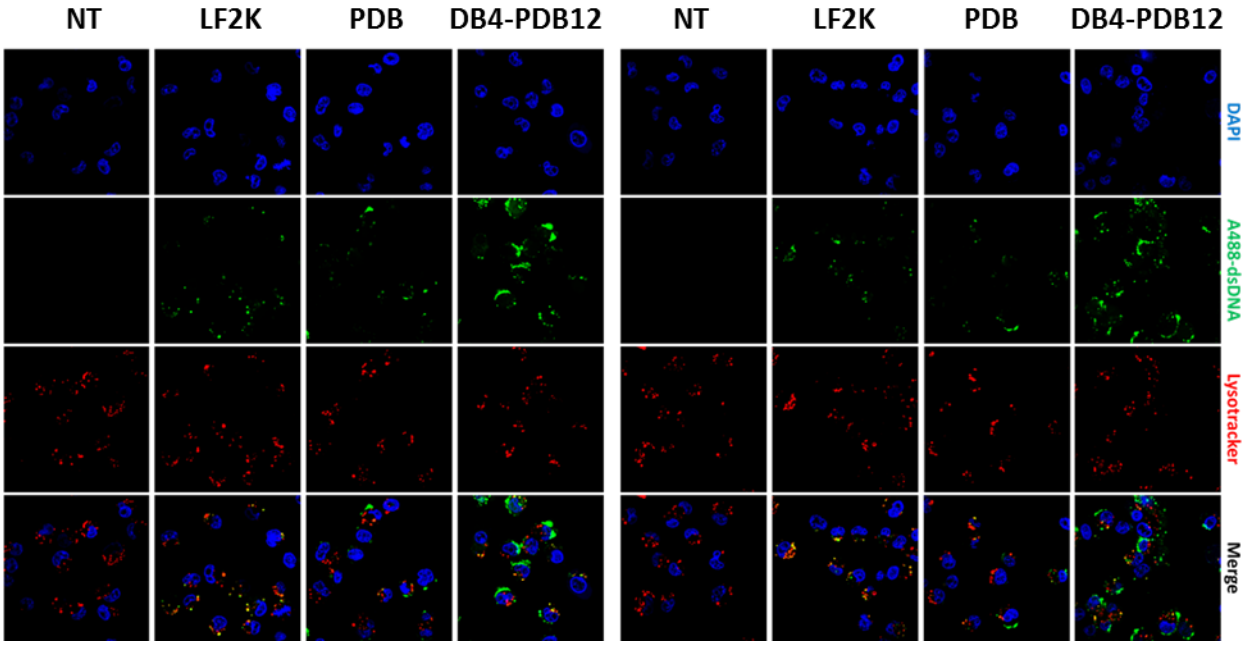

Figure B.12) Panel of confocal microscopy images at 60x magnification after 24 h treatment with PBS, LF2K, PDB, or DB4-PDB12 and acidic endolysosomal vesicle labeling by Lysotracker Red. LF2K is administered at the maximum tolerated dose of 25 nM. (LF2K = Lipofectamine 2000)

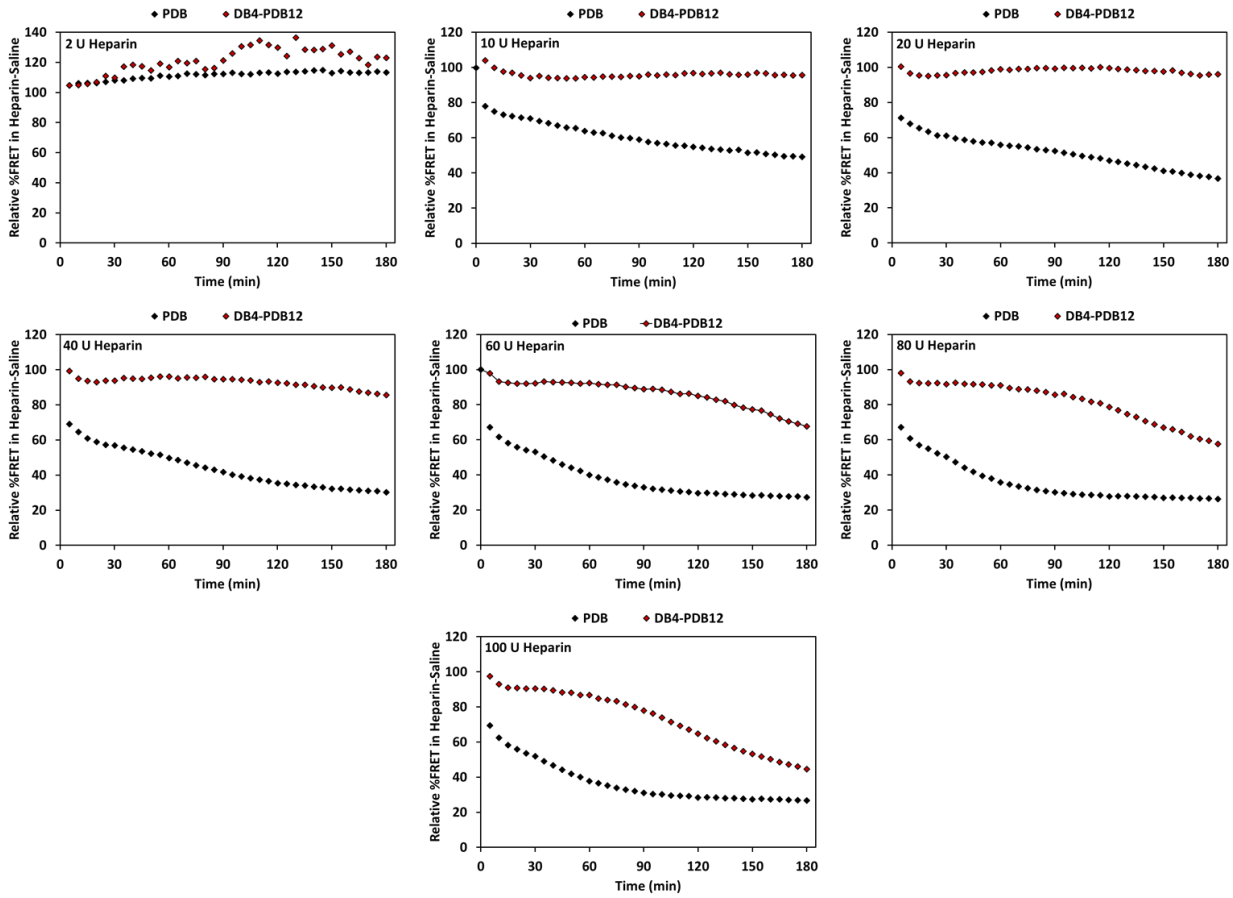

Figure B.13) Comprehensive panel of FRET-measured si-NP dissociation over time upon exposure to heparin-saline.

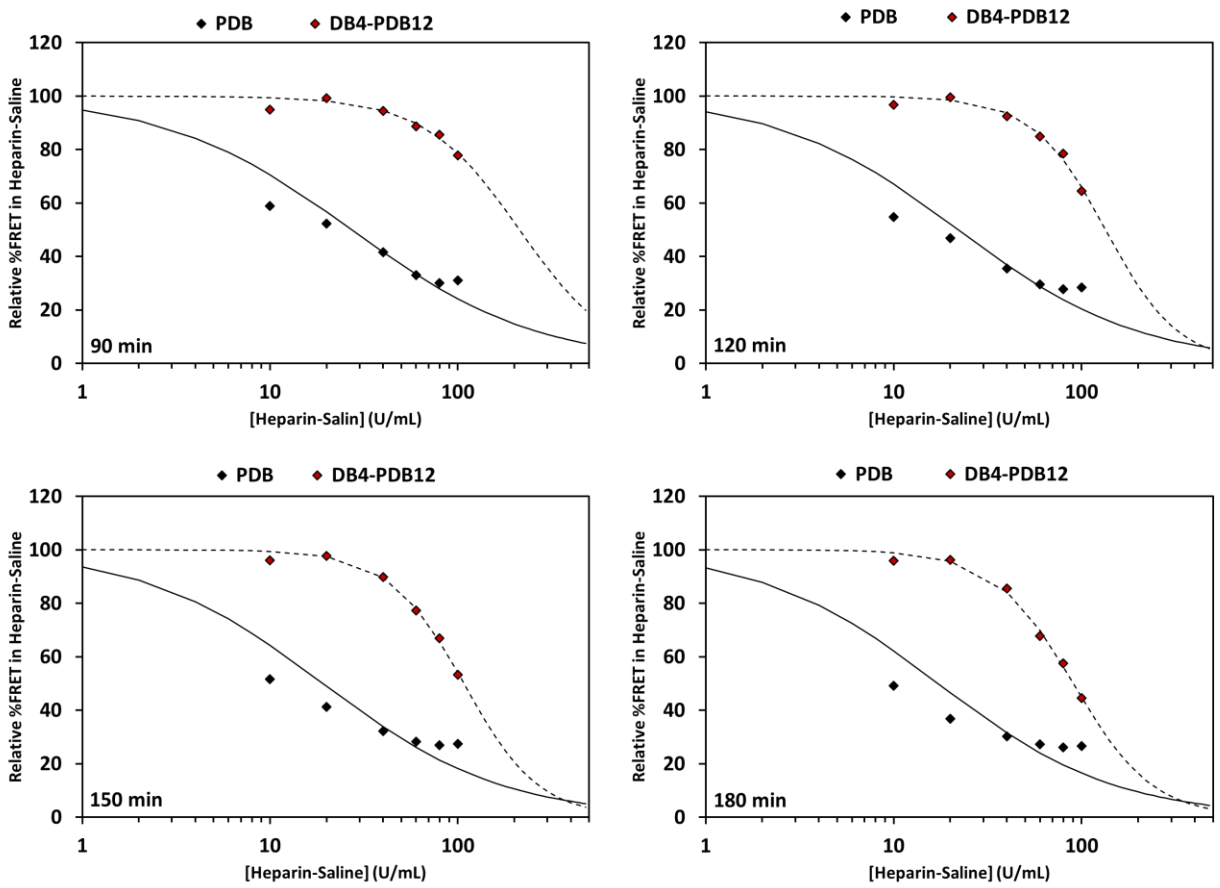

Figure B.14) Comprehensive panel of FRET-measured si-NP dissociation over range of heparin-saline doses. At time points earlier than 90 min, there is no measurable dissociation of DB4-PDB12 si-NPs.

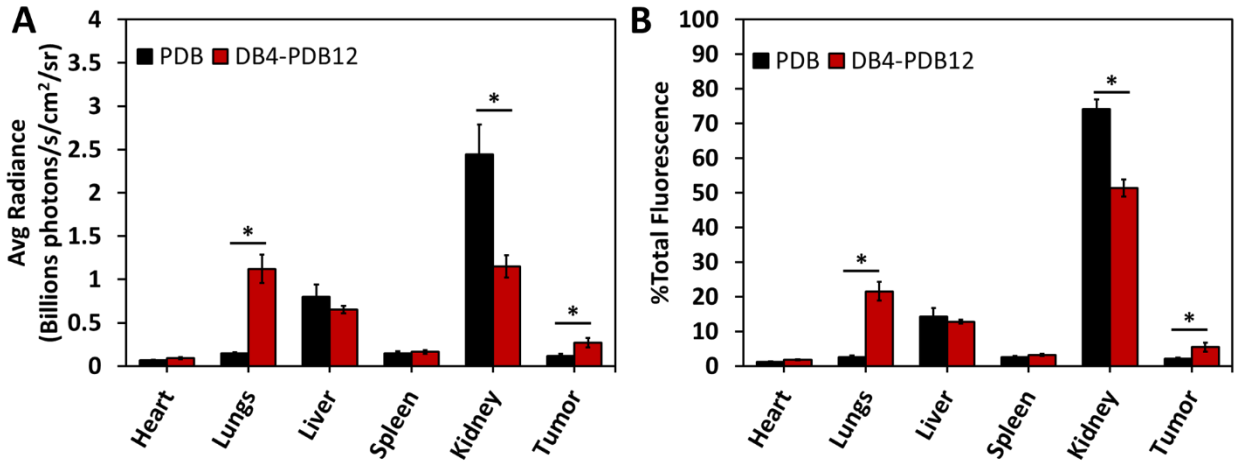

Figure B.15) Biodistribution of binary (PDB) and ternary (DB4-PDB12) si-NPs in tumor-bearing athymic nude mice represented as (A) average radiance and (B) percent of the total measured fluorescence in all organs.

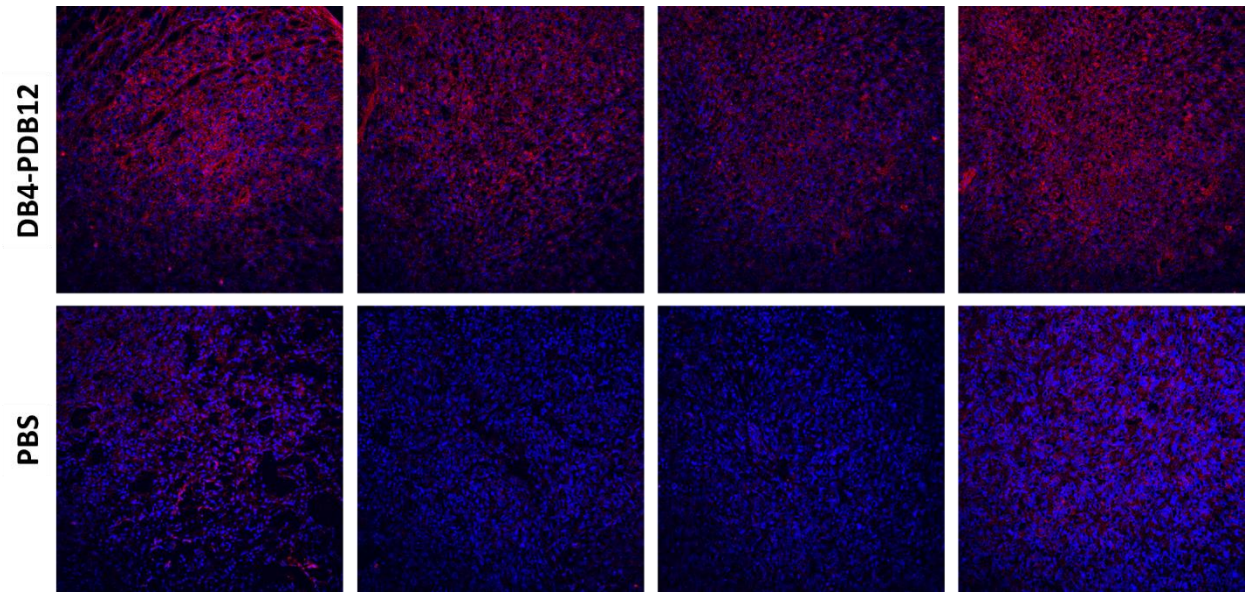

Figure B.16) Panel of confocal images of tumor sections from tumor-bearing mice treated with DB4-PDB12 si-NPs or PBS.

APPENDIX C

SUPPLEMENTARY MATERIAL FOR CHAPTER III

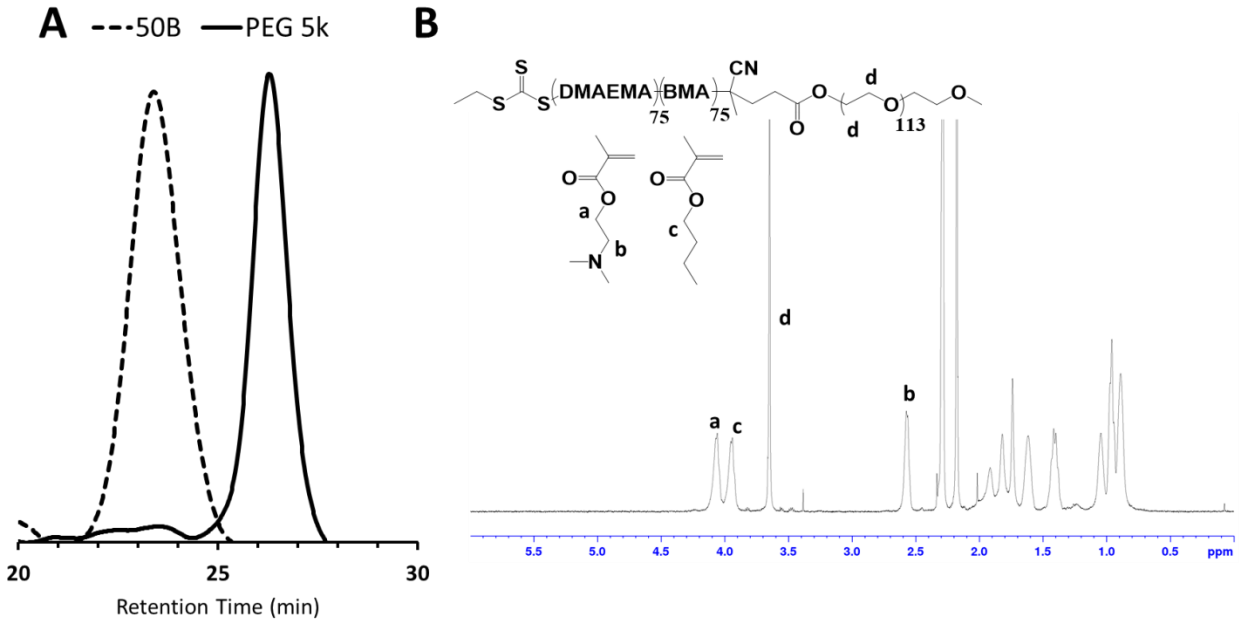

Polymer	RU[a]	%BMA[a]	%DMAEMA[a]	Mn[a]	Mw[b]	PDI[b]
50B	152	49.1	50.9	27800	28060	1.033

Figure C.1) Characterization of 50B polymer by (A) GPC and (B) ^{1}H-NMR.

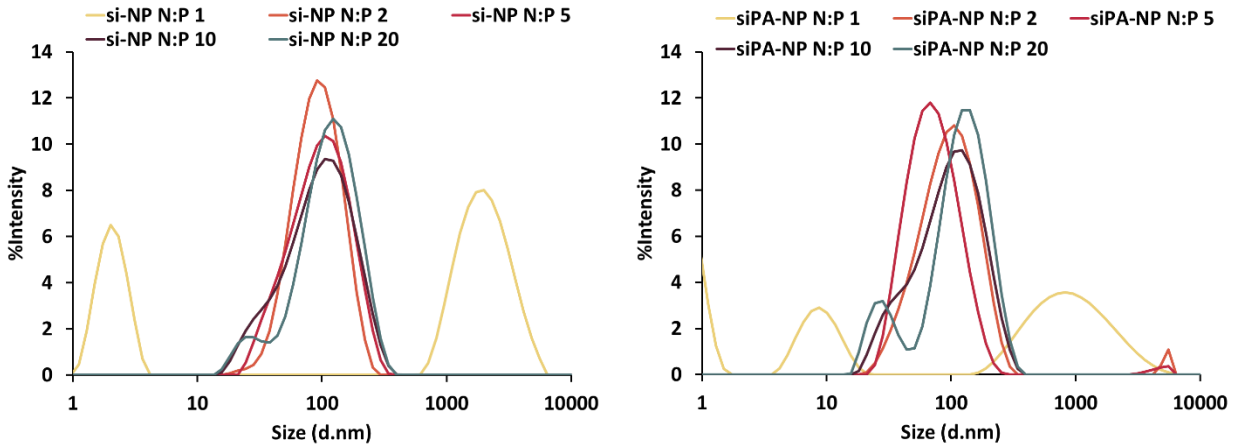

Figure C.2) DLS size characterization of siPA-NPs vs. si-NPs at a range of N:P ratios.

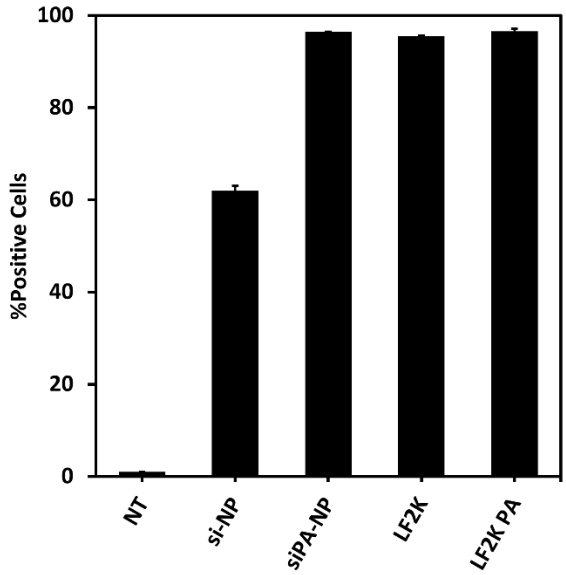

Figure C.3) Cell internalization of si-NPs and siPA-NPs at N:P = 10:1 plotted as percent positive cells compared to no treatment.

Parameter	Equation
1st Order Model	$C = C_o e^{-k_{el}t}$
$t_{1/2}$	$= \frac{\ln(2)}{k_{el}}$
$AUC_{0\text{-}t}$	$= \int_0^t C\,dt = \frac{C_o e^{-k_{el}t}}{-k_{el}}$
CL	$= \frac{D}{AUC}$

Where, C = Plasma Drug Concentration, C_o = Initial Plasma Drug Concentration, k_{el} = Elimination Constant, t = Time, $t_{1/2}$ = Plasma Half-Life, AUC = Area Under the Curve, CL = Clearance, D = Dose

Table C.1) Table of pharmacokinetic equations.

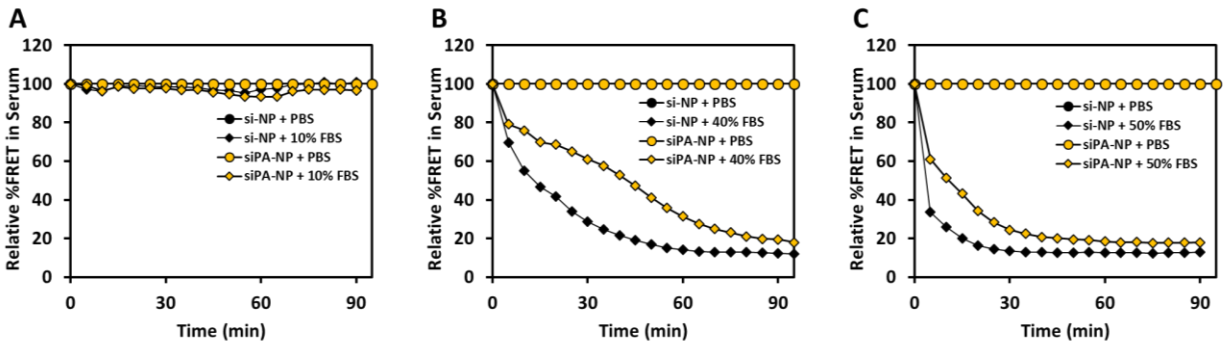

Figure C.4) Stability of si-NPs and siPA-NPs in (A) 10%, (B) 40%, and (C) 50% fetal bovine serum (FBS) monitored by FRET kinetics.

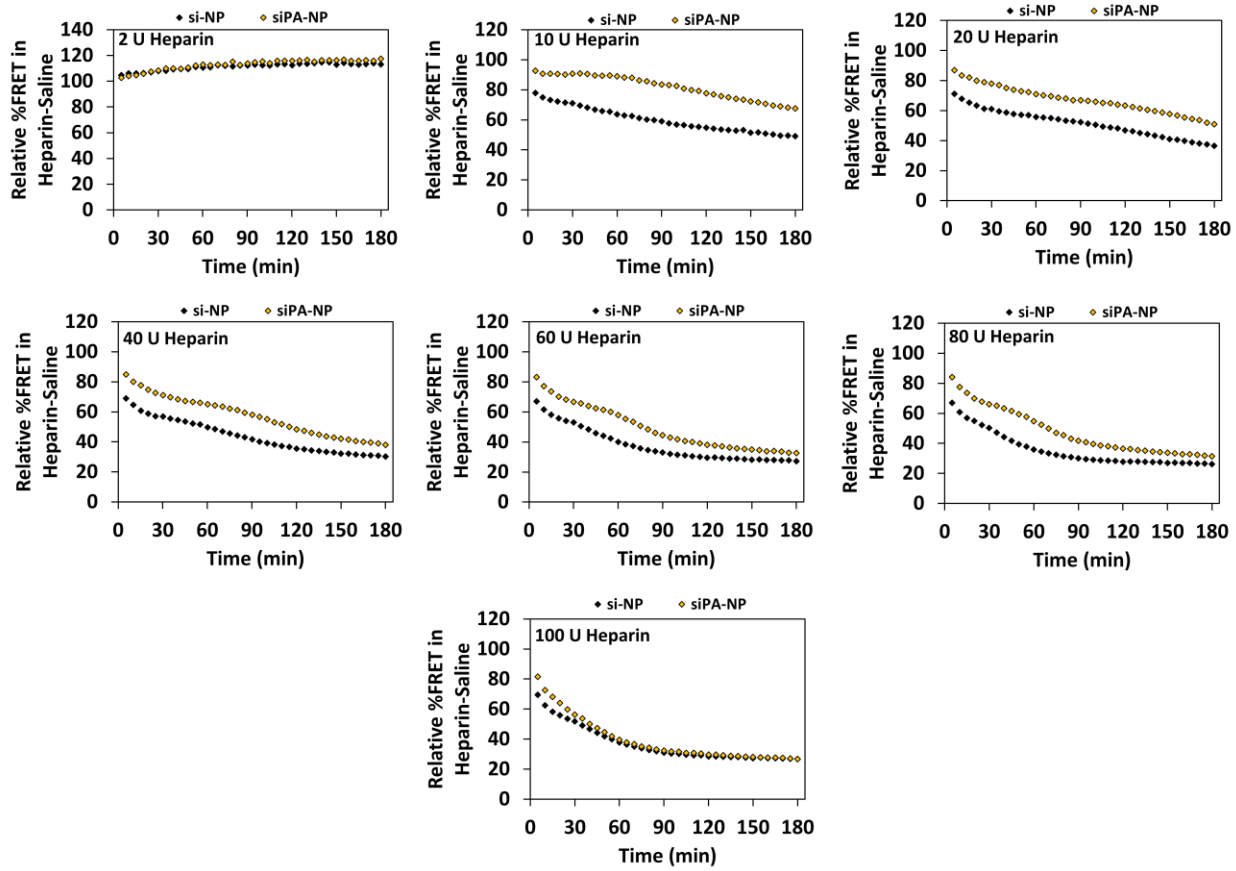

Figure C.5) Comprehensive panel of FRET-based heparin challenge assay. %FRET signal retained over time after exposure to varying concentrations of heparin saline.

Time (min)	si-NP	siPA-NP
30	73.9	140.6
60	37.0	76.7
90	27.2	50.9
120	22.0	39.9
150	19.1	33.1
180	17.2	28.0

Table C.2) EC50 values of heparin-dependent si-NP/siPA-NP dissociation as measured by FRET kinetics.

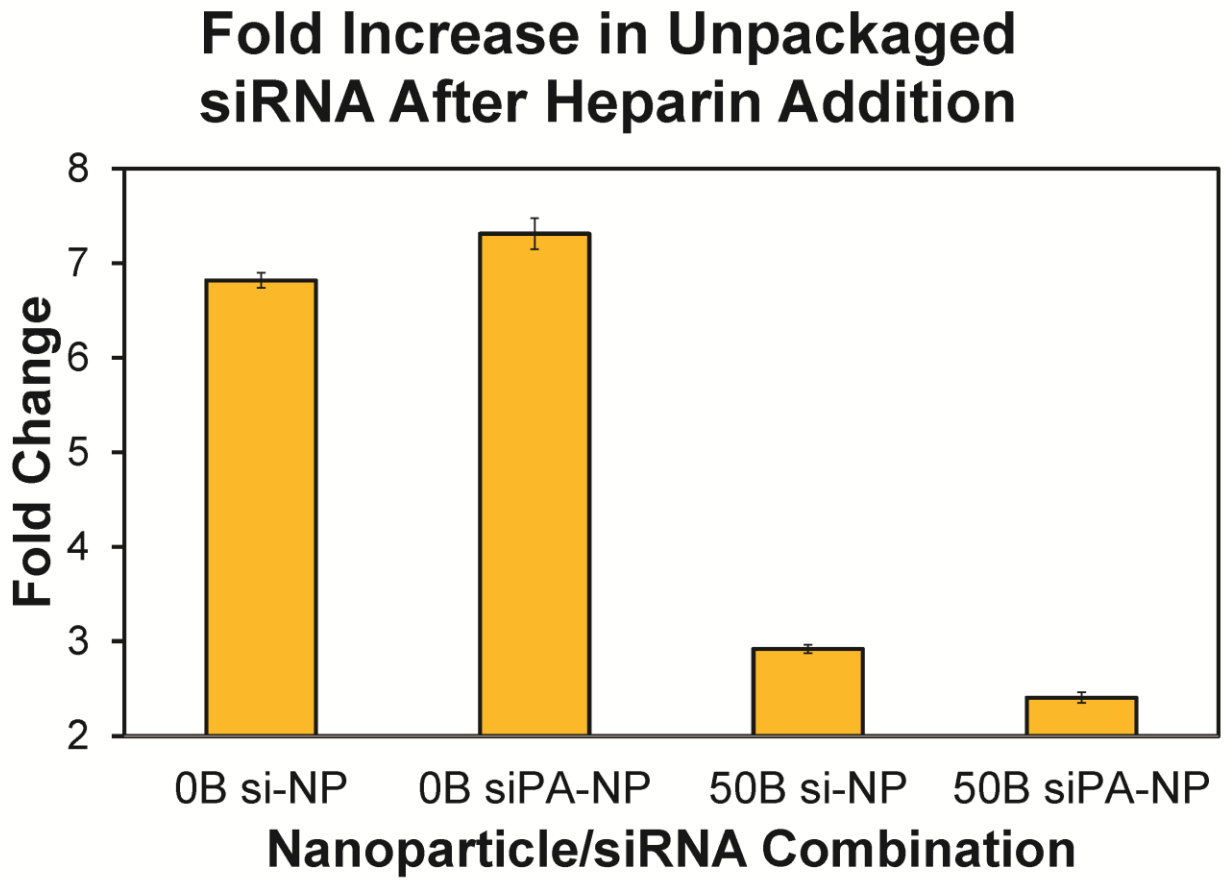

Figure C.6) PA-modified siRNA contributed to an improvement in stability of 50B polyplexes but not 0B polyplexes. As evaluated by a Ribogreen measure of unpackaged siRNA after 100 U/mL heparin addition and 15-minute incubation time.

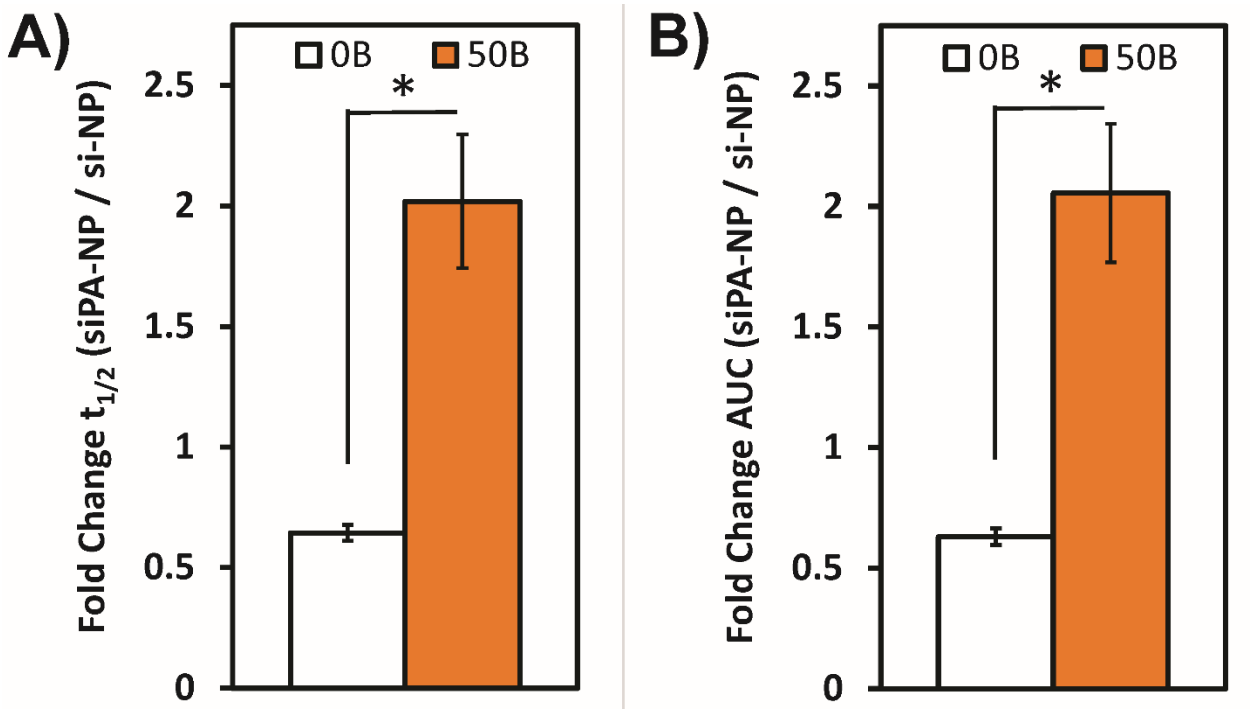

Figure C.7) Enhanced circulation time depends upon hydrophobic interactions between siPA and polymer NPs. In fully cationic polymer NPs (0B), siPA does not increase (A) circulation time half-life or (B) area under the curve (AUC) relative to unmodified siRNA, while in 50B NPs an increase in both is observed.

Oligonucleotide	Sequence (5' -> 3')	Source
Alexa488-Sense	GTCAGAAATAGAAACTGGTCATC	IDT
Alexa488-Antisense	[Alexa488]GATGACCAGTTTCTATTTCTGAC	IDT
Alexa546-Sense	GTCAGAAATAGAAACTGGTCATC	IDT
Alexa546-Antisense	[Alexa546]GATGACCAGTTTCTATTTCTGAC	IDT
Cy5-Sense	GTCAGAAATAGAAACTGGTCATC	Sigma
Cy5-Antisense	[Cyanine5]GATGACCAGTTTCTATTTCTGAC	Sigma
Luc-Sense	CAAUUGCACUGAUAAUGAACUCC[dT][dC]	Sigma
Luc-Antisense	GAGGAGUUCA[mU]U[mA]UCAGUGC[mA]A[mU]U[mG][mU][mU]	Sigma
Scr-Sense	CGUUAAUCGCGUAUAAUACGCGU[dA][dT]	Sigma
Scr-Antisense	AUACGCGUAU[mU]A[mU]ACGCGAU[mU]A[mA]C[mG][mA][mC]	Sigma

*Nomenclature: [d] = chiral DNA base, [m] = backbone 2'O-methyl modification

Table C.3) Table of oligonucleotide sequences.

APPENDIX D

SUPPLEMENTARY MATERIAL FOR CHAPTER IV

Supplementary Methods

All chemicals were purchased from Sigma-Aldrich (St. Louis, MO, USA) unless otherwise specified. DMAEMA and BMA monomers were passed twice through an activated basic alumina gravity column prior to use in order to remove inhibitors. 2,2-Azobis(2-methylpropionitrile) (AIBN) was recrystallized twice from methanol. All cell culture reagents were purchased through Fischer Scientific unless otherwise specified. Cell culture media and reagents, including Dulbecco's Modified Eagle Medium (DMEM), Fetal Bovine Serum (FBS), PBS (-/-), PBS (+/+), and anti-anti reagent were purchased through Life Technologies (Grand Island, NY, USA). For DLS experiments, dsDNA was used as a model for siRNA. For all fluorescent measurements, fluorophore-labeled dsDNA was used a model of siRNA. A list of oligonucleotides is provided in the supplement (**Supplementary Table D.2**). The naming scheme used for ternary si-NP formulation is as follows: [Binary Polymer] (Binary N:P)-[Ternary Polymer](Ternary N:P). Therefore, ternary si-NPs containing a DB core formulated at 4:1 N:P and PDB corona formulated to a final N:P of 12:1 are referred to as DB4-PDB12.

ECT, the reversible addition-fragmentation chain-transfer (RAFT) CTA, was synthesized according to a previously reported procedure[10]. The terminal carboxylic acid of ECT was then conjugated to PEG[16]. Briefly, methoxy-PEG (2 mmol, 10 g, Mn = 5000 Da), ECT (4 mmol, 1.045 g), and Dimethylaminopyridine (DMAP, 0.08 mmol, 10 mg) were dissolved in dry DCM (50 mL) and dicyclohexylcarbodiimide (DCC, 4 mmol, 0.82 g) was added while stirring. The reaction mixture was stirred for 48 h at room temperature (RT). Precipitated cyclohexyl urea was removed by filtration (0.2 μm pore size). The DCM layer was concentrated and precipitated into diethyl

ether twice. The precipitated PEG-ECT was washed thrice with diethyl ether and dried under vacuum. ^{1}H NMR (400 MHz Sprectrometer, Brüker, $CDCl_3$) showed 94% ECT conjugation to PEG.

RAFT controlled polymerization was used to synthesize both polymers, either from ECT or the PEG-ECT macro-CTA. Poly[(2-(dimethylamino)ethyl methacrylate)-*co*-(butyl methacrylate)] (p(DMAEMA-*co*-BMA); DB) was synthesized from ECT (**Supplementary Figure D.1**). The target degree of polymerization was 150, reaction volume was 3 mL (Dioxane), degassing was done for 30 min by nitrogen purge, and polymerization proceeded at 70°C for 24 h using AIBN as an initiator at 10:1 (CTA:AIBN) molar ratio. Reaction was stopped by removing the flask from heat and opening the reaction to air. The reaction mixture was precipitated thrice in a cold solution of pentane:diethyl ether (90:10) and dried under vacuum. PEG-*b*-p(DMAEMA-*co*-BMA) (PDB) was synthesized from the PEG-ECT macro-CTA (**Supplementary Figure D.1**). The target degree of polymerization was 150, reaction volume was 3 mL (Dioxane), degassing was done for 30 min by nitrogen purge, the polymerization proceeded at 70 °C for 24 h, and AIBN was used as an initiator at 10:1 (macro-CTA:AIBN) molar ratio. Reaction was stopped by removing the flask from heat and opening the reaction to air. The resulting diblock copolymer was precipitated in a cold solution of pentane:diethyl ether (90:10). The isolated polymer was dried, re-dissolved in ethanol, dialyzed one day against diH_2O and lyophilized to yield the final product.

Polymers were characterized for composition and molecular weight (Mn) by ^{1}H NMR (400 MHz Sprectrometer, Brüker, $CDCl_3$). Absolute molecular weight and polydispersity (PI) were further determined by gel permeation chromatography (GPC) using DMF + 0.1 M LiBr as the mobile phase with inline Agilent refractive index and Wyatt miniDAWN TREOS light scattering

detectors. Serial dilutions (10 mg/ml – 0.25 mg/ml) in DMF were measured on a digital refractometer to determine dn/dc values for calculating absolute molecular weight on GPC.

Each polymer was dissolved in pH 4.0 citric acid buffer (100 mM). The dsDNA was pre-condensed with the binary, core-forming polymer at each specified N:P ratio for 30 min at 0.5 mg/mL polymer concentration. Next, ternary, corona-forming polymer (3.33 mg/mL, 100 mM citric acid buffer at pH 4.0) was added in order to give the appropriate final N:P ratio and let complex for an additional 30 min. Polymer amount needed to yield the final N:P ratio was determined according to the following two equations for binary (1) and ternary (2) si-NPs:

(D.1)
$$nmol\ Pol = \frac{(nmol\ NA)(bp\ NA)(2)(N{:}P)}{(RU\ DMAEMA)(0.5)}$$

(D.2)
$$nmol\ Pol2 = \frac{(nmol\ NA)(bp\ NA)(2)(N{:}P) - (nmol\ Pol1)(RU\ DMAEMA1)(0.5)}{(RU\ DMAEMA2)(0.5)}$$

where nmol Pol is the nmol of binary polymer (DB), nmol NA is the nmol of nucleic acid, N:P is the ratio of primary amines to phosphates, RU DMAEMA is the number of repeating units of DMAEMA within the polymer backbone, nmol Pol2 is the nmol of ternary, corona-forming polymer (PDB), nmol Pol1 is the nmol of binary, core-forming polymer (DB), RU DMAEMA is the number of repeating units of DMAEMA within the binary, core-forming polymer backbone (DB), and RU DMAEMA2 is the number of repeating units of DMAEMA within the ternary, corona-forming polymer (PDB). A 5-fold excess of pH 8.0 phosphate buffer (100 mM) was added to adjust the pH to neutral before filtering through 0.45 μm pore syringe filters and measuring hydrodynamic diameter (D_h) of the resulting ternary si-NPs using dynamic light scattering (DLS) (Malvern Zetasizer Nano ZS, Malvern, UK). Before preparing TEM samples, si-NPs were

concentrated by centrifugation at 2000 x g in Amicon Ultra centrifugal filters (50,000 MW cut-off). Next, TEM samples were prepared by adding 5 μL of si-NP solution to pure carbon TEM grids (Ted Pella Inc, Redding, CA, USA), blotting dry (3 s) after 60 s, and counterstaining with 3% uranyl acetate (5 μL) for 20 s. The grids were dried overnight under vacuum prior to imaging on a FEI Tecnai Osiris microscope operating at 200 kV for TEM.

The hemolysis assay was used to assess ternary si-NP potential to escape the endolysosomal pathway. Red blood cells (RBCs) were obtained from anonymous donors and isolated by a well-established protocol[263]. After isolation, RBCs were incubated with varying concentrations (5, 15, and 30 μg/mL total polymer concentration) of ternary si-NPs at four pH's representative of extracellular and endolysosomal ranges (7.4, 6.8, 6.2, 5.6). After 1 h of incubation, intact RBCs and cellular debris were centrifuged out, and supernatants were removed. The supernatants were measured for absorbance at 451 nm (hemoglobin absorbance) and percent hemolysis was determined relative to 1% Triton-X100 detergent.

MDA-MB-361 cells (1e5 per well) were seeded in 6-well plates and allowed to adhere overnight. Cells were treated with DB4-PDB12 si-NPs carrying either Scrambled or Rictor siRNA (100 nM each) for 24 h, and protein was harvested 24, 48, and 96 h post-treatment. Western analyses using antibodies against Rictor (rabbit monoclonal, Sigma, 1:500) PSer473-Akt (rabbit monoclonal, Cell Signaling Technologies, 1:1000), Akt (mouse monoclonal, Cell Signaling Technologies, 1:1000), and Actin (mouse monoclonal, Sigma, 1:10,000) were performed on 20 micrograms cell lysate per lane resolved on 4-12% polyacrylamide gel (Novex) and transferred to nitrocellulose. Membranes were blocked in 3% gelatin in TBST (0.1% Tween-20) for 1 hour, incubated in primary antibody overnight at 4 degrees, washed 5 times for 5 minutes each in TBST,

incubated in HRP-conjugated goat anti-rabbit secondary (Pierce) for 1 hour at room temperature, washed 5 times, and developed using Pico-ECL (Pierce).

Tissue processing, H&E staining, and immunohistochemistry for Ki67 was performed by the Vanderbilt Translational Pathology Shared Resource. TUNEL staining was performed using the ApopTag In Situ Red Apoptosis Detection Kit (Millipore) as per manufacturer's protocol. Immunohistochemistry for Rictor and PSer473-Akt was performed through resources supported by the Vanderbilt Breast Specialized Program of Research Excellence (S.P.O.R.E.) Program. Photomicrographs acquired on an Olympus CK40 inverted microscope through an Optronics DEI-750C charge-coupled-device video camera using CellSens capture software. CellSens software was also used to quantify the average percentage of Ki67 or TUNEL positive nuclei in 3 to 4 fields/sample (10-20X magnification) as described previously[383]. Data are a representation of 4-5 independent tumors/condition. Expression of Rictor and PSer473-Akt were analyzed by IHC as described previously[384,385]. RNA was extracted from tumor tissue using a tissue lyser (Qiagen) and Qiazol and isolated using the RNEasy Universal Mini Kit (Qiagen) according to the manufacturer's protocol. Rictor mRNA levels were evaluated by RT-qPCR and normalized to the housekeeping gene, 36B4. Blood was collected by cardiac puncture, left at RT for 30 min, and then centrifuged at 2000 x g for 5 min. Resulting serum was harvested and tested by the Vanderbilt Translational Pathology Shared Resource for systemic levels of alanine aminotransferase (ALT), aspartate aminotransferase (AST), and blood urea nitrogen (BUN), and glucose (GLU).

Tumors were cut into small pieces, washed with HBSS containing Ca^{2+} and Mg^{2+}, and then processed using an enzyme mix containing collagenase (0.5 mg/mL, Roche Life Sciences, Indianapolis, IN, USA) and DNAse (0.19 mg/mL, BioRAD, Hercules, CA, USA) in DMEM. After 1 hour incubation in the enzyme mix at RT, the tumors were centrifuged and re-suspended in

HBSS without Ca^{2+} and Mg^{2+}, and then incubated with 5 mM EDTA for 20 minutes at RT. Tumors were then centrifuged and the pellets were re-suspended in HBSS with Ca^{2+} and Mg^{2+} and filtered using a 70 μm Nylon cell strainer. Filtrate was then washed once more with HBSS containing Ca^{2+} and Mg^{2+}, and then incubated in ACK lysis buffer (Thermo Fisher Scientific, USA) for 2 minutes before being diluted in 20 mL of PBS -/-. Cells were then pelleted and re-suspended in 1-2 mL PBS-/- prior to running on a flow cytometer (BD LSRii, BD Biosciences, San Jose, CA, USA). Uptake analysis was performed in FlowJo. Cell populations were isolated using forward and side scatter, then GFP positive tumor cells were selected, and Cy5 fluorescence intensity was measured.

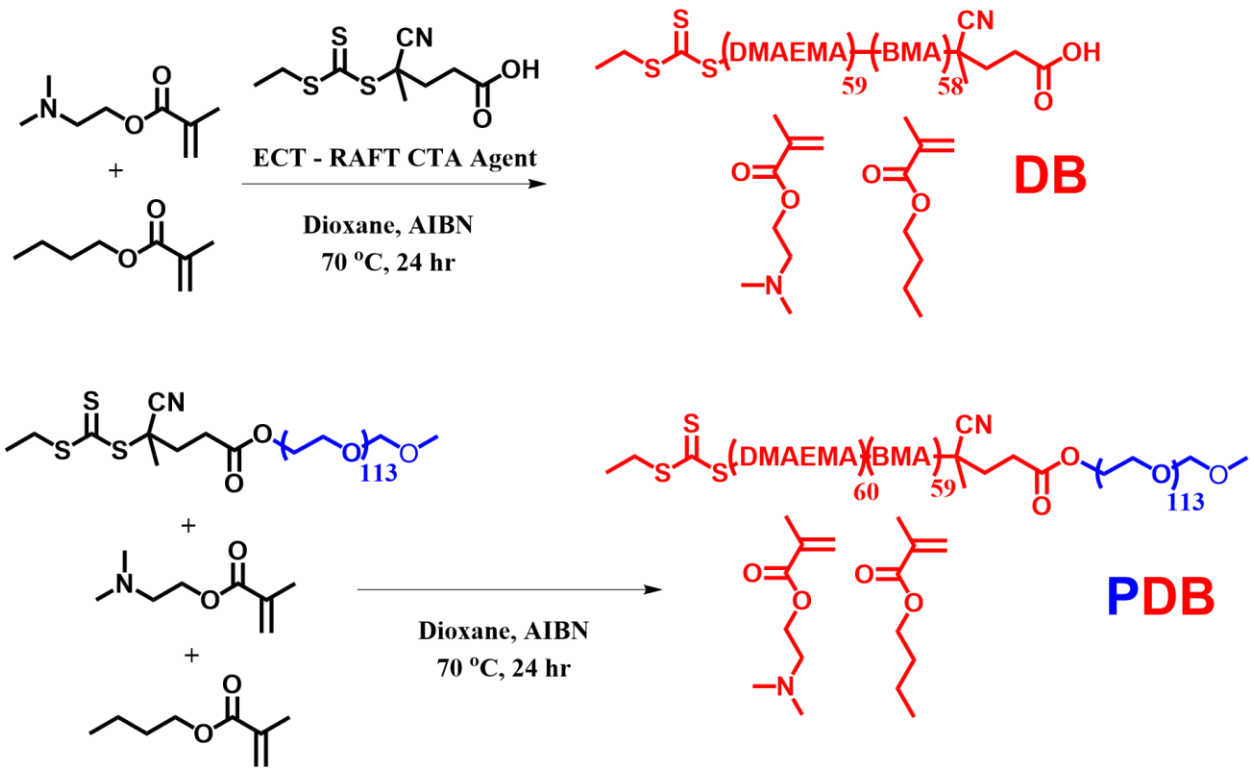

Figure D.1) RAFT Synthesis scheme for core-forming p(DMAEMA-*co*-BMA) (DB) and corona-forming PEG-*b*-p(DMAEMA-*co*-BMA) (PDB) polymers.

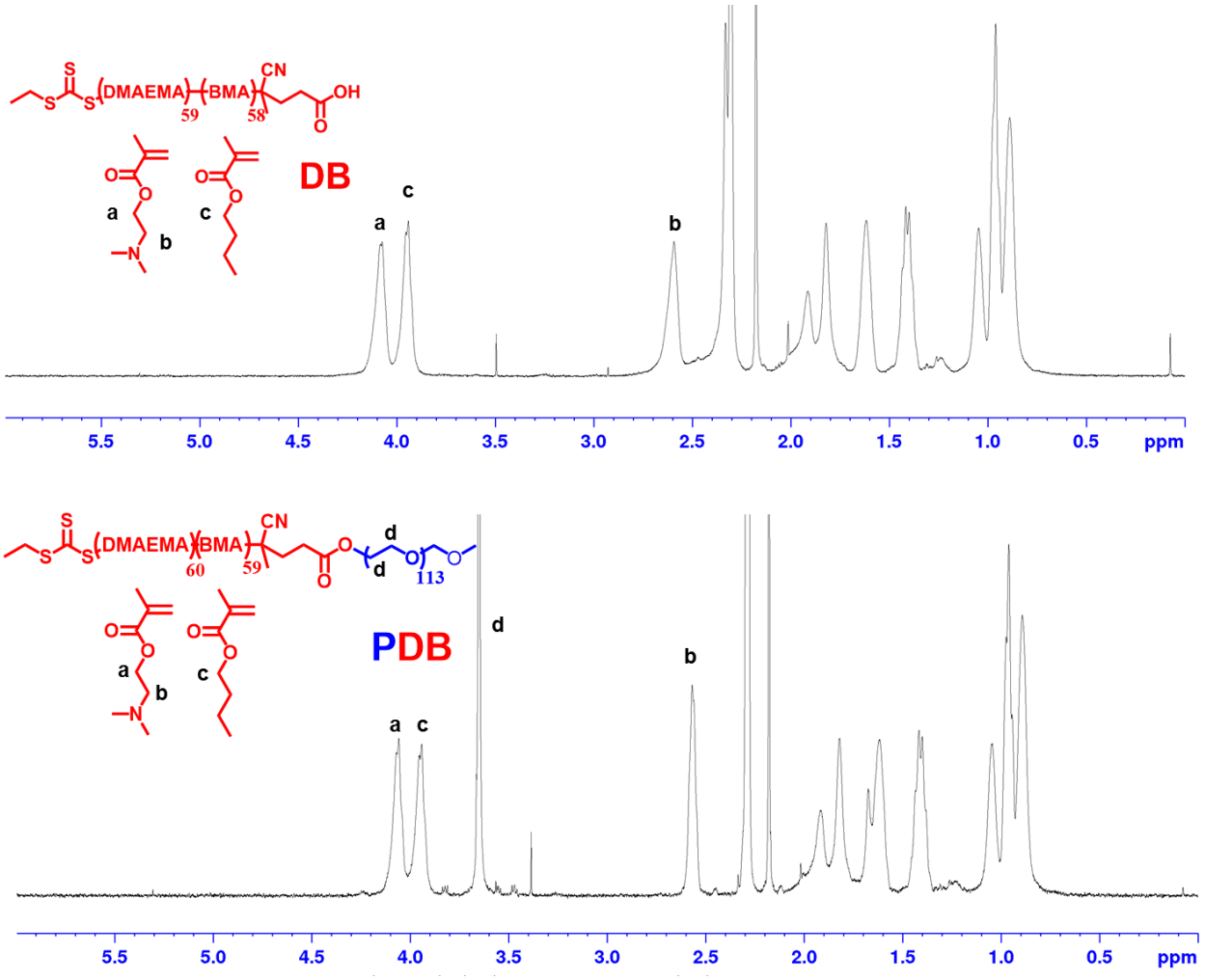

Figure D.2) ^{1}H-NMR characterization of DB and PDB polymers.

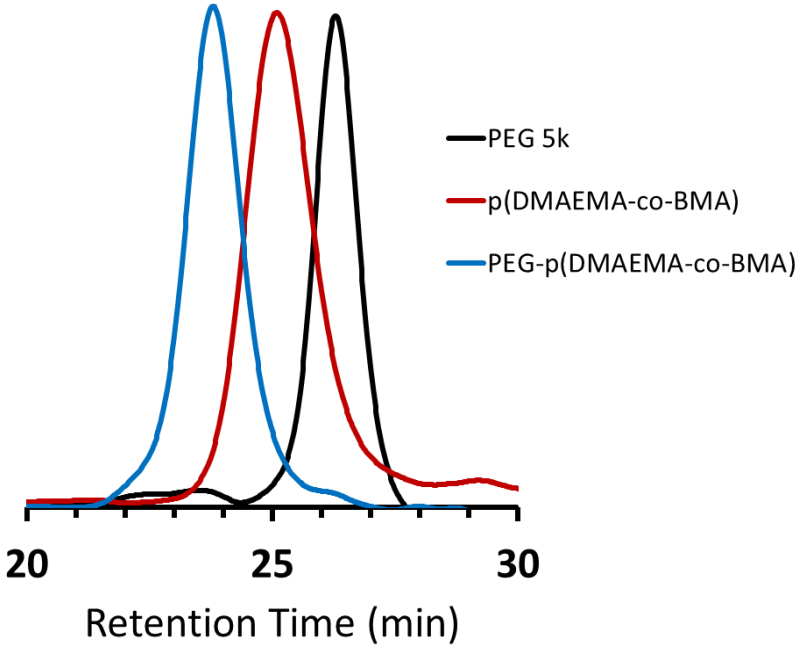

Figure D.3) Gel permeation chromatography (GPC) characterization of p(DMAEMA-co-BMA) (DB) and PEG-p(DMAEMA-co-BMA) (PDB) polymers.

Polymer	DP (NMR)	Composition (%BMA, NMR)	Mn (Da, NMR)	PI (GPC)
DB	117	49.6	17,500	1.05
PDB	119	49.6	22,800	1.03

Table D.1) Table of polymer chemical characterization values.

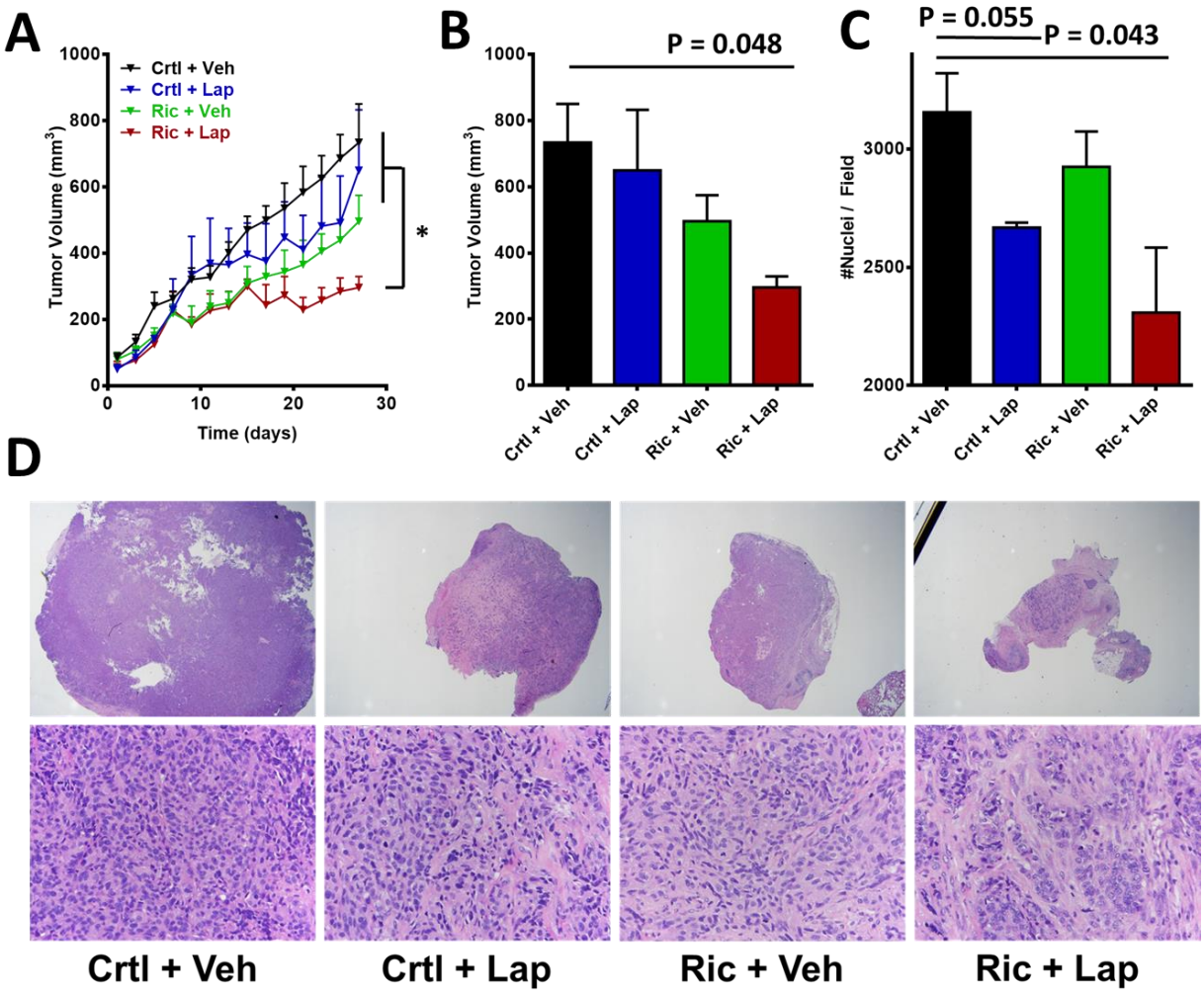

Figure D.4) Dual treatment of HER2+ BCs with Lapatinib and intratumoral Rictor RNAi inhibit tumor cell growth *in vivo*. (A) MDA-MB-361 tumor growth during treatment with Lapatinib (100 mg/kg daily, *i.p.*) and Rictor RNAi (1 mg/kg days 1, 3, and 5, *i.t.*). Lapatinib in combination with Rictor RNAi slows tumor progression most significantly. (B) MDA-MB-361 tumor volumes at the end of treatment (day 28). (C) Quantification of MDA-MB-361 cell density (number nuclei per field of view) at the end of 28 day study. (D) H&E stained tumor sections at 2x and 40x magnification.

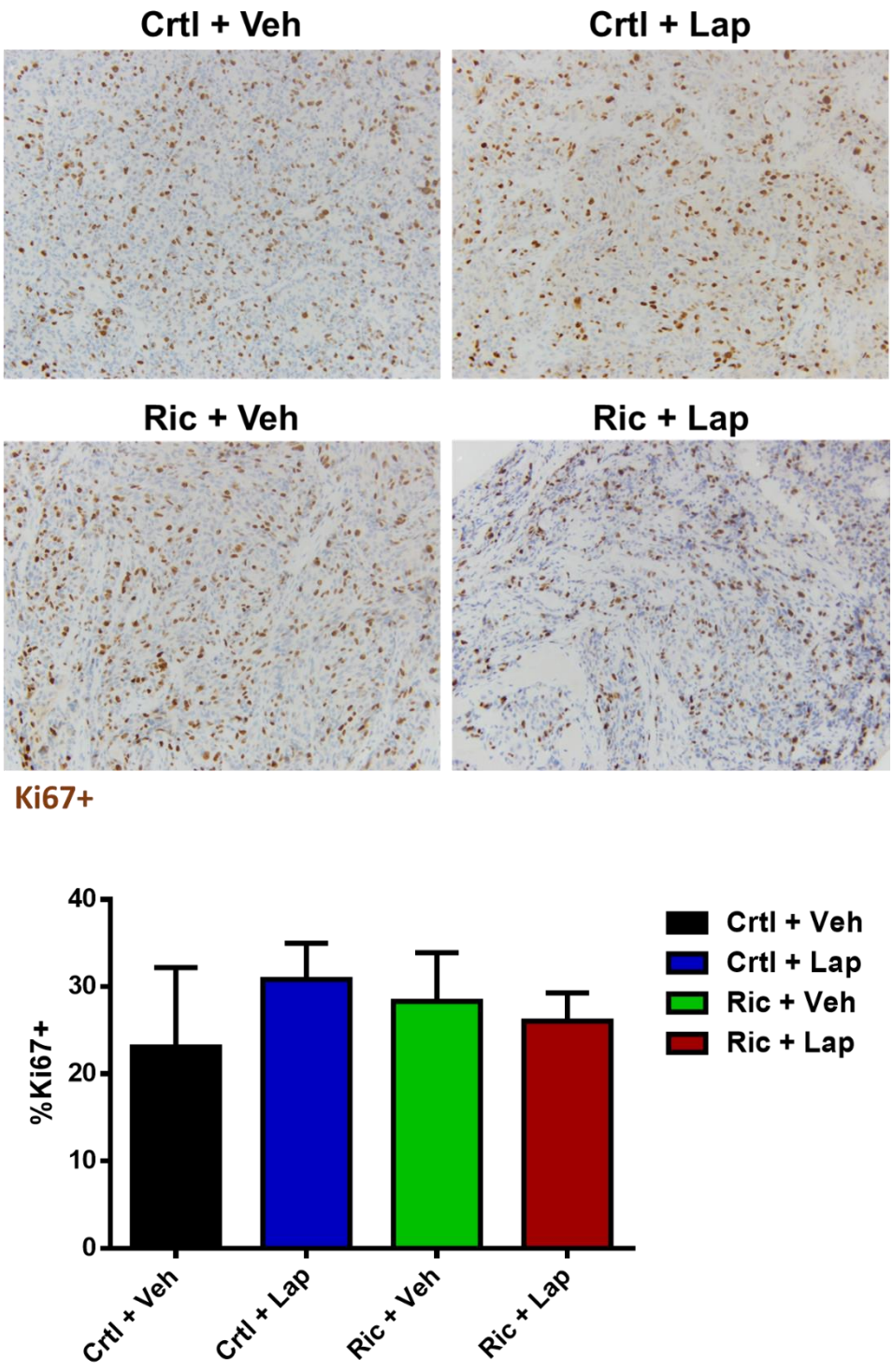

Figure D.5) Representative Ki67 IHC images and quantification at end of 28 day study. Rictor RNAi in combination with lapatinib therapy does not significantly affect tumor cell proliferation in MDA-MB-361 xenografts.

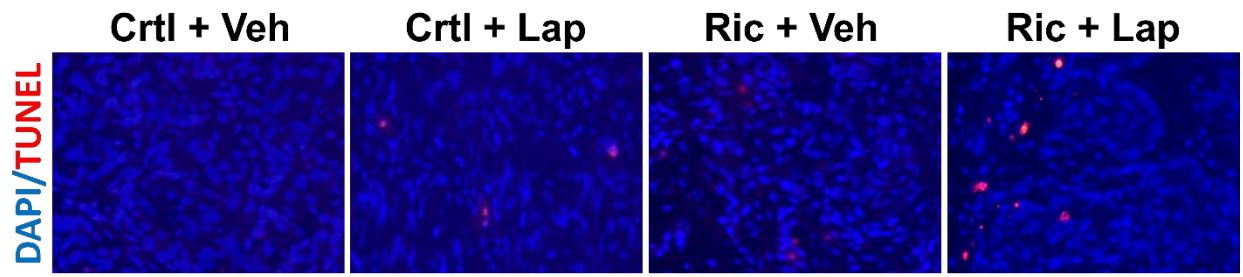

Figure D.6) Representative TUNEL IF images at treatment day 6 of the *i.v.* Rictor RNAi and Lapatinib trial.

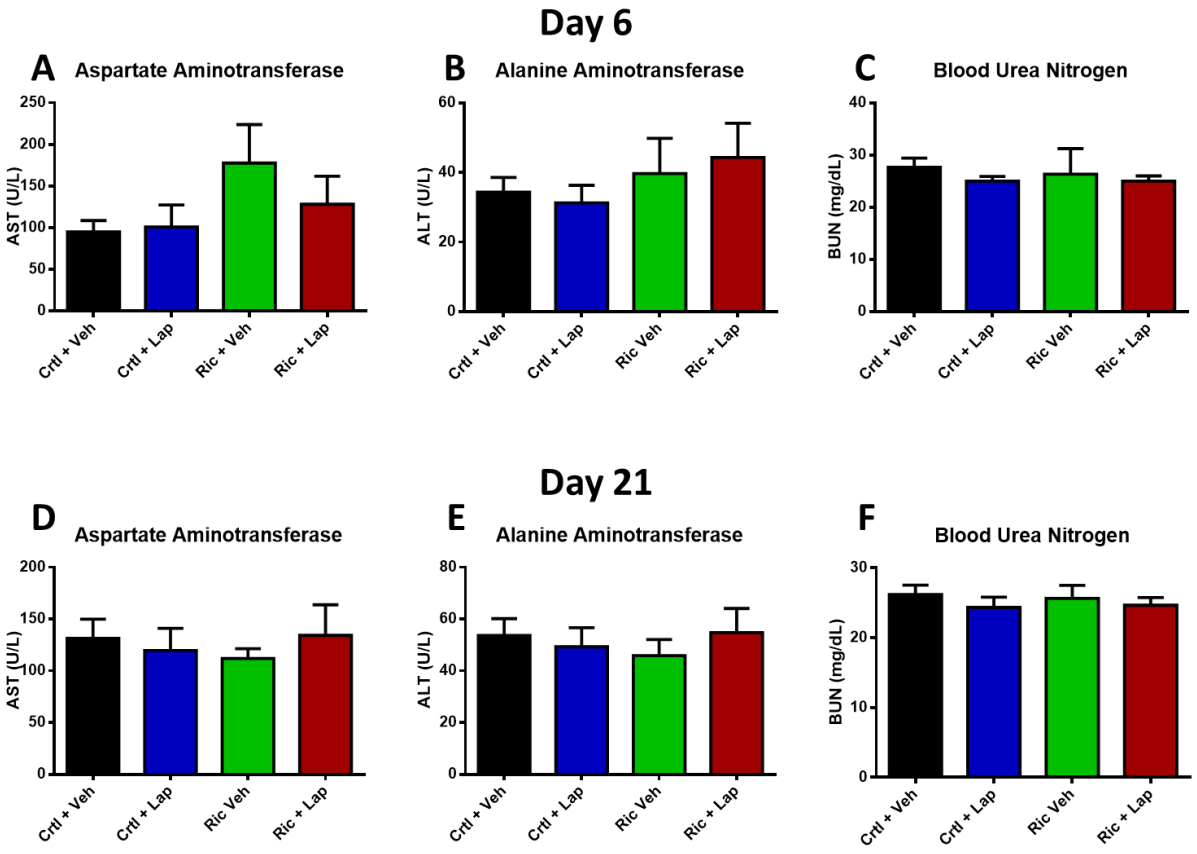

Figure D.7) Intravenous Rictor RNAi and lapatinib do not significantly affect blood levels of AST, ALT, and BUN at treatment days 6 (A, B, C) and 21 (D, E, F).

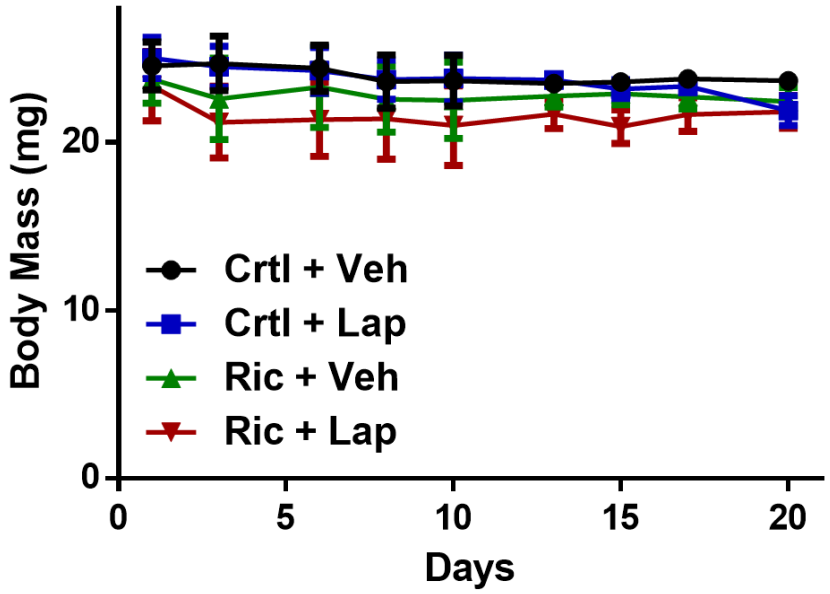

Figure D.8) Intravenous Rictor RNAi combined with oral lapatinib does not significantly affect mouse body mass using the treatment protocol in these studies.

Oligonucleotide	Sequence (5’ -> 3’)	Source
Cy5-Sense	dGdTdCdAdGdAdAdAdTdAdGdAdAdAdCdTdGdGdTdCdAdTdC	IDT
Cy5-Antisense	[Cyanine5]dGdAdTdGdAdCdCdAdGdTdTdTdCdTdAdTdTdTdCdTdGdAdC	IDT
Scr-Sense	rCrGrUrUrArArUrCrGrCrGrUrArUrArArUrArCrGrCrGrUdAdT	IDT
Scr-Antisense	rArUrArCrGrCrGrUrArUmUrAmUrArCrGrCrGrArUmUrAmArCmGmAmC	IDT
Rictor1-Sense	rGrArCrArCrArArGrCrArCrUrUrCrGrArUrUrArUrU	Dharmacon†
Rictor1-Antisense	rUrArArUrCrGrArArGrUrGrCrUrUrGrUrGrUrCrUrU	Dharmacon†
Rictor2-Sense	rGrArArGrArUrUrUrArUrUrGrArGrUrCrCrUrArUrU	Dharmacon†
Rictor2-Antisense	rUrArGrGrArCrUrCrArArUrArArArUrCrUrUrCrUrU	Dharmacon†
Rictor3-Sense	rGrCrGrArGrCrUrGrArUrGrUrArGrArArUrUrArUrU	Dharmacon†
Rictor3-Antisense	rUrArArUrUrCrUrArCrArUrCrArGrCrUrCrGrCrUrU	Dharmacon†
Rictor4-Sense	rGrGrGrArArUrArCrArArCrUrCrCrArArArUrArUrU	Dharmacon†
Rictor4-Antisense	rUrArUrUrUrGrGrArGrUrUrGrUrArUrUrCrCrCrUrU	Dharmacon†
Crtl-Sense	rUrGrGrUrUrUrArCrArUrGrUrCrGrArCrUrArArUrU	Dharmacon
Crtl-Antisense	rUrUrArGrUrCrGrArCrArUrGrUrArArArCrCrArUrU	Dharmacon
In Vivo Rictor-Sense	mGmArAmGrAmUrUrUrArUrUmGrAmGrUmCrCmUrArUrUrArAmUdC	IDT
In Vivo Rictor-Antisense	rGrAmUrUrArArUrAmGrGmArCmUrCrArArUrArArArUrCmUrUmCmUmU	IDT
Raptor-Sense	rUrGrGrCrUrArGrUrCrUrGrUrUrUrCrGrArArArUrU	Dharmacon
Raptor-Antisense	rUrUrUrCrGrArArArCrArGrArCrUrArGrCrCrArUrU	Dharmacon
Raptor – Fwd Primer	dCdGdGdGdGdAdGdGdTdCdTdGdGdGdTdCdTdTdCdAdA	IDT
Raptor – Rev Primer	dCdTdCdCdTdGdCdTdCdCdCdGdCdTdGdTdAdGdTdGdC	IDT
Rictor – Fwd Primer	dGdGdAdAdGdCdCdTdGdTdTdGdAdTdGdGdTdGdAdT	IDT
Rictor – Rev Primer	dGdGdCdAdGdCdCdTdGdTdTdTdTdAdTdGdGdTdGdT	IDT
GAPDH – Fwd Primer	dTdCdTdTdTdTdGdCdGdTdCdGdCdCdAdGdCdC	IDT
GAPDH – Rev Primer	dTdGdAdCdCdAdGdGdCdGdCdCdCdAdAdTdAdC	IDT
36B4 – Fwd Primer	dGdCdAdGdCdAdTdCdTdAdCdAdAdCdCdCdTdGdAdAdG	IDT
36B4 – Rev Primer	dCdAdCdTdGdGdCdAdAdCdAdTdTdGdCdGdGdAdC	IDT

***Nomenclature: d = DNA base, r = RNA base, m = backbone 2’O-methyl modification**
†SMARTPOOL used: equimolar combination of all 4 Rictor siRNAs

Table D.2) Oligonucleotide sequences used in the studies.

REFERENCES

1 Beavers, K. R., Nelson, C. E. & Duvall, C. L. MiRNA inhibition in tissue engineering and regenerative medicine. *Advanced Drug Delivery Reviews* **88**, 123-137, doi:http://dx.doi.org/10.1016/j.addr.2014.12.006 (2015).

2 Scott McIvor, R. Therapeutic Delivery of mRNA: The Medium Is the Message. *Molecular Therapy* **19**, 822-823, doi:http://dx.doi.org/10.1038/mt.2011.67 (2011).

3 Schwendener, R. A. Liposomes as vaccine delivery systems: a review of the recent advances. *Therapeutic Advances in Vaccines* **2**, 159-182, doi:10.1177/2051013614541440 (2014).

4 Silva, J. M., Videira, M., Gaspar, R., Préat, V. & Florindo, H. F. Immune system targeting by biodegradable nanoparticles for cancer vaccines. *Journal of Controlled Release* **168**, 179-199, doi:http://dx.doi.org/10.1016/j.jconrel.2013.03.010 (2013).

5 Kataoka, K., Harada, A. & Nagasaki, Y. Block copolymer micelles for drug delivery: design, characterization and biological significance. *Advanced Drug Delivery Reviews* **47**, 113-131, doi:http://dx.doi.org/10.1016/S0169-409X(00)00124-1 (2001).

6 Poon, G. M. & Gariepy, J. Cell-surface proteoglycans as molecular portals for cationic peptide and polymer entry into cells. *Biochemical Society transactions* **35**, 788-793, doi:10.1042/BST0350788 (2007).

7 Behr, J. The proton sponge, a means to enter cells viruses never thought of. *M S-Med Sci* **12**, 56 - 58 (1996).

8 Erbacher, P., Remy, J. S. & Behr, J. P. Gene transfer with synthetic virus-like particles via the integrin-mediated endocytosis pathway. *Gene therapy* **6**, 138-145, doi:10.1038/sj.gt.3300783 (1999).

9 Verbaan, F. *et al.* Intravenous fate of poly(2-(dimethylamino)ethyl methacrylate)-based polyplexes. *European journal of pharmaceutical sciences : official journal of the European Federation for Pharmaceutical Sciences* **20**, 419-427 (2003).

10 Convertine, A. J., Benoit, D. S., Duvall, C. L., Hoffman, A. S. & Stayton, P. S. Development of a novel endosomolytic diblock copolymer for siRNA delivery. *Journal of controlled release : official journal of the Controlled Release Society* **133**, 221-229, doi:10.1016/j.jconrel.2008.10.004 (2009).

11 Lundy, B. B., Convertine, A., Miteva, M. & Stayton, P. S. Neutral polymeric micelles for RNA delivery. *Bioconjug Chem* **24**, 398-407, doi:10.1021/bc300486k (2013).

12 Omedes Pujol, M., Coleman, D. J., Allen, C. D., Heidenreich, O. & Fulton, D. A. Determination of key structure-activity relationships in siRNA delivery with a mixed micelle system. *Journal of controlled release : official journal of the Controlled Release Society* **172**, 939-945, doi:10.1016/j.jconrel.2013.10.013 (2013).

13 Benoit, D. S., Srinivasan, S., Shubin, A. D. & Stayton, P. S. Synthesis of folate-functionalized RAFT polymers for targeted siRNA delivery. *Biomacromolecules* **12**, 2708-2714, doi:10.1021/bm200485b (2011).

14 Osada, K., Christie, R. J. & Kataoka, K. Polymeric micelles from poly(ethylene glycol)-poly(amino acid) block copolymer for drug and gene delivery. *Journal of the Royal Society, Interface / the Royal Society* **6 Suppl 3**, S325-339, doi:10.1098/rsif.2008.0547.focus (2009).

15 Wakebayashi, D. *et al.* Lactose-conjugated polyion complex micelles incorporating plasmid DNA as a targetable gene vector system: their preparation and gene transfecting efficiency against cultured HepG2 cells. *Journal of Controlled Release* **95**, 653-664, doi:http://dx.doi.org/10.1016/j.jconrel.2004.01.003 (2004).

16 Nelson, C. E. *et al.* Balancing Cationic and Hydrophobic Content of PEGylated siRNA Polyplexes Enhances Endosome Escape, Stability, Blood Circulation Time, and Bioactivity in Vivo. *ACS Nano* **7**, 8870-8880, doi:10.1021/nn403325f (2013).

17 Xiong, X. B., Uludag, H. & Lavasanifar, A. Virus-mimetic polymeric micelles for targeted siRNA delivery. *Biomaterials* **31**, 5886-5893, doi:10.1016/j.biomaterials.2010.03.075 (2010).

18 Xiong, X. B. & Lavasanifar, A. Traceable multifunctional micellar nanocarriers for cancer-targeted co-delivery of MDR-1 siRNA and doxorubicin. *ACS Nano* **5**, 5202-5213, doi:10.1021/nn2013707 (2011).

19 Smith, R., Sewell, S. L. & Giorgio, T. D. Proximity-activated nanoparticles: in vitro performance of specific structural modification by enzymatic cleavage. *International journal of nanomedicine* **3**, 95-103 (2008).

20 Li, H. *et al.* Matrix Metalloproteinase Responsive, Proximity-Activated Polymeric Nanoparticles for siRNA Delivery. *Advanced Functional Materials* **23**, 3040-3052, doi:10.1002/adfm.201202215 (2013).

21 Convertine, A. J. *et al.* pH-Responsive Polymeric Micelle Carriers for siRNA Drugs. *Biomacromolecules* **11**, 2904-2911, doi:10.1021/bm100652w (2010).

22 Lynn, D. M. & Langer, R. Degradable Poly(β-amino esters): Synthesis, Characterization, and Self-Assembly with Plasmid DNA. *Journal of the American Chemical Society* **122**, 10761-10768, doi:10.1021/ja0015388 (2000).

23 Akinc, A., Anderson, D. G., Lynn, D. M. & Langer, R. Synthesis of poly(beta-amino ester)s optimized for highly effective gene delivery. *Bioconjug Chem* **14**, 979-988, doi:10.1021/bc034067y (2003).

24 Green, J. J. *et al.* Combinatorial Modification of Degradable Polymers Enables Transfection of Human Cells Comparable to Adenovirus. *Advanced Materials* **19**, 2836-2842, doi:10.1002/adma.200700371 (2007).

25 Zhou, J. *et al.* Biodegradable poly(amine-co-ester) terpolymers for targeted gene delivery. *Nat Mater* **11**, 82-90, doi:http://www.nature.com/nmat/journal/v11/n1/abs/nmat3187.html#supplementary-information (2012).

26 Midoux, P. & Monsigny, M. Efficient gene transfer by histidylated polylysine/pDNA complexes. *Bioconjug Chem* **10**, 406-411, doi:10.1021/bc9801070 (1999).

27 Benns, J. M., Choi, J. S., Mahato, R. I., Park, J. S. & Kim, S. W. pH-sensitive cationic polymer gene delivery vehicle: N-Ac-poly(L-histidine)-graft-poly(L-lysine) comb shaped polymer. *Bioconjug Chem* **11**, 637-645 (2000).

28 Moreira, C. *et al.* Improving chitosan-mediated gene transfer by the introduction of intracellular buffering moieties into the chitosan backbone. *Acta biomaterialia* **5**, 2995-3006, doi:10.1016/j.actbio.2009.04.021 (2009).

29 Howard, K. A. *et al.* RNA interference in vitro and in vivo using a novel chitosan/siRNA nanoparticle system. *Molecular therapy : the journal of the American Society of Gene Therapy* **14**, 476-484, doi:10.1016/j.ymthe.2006.04.010 (2006).

30 Jiang, H. L. *et al.* Efficient gene delivery using chitosan-polyethylenimine hybrid systems. *Biomedical materials* **3**, 025013, doi:10.1088/1748-6041/3/2/025013 (2008).

31 Reineke, T. M. Poly(glycoamidoamine)s: Cationic glycopolymers for DNA delivery. *Journal of Polymer Science Part A: Polymer Chemistry* **44**, 6895-6908, doi:10.1002/pola.21697 (2006).

32 Srinivasachari, S., Liu, Y., Zhang, G., Prevette, L. & Reineke, T. M. Trehalose Click Polymers Inhibit Nanoparticle Aggregation and Promote pDNA Delivery in Serum. *Journal of the American Chemical Society* **128**, 8176-8184, doi:10.1021/ja0585580 (2006).

33 Smith, A. E., Sizovs, A., Grandinetti, G., Xue, L. & Reineke, T. M. Diblock Glycopolymers Promote Colloidal Stability of Polyplexes and Effective pDNA and siRNA Delivery under Physiological Salt and Serum Conditions. *Biomacromolecules* **12**, 3015-3022, doi:10.1021/bm200643c (2011).

34 Sizovs, A. *et al.* Poly(trehalose): Sugar-Coated Nanocomplexes Promote Stabilization and Effective Polyplex-Mediated siRNA Delivery. *Journal of the American Chemical Society* **135**, 15417-15424, doi:10.1021/ja404941p (2013).

35 Hwang, S. J., Bellocq, N. C. & Davis, M. E. Effects of Structure of β-Cyclodextrin-Containing Polymers on Gene Delivery. *Bioconjugate Chemistry* **12**, 280-290, doi:10.1021/bc0001084 (2001).

36 Pun, S. H. & Davis, M. E. Development of a Nonviral Gene Delivery Vehicle for Systemic Application. *Bioconjugate Chemistry* **13**, 630-639, doi:10.1021/bc0155768 (2002).

37 Bellocq, N. C., Pun, S. H., Jensen, G. S. & Davis, M. E. Transferrin-Containing, Cyclodextrin Polymer-Based Particles for Tumor-Targeted Gene Delivery. *Bioconjugate chemistry* **14**, 1122-1132, doi:10.1021/bc034125f (2003).

38 Davis, M. E. The first targeted delivery of siRNA in humans via a self-assembling, cyclodextrin polymer-based nanoparticle: from concept to clinic. *Molecular pharmaceutics* **6**, 659-668, doi:10.1021/mp900015y (2009).

39 Davis, M. E. *et al.* Evidence of RNAi in humans from systemically administered siRNA via targeted nanoparticles. *Nature* **464**, 1067-1070, doi:http://www.nature.com/nature/journal/v464/n7291/suppinfo/nature08956_S1.html (2010).

40 Fire, A. *et al.* Potent and specific genetic interference by double-stranded RNA in Caenorhabditis elegans. *Nature* **391**, 806-811, doi:10.1038/35888 (1998).

41 O'Reilly, R. K., Hawker, C. J. & Wooley, K. L. Cross-linked block copolymer micelles: functional nanostructures of great potential and versatility. *Chemical Society Reviews* **35**, 1068-1083, doi:10.1039/B514858H (2006).

42 Li, Y., Lokitz, B. S., Armes, S. P. & McCormick, C. L. Synthesis of Reversible Shell Cross-Linked Micelles for Controlled Release of Bioactive Agents†. *Macromolecules* **39**, 2726-2728, doi:10.1021/ma0604035 (2006).

43 Sumerlin, B. S. *et al.* Aqueous solution properties of pH-responsive AB diblock acrylamido–styrenic copolymers synthesized via aqueous reversible addition–fragmentation chain transfer. *Journal of Polymer Science Part A: Polymer Chemistry* **42**, 1724-1734, doi:10.1002/pola.11069 (2004).

44 Thurmond, K. B., Kowalewski, T. & Wooley, K. L. Water-Soluble Knedel-like Structures: The Preparation of Shell-Cross-Linked Small Particles. *Journal of the American Chemical Society* **118**, 7239-7240, doi:10.1021/ja961299h (1996).

45 Thurmond, K. B., Kowalewski, T. & Wooley, K. L. Shell Cross-Linked Knedels: A Synthetic Study of the Factors Affecting the Dimensions and Properties of Amphiphilic

Core-Shell Nanospheres. *Journal of the American Chemical Society* **119**, 6656-6665, doi:10.1021/ja9710520 (1997).

46 Pilon, L. N., Armes, S. P., Findlay, P. & Rannard, S. P. Synthesis and Characterization of Shell Cross-Linked Micelles with Hydroxy-Functional Coronas: A Pragmatic Alternative to Dendrimers? *Langmuir : the ACS journal of surfaces and colloids* **21**, 3808-3813, doi:10.1021/la047046g (2005).

47 Liu, S. & Armes, S. P. The facile one-pot synthesis of shell cross-linked micelles in aqueous solution at high solids. *J Am Chem Soc* **123**, 9910-9911 (2001).

48 O'Reilly, R. K., Joralemon, M. J., Wooley, K. L. & Hawker, C. J. Functionalization of Micelles and Shell Cross-linked Nanoparticles Using Click Chemistry. *Chemistry of Materials* **17**, 5976-5988, doi:10.1021/cm051047s (2005).

49 Jiang, X., Zhang, G., Narain, R. & Liu, S. Fabrication of Two Types of Shell-Cross-Linked Micelles with "Inverted" Structures in Aqueous Solution from Schizophrenic Water-Soluble ABC Triblock Copolymer via Click Chemistry. *Langmuir : the ACS journal of surfaces and colloids* **25**, 2046-2054, doi:10.1021/la803616d (2009).

50 Yu, S. S. *et al.* Macrophage-Specific RNA Interference Targeting via "Click", Mannosylated Polymeric Micelles. *Molecular pharmaceutics* **10**, 975-987, doi:10.1021/mp300434e (2013).

51 Kakizawa, Y., Harada, A. & Kataoka, K. Environment-Sensitive Stabilization of Core−Shell Structured Polyion Complex Micelle by Reversible Cross-Linking of the Core through Disulfide Bond. *Journal of the American Chemical Society* **121**, 11247-11248, doi:10.1021/ja993057y (1999).

52 Thurmond, K. B., 2nd, Remsen, E. E., Kowalewski, T. & Wooley, K. L. Packaging of DNA by shell crosslinked nanoparticles. *Nucleic acids research* **27**, 2966-2971 (1999).

53 Zhang, L. *et al.* Shell-Cross-Linked Micelles Containing Cationic Polymers Synthesized via the RAFT Process: Toward a More Biocompatible Gene Delivery System. *Biomacromolecules* **8**, 2890-2901, doi:10.1021/bm070370g (2007).

54 Zhang, K., Fang, H., Wang, Z., Taylor, J. S. & Wooley, K. L. Cationic shell-crosslinked knedel-like nanoparticles for highly efficient gene and oligonucleotide transfection of mammalian cells. *Biomaterials* **30**, 968-977, doi:10.1016/j.biomaterials.2008.10.057 (2009).

55 Zhang, K. *et al.* Structure-activity relationships of cationic shell-crosslinked knedel-like nanoparticles: shell composition and transfection efficiency/cytotoxicity. *Biomaterials* **31**, 1805-1813, doi:10.1016/j.biomaterials.2009.10.033 (2010).

56 Matsumoto, S. *et al.* Environment-Responsive Block Copolymer Micelles with a Disulfide Cross-Linked Core for Enhanced siRNA Delivery. *Biomacromolecules* **10**, 119-127, doi:10.1021/bm800985e (2008).

57 Fang, H., Zhang, K., Shen, G., Wooley, K. L. & Taylor, J. S. Cationic shell-cross-linked knedel-like (cSCK) nanoparticles for highly efficient PNA delivery. *Molecular pharmaceutics* **6**, 615-626, doi:10.1021/mp800199w (2009).

58 Shrestha, R., Elsabahy, M., Florez-Malaver, S., Samarajeewa, S. & Wooley, K. L. Endosomal escape and siRNA delivery with cationic shell crosslinked knedel-like nanoparticles with tunable buffering capacities. *Biomaterials* **33**, 8557-8568, doi:10.1016/j.biomaterials.2012.07.054 (2012).

59 Shrestha, R. *et al.* Hierarchically assembled theranostic nanostructures for siRNA delivery and imaging applications. *J Am Chem Soc* **134**, 17362-17365, doi:10.1021/ja306616n (2012).

60 Elsabahy, M. *et al.* Multifunctional hierarchically assembled nanostructures as complex stage-wise dual-delivery systems for coincidental yet differential trafficking of siRNA and paclitaxel. *Nano letters* **13**, 2172-2181, doi:10.1021/nl4006645 (2013).

61 Christian, D. A. *et al.* Polymersome carriers: from self-assembly to siRNA and protein therapeutics. *European journal of pharmaceutics and biopharmaceutics : official journal of Arbeitsgemeinschaft fur Pharmazeutische Verfahrenstechnik e.V* **71**, 463-474, doi:10.1016/j.ejpb.2008.09.025 (2009).

62 Discher, B. M. *et al.* Polymersomes: Tough Vesicles Made from Diblock Copolymers. *Science* **284**, 1143-1146, doi:10.1126/science.284.5417.1143 (1999).

63 Won, Y.-Y., Davis, H. T. & Bates, F. S. Giant Wormlike Rubber Micelles. *Science* **283**, 960-963, doi:10.1126/science.283.5404.960 (1999).

64 Aranda-Espinoza, H., Bermudez, H., Bates, F. S. & Discher, D. E. Electromechanical limits of polymersomes. *Physical review letters* **87**, 208301 (2001).

65 Srinivas, G., Discher, D. E. & Klein, M. L. Self-assembly and properties of diblock copolymers by coarse-grain molecular dynamics. *Nat Mater* **3**, 638-644, doi:http://www.nature.com/nmat/journal/v3/n9/suppinfo/nmat1185_S1.html (2004).

66 Srinivas, G., Discher, D. E. & Klein, M. L. Key roles for chain flexibility in block copolymer membranes that contain pores or make tubes. *Nano letters* **5**, 2343-2349, doi:10.1021/nl051515x (2005).

67 Rijcken, C. J., Soga, O., Hennink, W. E. & van Nostrum, C. F. Triggered destabilisation of polymeric micelles and vesicles by changing polymers polarity: an attractive tool for

drug delivery. *Journal of controlled release : official journal of the Controlled Release Society* **120**, 131-148, doi:10.1016/j.jconrel.2007.03.023 (2007).

68 Kros, A., Jansen, J. A., Holder, S. J., Nolte, R. J. M. & Sommerdijk, N. A. J. M. Silane-based hybrids for biomedical applications. *Journal of Adhesion Science and Technology* **16**, 143-155, doi:10.1163/156856102317293678 (2002).

69 Jiang, Y. *et al.* Reversible self-organization of a UV-responsive PEG-terminated malachite green derivative: vesicle formation and photoinduced disassembly. *Langmuir : the ACS journal of surfaces and colloids* **23**, 4029-4034, doi:10.1021/la063305l (2007).

70 Li, Y., Lokitz, B. S. & McCormick, C. L. Thermally Responsive Vesicles and Their Structural "Locking" through Polyelectrolyte Complex Formation. *Angewandte Chemie* **118**, 5924-5927, doi:10.1002/ange.200602168 (2006).

71 Qin, S., Geng, Y., Discher, D. E. & Yang, S. Temperature-Controlled Assembly and Release from Polymer Vesicles of Poly(ethylene oxide)-block- poly(N-isopropylacrylamide). *Advanced Materials* **18**, 2905-2909, doi:10.1002/adma.200601019 (2006).

72 Ahmed, F. & Discher, D. E. Self-porating polymersomes of PEG-PLA and PEG-PCL: hydrolysis-triggered controlled release vesicles. *Journal of controlled release : official journal of the Controlled Release Society* **96**, 37-53, doi:10.1016/j.jconrel.2003.12.021 (2004).

73 Ahmed, F. *et al.* Shrinkage of a rapidly growing tumor by drug-loaded polymersomes: pH-triggered release through copolymer degradation. *Molecular pharmaceutics* **3**, 340-350, doi:10.1021/mp050103u (2006).

74 Borchert, U. *et al.* pH-induced release from P2VP-PEO block copolymer vesicles. *Langmuir : the ACS journal of surfaces and colloids* **22**, 5843-5847, doi:10.1021/la060227t (2006).

75 Du, J., Tang, Y., Lewis, A. L. & Armes, S. P. pH-Sensitive Vesicles Based on a Biocompatible Zwitterionic Diblock Copolymer. *Journal of the American Chemical Society* **127**, 17982-17983, doi:10.1021/ja056514l (2005).

76 Cerritelli, S., Velluto, D. & Hubbell, J. A. PEG-SS-PPS: reduction-sensitive disulfide block copolymer vesicles for intracellular drug delivery. *Biomacromolecules* **8**, 1966-1972, doi:10.1021/bm070085x (2007).

77 Napoli, A. *et al.* Glucose-oxidase based self-destructing polymeric vesicles. *Langmuir : the ACS journal of surfaces and colloids* **20**, 3487-3491 (2004).

78 Napoli, A., Valentini, M., Tirelli, N., Muller, M. & Hubbell, J. A. Oxidation-responsive polymeric vesicles. *Nat Mater* **3**, 183-189, doi:http://www.nature.com/nmat/journal/v3/n3/suppinfo/nmat1081_S1.html (2004).

79 Cheng, R. *et al.* Glutathione-responsive nano-vehicles as a promising platform for targeted intracellular drug and gene delivery. *Journal of controlled release : official journal of the Controlled Release Society* **152**, 2-12, doi:10.1016/j.jconrel.2011.01.030 (2011).

80 Korobko, A. V., Backendorf, C. & van der Maarel, J. R. Plasmid DNA encapsulation within cationic diblock copolymer vesicles for gene delivery. *The journal of physical chemistry. B* **110**, 14550-14556, doi:10.1021/jp057363b (2006).

81 Korobko, A. V., Jesse, W. & van der Maarel, J. R. C. Encapsulation of DNA by Cationic Diblock Copolymer Vesicles. *Langmuir : the ACS journal of surfaces and colloids* **21**, 34-42, doi:10.1021/la047967r (2004).

82 Brown, M. D. *et al.* Preliminary Characterization of Novel Amino Acid Based Polymeric Vesicles as Gene and Drug Delivery Agents. *Bioconjugate Chemistry* **11**, 880-891, doi:10.1021/bc000052d (2000).

83 Brown, M. D. *et al.* In vitro and in vivo gene transfer with poly(amino acid) vesicles. *Journal of Controlled Release* **93**, 193-211, doi:http://dx.doi.org/10.1016/j.jconrel.2003.08.022 (2003).

84 Kim, Y. *et al.* Polymersome delivery of siRNA and antisense oligonucleotides. *Journal of Controlled Release* **134**, 132-140, doi:http://dx.doi.org/10.1016/j.jconrel.2008.10.020 (2009).

85 Torchilin, V. P. *et al.* p-Nitrophenylcarbonyl-PEG-PE-liposomes: fast and simple attachment of specific ligands, including monoclonal antibodies, to distal ends of PEG chains via p-nitrophenylcarbonyl groups. *Biochimica et biophysica acta* **1511**, 397-411 (2001).

86 Christian, N. A. *et al.* Tat-functionalized near-infrared emissive polymersomes for dendritic cell labeling. *Bioconjug Chem* **18**, 31-40, doi:10.1021/bc0601267 (2007).

87 Pourtau, L. *et al.* Antibody-Functionalized Magnetic Polymersomes: In vivo Targeting and Imaging of Bone Metastases using High Resolution MRI. *Advanced healthcare materials* **2**, 1420-1424, doi:10.1002/adhm.201300061 (2013).

88 Dalhaimer, P., Bermudez, H. & Discher, D. E. Biopolymer mimicry with polymeric wormlike micelles: Molecular weight scaled flexibility, locked-in curvature, and coexisting microphases. *Journal of Polymer Science Part B: Polymer Physics* **42**, 168-176, doi:10.1002/polb.10709 (2004).

89 Broz, P. *et al.* Cell targeting by a generic receptor-targeted polymer nanocontainer platform. *Journal of controlled release : official journal of the Controlled Release Society* **102**, 475-488, doi:10.1016/j.jconrel.2004.10.014 (2005).

90 Petersen, M. A., Yin, L., Kokkoli, E. & Hillmyer, M. A. Synthesis and characterization of reactive PEO-PMCL polymersomes. *Polymer Chemistry* **1**, 1281-1290, doi:10.1039/C0PY00143K (2010).

91 Pangburn, T. O., Bates, F. S. & Kokkoli, E. Polymersomes functionalized via "click" chemistry with the fibronectin mimetic peptides PR_b and GRGDSP for targeted delivery to cells with different levels of [small alpha]5[small beta]1 expression. *Soft Matter* **8**, 4449-4461, doi:10.1039/C2SM06922A (2012).

92 Pangburn, T. O., Georgiou, K., Bates, F. S. & Kokkoli, E. Targeted Polymersome Delivery of siRNA Induces Cell Death of Breast Cancer Cells Dependent upon Orai3 Protein Expression. *Langmuir : the ACS journal of surfaces and colloids* **28**, 12816-12830, doi:10.1021/la300874z (2012).

93 Peppas, N. A., Hilt, J. Z., Khademhosseini, A. & Langer, R. Hydrogels in Biology and Medicine: From Molecular Principles to Bionanotechnology. *Advanced Materials* **18**, 1345-1360, doi:10.1002/adma.200501612 (2006).

94 Lyon, L. A., Meng, Z., Singh, N., Sorrell, C. D. & St. John, A. Thermoresponsive microgel-based materials. *Chemical Society Reviews* **38**, 865-874, doi:10.1039/B715522K (2009).

95 Buddy Ratner, A. H., Frederick Schoen, Jack Lemons. *Bomaterials Science: An Introduction to Materials in Medicine*. (Elsevier, 2012).

96 Whitesides, G. M., Ostuni, E., Takayama, S., Jiang, X. & Ingber, D. E. Soft lithography in biology and biochemistry. *Annual review of biomedical engineering* **3**, 335-373, doi:10.1146/annurev.bioeng.3.1.335 (2001).

97 West, J. L. & Hubbell, J. A. Polymeric biomaterials with degradation sites for proteases involved in cell migration. *Macromolecules* **32**, 241-244 (1999).

98 Hern, D. L. & Hubbell, J. A. Incorporation of adhesion peptides into nonadhesive hydrogels useful for tissue resurfacing. *Journal of biomedical materials research* **39**, 266-276 (1998).

99 Kidane, A., Szabocsik, J. M. & Park, K. Accelerated study on lysozyme deposition on poly(HEMA) contact lenses. *Biomaterials* **19**, 2051-2055, doi:http://dx.doi.org/10.1016/S0142-9612(98)00111-2 (1998).

100 Peppas, N. A. & Merrill, E. W. Development of semicrystalline poly(vinyl alcohol) hydrogels for biomedical applications. *Journal of biomedical materials research* **11**, 423-434, doi:10.1002/jbm.820110309 (1977).

101 Martens, P. J., Bryant, S. J. & Anseth, K. S. Tailoring the degradation of hydrogels formed from multivinyl poly(ethylene glycol) and poly(vinyl alcohol) macromers for cartilage tissue engineering. *Biomacromolecules* **4**, 283-292, doi:10.1021/bm025666v (2003).

102 Drury, J. L. & Mooney, D. J. Hydrogels for tissue engineering: scaffold design variables and applications. *Biomaterials* **24**, 4337-4351 (2003).

103 Lee, C. R., Grodzinsky, A. J. & Spector, M. The effects of cross-linking of collagen-glycosaminoglycan scaffolds on compressive stiffness, chondrocyte-mediated contraction, proliferation and biosynthesis. *Biomaterials* **22**, 3145-3154 (2001).

104 Lutolf, M. P. *et al.* Synthetic matrix metalloproteinase-sensitive hydrogels for the conduction of tissue regeneration: engineering cell-invasion characteristics. *Proceedings of the National Academy of Sciences of the United States of America* **100**, 5413-5418, doi:10.1073/pnas.0737381100 (2003).

105 Burdick, J. A., Khademhosseini, A. & Langer, R. Fabrication of Gradient Hydrogels Using a Microfluidics/Photopolymerization Process. *Langmuir : the ACS journal of surfaces and colloids* **20**, 5153-5156, doi:10.1021/la049298n (2004).

106 Podual, K., Doyle, F. J., 3rd & Peppas, N. A. Glucose-sensitivity of glucose oxidase-containing cationic copolymer hydrogels having poly(ethylene glycol) grafts. *Journal of controlled release : official journal of the Controlled Release Society* **67**, 9-17 (2000).

107 Ehrick, J. D. *et al.* Genetically engineered protein in hydrogels tailors stimuli-responsive characteristics. *Nat Mater* **4**, 298-302, doi:10.1038/nmat1352 (2005).

108 Mann, B. K., Gobin, A. S., Tsai, A. T., Schmedlen, R. H. & West, J. L. Smooth muscle cell growth in photopolymerized hydrogels with cell adhesive and proteolytically degradable domains: synthetic ECM analogs for tissue engineering. *Biomaterials* **22**, 3045-3051, doi:http://dx.doi.org/10.1016/S0142-9612(01)00051-5 (2001).

109 Suzuki, Y. *et al.* Alginate hydrogel linked with synthetic oligopeptide derived from BMP-2 allows ectopic osteoinduction in vivo. *Journal of biomedical materials research* **50**, 405-409 (2000).

110 Zhang, S. Fabrication of novel biomaterials through molecular self-assembly. *Nature biotechnology* **21**, 1171-1178, doi:10.1038/nbt874 (2003).

111 Petka, W. A., Harden, J. L., McGrath, K. P., Wirtz, D. & Tirrell, D. A. Reversible hydrogels from self-assembling artificial proteins. *Science* **281**, 389-392 (1998).

112 Wang, C., Stewart, R. J. & Kopecek, J. Hybrid hydrogels assembled from synthetic polymers and coiled-coil protein domains. *Nature* **397**, 417-420, doi:10.1038/17092 (1999).

113 MacEwan, S. R. & Chilkoti, A. Applications of elastin-like polypeptides in drug delivery. *Journal of Controlled Release*, doi:http://dx.doi.org/10.1016/j.jconrel.2014.06.028.

114 Amiram, M., Quiroz, F. G., Callahan, D. J. & Chilkoti, A. A highly parallel method for synthesizing DNA repeats enables the discovery of 'smart' protein polymers. *Nat Mater* **10**, 141-148, doi:http://www.nature.com/nmat/journal/v10/n2/abs/nmat2942.html#supplementary-information (2011).

115 Alpar, H. O., Somavarapu, S., Atuah, K. N. & Bramwell, V. W. Biodegradable mucoadhesive particulates for nasal and pulmonary antigen and DNA delivery. *Advanced Drug Delivery Reviews* **57**, 411-430, doi:http://dx.doi.org/10.1016/j.addr.2004.09.004 (2005).

116 Vinogradov, S. V. Colloidal microgels in drug delivery applications. *Current pharmaceutical design* **12**, 4703-4712 (2006).

117 Peppas, N. A. & Huang, Y. Nanoscale technology of mucoadhesive interactions. *Adv Drug Deliv Rev* **56**, 1675-1687, doi:10.1016/j.addr.2004.03.001 (2004).

118 Chowdary, K. P. & Rao, Y. S. Mucoadhesive microspheres for controlled drug delivery. *Biological & pharmaceutical bulletin* **27**, 1717-1724 (2004).

119 Peppas, N. A., Wood, K. M. & Blanchette, J. O. Hydrogels for oral delivery of therapeutic proteins. *Expert opinion on biological therapy* **4**, 881-887, doi:10.1517/14712598.4.6.881 (2004).

120 Bromberg, L., Temchenko, M., Alakhov, V. & Hatton, T. A. Bioadhesive properties and rheology of polyether-modified poly(acrylic acid) hydrogels. *International journal of pharmaceutics* **282**, 45-60, doi:10.1016/j.ijpharm.2004.05.030 (2004).

121 Krauland, A. H. & Bernkop-Schnurch, A. Thiomers: development and in vitro evaluation of a peroral microparticulate peptide delivery system. *European journal of pharmaceutics and biopharmaceutics : official journal of Arbeitsgemeinschaft fur Pharmazeutische Verfahrenstechnik e.V* **57**, 181-187, doi:10.1016/j.ejpb.2003.09.011 (2004).

122 Jones, C. D. & Lyon, L. A. Synthesis and Characterization of Multiresponsive Core−Shell Microgels. *Macromolecules* **33**, 8301-8306, doi:10.1021/ma001398m (2000).

123 Serpe, M. J., Yarmey, K. A., Nolan, C. M. & Lyon, L. A. Doxorubicin Uptake and Release from Microgel Thin Films. *Biomacromolecules* **6**, 408-413, doi:10.1021/bm049455x (2004).

124 Gan, D. & Lyon, L. A. Tunable swelling kinetics in core--shell hydrogel nanoparticles. *J Am Chem Soc* **123**, 7511-7517 (2001).

125 Gan, D. & Lyon, L. A. Synthesis and Protein Adsorption Resistance of PEG-Modified Poly(N-isopropylacrylamide) Core/Shell Microgels. *Macromolecules* **35**, 9634-9639, doi:10.1021/ma021186k (2002).

126 Nayak, S., Lee, H., Chmielewski, J. & Lyon, L. A. Folate-Mediated Cell Targeting and Cytotoxicity Using Thermoresponsive Microgels. *Journal of the American Chemical Society* **126**, 10258-10259, doi:10.1021/ja0474143 (2004).

127 Peppas, N. A. & Franson, N. M. The swelling interface number as a criterion for prediction of diffusional solute release mechanisms in swellable polymers. *Journal of Polymer Science: Polymer Physics Edition* **21**, 983-997, doi:10.1002/pol.1983.180210614 (1983).

128 Ritger, P. L. & Peppas, N. A. A simple equation for description of solute release II. Fickian and anomalous release from swellable devices. *Journal of Controlled Release* **5**, 37-42, doi:http://dx.doi.org/10.1016/0168-3659(87)90035-6 (1987).

129 Ritger, P. L. & Peppas, N. A. A simple equation for description of solute release I. Fickian and non-fickian release from non-swellable devices in the form of slabs, spheres, cylinders or discs. *Journal of Controlled Release* **5**, 23-36, doi:http://dx.doi.org/10.1016/0168-3659(87)90034-4 (1987).

130 Morishita, M., Lowman, A. M., Takayama, K., Nagai, T. & Peppas, N. A. Elucidation of the mechanism of incorporation of insulin in controlled release systems based on complexation polymers. *Journal of Controlled Release* **81**, 25-32, doi:http://dx.doi.org/10.1016/S0168-3659(02)00019-6 (2002).

131 Elbert, D. L. & Hubbell, J. A. Surface Treatments of Polymers for Biocompatibility. *Annual Review of Materials Science* **26**, 365-394, doi:doi:10.1146/annurev.ms.26.080196.002053 (1996).

132 Elbert, D. L. & Hubbell, J. A. Reduction of fibrous adhesion formation by a copolymer possessing an affinity for anionic surfaces. *Journal of biomedical materials research* **42**, 55-65 (1998).

133 Elbert, D. L., Herbert, C. B. & Hubbell, J. A. Thin Polymer Layers Formed by Polyelectrolyte Multilayer Techniques on Biological Surfaces. *Langmuir : the ACS journal of surfaces and colloids* **15**, 5355-5362, doi:10.1021/la9815749 (1999).

134 Kenausis, G. L. *et al.* Poly(l-lysine)-g-Poly(ethylene glycol) Layers on Metal Oxide Surfaces: Attachment Mechanism and Effects of Polymer Architecture on Resistance to Protein Adsorption†. *The Journal of Physical Chemistry B* **104**, 3298-3309, doi:10.1021/jp993359m (2000).

135 Huang, N.-P. *et al.* Poly(l-lysine)-g-poly(ethylene glycol) Layers on Metal Oxide Surfaces: Surface-Analytical Characterization and Resistance to Serum and Fibrinogen

Adsorption. *Langmuir : the ACS journal of surfaces and colloids* **17**, 489-498, doi:10.1021/la000736+ (2000).

136 Scott, E. A. *et al.* Protein adsorption and cell adhesion on nanoscale bioactive coatings formed from poly(ethylene glycol) and albumin microgels. *Biomaterials* **29**, 4481-4493, doi:10.1016/j.biomaterials.2008.08.003 (2008).

137 Raemdonck, K. *et al.* Dextran Microgels for Time-Controlled Delivery of siRNA. *Advanced Functional Materials* **18**, 993-1001, doi:10.1002/adfm.200701039 (2008).

138 Costa, D., Valente, A. J., Miguel, M. G. & Queiroz, J. Plasmid DNA microgels for a therapeutical strategy combining the delivery of genes and anticancer drugs. *Macromolecular bioscience* **12**, 1243-1252, doi:10.1002/mabi.201200096 (2012).

139 Knipe, J. M., Chen, F. & Peppas, N. A. Multiresponsive polyanionic microgels with inverse pH responsive behavior by encapsulation of polycationic nanogels. *Journal of Applied Polymer Science* **131**, n/a-n/a, doi:10.1002/app.40098 (2014).

140 Wanakule, P., Liu, G. W., Fleury, A. T. & Roy, K. Nano-inside-micro: Disease-responsive microgels with encapsulated nanoparticles for intracellular drug delivery to the deep lung. *Journal of controlled release : official journal of the Controlled Release Society* **162**, 429-437, doi:10.1016/j.jconrel.2012.07.026 (2012).

141 Nelson, C. E. *et al.* Tunable Delivery of siRNA from a Biodegradable Scaffold to Promote Angiogenesis In Vivo. *Advanced Materials* **26**, 607-614, doi:10.1002/adma.201303520 (2014).

142 Nguyen, K., Dang, P. N. & Alsberg, E. Functionalized, biodegradable hydrogels for control over sustained and localized siRNA delivery to incorporated and surrounding cells. *Acta biomaterialia* **9**, 4487-4495, doi:http://dx.doi.org/10.1016/j.actbio.2012.08.012 (2013).

143 Krebs, M. D., Jeon, O. & Alsberg, E. Localized and Sustained Delivery of Silencing RNA from Macroscopic Biopolymer Hydrogels. *Journal of the American Chemical Society* **131**, 9204-9206, doi:10.1021/ja9037615 (2009).

144 Nguyen, M. K., Jeon, O., Krebs, M. D., Schapira, D. & Alsberg, E. Sustained localized presentation of RNA interfering molecules from in situ forming hydrogels to guide stem cell osteogenic differentiation. *Biomaterials* **35**, 6278-6286, doi:http://dx.doi.org/10.1016/j.biomaterials.2014.04.048 (2014).

145 Adolph, E. J. *et al.* Enhanced performance of plasmid DNA polyplexes stabilized by a combination of core hydrophobicity and surface PEGylation. *Journal of Materials Chemistry B*, doi:10.1039/C4TB00352G (2014).

146 Fine, D. *et al.* Silicon Micro- and Nanofabrication for Medicine. *Advanced healthcare materials* **2**, 632-666, doi:10.1002/adhm.201200214 (2013).

147 Zhang, M. *et al.* Polycation-functionalized nanoporous silicon particles for gene silencing on breast cancer cells. *Biomaterials* **35**, 423-431, doi:http://dx.doi.org/10.1016/j.biomaterials.2013.09.033 (2014).

148 Vinogradov, S. V., Bronich, T. K. & Kabanov, A. V. Nanosized cationic hydrogels for drug delivery: preparation, properties and interactions with cells. *Advanced Drug Delivery Reviews* **54**, 135-147, doi:http://dx.doi.org/10.1016/S0169-409X(01)00245-9 (2002).

149 Vinogradov, S., Batrakova, E. & Kabanov, A. Poly(ethylene glycol)–polyethyleneimine NanoGel™ particles: novel drug delivery systems for antisense oligonucleotides. *Colloids and Surfaces B: Biointerfaces* **16**, 291-304, doi:http://dx.doi.org/10.1016/S0927-7765(99)00080-6 (1999).

150 Vinogradov, S. V., Batrakova, E. V. & Kabanov, A. V. Nanogels for oligonucleotide delivery to the brain. *Bioconjug Chem* **15**, 50-60, doi:10.1021/bc034164r (2004).

151 Vinogradov, S. V., Zeman, A. D., Batrakova, E. V. & Kabanov, A. V. Polyplex Nanogel formulations for drug delivery of cytotoxic nucleoside analogs. *Journal of controlled release : official journal of the Controlled Release Society* **107**, 143-157, doi:10.1016/j.jconrel.2005.06.002 (2005).

152 Oishi, M., Hayashi, H., Itaka, K., Kataoka, K. & Nagasaki, Y. pH-Responsive PEGylated nanogels as targetable and low invasive endosomolytic agents to induce the enhanced transfection efficiency of nonviral gene vectors. *Colloid Polym Sci* **285**, 1055-1060, doi:10.1007/s00396-007-1660-6 (2007).

153 Tamura, A., Oishi, M. & Nagasaki, Y. Enhanced cytoplasmic delivery of siRNA using a stabilized polyion complex based on PEGylated nanogels with a cross-linked polyamine structure. *Biomacromolecules* **10**, 1818-1827, doi:10.1021/bm900252d (2009).

154 Tamura, A., Oishi, M. & Nagasaki, Y. Efficient siRNA delivery based on PEGylated and partially quaternized polyamine nanogels: enhanced gene silencing activity by the cooperative effect of tertiary and quaternary amino groups in the core. *Journal of controlled release : official journal of the Controlled Release Society* **146**, 378-387, doi:10.1016/j.jconrel.2010.05.031 (2010).

155 Mimi, H., Ho, K. M., Siu, Y. S., Wu, A. & Li, P. Polyethyleneimine-based core-shell nanogels: a promising siRNA carrier for argininosuccinate synthetase mRNA knockdown in HeLa cells. *Journal of controlled release : official journal of the Controlled Release Society* **158**, 123-130, doi:10.1016/j.jconrel.2011.10.035 (2012).

156 Lee, H., Mok, H., Lee, S., Oh, Y. K. & Park, T. G. Target-specific intracellular delivery of siRNA using degradable hyaluronic acid nanogels. *Journal of controlled release : official journal of the Controlled Release Society* **119**, 245-252, doi:10.1016/j.jconrel.2007.02.011 (2007).

157 Raemdonck, K., Naeye, B., Hogset, A., Demeester, J. & De Smedt, S. C. Prolonged gene silencing by combining siRNA nanogels and photochemical internalization. *Journal of controlled release : official journal of the Controlled Release Society* **145**, 281-288, doi:10.1016/j.jconrel.2010.04.012 (2010).

158 Naeye, B. *et al.* PEGylation of biodegradable dextran nanogels for siRNA delivery. *European journal of pharmaceutical sciences : official journal of the European Federation for Pharmaceutical Sciences* **40**, 342-351, doi:10.1016/j.ejps.2010.04.010 (2010).

159 Sunasee, R., Wattanaarsakit, P., Ahmed, M., Lollmahomed, F. B. & Narain, R. Biodegradable and Nontoxic Nanogels as Nonviral Gene Delivery Systems. *Bioconjugate Chemistry* **23**, 1925-1933, doi:10.1021/bc300314u (2012).

160 Ahmed, M. & Narain, R. Intracellular Delivery of DNA and Enzyme in Active Form Using Degradable Carbohydrate-Based Nanogels. *Molecular pharmaceutics* **9**, 3160-3170, doi:10.1021/mp300255p (2012).

161 Blackburn, W. H., Dickerson, E. B., Smith, M. H., McDonald, J. F. & Lyon, L. A. Peptide-functionalized nanogels for targeted siRNA delivery. *Bioconjug Chem* **20**, 960-968, doi:10.1021/bc800547c (2009).

162 Dickerson, E. B. *et al.* Chemosensitization of cancer cells by siRNA using targeted nanogel delivery. *BMC cancer* **10**, 10, doi:10.1186/1471-2407-10-10 (2010).

163 Dunn, S. S. *et al.* Reductively Responsive siRNA-Conjugated Hydrogel Nanoparticles for Gene Silencing. *Journal of the American Chemical Society* **134**, 7423-7430, doi:10.1021/ja300174v (2012).

164 Agarwal, R. *et al.* Mammalian cells preferentially internalize hydrogel nanodiscs over nanorods and use shape-specific uptake mechanisms. *Proceedings of the National Academy of Sciences*, doi:10.1073/pnas.1305000110 (2013).

165 Friedmann, T. Progress toward human gene therapy. *Science* **244**, 1275-1281, doi:10.1126/science.2660259 (1989).

166 Rosenberg, S. A. *et al.* Gene Transfer into Humans — Immunotherapy of Patients with Advanced Melanoma, Using Tumor-Infiltrating Lymphocytes Modified by Retroviral Gene Transduction. *New England Journal of Medicine* **323**, 570-578, doi:doi:10.1056/NEJM199008303230904 (1990).

167 Blaese, R. M. *et al.* T Lymphocyte-Directed Gene Therapy for ADA− SCID: Initial Trial Results After 4 Years. *Science* **270**, 475-480, doi:10.1126/science.270.5235.475 (1995).

168 Marcum, J. A. From the molecular genetics revolution to gene therapy: Translating basic research into medicine. *The Journal of laboratory and clinical medicine* **146**, 312-316 (2005).

169 Weiss, R. in *Washington Post* (2005).

170 Anderson, W. F. The Best of Times, the Worst of Times. *Science* **288**, 627-629, doi:10.1126/science.288.5466.627 (2000).

171 Kutzler, M. A. & Weiner, D. B. DNA vaccines: ready for prime time? *Nat Rev Genet* **9**, 776-788 (2008).

172 Ferraro, B. *et al.* Clinical applications of DNA vaccines: current progress. *Clinical infectious diseases : an official publication of the Infectious Diseases Society of America* **53**, 296-302, doi:10.1093/cid/cir334 (2011).

173 Kanasty, R., Dorkin, J. R., Vegas, A. & Anderson, D. Delivery materials for siRNA therapeutics. *Nat Mater* **12**, 967-977, doi:10.1038/nmat3765 (2013).

174 Ginn, S. L., Alexander, I. E., Edelstein, M. L., Abedi, M. R. & Wixon, J. Gene therapy clinical trials worldwide to 2012 - an update. *The journal of gene medicine* **15**, 65-77, doi:10.1002/jgm.2698 (2013).

175 Arteaga, C. L. *et al.* Treatment of HER2-positive breast cancer: current status and future perspectives. *Nat Rev Clin Oncol* **9**, 16-32, doi:http://www.nature.com/nrclinonc/journal/v9/n1/suppinfo/nrclinonc.2011.177_S1.html (2012).

176 Kennecke, H. *et al.* Metastatic Behavior of Breast Cancer Subtypes. *Journal of Clinical Oncology* **28**, 3271-3277 (2010).

177 Voduc, K. D. *et al.* Breast Cancer Subtypes and the Risk of Local and Regional Relapse. *Journal of Clinical Oncology* **28**, 1684-1691 (2010).

178 Cobleigh, M. A. *et al.* Multinational study of the efficacy and safety of humanized anti-HER2 monoclonal antibody in women who have HER2-overexpressing metastatic breast cancer that has progressed after chemotherapy for metastatic disease. *J Clin Oncol* **17** (1999).

179 Slamon, D. J. *et al.* Use of Chemotherapy plus a Monoclonal Antibody against HER2 for Metastatic Breast Cancer That Overexpresses HER2. *New England Journal of Medicine* **344**, 783-792, doi:10.1056/NEJM200103153441101 (2001).

180 Agus, D. B. *et al.* Phase I Clinical Study of Pertuzumab, a Novel HER Dimerization Inhibitor, in Patients With Advanced Cancer. *Journal of Clinical Oncology* **23**, 2534-2543 (2005).

181 Baselga, J. *et al.* Pertuzumab plus Trastuzumab plus Docetaxel for Metastatic Breast Cancer. *New England Journal of Medicine* **366**, 109-119, doi:10.1056/NEJMoa1113216 (2011).

182 Geyer, C. E. *et al.* Lapatinib plus Capecitabine for HER2-Positive Advanced Breast Cancer. *New England Journal of Medicine* **355**, 2733-2743, doi:10.1056/NEJMoa064320 (2006).

183 Cameron, D. *et al.* A phase III randomized comparison of lapatinib plus capecitabine versus capecitabine alone in women with advanced breast cancer that has progressed on trastuzumab: updated efficacy and biomarker analyses. *Breast Cancer Res Treat* **112** (2008).

184 Blackwell, K. L. *et al.* Randomized study of Lapatinib alone or in combination with trastuzumab in women with ErbB2-positive, trastuzumab-refractory metastatic breast cancer. *J Clin Oncol* **28** (2010).

185 Burstein, H. J. *et al.* Neratinib, an Irreversible ErbB Receptor Tyrosine Kinase Inhibitor, in Patients With Advanced ErbB2-Positive Breast Cancer. *Journal of Clinical Oncology* **28**, 1301-1307 (2010).

186 Engelman, J. A. Targeting PI3K signalling in cancer: opportunities, challenges and limitations. *Nat Rev Cancer* **9**, 550-562 (2009).

187 Yuan, T. L. & Cantley, L. C. PI3K pathway alterations in cancer: variations on a theme. *Oncogene* **27**, 5497-5510 (0000).

188 Berns, K. *et al.* A functional genetic approach identifies the PI3K pathway as a major determinant of trastuzumab resistance in breast cancer. *Cancer Cell* **12** (2007).

189 Samuels, Y. *et al.* High frequency of mutations of the PIK3CA gene in human cancers. *Science* **304** (2004).

190 Li, J. *et al.* PTEN, a Putative Protein Tyrosine Phosphatase Gene Mutated in Human Brain, Breast, and Prostate Cancer. *Science* **275**, 1943-1947 (1997).

191 Steck, P. A. *et al.* Identification of a candidate tumour suppressor gene, MMAC1, at chromosome 10q23.3 that is mutated in multiple advanced cancers. *Nat Genet* **15**, 356-362, doi:10.1038/ng0497-356 (1997).

192 Carpten, J. D. *et al.* A transforming mutation in the pleckstrin homology domain of AKT1 in cancer. *Nature* **448** (2007).

193 Ritter, C. A. *et al.* Human Breast Cancer Cells Selected for Resistance to Trastuzumab In vivo Overexpress Epidermal Growth Factor Receptor and ErbB Ligands and Remain Dependent on the ErbB Receptor Network. *Clinical Cancer Research* **13**, 4909-4919 (2007).

194 Sergina, N. V. *et al.* Escape from HER-family tyrosine kinase inhibitor therapy by the kinase-inactive HER3. *Nature* **445**, 437-441,

doi:http://www.nature.com/nature/journal/v445/n7126/suppinfo/nature05474_S1.html (2007).

195 Garrett, J. T. *et al.* Transcriptional and posttranslational up-regulation of HER3 (ErbB3) compensates for inhibition of the HER2 tyrosine kinase. *Proc Natl Acad Sci USA* **108** (2011).

196 Vaught, D. B. *et al.* HER3 Is Required for HER2-Induced Preneoplastic Changes to the Breast Epithelium and Tumor Formation. *Cancer Research* **72**, 2672-2682 (2012).

197 Huang, X. *et al.* Heterotrimerization of the Growth Factor Receptors erbB2, erbB3, and Insulin-like Growth Factor-I Receptor in Breast Cancer Cells Resistant to Herceptin. *Cancer Research* **70**, 1204-1214 (2010).

198 Shattuck, D. L., Miller, J. K., Carraway, K. L. & Sweeney, C. Met Receptor Contributes to Trastuzumab Resistance of Her2-Overexpressing Breast Cancer Cells. *Cancer Research* **68**, 1471-1477 (2008).

199 Caplen, N. J., Parrish, S., Imani, F., Fire, A. & Morgan, R. A. Specific inhibition of gene expression by small double-stranded RNAs in invertebrate and vertebrate systems. *Proc Natl Acad Sci U S A* **98**, 9742-9747, doi:10.1073/pnas.171251798 (2001).

200 Elbashir, S. M. *et al.* Duplexes of 21-nucleotide RNAs mediate RNA interference in cultured mammalian cells. *Nature* **411**, 494-498, doi:10.1038/35078107 (2001).

201 Soutschek, J. *et al.* Therapeutic silencing of an endogenous gene by systemic administration of modified siRNAs. *Nature* **432**, 173-178, doi:http://www.nature.com/nature/journal/v432/n7014/suppinfo/nature03121_S1.html (2004).

202 Dykxhoorn, D. M., Palliser, D. & Lieberman, J. The silent treatment: siRNAs as small molecule drugs. *Gene therapy* **13**, 541-552 (2006).

203 Wang, J., Lu, Z., Wientjes, M. G. & Au, J. S. Delivery of siRNA Therapeutics: Barriers and Carriers. *AAPS J* **12**, 492-503, doi:10.1208/s12248-010-9210-4 (2010).

204 Bartlett, D. W. & Davis, M. E. Effect of siRNA nuclease stability on the in vitro and in vivo kinetics of siRNA-mediated gene silencing. *Biotechnology and Bioengineering* **97**, 909-921, doi:10.1002/bit.21285 (2007).

205 Whitehead, K. A., Langer, R. & Anderson, D. G. Knocking down barriers: advances in siRNA delivery. *Nat Rev Drug Discov* **8**, 129-138 (2009).

206 Oh, Y.-K. & Park, T. G. siRNA delivery systems for cancer treatment. *Advanced Drug Delivery Reviews* **61**, 850-862, doi:http://dx.doi.org/10.1016/j.addr.2009.04.018 (2009).

207 Mislick, K. A. & Baldeschwieler, J. D. Evidence for the role of proteoglycans in cation-mediated gene transfer. *Proceedings of the National Academy of Sciences* **93**, 12349-12354 (1996).

208 Lammers, T., Rizzo, L. Y., Storm, G. & Kiessling, F. Personalized Nanomedicine. *Clinical Cancer Research* **18**, 4889-4894, doi:10.1158/1078-0432.ccr-12-1414 (2012).

209 Hansen, A. E. *et al.* Positron Emission Tomography Based Elucidation of the Enhanced Permeability and Retention Effect in Dogs with Cancer Using Copper-64 Liposomes. *ACS Nano* **9**, 6985-6995, doi:10.1021/acsnano.5b01324 (2015).

210 Gabizon, A., Shmeeda, H. & Barenholz, Y. Pharmacokinetics of Pegylated Liposomal Doxorubicin. *Clinical Pharmacokinetics* **42**, 419-436, doi:10.2165/00003088-200342050-00002 (2003).

211 Papahadjopoulos, D. *et al.* Sterically stabilized liposomes: improvements in pharmacokinetics and antitumor therapeutic efficacy. *Proceedings of the National Academy of Sciences* **88**, 11460-11464 (1991).

212 Torchilin, V. Tumor delivery of macromolecular drugs based on the EPR effect. *Adv Drug Deliv Rev* **63**, 131-135, doi:10.1016/j.addr.2010.03.011 (2011).

213 Maeda, H., Nakamura, H. & Fang, J. The EPR effect for macromolecular drug delivery to solid tumors: Improvement of tumor uptake, lowering of systemic toxicity, and distinct tumor imaging in vivo. *Adv Drug Deliv Rev* **65**, 71-79, doi:10.1016/j.addr.2012.10.002 (2013).

214 Venkataraman, S. *et al.* The role of PEG architecture and molecular weight in the gene transfection performance of PEGylated poly(dimethylaminoethyl methacrylate) based cationic polymers. *Biomaterials* **32**, 2369-2378, doi:http://dx.doi.org/10.1016/j.biomaterials.2010.11.070 (2011).

215 Mishra, S., Webster, P. & Davis, M. E. PEGylation significantly affects cellular uptake and intracellular trafficking of non-viral gene delivery particles. *European Journal of Cell Biology* **83**, 97-111, doi:http://dx.doi.org/10.1078/0171-9335-00363 (2004).

216 Sato, A. *et al.* Polymer brush-stabilized polyplex for a siRNA carrier with long circulatory half-life. *Journal of Controlled Release* **122**, 209-216, doi:http://dx.doi.org/10.1016/j.jconrel.2007.04.018 (2007).

217 Miteva, M. *et al.* Tuning PEGylation of mixed micelles to overcome intracellular and systemic siRNA delivery barriers. *Biomaterials* **38**, 97-107, doi:10.1016/j.biomaterials.2014.10.036 (2015).

218 Zuckerman, J. E., Choi, C. H., Han, H. & Davis, M. E. Polycation-siRNA nanoparticles can disassemble at the kidney glomerular basement membrane. *Proceedings of the*

National Academy of Sciences of the United States of America **109**, 3137-3142, doi:10.1073/pnas.1200718109 (2012).

219 Naeye, B. *et al.* In vivo disassembly of IV administered siRNA matrix nanoparticles at the renal filtration barrier. *Biomaterials* **34**, 2350-2358, doi:10.1016/j.biomaterials.2012.11.058 (2013).

220 Naeye, B. *et al.* In vivo disassembly of IV administered siRNA matrix nanoparticles at the renal filtration barrier. *Biomaterials* **34**, 2350-2358, doi:http://dx.doi.org/10.1016/j.biomaterials.2012.11.058 (2013).

221 Merkel, O. M. *et al.* Stability of siRNA polyplexes from poly(ethylenimine) and poly(ethylenimine)-g-poly(ethylene glycol) under in vivo conditions: Effects on pharmacokinetics and biodistribution measured by Fluorescence Fluctuation Spectroscopy and Single Photon Emission Computed Tomography (SPECT) imaging. *Journal of Controlled Release* **138**, 148-159, doi:http://dx.doi.org/10.1016/j.jconrel.2009.05.016 (2009).

222 Deng, Z. J. *et al.* Layer-by-Layer Nanoparticles for Systemic Codelivery of an Anticancer Drug and siRNA for Potential Triple-Negative Breast Cancer Treatment. *ACS Nano* **7**, 9571-9584, doi:10.1021/nn4047925 (2013).

223 Guertin, D. A. *et al.* Ablation in Mice of the mTORC Components raptor, rictor, or mLST8 Reveals that mTORC2 Is Required for Signaling to Akt-FOXO and PKCα, but Not S6K1. *Developmental Cell* **11**, 859-871, doi:http://dx.doi.org/10.1016/j.devcel.2006.10.007 (2006).

224 Zhang, Z., Zhang, G., Xu, X., Su, W. & Yu, B. mTOR-rictor is the Ser473 kinase for AKT1 in mouse one-cell stage embryos. *Molecular and Cellular Biochemistry* **361**, 249-257, doi:10.1007/s11010-011-1110-0 (2012).

225 Morrison-Joly, M. *et al.* Rictor/mTORC2 drives progression and therapeutic resistance of HER2-amplified breast cancers. *Cancer Research* (2016).

226 Wander, S. A., Hennessy, B. T. & Slingerland, J. M. Next-generation mTOR inhibitors in clinical oncology: how pathway complexity informs therapeutic strategy. *The Journal of Clinical Investigation* **121**, 1231-1241, doi:10.1172/JCI44145 (2011).

227 Guertin, D. A. *et al.* mTOR Complex 2 Is Required for the Development of Prostate Cancer Induced by Pten Loss in Mice. *Cancer Cell* **15**, 148-159, doi:http://dx.doi.org/10.1016/j.ccr.2008.12.017 (2009).

228 Masri, J. *et al.* mTORC2 Activity Is Elevated in Gliomas and Promotes Growth and Cell Motility via Overexpression of Rictor. *Cancer Research* **67**, 11712-11720, doi:10.1158/0008-5472.CAN-07-2223 (2007).

229 Li, H. *et al.* Targeting of mTORC2 prevents cell migration and promotes apoptosis in breast cancer. *Breast Cancer Research and Treatment* **134**, 1057-1066, doi:10.1007/s10549-012-2036-2 (2012).

230 Morrison, M. M. *et al.* mTOR Directs Breast Morphogenesis through the PKC-alpha-Rac1 Signaling Axis. *PLoS Genet* **11**, e1005291, doi:10.1371/journal.pgen.1005291 (2015).

231 Clark, A. R. & Toker, A. Signalling specificity in the Akt pathway in breast cancer. *Biochemical Society transactions* **42**, 1349-1355 (2014).

232 Miller, T., Rexer, B., Garrett, J. & Arteaga, C. Mutations in the phosphatidylinositol 3-kinase pathway: role in tumor progression and therapeutic implications in breast cancer. *Breast Cancer Research* **13**, 224 (2011).

233 Laplante, M. & Sabatini, David M. mTOR Signaling in Growth Control and Disease. *Cell* **149**, 274-293, doi:http://dx.doi.org/10.1016/j.cell.2012.03.017 (2012).

234 Banerji, U. *et al.* First results from a phase I trial of AZD8055, a dual mTORC1 and mTORC2 inhibitor. *ASCO Meeting Abstracts* **29**, 3096 (2011).

235 Asahina, H. *et al.* Safety and tolerability of AZD8055 in Japanese patients with advanced solid tumors; a dose-finding phase I study. *Investigational New Drugs* **31**, 677-684, doi:10.1007/s10637-012-9860-4 (2013).

236 Miller, T. W., Rexer, B. N., Garrett, J. T. & Arteaga, C. L. Mutations in the phosphatidylinositol 3-kinase pathway: role in tumor progression and therapeutic implications in breast cancer. *Breast Cancer Research* **13**, 1-12, doi:10.1186/bcr3039 (2011).

237 Miller, T. W., Balko, J. M. & Arteaga, C. L. Phosphatidylinositol 3-Kinase and Antiestrogen Resistance in Breast Cancer. *Journal of Clinical Oncology* **29**, 4452-4461, doi:10.1200/JCO.2010.34.4879 (2011).

238 Kim, D.-H. *et al.* mTOR Interacts with Raptor to Form a Nutrient-Sensitive Complex that Signals to the Cell Growth Machinery. *Cell* **110**, 163-175, doi:http://dx.doi.org/10.1016/S0092-8674(02)00808-5 (2002).

239 Oh, W. J. & Jacinto, E. mTOR complex 2 signaling and functions. *Cell Cycle* **10**, 2305-2316, doi:10.4161/cc.10.14.16586 (2011).

240 Meade, B. R. *et al.* Efficient delivery of RNAi prodrugs containing reversible charge-neutralizing phosphotriester backbone modifications. *Nature biotechnology* **32**, 1256-1261, doi:10.1038/nbt.3078 (2014).

241 Song, E. *et al.* Antibody mediated in vivo delivery of small interfering RNAs via cell-surface receptors. *Nat Biotech* **23**, 709-717 (2005).

242 Zimmermann, T. S. *et al.* RNAi-mediated gene silencing in non-human primates. *Nature* **441**, 111-114, doi:http://www.nature.com/nature/journal/v441/n7089/suppinfo/nature04688_S1.html (2006).

243 Dong, Y. *et al.* Lipopeptide nanoparticles for potent and selective siRNA delivery in rodents and nonhuman primates. *Proceedings of the National Academy of Sciences* **111**, 3955-3960 (2014).

244 Rahman, M. A. *et al.* Systemic delivery of siRNA nanoparticles targeting RRM2 suppresses head and neck tumor growth. *Journal of controlled release : official journal of the Controlled Release Society* **159**, 384-392, doi:10.1016/j.jconrel.2012.01.045 (2012).

245 Christie, R. J. *et al.* Targeted Polymeric Micelles for siRNA Treatment of Experimental Cancer by Intravenous Injection. *ACS Nano* **6**, 5174-5189, doi:10.1021/nn300942b (2012).

246 Verbaan, F. J. *et al.* Steric stabilization of poly(2-(dimethylamino)ethyl methacrylate)-based polyplexes mediates prolonged circulation and tumor targeting in mice. *The Journal of Gene Medicine* **6**, 64-75, doi:10.1002/jgm.475 (2004).

247 Bartlett, D. W., Su, H., Hildebrandt, I. J., Weber, W. A. & Davis, M. E. Impact of tumor-specific targeting on the biodistribution and efficacy of siRNA nanoparticles measured by multimodality in vivo imaging. *Proceedings of the National Academy of Sciences* **104**, 15549-15554, doi:10.1073/pnas.0707461104 (2007).

248 Oe, Y. *et al.* Actively-targeted polyion complex micelles stabilized by cholesterol and disulfide cross-linking for systemic delivery of siRNA to solid tumors. *Biomaterials* **35**, 7887-7895, doi:http://dx.doi.org/10.1016/j.biomaterials.2014.05.041 (2014).

249 Sarett, S. M. *et al.* Hydrophobic interactions between polymeric carrier and palmitic acid-conjugated siRNA improve PEGylated polyplex stability and enhance in vivo pharmacokinetics and tumor gene silencing. *Biomaterials* **97**, 122-132, doi:http://dx.doi.org/10.1016/j.biomaterials.2016.04.017 (2016).

250 Tzeng, S. Y. & Green, J. J. Subtle Changes to Polymer Structure and Degradation Mechanism Enable Highly Effective Nanoparticles for siRNA and DNA Delivery to Human Brain Cancer. *Advanced healthcare materials* **2**, 468-480, doi:10.1002/adhm.201200257 (2013).

251 Mangraviti, A. *et al.* Polymeric Nanoparticles for Nonviral Gene Therapy Extend Brain Tumor Survival in Vivo. *ACS Nano* **9**, 1236-1249, doi:10.1021/nn504905q (2015).

252 Dahlman, J. E. *et al.* In vivo endothelial siRNA delivery using polymeric nanoparticles with low molecular weight. *Nat Nano* **9**, 648-655, doi:10.1038/nnano.2014.84 http://www.nature.com/nnano/journal/v9/n8/abs/nnano.2014.84.html#supplementary-information (2014).

253 Alabi, C. A. *et al.* Multiparametric approach for the evaluation of lipid nanoparticles for siRNA delivery. *Proceedings of the National Academy of Sciences* **110**, 12881-12886, doi:10.1073/pnas.1306529110 (2013).

254 Akinc, A. *et al.* A combinatorial library of lipid-like materials for delivery of RNAi therapeutics. *Nat Biotech* **26**, 561-569, doi:http://www.nature.com/nbt/journal/v26/n5/suppinfo/nbt1402_S1.html (2008).

255 Siegwart, D. J. *et al.* Combinatorial synthesis of chemically diverse core-shell nanoparticles for intracellular delivery. *Proceedings of the National Academy of Sciences* **108**, 12996-13001 (2011).

256 Hao, J. *et al.* Rapid Synthesis of a Lipocationic Polyester Library via Ring-Opening Polymerization of Functional Valerolactones for Efficacious siRNA Delivery. *Journal of the American Chemical Society* **137**, 9206-9209, doi:10.1021/jacs.5b03429 (2015).

257 Zhou, K. *et al.* Modular degradable dendrimers enable small RNAs to extend survival in an aggressive liver cancer model. *Proceedings of the National Academy of Sciences* **113**, 520-525 (2016).

258 Love, K. T. *et al.* Lipid-like materials for low-dose, in vivo gene silencing. *Proceedings of the National Academy of Sciences* **107**, 1864-1869, doi:10.1073/pnas.0910603106 (2010).

259 Whitehead, K. A. *et al.* Degradable lipid nanoparticles with predictable in vivo siRNA delivery activity. *Nature Communications* **5**, 4277, doi:10.1038/ncomms5277 http://www.nature.com/articles/ncomms5277#supplementary-information (2014).

260 Sunshine, J. C., Akanda, M. I., Li, D., Kozielski, K. L. & Green, J. J. Effects of Base Polymer Hydrophobicity and End-Group Modification on Polymeric Gene Delivery. *Biomacromolecules* **12**, 3592-3600, doi:10.1021/bm200807s (2011).

261 Kozielski, K. L., Tzeng, S. Y., Hurtado De Mendoza, B. A. & Green, J. J. Bioreducible Cationic Polymer-Based Nanoparticles for Efficient and Environmentally Triggered Cytoplasmic siRNA Delivery to Primary Human Brain Cancer Cells. *ACS Nano* **8**, 3232-3241, doi:10.1021/nn500704t (2014).

262 Yan, Y. *et al.* Functional polyesters enable selective siRNA delivery to lung cancer over matched normal cells. *Proceedings of the National Academy of Sciences* **113**, E5702-E5710, doi:10.1073/pnas.1606886113 (2016).

263 Evans, B. C. *et al.* Ex Vivo Red Blood Cell Hemolysis Assay for the Evaluation of pH-responsive Endosomolytic Agents for Cytosolic Delivery of Biomacromolecular Drugs. e50166, doi:doi:10.3791/50166 (2013).

264 Bolte, S. & CordeliÈRes, F. P. A guided tour into subcellular colocalization analysis in light microscopy. *Journal of Microscopy* **224**, 213-232, doi:10.1111/j.1365-2818.2006.01706.x (2006).

265 Chiefari, J. *et al.* Living Free-Radical Polymerization by Reversible Addition−Fragmentation Chain Transfer: The RAFT Process. *Macromolecules* **31**, 5559-5562, doi:10.1021/ma9804951 (1998).

266 Boyer, C. *et al.* Bioapplications of RAFT Polymerization. *Chemical Reviews* **109**, 5402-5436, doi:10.1021/cr9001403 (2009).

267 Kong, W. H. *et al.* Efficient intracellular siRNA delivery strategy through rapid and simple two steps mixing involving noncovalent post-PEGylation. *J Control Release* **138**, 141-147, doi:10.1016/j.jconrel.2009.04.034 (2009).

268 Medina-Kauwe, L. K., Xie, J. & Hamm-Alvarez, S. Intracellular trafficking of nonviral vectors. *Gene therapy* **12**, 1734-1751, doi:10.1038/sj.gt.3302592 (2005).

269 Gilleron, J. *et al.* Image-based analysis of lipid nanoparticle-mediated siRNA delivery, intracellular trafficking and endosomal escape. *Nat Biotech* **31**, 638-646, doi:10.1038/nbt.2612 http://www.nature.com/nbt/journal/v31/n7/abs/nbt.2612.html#supplementary-information (2013).

270 Li, H., E. Nelson, C., C. Evans, B. & L. Duvall, C. Delivery of Intracellular-Acting Biologics in Pro-Apoptotic Therapies. *Current Pharmaceutical Design* **17**, 293-319, doi:10.2174/138161211795049642 (2011).

271 Evans, B. C. *et al.* Ex vivo red blood cell hemolysis assay for the evaluation of pH-responsive endosomolytic agents for cytosolic delivery of biomacromolecular drugs. *J Vis Exp*, e50166, doi:10.3791/50166 (2013).

272 Sohaebuddin, S. K., Thevenot, P. T., Baker, D., Eaton, J. W. & Tang, L. Nanomaterial cytotoxicity is composition, size, and cell type dependent. *Particle and Fibre Toxicology* **7**, 1-17, doi:10.1186/1743-8977-7-22 (2010).

273 Xia, T., Kovochich, M., Liong, M., Zink, J. I. & Nel, A. E. Cationic Polystyrene Nanosphere Toxicity Depends on Cell-Specific Endocytic and Mitochondrial Injury Pathways. *ACS Nano* **2**, 85-96, doi:10.1021/nn700256c (2008).

274 Frank-Kamenetsky, M. *et al.* Therapeutic RNAi targeting PCSK9 acutely lowers plasma cholesterol in rodents and LDL cholesterol in nonhuman primates. *Proceedings of the National Academy of Sciences* (2008).

275 Gao, S. *et al.* The Effect of Chemical Modification and Nanoparticle Formulation on Stability and Biodistribution of siRNA in Mice. *Mol Ther* **17**, 1225-1233 (2009).

276 Huang, Y. *et al.* Binary and ternary complexes based on polycaprolactone-graft-poly (N, N-dimethylaminoethyl methacrylate) for targeted siRNA delivery. *Biomaterials* **33**, 4653-4664, doi:10.1016/j.biomaterials.2012.02.052 (2012).

277 Han, S. *et al.* Effects of hydrophobic core components in amphiphilic PDMAEMA nanoparticles on siRNA delivery. *Biomaterials* **48**, 45-55, doi:http://dx.doi.org/10.1016/j.biomaterials.2015.01.026 (2015).

278 Miller, M. A. *et al.* Predicting therapeutic nanomedicine efficacy using a companion magnetic resonance imaging nanoparticle. *Science Translational Medicine* **7**, 314ra183-314ra183 (2015).

279 Clark, A. J. *et al.* CRLX101 nanoparticles localize in human tumors and not in adjacent, nonneoplastic tissue after intravenous dosing. *Proceedings of the National Academy of Sciences* (2016).

280 Wang, J., Lu, Z., Wientjes, M. G. & Au, J. L. Delivery of siRNA therapeutics: barriers and carriers. *The AAPS journal* **12**, 492-503, doi:10.1208/s12248-010-9210-4 (2010).

281 Gilleron, J. *et al.* Image-based analysis of lipid nanoparticle-mediated siRNA delivery, intracellular trafficking and endosomal escape. *Nature biotechnology* **31**, 638-646, doi:10.1038/nbt.2612 (2013).

282 Haussecker, D. Current issues of RNAi therapeutics delivery and development. *Journal of controlled release : official journal of the Controlled Release Society* **195**, 49-54, doi:10.1016/j.jconrel.2014.07.056 (2014).

283 Oe, Y. *et al.* Actively-targeted polyion complex micelles stabilized by cholesterol and disulfide cross-linking for systemic delivery of siRNA to solid tumors. *Biomaterials* **35**, 7887-7895, doi:10.1016/j.biomaterials.2014.05.041 (2014).

284 Li, H. *et al.* Dual MMP7-Proximity-Activated and Folate Receptor-Targeted Nanoparticles for siRNA Delivery. *Biomacromolecules* **16**, 192-201, doi:10.1021/bm501394m (2015).

285 Yin, H. *et al.* Non-viral vectors for gene-based therapy. *Nature reviews. Genetics* **15**, 541-555, doi:10.1038/nrg3763 (2014).

286 Alam, M. R. *et al.* Multivalent cyclic RGD conjugates for targeted delivery of small interfering RNA. *Bioconjugate chemistry* **22**, 1673-1681, doi:10.1021/bc200235q (2011).

287 Kubo, T., Takei, Y., Mihara, K., Yanagihara, K. & Seyama, T. Amino-modified and lipid-conjugated dicer-substrate siRNA enhances RNAi efficacy. *Bioconjugate chemistry* **23**, 164-173, doi:10.1021/bc200333w (2012).

288 Jeong, J. H., Mok, H., Oh, Y., and Park, T.G. siRNA Conjugate Delivery Systems. *Bioconjugate Chem* **20**, 5-14 (2009).

289 Matsuda, S. *et al.* siRNA Conjugates Carrying Sequentially Assembled Trivalent N-Acetylgalactosamine Linked Through Nucleosides Elicit Robust Gene Silencing In Vivo in Hepatocytes. *ACS chemical biology* **10**, 1181-1187, doi:10.1021/cb501028c (2015).

290 Nishina, K. *et al.* Efficient in vivo delivery of siRNA to the liver by conjugation of alpha-tocopherol. *Molecular therapy : the journal of the American Society of Gene Therapy* **16**, 734-740, doi:10.1038/mt.2008.14 (2008).

291 Nelson, C. E., Kintzing, R. J., Hanna, A., Shannon, J. M., Gupta, M. K., Duvall, C. L. Balancing Cationic and Hydrophobic Content of PEGylated siRNA Polyplexes Enhances Endosome Escape, Stability, Blood Circulation Time, and Bioactivity in Vivo. *ACS Nano* **7**, 8870-8880 (2013).

292 Poon, Z., Chang, D., Zhao, X. & Hammond, P. T. Layer-by-Layer Nanoparticles with a pH-Sheddable Layer for in Vivo Targeting of Tumor Hypoxia. *ACS Nano* **5**, 4284-4292, doi:10.1021/nn200876f (2011).

293 Wei, H. *et al.* Dual Responsive, Stabilized Nanoparticles for Efficient In Vivo Plasmid Delivery. *Angewandte Chemie International Edition* **52**, 5377-5381, doi:10.1002/anie.201301896 (2013).

294 Foster, A. A., Greco, C. T., Green, M. D., Epps, T. H. & Sullivan, M. O. Light-Mediated Activation of siRNA Release in Diblock Copolymer Assemblies for Controlled Gene Silencing. *Advanced healthcare materials* **4**, 760-770, doi:10.1002/adhm.201400671 (2015).

295 Nakayama, T. *et al.* Harnessing a physiologic mechanism for siRNA delivery with mimetic lipoprotein particles. *Molecular therapy : the journal of the American Society of Gene Therapy* **20**, 1582-1589, doi:10.1038/mt.2012.33 (2012).

296 Rajeev, K. G. *et al.* Hepatocyte-Specific Delivery of siRNAs Conjugated to Novel Non-nucleosidic Trivalent N-Acetylgalactosamine Elicits Robust Gene Silencing in Vivo. *Chembiochem : a European journal of chemical biology* **16**, 903-908, doi:10.1002/cbic.201500023 (2015).

297 Yasuda, M. *et al.* RNAi-mediated silencing of hepatic Alas1 effectively prevents and treats the induced acute attacks in acute intermittent porphyria mice. *Proceedings of the National Academy of Sciences of the United States of America* **111**, 7777-7782, doi:10.1073/pnas.1406228111 (2014).

298 Coelho, T. *et al.* Safety and efficacy of RNAi therapy for transthyretin amyloidosis. *The New England journal of medicine* **369**, 819-829, doi:10.1056/NEJMoa1208760 (2013).

299 Frank-Kamenetsky, M. *et al.* Therapeutic RNAi targeting PCSK9 acutely lowers plasma cholesterol in rodents and LDL cholesterol in nonhuman primates. *Proceedings of the*

National Academy of Sciences of the United States of America **105**, 11915-11920, doi:10.1073/pnas.0805434105 (2008).

300 Zhu, X. *et al.* Long-circulating siRNA nanoparticles for validating Prohibitin1-targeted non-small cell lung cancer treatment. *Proceedings of the National Academy of Sciences* **112**, 7779-7784, doi:10.1073/pnas.1505629112 (2015).

301 Kubo, T. *et al.* Gene-Silencing Potency of Symmetric and Asymmetric Lipid-Conjugated siRNAs and Its Correlation with Dicer Recognition. *Bioconjugate chemistry* **24**, 2045-2057, doi:10.1021/bc400391n (2013).

302 Ambardekar, V. V. *et al.* The modification of siRNA with 3' cholesterol to increase nuclease protection and suppression of native mRNA by select siRNA polyplexes. *Biomaterials* **32**, 1404-1411, doi:10.1016/j.biomaterials.2010.10.019 (2011).

303 Uno, Y. *et al.* High-density lipoprotein facilitates in vivo delivery of alpha-tocopherol-conjugated short-interfering RNA to the brain. *Human gene therapy* **22**, 711-719, doi:10.1089/hum.2010.083 (2011).

304 Sarett, S. M., Kilchrist, K. V., Miteva, M. & Duvall, C. L. Conjugation of Palmitic Acid Improves Potency and Longevity of siRNA Delivered via Endosomolytic Polymer Nanoparticles. *Journal of biomedical materials research. Part A*, doi:10.1002/jbm.a.35413 (2015).

305 Oba, M. *et al.* Polyplex micelles prepared from omega-cholesteryl PEG-polycation block copolymers for systemic gene delivery. *Biomaterials* **32**, 652-663, doi:10.1016/j.biomaterials.2010.09.022 (2011).

306 Falamarzian, A. *et al.* Effective down-regulation of signal transducer and activator of transcription 3 (STAT3) by polyplexes of siRNA and lipid-substituted polyethyleneimine for sensitization of breast tumor cells to conventional chemotherapy. *Journal of biomedical materials research. Part A* **102**, 3216-3228, doi:10.1002/jbm.a.34992 (2014).

307 Wei, H. *et al.* Dual responsive, stabilized nanoparticles for efficient in vivo plasmid delivery. *Angewandte Chemie* **52**, 5377-5381, doi:10.1002/anie.201301896 (2013).

308 Kim, J., Sunshine, J. C., Green, J. J. Differential Polymer Structure Tunes Mechanism of Cellular Uptake and Transfection Routes of Poly(β-amino ester) Polyplexes in Human Breast Cancer Cells. *Bioconjugate chemistry* **25**, doi:10.1021/bc4002322 (2014).

309 Bishop, C. J., Abubaker-Sharif, B., Guiriba, T., Tzeng, S. Y. & Green, J. J. Gene delivery polymer structure-function relationships elucidated via principal component analysis. *Chemical Communications* **51**, 12134-12137, doi:10.1039/C5CC04417K (2015).

310 Liu, H. *et al.* SiRNA-phospholipid conjugates for gene and drug delivery in cancer treatment. *Biomaterials* **35**, 6519-6533, doi:10.1016/j.biomaterials.2014.04.033 (2014).

311 He, C., Hu, Y., Yin, L., Tang, C. & Yin, C. Effects of particle size and surface charge on cellular uptake and biodistribution of polymeric nanoparticles. *Biomaterials* **31**, 3657-3666, doi:http://dx.doi.org/10.1016/j.biomaterials.2010.01.065 (2010).

312 Tang, L., Fan, T. M., Borst, L. B. & Cheng, J. Synthesis and Biological Response of Size-Specific, Monodisperse Drug–Silica Nanoconjugates. *ACS Nano* **6**, 3954-3966, doi:10.1021/nn300149c (2012).

313 Gratton, S. E. A. *et al.* The effect of particle design on cellular internalization pathways. *Proceedings of the National Academy of Sciences* **105**, 11613-11618, doi:10.1073/pnas.0801763105 (2008).

314 Perry, J. L. *et al.* PEGylated PRINT Nanoparticles: The Impact of PEG Density on Protein Binding, Macrophage Association, Biodistribution, and Pharmacokinetics. *Nano Letters* **12**, 5304-5310, doi:10.1021/nl302638g (2012).

315 Anselmo, A. C. *et al.* Elasticity of Nanoparticles Influences Their Blood Circulation, Phagocytosis, Endocytosis, and Targeting. *ACS Nano* **9**, 3169-3177, doi:10.1021/acsnano.5b00147 (2015).

316 Nam, H. Y. *et al.* Cellular uptake mechanism and intracellular fate of hydrophobically modified glycol chitosan nanoparticles. *Journal of Controlled Release* **135**, 259-267, doi:http://dx.doi.org/10.1016/j.jconrel.2009.01.018 (2009).

317 Sahay, G. *et al.* Efficiency of siRNA delivery by lipid nanoparticles is limited by endocytic recycling. *Nat Biotech* **31**, 653-658, doi:10.1038/nbt.2614 http://www.nature.com/nbt/journal/v31/n7/abs/nbt.2614.html#supplementary-information (2013).

318 Werfel, T. A. *et al.* Hydrolytic charge-reversal of PEGylated polyplexes enhances intracellular un-packaging and activity of siRNA. *Journal of Biomedical Materials Research Part A* **104**, 917-927, doi:10.1002/jbm.a.35629 (2016).

319 Evans BC, H. K., Osgood MJ, Voskresensky I, Dmowska J, Kilchrist KV, Brophy CM, Duvall, CL. MK2 inhibitory peptide delivered in nanopolyplexes prevents vascular graft intimal hyperplasia. *Science Translational Medicine* **7** (2015).

320 Gabizon, A., Shmeeda, H., Horowitz, A. T. & Zalipsky, S. Tumor cell targeting of liposome-entrapped drugs with phospholipid-anchored folic acid–PEG conjugates. *Advanced drug delivery reviews* **56**, 1177-1192 (2004).

321 Choi, K. Y. *et al.* Self-assembled hyaluronic acid nanoparticles for active tumor targeting. *Biomaterials* **31**, 106-114 (2010).

322 Arap, W., Pasqualini, R. & Ruoslahti, E. Cancer treatment by targeted drug delivery to tumor vasculature in a mouse model. *Science* **279**, 377-380 (1998).

323 Pollaro, L. & Heinis, C. Strategies to prolong the plasma residence time of peptide drugs. *MedChemComm* **1**, 319, doi:10.1039/c0md00111b (2010).

324 Wolfrum, C. *et al.* Mechanisms and optimization of in vivo delivery of lipophilic siRNAs. *Nature biotechnology* **25**, 1149-1157, doi:10.1038/nbt1339 (2007).

325 Ross, J. S. & Fletcher, J. A. The HER-2/neu Oncogene in Breast Cancer: Prognostic Factor, Predictive Factor, and Target for Therapy. *STEM CELLS* **16**, 413-428, doi:10.1002/stem.160413 (1998).

326 Baselga, J. *et al.* Phase II randomized study of neoadjuvant everolimus plus letrozole compared with placebo plus letrozole in patients with estrogen receptor-positive breast cancer. *J Clin Oncol* **27** (2009).

327 deGraffenried, L. A. *et al.* Inhibition of mTOR Activity Restores Tamoxifen Response in Breast Cancer Cells with Aberrant Akt Activity. *Clinical Cancer Research* **10**, 8059 (2004).

328 Driscoll, D. R. *et al.* mTORC2 Signaling Drives the Development and Progression of Pancreatic Cancer. *Cancer Research* **76**, 6911 (2016).

329 Cheng, H. *et al.* RICTOR Amplification Defines a Novel Subset of Patients with Lung Cancer Who May Benefit from Treatment with mTORC1/2 Inhibitors. *Cancer Discovery* **5**, 1262 (2015).

330 O'Reilly, K. E. *et al.* mTOR Inhibition Induces Upstream Receptor Tyrosine Kinase Signaling and Activates Akt. *Cancer Research* **66**, 1500-1508 (2006).

331 Carracedo, A. *et al.* Inhibition of mTORC1 leads to MAPK pathway activation through a PI3K-dependent feedback loop in human cancer. *J Clin Invest* **118** (2008).

332 Palm, W. *et al.* The Utilization of Extracellular Proteins as Nutrients Is Suppressed by mTORC1. *Cell* **162**, 259-270, doi:http://dx.doi.org/10.1016/j.cell.2015.06.017 (2015).

333 Kilchrist, K. V., Evans, B. C., Brophy, C. M. & Duvall, C. L. Mechanism of Enhanced Cellular Uptake and Cytosolic Retention of MK2 Inhibitory Peptide Nano-polyplexes. *Cellular and Molecular Bioengineering* **9**, 368-381, doi:10.1007/s12195-016-0446-7 (2016).

334 Brantley-Sieders, D. M. *et al.* Angiocrine factors modulate tumor proliferation and motility through EphA2 repression of Slit2 tumor suppressor function in endothelium. *Cancer research* **71**, 976-987, doi:10.1158/0008-5472.CAN-10-3396 (2011).

335 Bergers, G. *et al.* Matrix metalloproteinase-9 triggers the angiogenic switch during carcinogenesis. *Nature cell biology* **2**, 737-744, doi:10.1038/35036374 (2000).

336 Pan, D. W. & Davis, M. E. Cationic Mucic Acid Polymer-Based siRNA Delivery Systems. *Bioconjugate Chemistry* **26**, 1791-1803, doi:10.1021/acs.bioconjchem.5b00324 (2015).

337 Wittrup, A. *et al.* Visualizing lipid-formulated siRNA release from endosomes and target gene knockdown. *Nat Biotech* **33**, 870-876, doi:10.1038/nbt.3298 http://www.nature.com/nbt/journal/v33/n8/abs/nbt.3298.html#supplementary-information (2015).

338 Pérez-Medina, C. *et al.* Nanoreporter PET predicts the efficacy of anti-cancer nanotherapy. *Nature Communications* **7**, 11838, doi:10.1038/ncomms11838 http://www.nature.com/articles/ncomms11838#supplementary-information (2016).

339 Bae, Y. H. & Park, K. Targeted drug delivery to tumors: Myths, reality and possibility. *Journal of Controlled Release* **153**, 198-205, doi:http://dx.doi.org/10.1016/j.jconrel.2011.06.001 (2011).

340 Zuckerman, J. E. *et al.* Correlating animal and human phase Ia/Ib clinical data with CALAA-01, a targeted, polymer-based nanoparticle containing siRNA. *Proceedings of the National Academy of Sciences* **111**, 11449-11454 (2014).

341 O'Reilly, K. E. *et al.* mTOR inhibition induces upstream receptor tyrosine kinase signaling and activates Akt. *Cancer Res* **66** (2006).

342 Swain, S. M. *et al.* Pertuzumab, Trastuzumab, and Docetaxel in HER2-Positive Metastatic Breast Cancer. *New England Journal of Medicine* **372**, 724-734, doi:10.1056/NEJMoa1413513 (2015).

343 Balko, J. M. *et al.* Molecular Profiling of the Residual Disease of Triple-Negative Breast Cancers after Neoadjuvant Chemotherapy Identifies Actionable Therapeutic Targets. *Cancer Discovery* **4**, 232 (2014).

344 Burnett, J. C., Rossi, J. J. & Tiemann, K. Current progress of siRNA/shRNA therapeutics in clinical trials. *Biotechnology journal* **6**, 1130-1146, doi:10.1002/biot.201100054 (2011).

345 Caplen, N. J., Parrish, S., Imani, F., Fire, A. & Morgan, R. A. Specific inhibition of gene expression by small double-stranded RNAs in invertebrate and vertebrate systems. *Proceedings of the National Academy of Sciences* **98**, 9742-9747, doi:10.1073/pnas.171251798 (2001).

346 Elbashir, S. M. *et al.* Duplexes of 21-nucleotide RNAs mediate RNA interference in cultured mammalian cells. *Nature* **411**, 494-498 (2001).

347 Kasper, J. C., Schaffert, D., Ogris, M., Wagner, E. & Friess, W. Development of a lyophilized plasmid/LPEI polyplex formulation with long-term stability—A step closer

from promising technology to application. *Journal of Controlled Release* **151**, 246-255, doi:http://dx.doi.org/10.1016/j.jconrel.2011.01.003 (2011).

348 Wilhelm, S. *et al.* Analysis of nanoparticle delivery to tumours. *Nature Reviews Materials* **1**, 16014, doi:10.1038/natrevmats.2016.14 http://www.nature.com/articles/natrevmats201614#supplementary-information (2016).

349 Tang, L. *et al.* Investigating the optimal size of anticancer nanomedicine. *Proceedings of the National Academy of Sciences* **111**, 15344-15349, doi:10.1073/pnas.1411499111 (2014).

350 Cabral, H. *et al.* Accumulation of sub-100 nm polymeric micelles in poorly permeable tumours depends on size. *Nat Nanotechnol* **6**, 815-823, doi:10.1038/nnano.2011.166 (2011).

351 Nichols, J. W. & Bae, Y. H. EPR: Evidence and fallacy. *Journal of Controlled Release* **190**, 451-464, doi:http://dx.doi.org/10.1016/j.jconrel.2014.03.057 (2014).

352 Danhier, F., Feron, O. & Préat, V. To exploit the tumor microenvironment: passive and active tumor targeting of nanocarriers for anti-cancer drug delivery. *Journal of Controlled Release* **148**, 135-146 (2010).

353 Pelaz, B. *et al.* Surface Functionalization of Nanoparticles with Polyethylene Glycol: Effects on Protein Adsorption and Cellular Uptake. *ACS Nano* **9**, 6996-7008, doi:10.1021/acsnano.5b01326 (2015).

354 Liu, Y. *et al.* Theranostic near-infrared fluorescent nanoplatform for imaging and systemic siRNA delivery to metastatic anaplastic thyroid cancer. *Proceedings of the National Academy of Sciences* **113**, 7750-7755 (2016).

355 Nair, J. K. *et al.* Multivalent N-Acetylgalactosamine-Conjugated siRNA Localizes in Hepatocytes and Elicits Robust RNAi-Mediated Gene Silencing. *Journal of the American Chemical Society* **136**, 16958-16961, doi:10.1021/ja505986a (2014).

356 Wolfrum, C. *et al.* Mechanisms and optimization of in vivo delivery of lipophilic siRNAs. *Nat Biotech* **25**, 1149-1157, doi:http://www.nature.com/nbt/journal/v25/n10/suppinfo/nbt1339_S1.html (2007).

357 Zhang, Y.-N., Poon, W., Tavares, A. J., McGilvray, I. D. & Chan, W. C. W. Nanoparticle–liver interactions: Cellular uptake and hepatobiliary elimination. *Journal of Controlled Release* **240**, 332-348, doi:http://dx.doi.org/10.1016/j.jconrel.2016.01.020 (2016).

358 Liu, H.-L. *et al.* Magnetic resonance monitoring of focused ultrasound/magnetic nanoparticle targeting delivery of therapeutic agents to the brain. *Proceedings of the National Academy of Sciences* **107**, 15205-15210 (2010).

359 Jones, S. W. *et al.* Nanoparticle clearance is governed by Th1/Th2 immunity and strain background. *The Journal of Clinical Investigation* **123**, 3061-3073, doi:10.1172/JCI66895 (2013).

360 Perche, F. *et al.* Hydroxychloroquine-conjugated gold nanoparticles for improved siRNA activity. *Biomaterials* **90**, 62-71, doi:http://dx.doi.org/10.1016/j.biomaterials.2016.02.027 (2016).

361 Dahlman, J. E. *et al.* Barcoded nanoparticles for high throughput in vivo discovery of targeted therapeutics. *Proceedings of the National Academy of Sciences*, doi:10.1073/pnas.1620874114 (2017).

362 Iorio, M. V. *et al.* MicroRNA Gene Expression Deregulation in Human Breast Cancer. *Cancer Research* **65**, 7065 (2005).

363 Hanson, M. C. *et al.* Nanoparticulate STING agonists are potent lymph node–targeted vaccine adjuvants. *The Journal of Clinical Investigation* **125**, 2532-2546, doi:10.1172/JCI79915 (2015).

364 Lv, H., Zhang, S., Wang, B., Cui, S. & Yan, J. Toxicity of cationic lipids and cationic polymers in gene delivery. *Journal of Controlled Release* **114**, 100-109, doi:http://dx.doi.org/10.1016/j.jconrel.2006.04.014 (2006).

365 Alexis, F., Pridgen, E., Molnar, L. K. & Farokhzad, O. C. Factors Affecting the Clearance and Biodistribution of Polymeric Nanoparticles. *Molecular pharmaceutics* **5**, 505-515, doi:10.1021/mp800051m (2008).

366 Zuckerman, J. E. *et al.* Correlating animal and human phase Ia/Ib clinical data with CALAA-01, a targeted, polymer-based nanoparticle containing siRNA. *Proceedings of the National Academy of Sciences of the United States of America* **111**, 11449-11454, doi:10.1073/pnas.1411393111 (2014).

367 Li, H. *et al.* Dual MMP7-Proximity-Activated and Folate Receptor-Targeted Nanoparticles for siRNA Delivery. *Biomacromolecules* **16**, 192-201, doi:10.1021/bm501394m (2014).

368 Sun, H. *et al.* Biodegradable micelles with sheddable poly(ethylene glycol) shells for triggered intracellular release of doxorubicin. *Biomaterials* **30**, 6358-6366, doi:http://dx.doi.org/10.1016/j.biomaterials.2009.07.051 (2009).

369 Cheng, R., Meng, F., Deng, C., Klok, H.-A. & Zhong, Z. Dual and multi-stimuli responsive polymeric nanoparticles for programmed site-specific drug delivery. *Biomaterials* **34**, 3647-3657, doi:http://dx.doi.org/10.1016/j.biomaterials.2013.01.084 (2013).

370 Meng, F., Zhong, Z. & Feijen, J. Stimuli-Responsive Polymersomes for Programmed Drug Delivery. *Biomacromolecules* **10**, 197-209, doi:10.1021/bm801127d (2009).

371 Zhu, C. *et al.* Co-delivery of siRNA and paclitaxel into cancer cells by biodegradable cationic micelles based on PDMAEMA–PCL–PDMAEMA triblock copolymers. *Biomaterials* **31**, 2408-2416, doi:http://dx.doi.org/10.1016/j.biomaterials.2009.11.077 (2010).

372 Prata, C. A. H. *et al.* Charge-Reversal Amphiphiles for Gene Delivery. *Journal of the American Chemical Society* **126**, 12196-12197, doi:10.1021/ja0474906 (2004).

373 Gu, W. *et al.* Polymer Nanocarrier System for Endosome Escape and Timed Release of siRNA with Complete Gene Silencing and Cell Death in Cancer Cells. *Biomacromolecules* **14**, 3386-3389, doi:10.1021/bm401139e (2013).

374 Truong, N. P. *et al.* An influenza virus-inspired polymer system for the timed release of siRNA. *Nat Commun* **4**, 1902, doi:10.1038/ncomms2905 (2013).

375 Convertine, A. J., Benoit, D. S. W., Duvall, C. L., Hoffman, A. S. & Stayton, P. S. Development of a novel endosomolytic diblock copolymer for siRNA delivery. *Journal of Controlled Release* **133**, 221-229, doi:http://dx.doi.org/10.1016/j.jconrel.2008.10.004 (2009).

376 Moad, G., Chong, Y. K., Postma, A., Rizzardo, E. & Thang, S. H. Advances in RAFT polymerization: the synthesis of polymers with defined end-groups. *Polymer* **46**, 8458-8468, doi:http://dx.doi.org/10.1016/j.polymer.2004.12.061 (2005).

377 Chong, Y. K., Le, T. P. T., Moad, G., Rizzardo, E. & Thang, S. H. A More Versatile Route to Block Copolymers and Other Polymers of Complex Architecture by Living Radical Polymerization: The RAFT Process. *Macromolecules* **32**, 2071-2074, doi:10.1021/ma981472p (1999).

378 Alabi, C. A. *et al.* FRET-Labeled siRNA Probes for Tracking Assembly and Disassembly of siRNA Nanocomplexes. *ACS Nano* **6**, 6133-6141, doi:10.1021/nn3013838 (2012).

379 Miteva, M. *et al.* Tuning PEGylation of mixed micelles to overcome intracellular and systemic siRNA delivery barriers. *Biomaterials* **38**, 97-107, doi:http://dx.doi.org/10.1016/j.biomaterials.2014.10.036 (2015).

380 Tran, N. T. D. *et al.* Timed-Release Polymer Nanoparticles. *Biomacromolecules* **14**, 495-502, doi:10.1021/bm301721k (2013).

381 Truong, N. P., Jia, Z., Burges, M., McMillan, N. A. J. & Monteiro, M. J. Self-Catalyzed Degradation of Linear Cationic Poly(2-dimethylaminoethyl acrylate) in Water. *Biomacromolecules* **12**, 1876-1882, doi:10.1021/bm200219e (2011).

382 Novo, L. *et al.* Targeted Decationized Polyplexes for siRNA Delivery. *Molecular pharmaceutics* **12**, 150-161, doi:10.1021/mp500499x (2014).

383 Youngblood, V. *et al.* Elevated Slit2 Activity Impairs VEGF-Induced Angiogenesis and Tumor Neovascularization in EphA2-Deficient Endothelium. *Molecular cancer research : MCR* **13**, 524-537, doi:10.1158/1541-7786.MCR-14-0142 (2015).

384 Brantley-Sieders, D. M. *et al.* The receptor tyrosine kinase EphA2 promotes mammary adenocarcinoma tumorigenesis and metastatic progression in mice by amplifying ErbB2 signaling. *J Clin Invest* **118**, 64-78 (2008).

385 Dunaway, C. M. *et al.* Cooperative signaling between Slit2 and Ephrin-A1 regulates a balance between angiogenesis and angiostasis. *Mol Cell Biol* **31**, 404-416, doi:MCB.00667-10 [pii]10.1128/MCB.00667-10 (2011).